BEILSTEIN JOURNAL OF ORGANIC CHEMISTRY

Photocatalysis and photochemistry in organic synthesis

Edited by Timothy Noël and Bartholomäus (Bart) Pieber

Imprint

Beilstein Journal of Organic Chemistry
www.bjoc.org
ISSN 1860-5397
Email: journals-support@beilstein-institut.de

The *Beilstein Journal of Organic Chemistry* is published by the Beilstein-Institut zur Förderung der Chemischen Wissenschaften.

Beilstein-Institut zur Förderung der Chemischen Wissenschaften
Trakehner Straße 7–9
60487 Frankfurt am Main
Germany
www.beilstein-institut.de

BEILSTEIN JOURNAL OF ORGANIC CHEMISTRY

Photocatalysis and photochemistry in organic synthesis

Timothy Noël[*1] and Bartholomäus Pieber[*2]

Editorial

Open Access

Address:
[1]Van't Hoff Institute for Molecular Sciences (HIMS), University of Amsterdam, Science Park 904, 1098 XH Amsterdam, Netherlands and [2]Institute of Science and Technology Austria (ISTA), Am Campus 1, 3400 Klosterneuburg, Austria

Email:
Timothy Noël[*] - t.noel@uva.nl;
Bartholomäus Pieber[*] - bartholomaeus.pieber@ista.ac.at

* Corresponding author

Keywords:
photocatalysis; photochemistry

Beilstein J. Org. Chem. **2025,** *21,* 1645–1647.
https://doi.org/10.3762/bjoc.21.128

Received: 05 August 2025
Accepted: 13 August 2025
Published: 18 August 2025

This article is part of the thematic issue "Photocatalysis and photochemistry in organic synthesis".

Guest Editors: T. Noël and B. Pieber

Soon after its first reported synthesis in 1936 [1], $[Ru(bpy)_3]Cl_2$ (bpy = 2,2'-bipyridine) and its derivatives attracted significant attention due to their photophysical properties [2-4]. These complexes can efficiently absorb visible light through a metal-to-ligand charge transfer (MLCT) transition, resulting in a long-lived charge-separated species. In this excited state, $[Ru(bpy)_3]Cl_2$ is both a more potent oxidant and reductant than in its ground state. This reactivity, in combination with the reversible redox behavior of the metal complex, enables reductive or oxidative quenching cycles in the presence of electron donors and acceptors. Furthermore, $[Ru(bpy)_3]Cl_2$ can engage in Förster and Dexter energy transfer processes, enabling the transfer of excited-state energy to molecules that do not themselves absorb visible light. This versatility is arguably the reason for the tremendous impact of $[Ru(bpy)_3]Cl_2$ on several research areas, including solar energy conversion [5], optosensing [6], photodynamic therapy [7,8] and bioimaging [9].

Scattered examples of $[Ru(bpy)_3]Cl_2$ being used as a photocatalyst for visible-light-driven organic synthesis appeared in the scientific literature as early as the 1970s [10]. However, these remained largely isolated cases – more mechanistic curiosities than general synthetic platforms.

The narrative shifted significantly in the late 2000s, when interest in early pioneering work on photocatalysis was revisited, and systematic investigations began to demonstrate its broad applicability [11]. This renewed momentum was driven by contributions from numerous groups across the field. At the same time, advances in technology – particularly the accessibility of various light sources (most notably LEDs) – made photochemical transformations much more practical to implement. Two decades later, photocatalysis and photochemistry remain among the most studied topics in modern organic synthesis. Nowadays, chemists can choose from a wide range of organometallic [12,13], organic [14,15], or heterogeneous photocatalysts [16,17] to trigger visible-light photoredox catalysis, and this arsenal of catalysts is constantly expanding. In this thematic issue, the Dell'Amico group describes the development of a new class of organic donor–acceptor photocatalysts that show promising activity for several transformations [18]. Additionally, Hoffmann and co-workers contributed a Review article discussing photocatalysts capable of harnessing low-energy red light to trigger chemical reactions [19].

In addition to photoredox catalysis, several mechanistic platforms that leverage light – such as the use of electron donor–acceptor complexes [20], proton-coupled electron

transfer [21], hydrogen atom transfer [22], halogen atom transfer [23], and energy transfer catalysis [24,25] – have been established as powerful additions to the arsenal of photon-driven reactions. Three articles in this thematic issue exemplify this: The Molloy group developed an intramolecular [2 + 2]-cycloaddition of alkenylboronic esters using energy transfer catalysis [26]. Gualandi and co-workers leveraged a combination of photoredox and HAT catalysis to realize the intramolecular nucleophilic amidation of alkenes with β-lactams [27]. Further, Luridiana and colleagues developed a method for the alkylation of a dehydroalanine derivative using silane-mediated halogen atom transfer [28].

Dual catalytic approaches that merge photocatalysis with Lewis acid [29], organo- [30], or transition metal catalysis [31] have enabled access to bond formations that are otherwise challenging to achieve. In particular, the combination of nickel catalysis and photoredox catalysis has become one of the most studied strategies to forge carbon–carbon bonds. The groups of Soengas and Rodríguez-Solla used this strategy to develop a general method for the synthesis of enaminones [32].

Light-induced transition metal catalysis that does not require exogenous photocatalysts has emerged as a new paradigm in photochemical synthesis [33]. Here, a transition metal complex plays a dual role by harnessing photon energy to facilitate bond-breaking and bond-forming events. For example, Sipos and co-workers demonstrate in this thematic issue that visible light increases the reaction rate of palladium-catalyzed Negishi cross-couplings [34].

The integration of enabling technologies has also contributed to the success of photocatalytic organic synthesis [35]. Automated reaction platforms, high-throughput experimentation techniques, and flow chemistry are being harnessed to push the limits of light-driven reactions [36]. Terada and colleagues show in this thematic issue how flow chemistry is used to significantly improve the yield of a π-Lewis acidic metal-catalyzed cyclization–radical addition sequence [37]. Recently, chemists have begun studying reactions that combine the advantages of photochemical methods and mechanochemistry. This thematic issue contains a Perspective article from the Capaldo laboratory that surveys these efforts and discusses future possibilities [38].

Without a doubt, the growing interest in light-mediated organic synthesis has also resulted in a renaissance of radical chemistry. Once regarded as "[…] messy, unpredictable, unpromising and essentially mysterious" [39], radical-based methods have become central to modern organic chemistry, spanning applications in the life sciences. The Perspective article from the Molander group on the photocatalyzed elaboration of antibody-based bioconjugates underscores this impact [40].

This thematic issue celebrates the profound impact of light-mediated synthesis across fundamental, methodological, and applied domains. As guest editors, we are deeply grateful to all contributors and thank all referees for their careful evaluations, which helped maintain the scientific rigor of this collection. We hope this collection inspires further exploration and innovation in this rapidly advancing field.

Timothy Noël and Bartholomäus Pieber

Amsterdam and Klosterneuburg, August 2025

Acknowledgements

The Graphical Abstract was created with the AI tool https://wordart.com. This content is not subject to CC BY 4.0.

Data Availability Statement

Data sharing is not applicable as no new data was generated or analyzed in this study.

References

1. Burstall, F. H. *J. Chem. Soc.* **1936,** 173–175. doi:10.1039/jr9360000173
2. Villani, E.; Sakanoue, K.; Einaga, Y.; Inagi, S.; Fiorani, A. *J. Electroanal. Chem.* **2022,** *921,* 116677. doi:10.1016/j.jelechem.2022.116677
3. Arias-Rotondo, D. M.; McCusker, J. K. An Overview of the Physical and Photophysical Properties of [Ru(bpy)$_3$]2+. In *Visible Light Photocatalysis in Organic Chemistry;* Stephenson, C. R. J.; Yoon, T. P.; MacMillan, D. W. C., Eds.; Wiley-VCH: Weinheim, Germany, 2018; pp 1–24. doi:10.1002/9783527674145.ch1
4. Juris, A.; Balzani, V.; Barigelletti, F.; Campagna, S.; Belser, P.; von Zelewsky, A. *Coord. Chem. Rev.* **1988,** *84,* 85–277. doi:10.1016/0010-8545(88)80032-8
5. Kalyanasundaram, K. *Coord. Chem. Rev.* **1982,** *46,* 159–244. doi:10.1016/0010-8545(82)85003-0
6. Orellana, G.; García-Fresnadillo, D. Environmental and Industrial Optosensing with Tailored Luminescent Ru(II) Polypyridyl Complexes. In *Optical Sensors: Industrial Environmental and Diagnostic Applications;* Narayanaswamy, R.; Wolfbeis, O. S., Eds.; Springer: Berlin, Heidelberg, 2004; pp 309–357. doi:10.1007/978-3-662-09111-1_13
7. Heinemann, F.; Karges, J.; Gasser, G. *Acc. Chem. Res.* **2017,** *50,* 2727–2736. doi:10.1021/acs.accounts.7b00180
8. Ng, X. Y.; Fong, K. W.; Kiew, L. V.; Chung, P. Y.; Liew, Y. K.; Delsuc, N.; Zulkefeli, M.; Low, M. L. *J. Inorg. Biochem.* **2024,** *250,* 112425. doi:10.1016/j.jinorgbio.2023.112425
9. Fillaut, J.-L. *Coord. Chem. Rev.* **2024,** *518,* 216050. doi:10.1016/j.ccr.2024.216050
10. Schroll, P. Early pioneers of organic photochemistry. In *Chemical Photocatalysis;* König, B., Ed.; Walter de Gruyter: Berlin, Germany, 2020; pp 1–16. doi:10.1515/9783110576764-001

11. Shaw, M. H.; Twilton, J.; MacMillan, D. W. C. *J. Org. Chem.* **2016,** *81,* 6898–6926. doi:10.1021/acs.joc.6b01449
12. Arias-Rotondo, D. M.; McCusker, J. K. *Chem. Soc. Rev.* **2016,** *45,* 5803–5820. doi:10.1039/c6cs00526h
13. Hossain, A.; Bhattacharyya, A.; Reiser, O. *Science* **2019,** *364,* eaav9713. doi:10.1126/science.aav9713
14. Romero, N. A.; Nicewicz, D. A. *Chem. Rev.* **2016,** *116,* 10075–10166. doi:10.1021/acs.chemrev.6b00057
15. Bonardi, A.-H.; Dumur, F.; Noirbent, G.; Lalevée, J.; Gigmes, D. *Beilstein J. Org. Chem.* **2018,** *14,* 3025–3046. doi:10.3762/bjoc.14.282
16. Gisbertz, S.; Pieber, B. *ChemPhotoChem* **2020,** *4,* 456–475. doi:10.1002/cptc.202000014
17. Riente, P.; Noël, T. *Catal. Sci. Technol.* **2019,** *9,* 5186–5232. doi:10.1039/c9cy01170f
18. Medrano-Uribe, K.; Humbrías-Martín, J.; Dell'Amico, L. *Beilstein J. Org. Chem.* **2025,** *21,* 935–944. doi:10.3762/bjoc.21.76
19. Fortier, L.; Lefebvre, C.; Hoffmann, N. *Beilstein J. Org. Chem.* **2025,** *21,* 296–326. doi:10.3762/bjoc.21.22
20. Crisenza, G. E. M.; Mazzarella, D.; Melchiorre, P. *J. Am. Chem. Soc.* **2020,** *142,* 5461–5476. doi:10.1021/jacs.0c01416
21. Miller, D. C.; Tarantino, K. T.; Knowles, R. R. *Top. Curr. Chem.* **2016,** *374,* 30. doi:10.1007/s41061-016-0030-6
22. Capaldo, L.; Ravelli, D.; Fagnoni, M. *Chem. Rev.* **2022,** *122,* 1875–1924. doi:10.1021/acs.chemrev.1c00263
23. Juliá, F.; Constantin, T.; Leonori, D. *Chem. Rev.* **2022,** *122,* 2292–2352. doi:10.1021/acs.chemrev.1c00558
24. Strieth-Kalthoff, F.; James, M. J.; Teders, M.; Pitzer, L.; Glorius, F. *Chem. Soc. Rev.* **2018,** *47,* 7190–7202. doi:10.1039/c8cs00054a
25. Neveselý, T.; Wienhold, M.; Molloy, J. J.; Gilmour, R. *Chem. Rev.* **2022,** *122,* 2650–2694. doi:10.1021/acs.chemrev.1c00324
26. McGhie, L.; Kortman, H. M.; Rumpf, J.; Seeberger, P. H.; Molloy, J. J. *Beilstein J. Org. Chem.* **2025,** *21,* 854–863. doi:10.3762/bjoc.21.69
27. Giraldi, V.; Magagnano, G.; Giacomini, D.; Cozzi, P. G.; Gualandi, A. *Beilstein J. Org. Chem.* **2024,** *20,* 2461–2468. doi:10.3762/bjoc.20.210
28. van der Heide, P.; Retini, M.; Fanini, F.; Piersanti, G.; Secci, F.; Mazzarella, D.; Noël, T.; Luridiana, A. *Beilstein J. Org. Chem.* **2024,** *20,* 3274–3280. doi:10.3762/bjoc.20.271
29. Yoon, T. P. *Acc. Chem. Res.* **2016,** *49,* 2307–2315. doi:10.1021/acs.accounts.6b00280
30. Shen, J.-H.; Shi, M.; Wei, Y. *Chem. – Eur. J.* **2023,** *29,* e202301157. doi:10.1002/chem.202301157
31. Chan, A. Y.; Perry, I. B.; Bissonnette, N. B.; Buksh, B. F.; Edwards, G. A.; Frye, L. I.; Garry, O. L.; Lavagnino, M. N.; Li, B. X.; Liang, Y.; Mao, E.; Millet, A.; Oakley, J. V.; Reed, N. L.; Sakai, H. A.; Seath, C. P.; MacMillan, D. W. C. *Chem. Rev.* **2022,** *122,* 1485–1542. doi:10.1021/acs.chemrev.1c00383
32. Pérez-Ramos, P.; Soengas, R. G.; Rodríguez-Solla, H. *Beilstein J. Org. Chem.* **2025,** *21,* 1535–1543. doi:10.3762/bjoc.21.116
33. Cheung, K. P. S.; Sarkar, S.; Gevorgyan, V. *Chem. Rev.* **2022,** *122,* 1543–1625. doi:10.1021/acs.chemrev.1c00403
34. Gasparetto, M.; Fődi, B.; Sipos, G. *Beilstein J. Org. Chem.* **2024,** *20,* 1922–1932. doi:10.3762/bjoc.20.168
35. Buglioni, L.; Raymenants, F.; Slattery, A.; Zondag, S. D. A.; Noël, T. *Chem. Rev.* **2022,** *122,* 2752–2906. doi:10.1021/acs.chemrev.1c00332
36. Bonciolini, S.; Pulcinella, A.; Noël, T. *J. Am. Chem. Soc.* **2025,** *147,* 28523–28545. doi:10.1021/jacs.5c10303
37. Terada, M.; Iwasaki, Z.; Yazaki, R.; Umemiya, S.; Kikuchi, J. *Beilstein J. Org. Chem.* **2024,** *20,* 1973–1980. doi:10.3762/bjoc.20.173
38. Mele, F.; Constantin, A. M.; Porcheddu, A.; Maggi, R.; Maestri, G.; Ca', N. D.; Capaldo, L. *Beilstein J. Org. Chem.* **2025,** *21,* 458–472. doi:10.3762/bjoc.21.33
39. Walling, C. *Tetrahedron* **1985,** *41,* 3887–3900. doi:10.1016/s0040-4020(01)97172-8
40. Le Stum, M.; Romero, E.; Molander, G. A. *Beilstein J. Org. Chem.* **2025,** *21,* 616–629. doi:10.3762/bjoc.21.49

License and Terms

BEILSTEIN JOURNAL OF ORGANIC CHEMISTRY

Negishi-coupling-enabled synthesis of α-heteroaryl-α-amino acid building blocks for DNA-encoded chemical library applications

Matteo Gasparetto, Balázs Fődi and Gellért Sipos*

Full Research Paper

Open Access

Address:
X-Chem Zrt., Záhony u. 7, DA Building, Graphisoft Park, Budapest, 1031, Hungary

Email:
Gellért Sipos* - gellert.sipos@x-chemrx.com

* Corresponding author

Keywords:
amino acids; DEL; flow chemistry; Negishi; on-DNA chemistry

Beilstein J. Org. Chem. **2024,** *20,* 1922–1932.
https://doi.org/10.3762/bjoc.20.168

Received: 30 May 2024
Accepted: 26 July 2024
Published: 08 August 2024

This article is part of the thematic issue "Photocatalysis and photochemistry in organic synthesis".

Guest Editor: T. Noël

Abstract

Amino acids are vital motifs in the domain of biochemistry, serving as the foundational unit for peptides and proteins, while also holding a crucial function in many biological processes. Due to their bifunctional character, they have been also used for combinatorial chemistry purposes, such as the preparation of DNA-encoded chemical libraries. We developed a practical synthesis for α-heteroaryl-α-amino acids starting from an array of small heteroaromatic halides. The reaction sequence utilizes a photochemically enhanced Negishi cross-coupling as a key step, followed by oximation and reduction. The prepared amino esters were validated for on-DNA reactivity via a reverse amidation–hydrolysis–reverse amidation protocol.

Introduction

DNA-encoded chemical library (DEL) technology is a powerful tool for hit identification [1,2]. DELs are chemically synthesized libraries in which every member is covalently attached to a unique DNA sequence serving as a molecular "barcode" [3]. The success of this technology ultimately relies on the quality and diversity of the libraries. DEL synthesis must employ DNA-compatible reactions; hence it operates under a limited set of conditions [4,5]. DELs are typically produced via split-and-pool combinatorial chemistry methods. Using bifunctional building blocks (BBs) can quickly increase the diversity of these molecular libraries [6]. Hence, DEL practitioners constantly seek access to novel building blocks [7].

Amino acids (AAs) are vital motifs in the domain of biochemistry, serving as the foundational unit for peptides and proteins, while also holding a crucial function in many biological processes [8]. Non-canonical amino acids (NCAs) are widely used in medicinal chemistry [9]. Not surprisingly, they also find broad use as bifunctional building blocks (BBs) for DELs. In an early example, an 800-million-members DEL utilized Fmoc-amino acids as primary diversity elements [10].

The pursuit of achieving the efficient synthesis of α-amino acids has been an ongoing challenge since 1850, marked by the initial report of the Strecker condensation [11]. The Strecker synthesis

and the related Bucherer–Bergs hydantoin formation remains the most employed approach for producing this family of substrates [12]. Despite its effectiveness, this approach requires hazardous cyanides and harsh conditions for the subsequent hydrolysis of the nitrile or the hydantoin. Additionally, it carries significant limitations in its scope, reducing its overall applicability.

A different approach for the synthesis of α-amino acids involves the formation of dehydroamino acids and subsequent hydrogenation [13,14]. More recently, there have been reports of techniques that utilize phase transfer catalysts (PTCs) to alkylate glycine derivatives [15,16]. A range of less widely applicable strategies have been developed as well [17-22].

The above-mentioned methods focus on the synthesis of α-alkyl-amino acids. Moving to α-aryl-amino acids, the Clayden group published an excellent asymmetric α-arylation method to access quaternary amino acids with high enantiomeric purity [23]. The synthesis of formally glycine-derived tertiary α-aryl-amino acids is much less developed. The most common strategy for obtaining these substrates is by lithiation of an aromatic ring followed by coupling with a glycine derivative (Scheme 1a). For example, this approach was applied to the synthesis of *N*-substituted pyrazoles and poly-substituted isothiazoles [24,25]. Glycine derivatives can be reacted with indoles using copper catalysis or metallophotoredox catalysis [26]. Le et al. reported the use of the same approach for imidazo[1,2-*a*]pyridines [27,28]. However, the selectivity of these photoredox reactions is driven by the structural properties of the heteroaromatic ring. During the preparation of this article, the Meggers group published an outstanding enantioselective iron-catalyzed α-amination pathway (Scheme 1b) [29]. The method is widely applicable to a broad range of substrates, however, it utilizes a catalyst that is not commercially available and small heteroaromatic rings are underrepresented in the scope.

Recognizing the importance of small heteroaromatic rings and the amino acid motif in medicinal chemistry [30-33], and aiming to expand our in-house DEL BB collection, we sought to develop a synthetic route capable of providing a broad range of α-heteroaryl-α-amino acids in a cost-effective manner (Scheme 1c).

Herein, we describe the synthesis and on-DNA validation of non-canonical α-heteroaryl-α-amino acids. We envisioned that α-heteroaryl acetates accessed through Negishi coupling can be used as key intermediates towards NCAs (Scheme 1c). Indeed, oximation of these motifs followed by reduction gave access to the desired NCAs.

Results and Discussion

Negishi cross-coupling step

The Negishi reaction provides convenient access to compounds featuring C(sp^2)–C(sp^3) bonds. However, the general view is

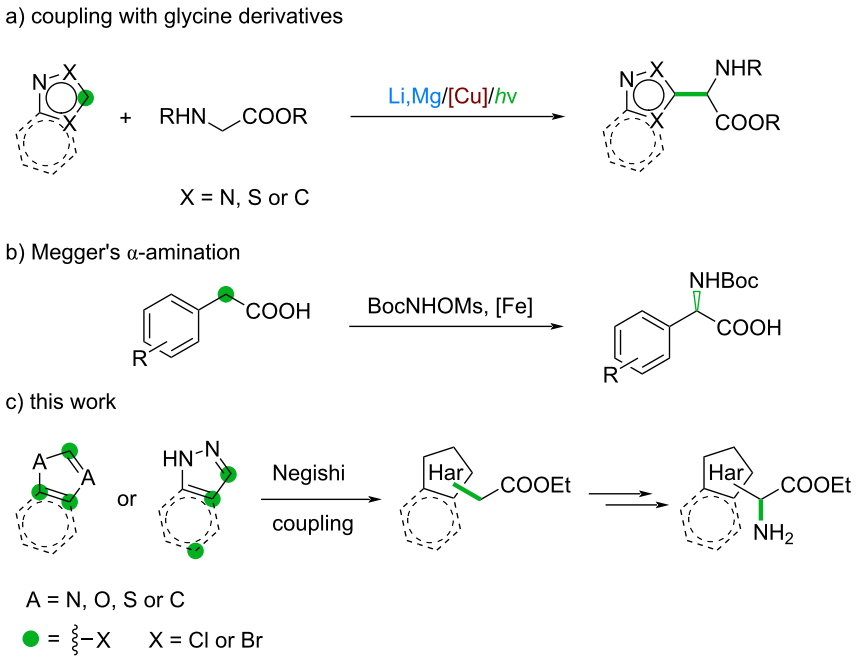

Scheme 1: Known and improved synthetic strategies to access α-(hetero)aryl-amino acids.

that this transformation is less reliable than its orthogonal counterpart, the Suzuki reaction. Recent years have seen significant developments in Negishi reaction methodologies [34-39]. In particular, Alcazar et al. developed continuous flow protocols for both the generation of alkylzinc halides and for the subsequent Negishi cross-coupling reaction [40-44]. We successfully adapted Alcazar's protocols for the synthesis of otherwise challenging heteroaryl–alkyl connections (see Table S1 in Supporting Information File 1). We decided to explore the potential of this methodology for the formation of α-heteroarylacetates. In particular, we were curious to see whether this methodology translates well for five-membered heteroarene substrates (e.g., thiazoles, pyrazoles, imidazoles) which are usually underrepresented in the peer-reviewed literature in comparison to phenyl groups or their six-membered counterparts (e.g., pyridines, pyrimidines) [42]. Furthermore, the increasing importance of small heteroaromatic rings containing nitrogen, sulfur and/or oxygen in medicinal chemistry is well depicted by the list of recently approved drugs by the FDA [31]. Fezolinetant (an NK3 receptor antagonist) and quizartinib (FLT3 inhibitor) are just a couple of examples among the drugs reaching the market in the last year.

As shown in Scheme 2, ethyl (bromozinc)acetate (**1a**) was synthesized in flow by pumping a solution of ethyl 2-bromoacetate through a pre-activated zinc column (see page 11 in Supporting Information File 1) [44]. The Reformatsky reagent could be obtained in yields varying from 70 to 90% depending on the activation state of the column. The yield of the reaction was determined by titration with iodine (see page 11 Supporting Information File 1), affording final concentrations between 0.35 to 0.45 M in THF. The solution can be stored in the fridge under argon for one week before being used in the Negishi reaction. With concentrations above 0.4 M we observed crystallization of ethyl (bromozinc)acetate at the bottom of the vial after a few hours of storage in the fridge. The solid can be easily re-dissolved by gentle heating, and without affecting the product concentration and integrity.

After a brief screening, $Pd(dba)_2$ and X-Phos (in a 1:2 ratio) were selected as the catalyst system for the Negishi reaction (Supporting Information File 1). Preliminary experiments were carried out with and without blue light irradiation in the PhotoCube^{TM} photoreactor [45]. These experiments revealed that while the conversion of imidazoles and pyrazoles benefits from irradiation, thiazoles seem to be largely unaffected by the presence of light (see pages 5 and 6 in Supporting Information File 1). In the case of indazoles, increased reaction rates were observed in the presence of light, but the overall yield was the same for the dark and irradiated experiments. Although these reactions are typically complete within 4 h in the dark, irradiation with blue light halves the reaction time for many compounds. Overall, these observations are in line with those of Alcazar et al. [43]. In their work, the authors demonstrated the formation of a complex between palladium and the organozinc reagent which is absorbing in the blue region. This complex then accelerates the oxidative addition of the aryl halide to the metal, which is usually the rate-limiting step for palladium-catalyzed cross-couplings. Based on these results we decided to perform all Negishi reactions under blue light irradiation.

With the optimized conditions in hand, we proceeded with the investigation of the heteroaryl halide scope in batch (Scheme 3). Thiazoles proved to be challenging substrates typically affording the desired products in moderate yields (**2b**–**h**). While 2-chlorothiazole led to the production of **2b** in 44% yield, 2-bromo-5-chlorothiazole only afforded 21% yield (**2d**). Gratifyingly, the reaction selectively proceeded in position 2 of the ring. Position 4 seems to be inert to the Negishi coupling conditions as illustrated by substrates **2c** and **2g**. Somewhat surprisingly, LCMS analysis indicated that **1g** did not go through oxidative addition and remained unreacted. Formation of **2h** did not occur, however, we observed the formation of unidentified side products. Interestingly, the presence of a free carboxylic group is well tolerated (**2f**). Benzothiazole **1i** proved to be an excellent substrate for this reaction, leading to the desired acetate **2i** in high yield. A similar result was obtained for the furanyl derivative **2j**. Pyrazoles were the only substrate class which clearly benefited from light irradiation (**2k**–**o**), displaying not just a shorter reaction time but also higher yields. Even unprotected pyrazoles (**2k**, **2m**, **2n**) performed well, showing that *N*-protection is not mandatory for this transformation.

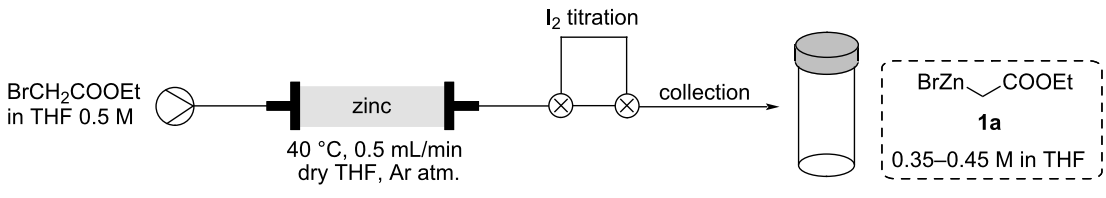

Scheme 2: Reformatsky reagent production.

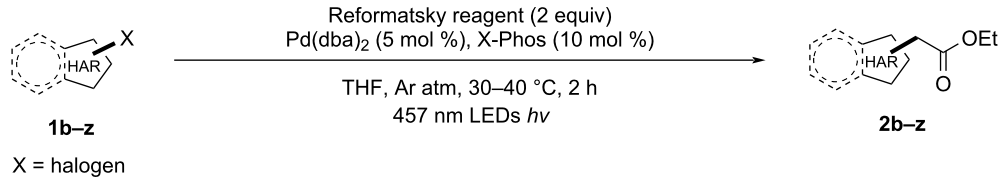

1b–z

X = halogen

2b–z

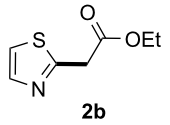

2b

44% (X = Cl)

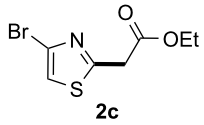

2c

62% (X = Br)

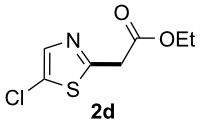

2d

21% (X = Br)

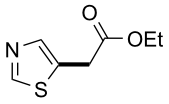

2e

50% (X = Br)

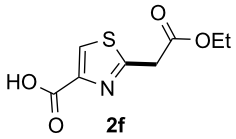

2f

61% (X = Br)

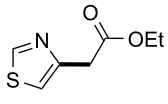

2g

– (X = Br)

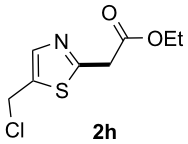

2h

– (X = Cl)

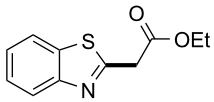

2i

87% (X = Br)

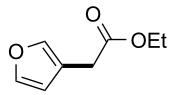

2j

87% (X = Br)

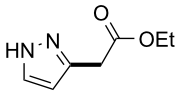

2k

73% (X = Br)
not irradiated: 45%*

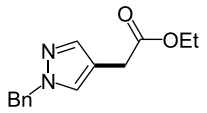

2l

80% (X = Br)
not irradiated: 58%*

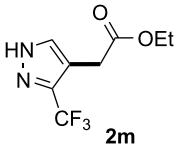

2m

95% (X = Br)
not irradiated: 66%*

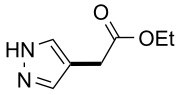

2n

48% (X = Br)
not irradiated: 26%*

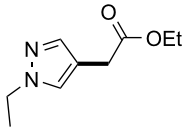

2o

87% (X = Br)

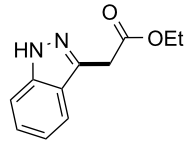

2p

39% (X = Cl)

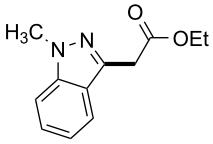

2q

48% (X = Br)

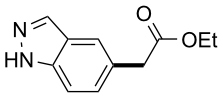

2r

82% (X = Br)

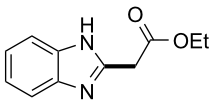

2s

– (X = Br)

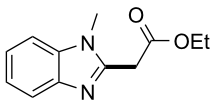

2t

77% (X = Br)

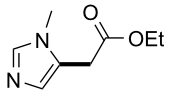

2u

92% (X = Br)

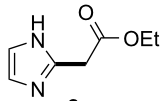

2v

– (X = Br)

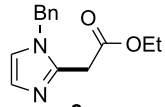

2z

– (X = Br)

Scheme 3: Scope of ethyl heteroarylacetates. Isolated yields are given. *Dark reactions were carried out for 4 h.

3-Bromo- and 3-chloroindazoles offered moderate yields (39% and 48% for **2p** and **2q**, respectively), while 5-substituted **2r** was isolated with 82% yield. In contrast to pyrazoles and indazoles, benzimidazoles and imidazoles required the protection of the aromatic NH group (**2s** vs **2t**; **2v** vs **2u**). Reactions with unprotected imidazoles **1s** and **1v** led to immediate formation of a precipitate upon addition of the Reformatsky reagent. Surprisingly, **1z** did not afford the expected product (**2z**).

The synthesis of the Reformatsky reagent can be combined with the Negishi cross-coupling step in a continuous flow manner [41-43]. Continuous flow chemistry offers superior control over reaction parameters compared to traditional batch methods. This approach leads to reproducible reactions, improved safety features, and it can facilitate high-throughput screening and rapid optimization [46,47]. Homogenous heating and mixing in flow reactors can lead to higher reaction rates and yields. In terms of photochemistry, continuous flow setups provide enhanced light irradiation as well [48,49]. These advantages make flow chemistry a powerful tool for chemical synthesis and industrial applications [50,51].

To assess the advantage of moving from batch to flow, the production of compounds **2b** and **2i** was carried out with the telescoped approach. Despite the difference in the yield being minimal, the rate of the transformation showed a significant improvement under continuous flow conditions, leading to reaction completion within 30 minutes (Scheme 4).

Oxime formation

Once the ethyl heteroarylacetates scope was completed we turned our attention to the incorporation of the amino group. There are precedents for α-aminations, but we were not able to find a method suitable for our needs [52,53]. Benzylic bromination followed by nucleophilic substitution offers a general approach for the introduction of the nitrogen atom [54-56]. Consequently, the continuous flow Wohl–Ziegler bromination of **2b** was attempted [57]. Even though we could observe excellent LCMS-conversion for the mono-brominated compound, we encountered several problems related to the stability of the product (see Supporting Information File 1).

To circumvent these issues, we came across the possibility of inserting an oximino group into the benzylic position which can then be converted into an amino group by reduction. We reasoned that increasing the sp^2 fraction and the rigidity of the whole structure will lead to increased stability of these derivatives. The first exploratory attempts demonstrated the easy preparation and the high bench stability of the oxime derivatives, therefore we opted to proceed using this route. In this study, we explored three distinct approaches commonly employed for the introduction of the oximino group into a molecule. The first approach is based on the generation of the nitrosonium ion from sodium nitrite under acidic conditions (Scheme 5, top) [58,59]. Additionally, another very common method involves the employment of a strong base, typically sodium ethoxide or methoxide, in combination with an alkyl nitrite to promote the incorporation of the oximino group (Scheme 5, middle) [60,61]. Furthermore, a widely adopted strategy involves the conversion of a carbonyl group to an oxime through condensation with hydroxylamine (Scheme 5, bottom) [62-64].

In order to develop a synthetic approach applicable to several different substrates, we decided to screen the three methods on one example from each type of heteroaryl halides. According to

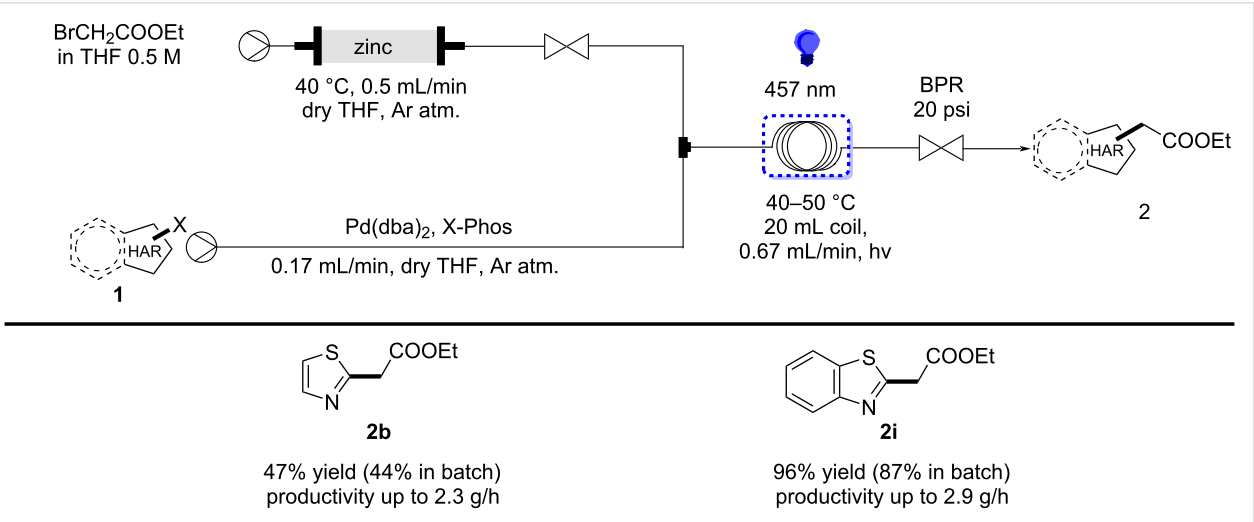

Scheme 4: Telescoped flow synthesis of heteroarylacetates.

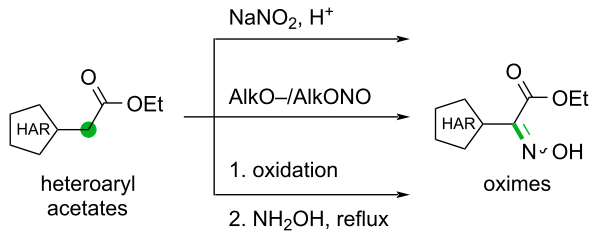

Scheme 5: Potential routes for the preparation of oximes.

our experimental results, thiazole **2b**, benzothiazole **2i** and benzimidazole **2t** react very well with sodium nitrite in an acidic environment (Scheme 6, red section). Among the various subclasses of compounds, pyrazole **2l** exhibited a high reactivity using *t*-BuONO and EtONa in ethanol (Scheme 6, red section). On the other hand, no reaction was observed with indazoles and furans using the first two conditions, requiring the formation of the ketoesters **4j** and **4r** first, followed by the functional group interconversion (FGI) with $NH_2OH{\cdot}HCl$ (Scheme 6, blue and green sections).

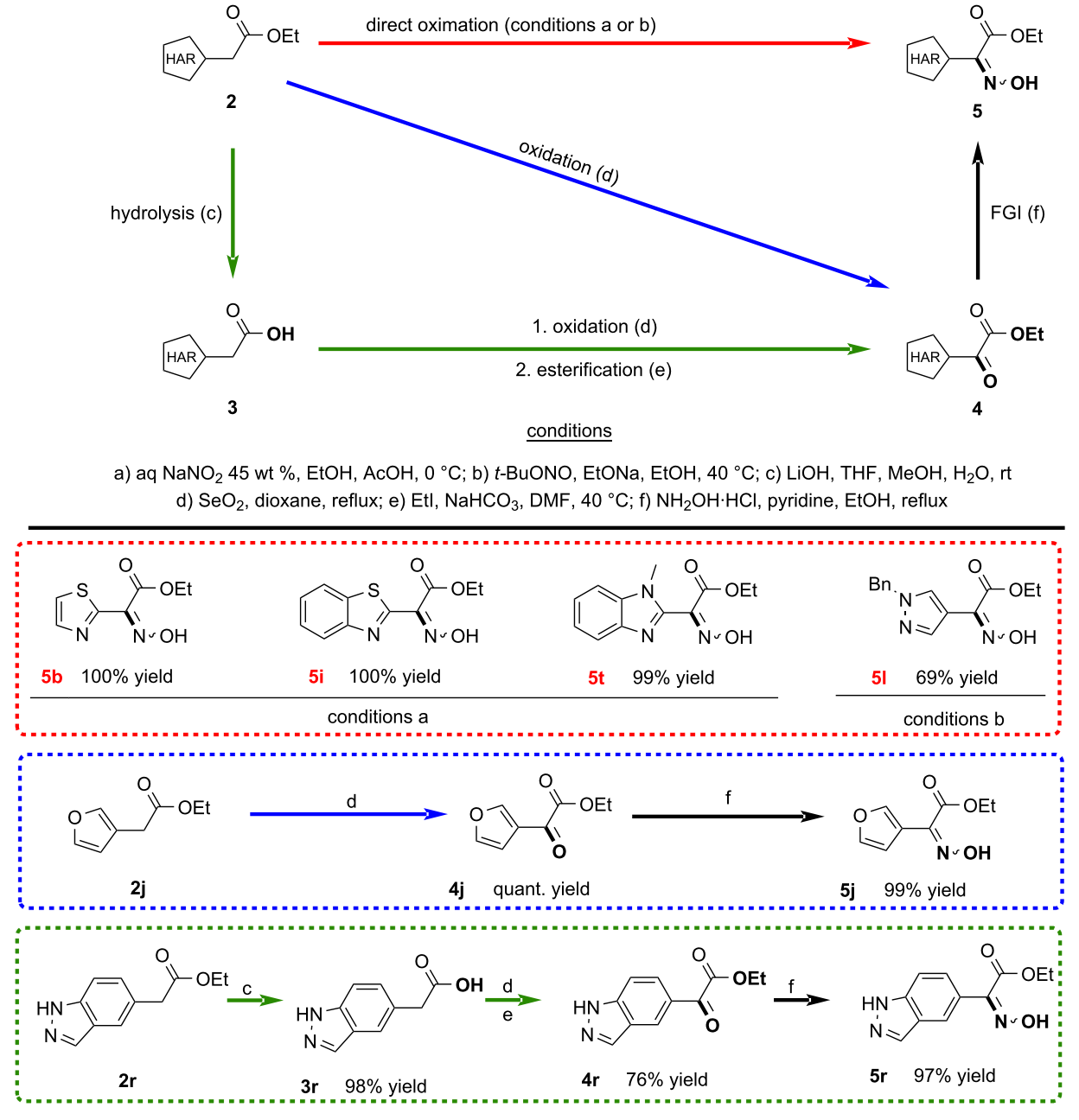

Scheme 6: Oxime group insertion step.

The Riley oxidation of the furanyl derivative **2j** proceeded smoothly yielding **4j** in quantitative yield. However, obtaining compound **4r** presented some challenges due to the resistance of ester **2r** towards conventional oxidation methods (see Table S5 in Supporting Information File 1). Consequently, a multistep process involving ester hydrolysis and subsequent re-esterification was necessary to achieve the desired ketoester.

Reduction of the oximes

Oximes are commonly reduced to the corresponding amines using either palladium on activated carbon and hydrogen gas [65-68], or with zinc and a Brønsted acid as source of hydrogen [68,69]. Both methods were tested and after a brief optimization process, zinc dust and HCl in a mixture of EtOH/dioxane proved to be the best conditions in order to maximize the yield and limit the amino ester instability issues (see Table S6 in Supporting Information File 1). By slightly adjusting the reaction time and the temperature, all oxime derivatives underwent reduction to yield the corresponding amine. The amino esters were effectively safeguarded against degradation through the immediate formation of the HCl salt or by Boc-protection. This procedure allowed us to obtain all the protected amino acids in a yield that varies from 56 to 74% (Scheme 7).

Gram scale experiment

With the optimized synthetic route, we were able to reach the final targets in good to excellent overall yields (from 25% to 64%, see Scheme 7). To test the robustness of our approach, the synthesis of compound **6i** was carried out on gram scale starting from 2.1 g of 2-bromobenzothiazole (**1i**). The gram scale production showed comparable results to those obtained in the small-scale procedure, leading to the formation of 1.8 g (67% overall yield) of the final product **6i** (Scheme 7, bottom).

On-DNA validation

Due to the large complexity of DELs, there is only limited opportunity to track the efficiency of individual reactions during library synthesis. Therefore, BBs need to pass validation before being used in library synthesis settings. For these bifunctional amino esters, we performed a three-step validation where they were first attached to carboxylic acid functionalized DNA headpiece **7a** (first reverse amidation). Next, the ester was hydrolyzed to obtain acid **9**, and finally, a second reverse amidation with aniline afforded **10**.

Both the reverse amidation and the ester hydrolysis were performed following literature protocols [70,71]. In these experiments, compounds **6b** and **6i** proved to be unstable under on-DNA conditions as they failed to form esters **8b** and **8i**. Closely related structures, such as α-aminobenzothiazol-2-ylacetic acid is known to undergo decarboxylation at room temperature [72]. Compound **8t** underwent decarboxylation during the hydrolysis step. Compounds **6j**, **6l** and **6r** passed validation in moderate to good yields (Scheme 8).

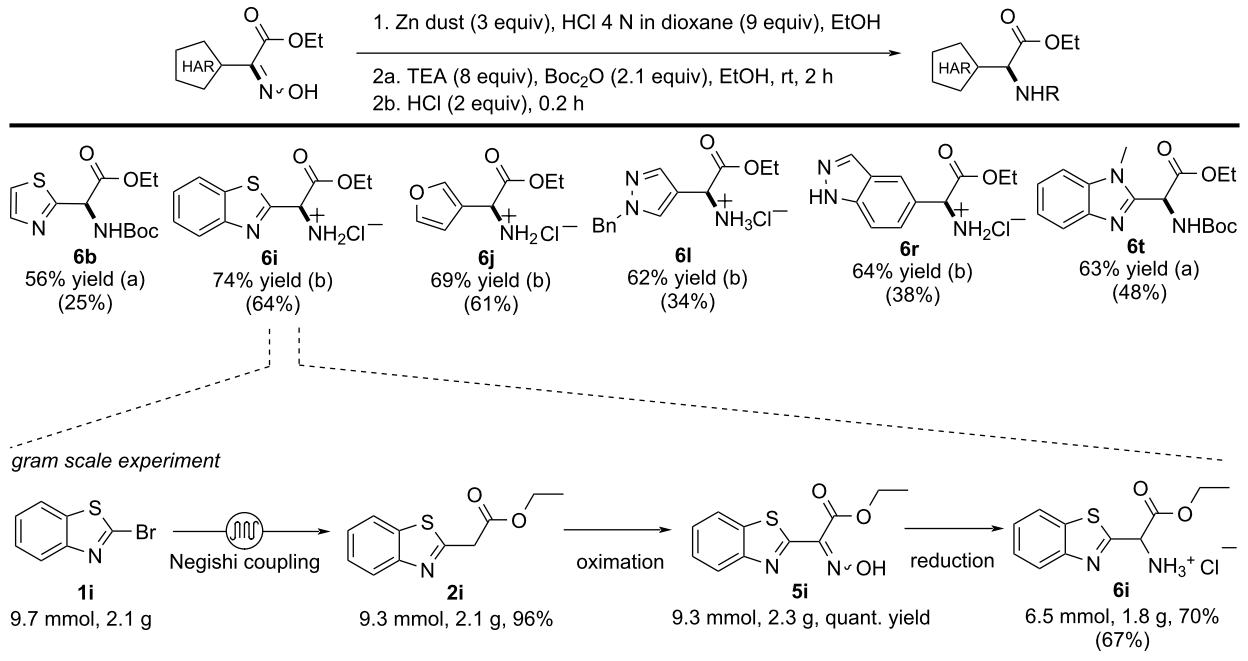

Scheme 7: Amino ester production: general scheme, scope and gram scale experiment. The numbers in brackets represent the overall yield for the synthesis of the amino esters from the Negishi coupling till the reduction/protection step.

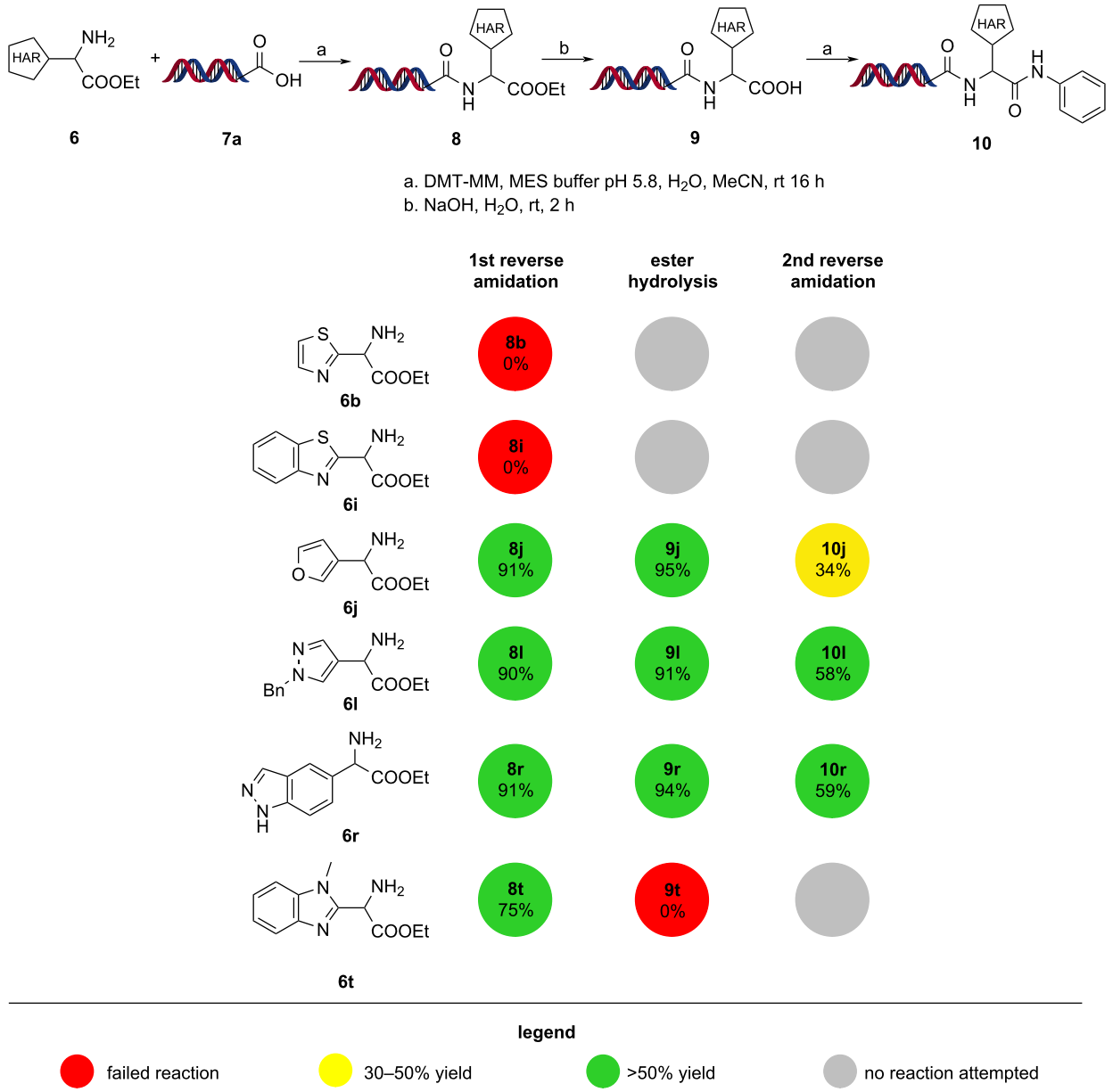

Scheme 8: Reactions scheme and results for the on-DNA experiments. The reported values represent the normalized yield for each reaction (Supporting Information File 1).

Conclusion

In conclusion, by taking advantage of the recent advances in the Negishi cross-coupling reaction we obtained a broad range of heteroarylacetates starting from heteroaromatic halides. One compound from each subclass of medicinal chemistry-relevant substrates (thiazoles, pyrazoles, etc.) was used for the preparation of α-heteroaryl-α-amino esters via the insertion of an oxime group and subsequent reduction step. The procedure relies solely on readily available and widely used reagents, rendering our approach well-suited for both industrial and academic settings. The synthesized amino esters were engaged in a three-step on-DNA validation protocol, demonstrating their possible application for DEL production.

Supporting Information

Supporting Information File 1

Experimental part and NMR spectra.
[https://www.beilstein-journals.org/bjoc/content/supplementary/1860-5397-20-168-S1.pdf]

Acknowledgements

The authors thank Dr. Attila Sveiczer and Dr. Mounir Raji for the consultations and technical support during the practical work of the project, and Dr. Veronika Papp-Kádár for the support during the on-DNA validation experiment. The authors thank Dr. Ying Zhang and Dr. Anthony Keefe for proofreading the manuscript.

Funding

M.G. thanks the European Union for funding under the PhotoReAct Project, H2020 Marie Sklodowska-Curie grant agreement No.956324 (MSCAITN: PhotoReAct).

ORCID® iDs

Matteo Gasparetto - https://orcid.org/0009-0005-9354-6559
Gellért Sipos - https://orcid.org/0000-0001-6956-9009

Data Availability Statement

All data that supports the findings of this study is available in the published article and/or the supporting information to this article.

References

1. Xia, B.; Franklin, G. J.; Lu, X.; Bedard, K. L.; Grady, L. C.; Summerfield, J. D.; Shi, E. X.; King, B. W.; Lind, K. E.; Chiu, C.; Watts, E.; Bodmer, V.; Bai, X.; Marcaurelle, L. A. *ACS Med. Chem. Lett.* **2021,** *12,* 1166–1172. doi:10.1021/acsmedchemlett.1c00156
2. Goodnow, R. A., Jr. *A Handbook for DNA-Encoded Chemistry;* John Wiley & Sons: New York, NY, USA, 2014. doi:10.1002/9781118832738
3. Favalli, N.; Bassi, G.; Scheuermann, J.; Neri, D. *FEBS Lett.* **2018,** *592,* 2168–2180. doi:10.1002/1873-3468.13068
4. Fair, R. J.; Walsh, R. T.; Hupp, C. D. *Bioorg. Med. Chem. Lett.* **2021,** *51,* 128339. doi:10.1016/j.bmcl.2021.128339
5. Fitzgerald, P. R.; Paegel, B. M. *Chem. Rev.* **2021,** *121,* 7155–7177. doi:10.1021/acs.chemrev.0c00789
6. Zhang, Y.; Clark, M. A. *Bioorg. Med. Chem.* **2021,** *41,* 116189. doi:10.1016/j.bmc.2021.116189
7. Geigle, S. N.; Petersen, A. C.; Satz, A. L. *Org. Lett.* **2019,** *21,* 9001–9004. doi:10.1021/acs.orglett.9b03406
8. Wu, G. *Amino Acids* **2009,** *37,* 1–17. doi:10.1007/s00726-009-0269-0
9. Liu, R.; Li, X.; Lam, K. S. *Curr. Opin. Chem. Biol.* **2017,** *38,* 117–126. doi:10.1016/j.cbpa.2017.03.017
10. Clark, M. A.; Acharya, R. A.; Arico-Muendel, C. C.; Belyanskaya, S. L.; Benjamin, D. R.; Carlson, N. R.; Centrella, P. A.; Chiu, C. H.; Creaser, S. P.; Cuozzo, J. W.; Davie, C. P.; Ding, Y.; Franklin, G. J.; Franzen, K. D.; Gefter, M. L.; Hale, S. P.; Hansen, N. J. V.; Israel, D. I.; Jiang, J.; Kavarana, M. J.; Kelley, M. S.; Kollmann, C. S.; Li, F.; Lind, K.; Mataruse, S.; Medeiros, P. F.; Messer, J. A.; Myers, P.; O'Keefe, H.; Oliff, M. C.; Rise, C. E.; Satz, A. L.; Skinner, S. R.; Svendsen, J. L.; Tang, L.; van Vloten, K.; Wagner, R. W.; Yao, G.; Zhao, B.; Morgan, B. A. *Nat. Chem. Biol.* **2009,** *5,* 647–654. doi:10.1038/nchembio.211
11. Strecker, A. *Justus Liebigs Ann. Chem.* **1850,** *75,* 46–51. doi:10.1002/jlac.18500750104
12. Wang, J.; Liu, X.; Feng, X. *Chem. Rev.* **2011,** *111,* 6947–6983. doi:10.1021/cr200057t
13. Mazurkiewicz, R.; Kuźnik, A.; Grymel, M.; Kuźnik, N. *Monatsh. Chem.* **2004,** *135,* 807–815. doi:10.1007/s00706-003-0167-1
14. Dai, Y.; Chen, J.; Wang, Z.; Wang, T.; Wang, L.; Yang, Y.; Qiao, X.; Fan, B. *J. Org. Chem.* **2021,** *86,* 7141–7147. doi:10.1021/acs.joc.1c00426
15. O'Donnell, M. J. *Acc. Chem. Res.* **2004,** *37,* 506–517. doi:10.1021/ar0300625
16. Maruoka, K.; Ooi, T. *Chem. Rev.* **2003,** *103,* 3013–3028. doi:10.1021/cr020020e
17. Dauzonne, D.; Royer, R. *Synthesis* **1987,** 399–401. doi:10.1055/s-1987-27962
18. Corey, E. J.; Link, J. O. *J. Am. Chem. Soc.* **1992,** *114,* 1906–1908. doi:10.1021/ja00031a069
19. Faraggi, T. M.; Rouget-Virbel, C.; Rincón, J. A.; Barberis, M.; Mateos, C.; García-Cerrada, S.; Agejas, J.; de Frutos, O.; MacMillan, D. W. C. *Org. Process Res. Dev.* **2021,** *25,* 1966–1973. doi:10.1021/acs.oprd.1c00208
20. Ni, S.; Garrido-Castro, A. F.; Merchant, R. R.; de Gruyter, J. N.; Schmitt, D. C.; Mousseau, J. J.; Gallego, G. M.; Yang, S.; Collins, M. R.; Qiao, J. X.; Yeung, K.-S.; Langley, D. R.; Poss, M. A.; Scola, P. M.; Qin, T.; Baran, P. S. *Angew. Chem.* **2018,** *130,* 14768–14773. doi:10.1002/ange.201809310
21. Curto, J. M.; Dickstein, J. S.; Berritt, S.; Kozlowski, M. C. *Org. Lett.* **2014,** *16,* 1948–1951. doi:10.1021/ol500506t
22. Bombonato, E.; Fasano, V.; Pecorari, D.; Fornasari, L.; Castagnini, F.; Marcaccio, M.; Ronchi, P. *ACS Omega* **2024,** *9,* 13081–13085. doi:10.1021/acsomega.3c09357
23. Leonard, D. J.; Ward, J. W.; Clayden, J. *Nature* **2018,** *562,* 105–109. doi:10.1038/s41586-018-0553-9
24. Bunch, L.; Krogsgaard-Larsen, P.; Madsen, U. *J. Org. Chem.* **2002,** *67,* 2375–2377. doi:10.1021/jo0162134
25. Jørgensen, C. G.; Clausen, R. P.; Hansen, K. B.; Bräuner-Osborne, H.; Nielsen, B.; Metzler, B.; Kehler, J.; Krogsgaard-Larsen, P.; Madsen, U. *Org. Biomol. Chem.* **2007,** *5,* 463–471. doi:10.1039/b615162k
26. Zhu, S.; Rueping, M. *Chem. Commun.* **2012,** *48,* 11960–11962. doi:10.1039/c2cc36995h
27. Zhu, Z.-Q.; Xiao, L.-J.; Chen, Y.; Xie, Z.-B.; Zhu, H.-B.; Le, Z.-G. *Synthesis* **2018,** *50,* 2775–2783. doi:10.1055/s-0036-1609845
28. Zhu, Z.-Q.; Xiao, L.-J.; Zhou, C.-C.; Song, H.-L.; Xie, Z.-B.; Le, Z.-G. *Tetrahedron Lett.* **2018,** *59,* 3326–3331. doi:10.1016/j.tetlet.2018.07.047
29. Ye, C.-X.; Dansby, D. R.; Chen, S.; Meggers, E. *Nat. Synth.* **2023,** *2,* 645–652. doi:10.1038/s44160-023-00267-w
30. Frühauf, A.; Behringer, M.; Meyer-Almes, F.-J. *Molecules* **2023,** *28,* 5686. doi:10.3390/molecules28155686
31. Wang, Y.-T.; Yang, P.-C.; Zhang, Y.-F.; Sun, J.-F. *Eur. J. Med. Chem.* **2024,** *265,* 116124. doi:10.1016/j.ejmech.2024.116124
32. Polêto, M. D.; Rusu, V. H.; Grisci, B. I.; Dorn, M.; Lins, R. D.; Verli, H. *Front. Pharmacol.* **2018,** *9,* 395. doi:10.3389/fphar.2018.00395
33. Gupta, K.; Sirbaiya, A. K.; Kumar, V.; Rahman, M. A. *Mini-Rev. Med. Chem.* **2022,** *22,* 1895–1935. doi:10.2174/1389557522666220217101805
34. Negishi, E.-i. *Angew. Chem., Int. Ed.* **2011,** *50,* 6738–6764. doi:10.1002/anie.201101380
35. Valente, C.; Belowich, M. E.; Hadei, N.; Organ, M. G. *Eur. J. Org. Chem.* **2010,** 4343–4354. doi:10.1002/ejoc.201000359
36. Wei, B.; Knochel, P. *Synthesis* **2022,** *54,* 246–254. doi:10.1055/a-1589-0150

37. Cossy, J., Ed. *Organozinc Derivatives and Transition Metal Catalysts: Formation of C-C Bonds by Cross-coupling;* De Gruyter: Berlin, Germany, 2023. doi:10.1515/9783110728859
38. Haas, D.; Hammann, J. M.; Greiner, R.; Knochel, P. *ACS Catal.* **2016,** *6,* 1540–1552. doi:10.1021/acscatal.5b02718
39. Muzammil; Zahoor, A. F.; Parveen, B.; Javed, S.; Akhtar, R.; Tabassum, S. *Chem. Pap.* **2024,** *78,* 3399–3430. doi:10.1007/s11696-024-03369-7
40. Abdiaj, I.; Cañellas, S.; Dieguez, A.; Linares, M. L.; Pijper, B.; Fontana, A.; Rodriguez, R.; Trabanco, A.; Palao, E.; Alcázar, J. *J. Med. Chem.* **2023,** *66,* 716–732. doi:10.1021/acs.jmedchem.2c01646
41. Abdiaj, I.; Fontana, A.; Gomez, M. V.; de la Hoz, A.; Alcázar, J. *Angew. Chem., Int. Ed.* **2018,** *57,* 8473–8477. doi:10.1002/anie.201802656
42. Alonso, N.; Miller, L. Z.; Muñoz, J. d. M.; Alcázar, J.; McQuade, D. T. *Adv. Synth. Catal.* **2014,** *356,* 3737–3741. doi:10.1002/adsc.201400243
43. Abdiaj, I.; Huck, L.; Mateo, J. M.; de la Hoz, A.; Gomez, M. V.; Díaz-Ortiz, A.; Alcázar, J. *Angew. Chem., Int. Ed.* **2018,** *57,* 13231–13236. doi:10.1002/anie.201808654
44. Berton, M.; Huck, L.; Alcázar, J. *Nat. Protoc.* **2018,** *13,* 324–334. doi:10.1038/nprot.2017.141
45. PhotoCube - ThalesNano. https://thalesnano.com/products-and-services/photocube/ (accessed May 29, 2024).
46. Capaldo, L.; Wen, Z.; Noël, T. *Chem. Sci.* **2023,** *14,* 4230–4247. doi:10.1039/d3sc00992k
47. Vázquez-Amaya, L. Y.; Coppola, G. A.; Van der Eycken, E. V.; Sharma, U. K. *J. Flow Chem.* **2024,** *14,* 257–279. doi:10.1007/s41981-024-00312-5
48. Zondag, S. D. A.; Mazzarella, D.; Noël, T. *Annu. Rev. Chem. Biomol. Eng.* **2023,** *14,* 283–300. doi:10.1146/annurev-chembioeng-101121-074313
49. Buglioni, L.; Raymenants, F.; Slattery, A.; Zondag, S. D. A.; Noël, T. *Chem. Rev.* **2022,** *122,* 2752–2906. doi:10.1021/acs.chemrev.1c00332
50. Wei, X.-J.; Abdiaj, I.; Sambiagio, C.; Li, C.; Zysman-Colman, E.; Alcázar, J.; Noël, T. *Angew. Chem.* **2019,** *131,* 13164–13168. doi:10.1002/ange.201906462
51. Bonciolini, S.; Pulcinella, A.; Leone, M.; Schiroli, D.; Ruiz, A. L.; Sorato, A.; Dubois, M. A. J.; Gopalakrishnan, R.; Masson, G.; Della Ca', N.; Protti, S.; Fagnoni, M.; Zysman-Colman, E.; Johansson, M.; Noël, T. *Nat. Commun.* **2024,** *15,* 1509. doi:10.1038/s41467-024-45804-z
52. Feng, M.; Tinelli, R.; Meyrelles, R.; González, L.; Maryasin, B.; Maulide, N. *Angew. Chem., Int. Ed.* **2023,** *62,* e202212399. doi:10.1002/anie.202212399
53. Cecere, G.; König, C. M.; Alleva, J. L.; MacMillan, D. W. C. *J. Am. Chem. Soc.* **2013,** *135,* 11521–11524. doi:10.1021/ja406181e
54. Liu, Y.; Zhang, Z.; Ran, F.; Guo, K.; Chen, X.; Zhao, G. *Bioorg. Chem.* **2020,** *97,* 103671. doi:10.1016/j.bioorg.2020.103671
55. Laufer, R.; Ng, G.; Liu, Y.; Patel, N. K. B.; Edwards, L. G.; Lang, Y.; Li, S.-W.; Feher, M.; Awrey, D. E.; Leung, G.; Beletskaya, I.; Plotnikova, O.; Mason, J. M.; Hodgson, R.; Wei, X.; Mao, G.; Luo, X.; Huang, P.; Green, E.; Kiarash, R.; Lin, D. C.-C.; Harris-Brandts, M.; Ban, F.; Nadeem, V.; Mak, T. W.; Pan, G. J.; Qiu, W.; Chirgadze, N. Y.; Pauls, H. W. *Bioorg. Med. Chem.* **2014,** *22,* 4968–4997. doi:10.1016/j.bmc.2014.06.027
56. Lopchuk, J. M.; Hughes, R. P.; Gribble, G. W. *Org. Lett.* **2013,** *15,* 5218–5221. doi:10.1021/ol402385v
57. Cantillo, D.; de Frutos, O.; Rincon, J. A.; Mateos, C.; Kappe, C. O. *J. Org. Chem.* **2014,** *79,* 223–229. doi:10.1021/jo402409k
58. Saito, T.; Saheki, N.; Hatanaka, M.; Ishimaru, T. *J. Heterocycl. Chem.* **1983,** *20,* 73–75. doi:10.1002/jhet.5570200117
59. Zhang, Q.; Zhao, C.; Zhang, X.; He, C.; Pang, S. *New J. Chem.* **2022,** *46,* 1489–1493. doi:10.1039/d1nj05510k
60. Hrib, N. J.; Jurcak, J. G.; Burgher, K. L.; Conway, P. G.; Hartman, H. B.; Kerman, L. L.; Roehr, J. E.; Woods, A. T. *J. Med. Chem.* **1994,** *37,* 2308–2314. doi:10.1021/jm00041a009
61. Baruah, P. K.; Dinsmore, J.; King, A. M.; Salomé, C.; De Ryck, M.; Kaminski, R.; Provins, L.; Kohn, H. *Bioorg. Med. Chem.* **2012,** *20,* 3551–3564. doi:10.1016/j.bmc.2012.04.002
62. Desmarchelier, A.; Ortiz, P.; Harutyunyan, S. R. *Chem. Commun.* **2015,** *51,* 703–706. doi:10.1039/c4cc06719c
63. Angeles-Dunham, V. V.; Nickerson, D. M.; Ray, D. M.; Mattson, A. E. *Angew. Chem., Int. Ed.* **2014,** *53,* 14538–14541. doi:10.1002/anie.201408613
64. Ramalingan, C.; Park, Y.-T. *J. Org. Chem.* **2007,** *72,* 4536–4538. doi:10.1021/jo070297k
65. Paine, J. B., III; Brough, J. R.; Buller, K. K.; Erikson, E. E. *J. Org. Chem.* **1987,** *52,* 3986–3993. doi:10.1021/jo00227a009
66. Jnaneshwara, G. K.; Sudalai, A.; Deshpande, V. H. *J. Chem. Res., Synop.* **1998,** 160–161. doi:10.1039/a705957d
67. Garg, N. K.; Sarpong, R.; Stoltz, B. M. *J. Am. Chem. Soc.* **2002,** *124,* 13179–13184. doi:10.1021/ja027822b
68. Günther, M.; Lategahn, J.; Juchum, M.; Döring, E.; Keul, M.; Engel, J.; Tumbrink, H. L.; Rauh, D.; Laufer, S. *J. Med. Chem.* **2017,** *60,* 5613–5637. doi:10.1021/acs.jmedchem.7b00316
69. Coutant, E. P.; Hervin, V.; Gagnot, G.; Ford, C.; Baatallah, R.; Janin, Y. L. *Beilstein J. Org. Chem.* **2018,** *14,* 2853–2860. doi:10.3762/bjoc.14.264
70. Du, H.-C.; Simmons, N.; Faver, J. C.; Yu, Z.; Palaniappan, M.; Riehle, K.; Matzuk, M. M. *Org. Lett.* **2019,** *21,* 2194–2199. doi:10.1021/acs.orglett.9b00497
71. Satz, A. L.; Cai, J.; Chen, Y.; Goodnow, R.; Gruber, F.; Kowalczyk, A.; Petersen, A.; Naderi-Oboodi, G.; Orzechowski, L.; Strebel, Q. *Bioconjugate Chem.* **2015,** *26,* 1623–1632. doi:10.1021/acs.bioconjchem.5b00239
72. Baudet, P.; Otten, C. *Helv. Chim. Acta* **1970,** *53,* 1683–1693. doi:10.1002/hlca.19700530715

BEILSTEIN JOURNAL OF ORGANIC CHEMISTRY

Development of a flow photochemical process for a π-Lewis acidic metal-catalyzed cyclization/radical addition sequence: in situ-generated 2-benzopyrylium as photoredox catalyst and reactive intermediate

Masahiro Terada*[1], Zen Iwasaki[1], Ryohei Yazaki[1], Shigenobu Umemiya[1] and Jun Kikuchi[1,2]

Full Research Paper

Open Access

Address:
[1]Department of Chemistry, Graduate School of Science, Tohoku University, Aoba-ku, Sendai 980-8578, Japan and [2]Graduate School of Pharmaceutical Science, Tohoku University, Aoba-ku, Sendai 980-8578, Japan

Email:
Masahiro Terada* - mterada@tohoku.ac.jp

* Corresponding author

Keywords:
2-benzopyrylium; flow chemistry; isocromene; photochemical reaction; π-Lewis acidic metal

Beilstein J. Org. Chem. **2024,** *20,* 1973–1980.
https://doi.org/10.3762/bjoc.20.173

Received: 27 March 2024
Accepted: 30 July 2024
Published: 13 August 2024

This article is part of the thematic issue "Photocatalysis and photochemistry in organic synthesis".

Guest Editor: T. Noël

Abstract

A flow photochemical reaction system for a π-Lewis acidic metal-catalyzed cyclization/radical addition sequence was developed, which utilizes in situ-generated 2-benzopyrylium intermediates as the photoredox catalyst and electrophilic substrates. The key 2-benzopyrylium intermediates were generated in the flow reaction system through the intramolecular cyclization of *ortho*-carbonyl alkynylbenzene derivatives by the π-Lewis acidic metal catalyst $AgNTf_2$ and the subsequent proto-demetalation with trifluoroacetic acid. The 2-benzopyrylium intermediates underwent further photoreactions with benzyltrimethylsilane derivatives as the donor molecule in the flow photoreactor to provide 1*H*-isochromene derivatives in higher yields in most cases than the batch reaction system.

Introduction

Flow chemistry has been actively studied in recent years as a method to run a reaction continuously using a flow path or tube, rather than in a flask [1-16]. This method has attracted much attention because, unlike a batch reaction system, it allows for rapid generation of unstable chemical species by controlling parameters such as flow velocity and mixing properties, and in some cases makes it possible to achieve reactions that are difficult to perform using batch chemistry [17-21]. In general, efficient two-phase mixing and heat transfer, as well as ease of scale-up, are the advantages of using a flow system. In addition, reproducibility in a liquid–liquid flow system is improved because the flow velocity and temperature can be precisely con-

trolled by using a syringe pump and a temperature control unit, respectively. Moreover, as the reaction mixture continues to flow and the reaction can be quenched immediately when necessary, the decomposition of an unstable product under the reaction conditions can be avoided [22-25]. Furthermore, when a photoreaction is performed in a flow system, there is an advantage that the light irradiation efficiency [26-29] is increased. Thus, the flow photochemical process is crucial and beneficial to product formation.

Recently, we reported a sequential transformation consisting of a π-Lewis acidic metal-catalyzed cyclization [30-45] and subsequent photochemical radical addition [46-54], which affords 1*H*-isochromene derivatives **3** through three catalytic cycles (Scheme 1a) [55]: catalytic cycles I and II and a photoredox cycle of the photocatalyst [56,57] (see Supporting Information File 1 for the overall catalytic cycles). In catalytic cycle I, the key cationic components, 2-benzopyrylium intermediates **A**, are generated in situ by the activation of the alkyne moiety of *ortho*-carbonyl alkynylbenzene derivatives **1** in the presence of the π-Lewis acidic metal catalyst [M]X [$AgNTf_2$ or $Cu(NTf_2)_2$] and subsequent intramolecular cyclization followed by protodemetalation with trifluoroacetic acid (TFA). In catalytic cycle II, photoexcitation of the generated 2-benzopyrylium intermediates **A** under light irradiation facilitates single-electron transfer (SET) from benzyltrimethylsilane derivatives **2** as the donor molecule, initiating further radical reactions through the formation of radical cations **B**. Nucleophilic arylmethyl radicals **C**, which are generated from radical cations **B** by desilylation, undergo an addition reaction with 2-benzopyrylium intermediates **A**, giving rise to the corresponding radical cation. Catalytic cycle II is completed through a SET from **D**, a reduced form of the photoredox catalyst 2-benzopyrylium intermediates **A**, to the generated radical cation, affording 1*H*-isochromene derivatives **3**. The photoredox cycle is also completed with the regeneration of cations **A** through SET from **D**.

The most distinctive feature of this sequential transformation is that the in situ-generated 2-benzopyrylium intermediates **A** are used not only as an electrophile but also as a photoredox catalyst. However, as this reaction is carried out under relatively harsh conditions (i.e., light irradiation, use of an excess amount of TFA), the stability of products **3** was a concern. Indeed, subjecting product **3a** to the optimal reaction conditions with either $AgNTf_2$ or $Cu(NTf_2)_2$ resulted in the significant degradation of **3a**, although the degradation of **3a** was partially suppressed when $AgNTf_2$ was used (Scheme 1b). Accordingly, we envisioned that the characteristics of the flow photochemical process, i.e., efficient light irradiation and immediate separation of the formed product from the reaction system, would be suitable for this sequential reaction. Here, we report the results of our investigation on the use of a flow photochemical reaction system to improve the yield of the present sequential transformation.

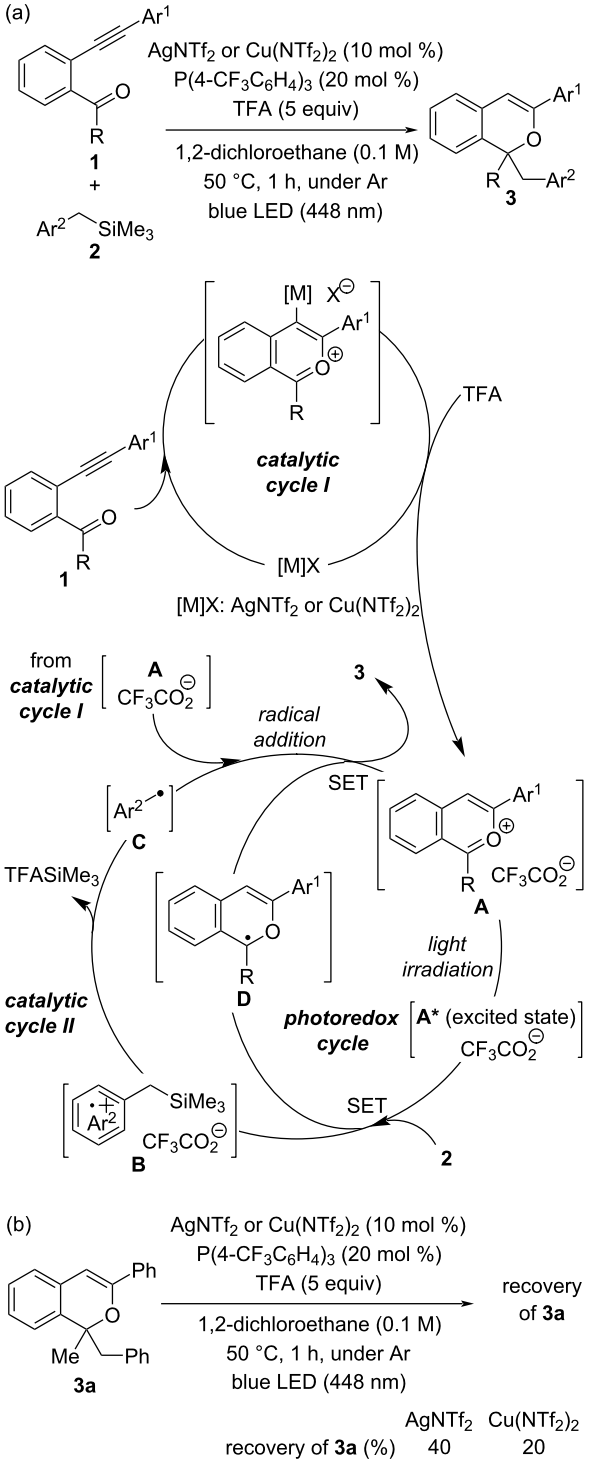

Scheme 1: (a) Sequential π-Lewis acidic metal-catalyzed cyclization/photochemical radical addition for the formation of 1*H*-isochromene derivatives **3** and its plausible catalytic cycles. (b) Stability of **3a** under the optimal reaction conditions of the batch reaction.

Results and Discussion

At the outset of our studies to optimize the flow reaction conditions, we employed $AgNTf_2$ as the π-Lewis acidic metal catalyst because of its high solubility in 1,2-dichloroethane (1,2-DCE) [58] and ability to partially suppress the degradation of the product formed (Scheme 1b). When designing a flow reaction system for the present sequential transformation, we considered the fact that the transformation involves three catalytic cycles. In particular, given that catalytic cycle I (see Scheme 1a) generates, e.g., key cationic components, 2-benzopyrylium intermediates **A** without light irradiation, it is necessary to ensure that the reaction time of catalytic cycle I is not affected by the timescale of the flow reaction. Therefore, we adopted a dual syringe system in which two solutions are mixed before being introduced into the photoreactor (volume: 1.0 mL) (Table 1, top right). After several trials, we decided to fill syringe A with *o*-alkynylacetophenone **1a** and syringe B with $AgNTf_2$, $P(4\text{-}CF_3C_6H_4)_3$, benzyltrimethylsilane (**2a**, TMSBn), and TFA (see Supporting Information File 1 for details). At this time, the volumes of the solutions placed in the two syringes were adjusted to be approximately the same. The initial conditions of the flow reaction were based on those of the batch reaction [0.1 mmol of **1a**, 10 μmol (10 mol %) of $AgNTf_2$, 20 μmol (20 mol %) of $P(4\text{-}CF_3C_6H_4)_3$, 1.0 mmol (10 equiv) of **2a**, and 0.5 mmol (5 equiv) of TFA under light irradiation (blue LED: λ_{max} = 448 nm) at 50 °C for 1 h in 1 mL (total volume) of 1,2-DCE] [55] with a flow rate of 3 mL/h (light irradiation time: 20 min in the flow reaction, 1 h in the batch reaction). As shown in Table 1, product **3a** was obtained in moderate yield (entry 1: 42%, cf. batch reaction: 76%). Lowering the reaction temperature to 25 °C reduced the yield (Table 1, entry 2: 35%), but decreasing the amount of the phosphine ligand from 20 mol % to 5 mol % markedly improved the yield (Table 1, entry 3: 53%). Even when the flow rate was increased from 3 mL/h to 24 mL/h (light irradiation time was shortened from 20 min to 2.5 min), the yield of **3a** was maintained (Table 1, entry 4: 53%). Under these conditions, no improvement in yield was observed when the premixing zone (0.7 mL) was provided

Table 1: Screening of reaction conditions in the flow reaction system[a].

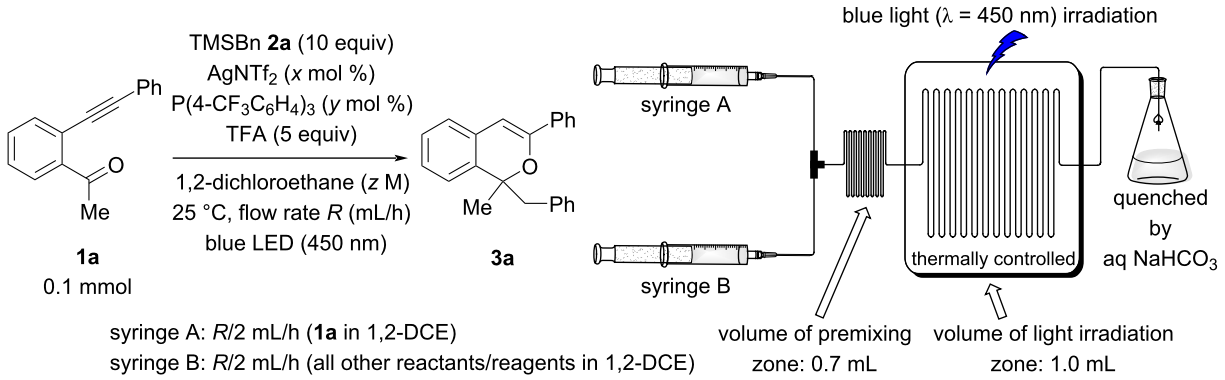

Entry	$AgNTf_2$ (*x* mol %)	$P(4\text{-}CF_3C_6H_4)_3$ (*y* mol %)	Conc. of **1a** (*z* M)	Flow rate (*R* mL/h)	Premixing zone (mL)	Yield of **3a** (%)[b]	Recovery of **1a** (%)[b]
1[c]	10	20	0.1	3	none	42	0
2	10	20	0.1	3	none	35	22
3	10	5	0.1	3	none	53	1
4	10	5	0.1	24	none	53	0
5	10	5	0.1	24	0.7	52	9
6	5	2.5	0.1	24	none	26	14
7	5	2.5	0.1	24	0.7	49	0
8	5	2.5	0.05	24	0.7	61	0
9	2	1	0.05	24	0.7	28	28
10[d]	5	2.5	0.05	24	0.7	77	0

[a]Unless otherwise noted, all reactions were carried out in a flow photochemical reactor (volume: 1.0 mL, λ_{max} = 450 nm) using a dual syringe system, as shown in the table scheme. Syringe A: 0.1 mmol of **1a** in 1,2-DCE (0.55 mL). Syringe B: $AgNTf_2$, $P(4\text{-}CF_3C_6H_4)_3$, TMSBn (**2a**), and TFA in 1,2-DCE (0.45 mL); [b]Yield was determined by NMR analysis using 1,1,2,2-tetrabromoethane as an internal standard; [c]At 50 °C. [d]Reaction was conducted on a 0.5 mmol scale. Syringe A: 0.5 mmol of **1a** in 1,2-DCE (5.4 mL). Syringe B: 25 μmol (5 mol %) of $AgNTf_2$, 12.5 μmol (2.5 mol %) of $P(4\text{-}CF_3C_6H_4)_3$, 5 mmol (10 equiv) of TMSBn (**2a**), and 2.5 mmol (5 equiv) of TFA in 1,2-DCE (4.6 mL).

(Table 1, entry 5: 52%); however, the effect of adding the premixing zone was remarkable when the amount of $AgNTf_2$ was reduced by half (5 mol %; Table 1, entry 6 vs entry 7: 26% vs 49%). These results suggest that the generation of 2-benzopyrylium intermediates **A**, (i.e., catalytic cycle I) requires a certain reaction time (at this flow rate: ca. 2 min). Moreover, the yield of **3a** was improved when the concentration of **1a** was lowered from 0.1 M to 0.05 M (Table 1, entry 8: 61%). Meanwhile, further reducing the catalyst loading from 5 mol % to 2 mol % resulted in a significant decrease in yield (Table 1, entry 9: 28%). When the reaction was scaled up from 0.1 mmol to 0.5 mmol of **1a** in consideration of the dead volume of the flow reactor, the product **3a** was obtained in markedly improved yield (Table 1, entry 10: 77%) [59] which was comparable to that of the batch reaction (76%). Notably, however, the present flow reaction was performed at 25 °C (batch: 50 °C) with half the amount of $AgNTf_2$ (flow: 5 mol %, batch: 10 mol %), and the light irradiation time was shortened to only 2.5 minutes (batch: 1 h). Thus, under the optimal conditions (Table 1, entry 10), the flow reaction system proved extremely useful for improving the efficiency of the present photochemical sequential transformation.

With the optimal flow reaction conditions in hand, we next investigated the scope of substrates **1** by introducing a series of substituents to the terminal phenyl group. The results of the batch reaction system are also shown for comparison in Table 2 (right-hand side) [55]. As expected, the use of the flow reaction system significantly increased yields, although the yields obtained in the reactions of substrates having an electron-donating methoxy group were low to moderate regardless of the substitution pattern (Table 2, entries 1, 2, and 6). Indeed, when a methoxy group was introduced at the *para*-position, product **3b** was obtained in low yield (Table 2, entry 1: 14%). Because this yield was lower than that obtained in the batch reaction (48%), the flow reaction conditions for **1b** were thoroughly reconsidered (see Supporting Information File 1 for details). As a result, extending the premixing time and the light irradiation time

Table 2: Scope of substrates[a].

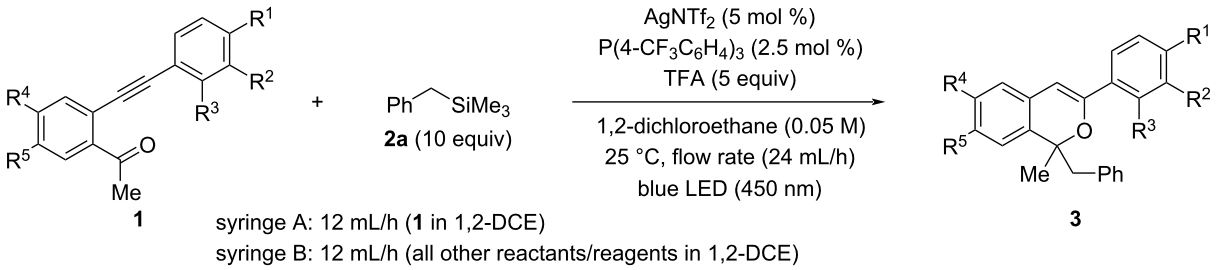

Entry	1	R^1	R^2	R^3	R^4	R^5	3	Yield of 3 (%)[b]	Batch reaction using $AgNTf_2$. Yield of 3 (%)[b,c]
1	**1b**	MeO	H	H	H	H	**3b**	14	48[d]
2[e]	**1b**						**3b**	54	
3	**1c**	Me	H	H	H	H	**3c**	76	21
4	**1d**	Br	H	H	H	H	**3d**	57	10
5	**1e**	CF_3	H	H	H	H	**3e**	77	65
6	**1f**	H	MeO	H	H	H	**3f**	39	40
7	**1g**	H	Me	H	H	H	**3g**	75	50
8	**1h**	H	Br	H	H	H	**3h**	68	63
9	**1i**	H	CF_3	H	H	H	**3i**	65	42
10	**1j**	H	H	Me	H	H	**3j**	76	72
11	**1k**	H	H	H	F	H	**3k**	79	–
12	**1l**	H	H	H	H	F	**3l**	75	–

[a]Unless otherwise noted, all reactions were carried out in the flow photochemical reactor (volume: 1.0 mL, λ_{max} = 450 nm) having a 0.7 mL premixing zone using a dual syringe system with a flow rate of 24 mL/h (12 mL/h for each syringe) at 25 °C. Syringe A: 0.5 mmol of **1** in 1,2-DCE (5.4 mL). Syringe B: 25 μmol (5 mol %) of $AgNTf_2$, 12.5 μmol (2.5 mol %) of $P(4\text{-}CF_3C_6H_4)_3$, 5 mmol (10 equiv) of TMSBn (**2a**), and 2.5 mmol (5 equiv) of TFA in 1,2-DCE (4.6 mL). [b]Yield was determined by NMR analysis using 1,1,2,2-tetrabromoethane as an internal standard. Substrates **1** were not recovered in all cases. All products **3** were isolated before structural assignment. [c]Batch reaction conditions (see ref. [55]): Unless otherwise noted, all reactions were carried out using blue LED (λ_{max} = 448 nm), 0.1 mmol of **1**, 1.0 mmol (10 equiv) of TMSBn (**2a**), 10 μmol (10 mol %) of $AgNTf_2$, 20 μmol (20 mol %) of $P(4\text{-}CF_3C_6H_4)_3$, and 5 equiv of TFA in 1,2-DCE (1.0 mL: 0.1 M of **1**) at 50 °C for 1 h. [d]At 0 °C for 6 h. [e]The flow photochemical reactor having a 1.1 mL premixing zone using a dual syringe system with a flow rate of 6 mL/h (3 mL/h for each syringe).

(Table 2, entry 2) led to an improved yield; the obtained yield was higher than that of the batch reaction system even when half the amount of $AgNTf_2$ was used with the temperature reduced to 25 °C (flow: 54% vs batch: 48%). Meanwhile, the reaction of substrate **1c** having a methyl group as a weak electron-donating group at the *para*-position afforded product **3c** in high yield (Table 2, entry 3: 76%). In addition, the reaction of **1d** having a bromo group resulted in a moderate yield, but with a significant improvement compared with the batch reaction (Table 2, entry 4: 57% vs 10%). The reaction of **1e** substituted with a strong electron-withdrawing trifluoromethyl group afforded the product **3e** in high yield (Table 2, entry 5: 77%), again confirming the high efficiency of the flow reaction system (batch: 54%). Next, the effects of the substituent at the *meta*-position were investigated. Substrate **1f** having a methoxy group afforded compound **3f** in only moderate yield (Table 2, entry 6: 39%), similar to the batch reaction (40%). The reactions of substrates having a methyl, bromo, or trifluoromethyl group gave the corresponding products **3g**–**i**, respectively, in good yields (Table 2, entries 7–9). The *ortho*-methyl-substituted substrate **1j** was also compatible, affording product **3j** in good yield (Table 2, entry 10: 76%). This yield was comparable to that of the substrate having a methyl group at the *para*- or *meta*-position, despite the steric hindrance of the *ortho*-substituent (Table 2, entry 10 vs entries 3 and 7). When a fluoro group was introduced to the tethering phenyl backbone, a high yield was obtained regardless of whether it was introduced at the 6- or 7-position (Table 2, entries 11 and 12).

Next, the effects of a carbonyl substituent, instead of a methyl ketone substituent, were investigated (Table 3). First, the reaction was performed with phenyl ketone **1m**, but product **3m** was obtained in low yield (Table 3, entry 1: 7%). This yield was lower than that obtained in the batch reaction (30%), and because 28% of **1m** were recovered, the flow reaction conditions were further examined (see Supporting Information File 1 for details). Although the yield of **3m** was improved to 19% (Table 3, entry 2) by increasing the temperature of the premixing zone from room temperature to 50 °C and reducing the flow rate from 24 mL/h to 6 mL/h (light irradiation time was extended from 2.5 min to 10 min), it did not exceed the yield of the batch reaction. In contrast, aldehyde **1n** having a simple phenyl group gave product **3n** in good yield (Table 3, entry 3: 72%). Because the yield of this flow reaction was better than that of the batch reaction (65%), the reactions of aldehydes with a series of substituents introduced to the terminal phenyl group were further investigated (Table 3, entries 4–7). Aldehydes having an electron-donating methyl group and an electron-with-

Table 3: Sequential transformation of phenyl ketone **1m** and aldehydes **1n**–**r**[a].

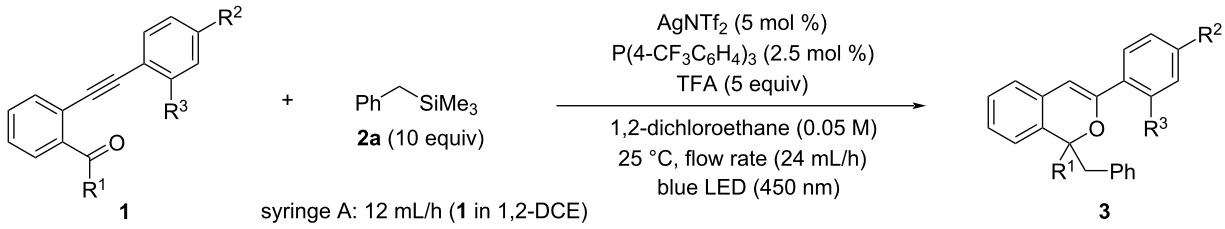

Entry	**1**	R^1	R^2	R^3	**3**	Yield of **3** (%)[b]	Recovery of **1** (%)[b]	Batch reaction using $AgNTf_2$. Yield of **3** (%)[c]
1	**1m**	Ph	H	H	**3m**	7	29	30
2[d,e]	**1m**				**3m**	19	0	
3	**1n**	H	H	H	**3n**	72	0	65[f]
4	**1o**	H	Me	H	**3o**	82	5	–
5	**1p**	H	Br	H	**3p**	75	0	34[f]
6	**1q**	H	CF_3	H	**3q**	63	18	–
7[e]	**1r**	H	H	Me	**3r**	73	8	–

[a]Unless otherwise noted, all reactions were carried out in the flow photochemical reactor (volume: 1.0 mL, λ_{max} = 450 nm) having a 0.7 mL premixing zone using a dual syringe system with a flow rate of 24 mL/h (12 mL/h for each syringe) at 25 °C. Syringe A: 0.5 mmol of **1** in 1,2-DCE (5.4 mL). Syringe B: 25 μmol (5 mol %) of $AgNTf_2$, 12.5 μmol (2.5 mol %) of $P(4\text{-}CF_3C_6H_4)_3$, 5 mmol (10 equiv) of TMSBn (**2a**), and 2.5 mmol (5 equiv) of TFA in 1,2-DCE (4.6 mL). [b]Yield was determined by NMR analysis using 1,1,2,2-tetrabromoethane as an internal standard. All products **3** were isolated before structural assignment. [c]Batch reaction conditions: unless otherwise noted, reactions were carried out using 0.1 mmol of **1**, 1.0 mmol (10 equiv) of TMSBn (**2a**), 10 μmol (10 mol %) of $AgNTf_2$, 20 μmol (20 mol %) of $P(4\text{-}CF_3C_6H_4)_3$, and 5 equiv of TFA in 1,2-DCE (1 mL: 0.1 M of **1**) at 50 °C for 1 h. [d]The flow photochemical reactor having a 0.5 mL premixing zone using a dual syringe system with a flow rate of 6 mL/h (3 mL/h for each syringe). [e]The temperature of the premixing zone was increased to 50 °C. [f]The reaction was performed using 0.05 M of **1** and 2.5 equiv of TFA for 2 h.

drawing bromo group at the *para*-position of the phenyl moiety gave products **3o** and **3p**, respectively, in high yields (Table 3, entries 4 and 5). The aldehyde **1q** bearing a strong electron-withdrawing trifluoromethyl group at the *para*-position gave product **3q** in moderate yield (Table 3, entry 6: 63%), with the recovery of substrate **1q** (18%). The reaction of *ortho*-methyl-substituted aldehyde **1r** afforded the product **3r** in high yield when the temperature of the premixing zone was increased to 50 °C (Table 3, entry 7: 73%).

The scope of donor molecules **2b** and **2c** having an electron-withdrawing trifluoromethyl group and an electron-donating methoxy group [60,61] at the *para*-position of the benzyltrimethylsilane, respectively, was also investigated in the present flow reaction system (Scheme 2). As expected, the flow reaction of **2b** having a trifluoromethyl group afforded product **3s** in higher yield (50%) than that of the batch reaction (18%) under the optimal reaction conditions. In contrast, in the flow reaction of **2c** having a methoxy group, product **3t** was obtained in a markedly lower yield (32%) than that of the batch reaction (54%). However, extending the light irradiation time by reducing the flow rate from 24 mL/h to 6 mL/h (light irradiation time: 24 mL/h = 2.5 min, 6 mL/h = 10 min) significantly improved the yield of **3t** (78%), presumably because of the retardation of the desilylation process (from **B** to **C** in Scheme 1a).

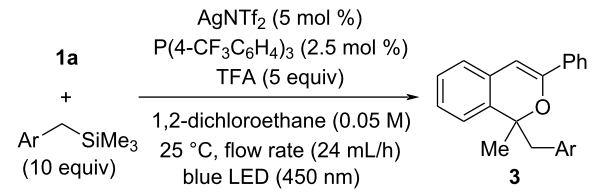

2b: Ar = 4-$CF_3C_6H_4$-
2c: Ar = 4-$MeOC_6H_4$-

syringe A: 12 mL/h (**1a** in 1,2-DCE)
syringe B: 12 mL/h (all other reactants/reagents in 1,2-DCE)

	yield of **3** (%)	flow reaction	cf. batch reaction (ref. [55])
3s: Ar = 4-$CF_3C_6H_4$-	50		18
3t: Ar = 4-$MeOC_6H_4$-	32 (78)[a]		54

Scheme 2: The reaction with benzyltrimethylsilane derivatives **2**.
[a]Flow rate was 6 mL/h and premixing zone was 0.2 mL.

Conclusion

We have demonstrated a flow reaction system for a π-Lewis acidic metal-catalyzed cyclization/photochemical radical addition sequence, affording, in most cases, the 1*H*-isochromene derivatives in higher yields than the batch reaction system, even with the amount of the π-Lewis acidic metal catalyst reduced by half. In the present sequential transformation, the key cationic species, 2-benzopyrylium intermediates, were generated in situ through the $AgNTf_2$-catalyzed intramolecular cyclization of *ortho*-carbonyl alkynylbenzene derivatives and subsequent proto-demetalation with TFA. Further photoreactions of 2-benzopyrylium intermediates with benzyltrimethylsilane derivatives as the donor molecule were conducted in the flow photoreactor. We confirmed that the flow reaction system is an excellent method for improving the efficiency of the present sequential transformation, avoiding product degradation under photochemical reaction conditions. Further investigation of other flow photochemical reactions using in situ-generated organic cations is in progress in our laboratory.

Supporting Information

Supporting Information File 1

The exploratory investigation, experimental procedures, and characterization data.
[https://www.beilstein-journals.org/bjoc/content/supplementary/1860-5397-20-173-S1.pdf]

Supporting Information File 2

Copies of NMR spectra.
[https://www.beilstein-journals.org/bjoc/content/supplementary/1860-5397-20-173-S2.pdf]

Funding

This work was partially supported by a Grant-in-Aid for Scientific Research on Innovative Areas “Hybrid Catalysis for Enabling Molecular Synthesis on Demand” (JP17H06447) and a Grant-in-Aid for Transformative Research Areas (A) “Green Catalysis Science for Renovating Transformation of Carbon-Based Resources” (JP23H04908) from MEXT, Japan and a Grant-in-Aid for Young Scientists (JP19K15552) from JSPS.

Author Contributions

Masahiro Terada: conceptualization; funding acquisition; methodology; project administration; resources; supervision; visualization; writing – original draft; writing – review & editing. Zen Iwasaki: data curation; formal analysis; investigation; validation; visualization. Ryohei Yazaki: data curation; formal analysis; investigation. Shigenobu Umemiya: data curation; formal analysis; investigation; methodology; supervision; writing – review & editing. Jun Kikuchi: conceptualization; funding acquisition; investigation; methodology; project administration; supervision; visualization; writing – review & editing.

ORCID® iDs

Masahiro Terada - https://orcid.org/0000-0002-0554-8652
Shigenobu Umemiya - https://orcid.org/0000-0002-1793-856X
Jun Kikuchi - https://orcid.org/0000-0001-9892-8832

Data Availability Statement

All data that supports the findings of this study is available in the published article and/or the supporting information to this article.

References

1. Ehrfeld, W.; Hessel, V.; Löwe, H. *Microreactors;* Wiley-VCH: Weinheim, Germany, 2000. doi:10.1002/3527601953
2. Yoshida, J. *Basics of Flow Microreactor Synthesis;* Springer: Tokyo, Japan, 2015. doi:10.1007/978-4-431-55513-1
3. Noël, T., Ed. *Organometallic Flow Chemistry;* Topics in Organometallic Chemistry, Vol. 57; Springer International Publishing: Cham, Switzerland, 2016. doi:10.1007/978-3-319-33243-7
4. Mason, B. P.; Price, K. E.; Steinbacher, J. L.; Bogdan, A. R.; McQuade, D. T. *Chem. Rev.* **2007,** *107,* 2300–2318. doi:10.1021/cr050944c
5. Ahmed-Omer, B.; Brandt, J. C.; Wirth, T. *Org. Biomol. Chem.* **2007,** *5,* 733–740. doi:10.1039/b615072a
6. Watts, P.; Wiles, C. *Chem. Commun.* **2007,** 443–467. doi:10.1039/b609428g
7. McMullen, J. P.; Jensen, K. F. *Annu. Rev. Anal. Chem.* **2010,** *3,* 19–42. doi:10.1146/annurev.anchem.111808.073718
8. Yoshida, J.; Kim, H.; Nagaki, A. *ChemSusChem* **2011,** *4,* 331–340. doi:10.1002/cssc.201000271
9. Wiles, C.; Watts, P. *Green Chem.* **2012,** *14,* 38–54. doi:10.1039/c1gc16022b
10. Kirschning, A.; Kupracz, L.; Hartwig, J. *Chem. Lett.* **2012,** *41,* 562–570. doi:10.1246/cl.2012.562
11. McQuade, D. T.; Seeberger, P. H. *J. Org. Chem.* **2013,** *78,* 6384–6389. doi:10.1021/jo400583m
12. Elvira, K. S.; i Solvas, X. C.; Wootton, R. C. R.; deMello, A. J. *Nat. Chem.* **2013,** *5,* 905–915. doi:10.1038/nchem.1753
13. Pastre, J. C.; Browne, D. L.; Ley, S. V. *Chem. Soc. Rev.* **2013,** *42,* 8849–8869. doi:10.1039/c3cs60246j
14. Cambié, D.; Bottecchia, C.; Straathof, N. J. W.; Hessel, V.; Noël, T. *Chem. Rev.* **2016,** *116,* 10276–10341. doi:10.1021/acs.chemrev.5b00707
15. Plutschack, M. B.; Pieber, B.; Gilmore, K.; Seeberger, P. H. *Chem. Rev.* **2017,** *117,* 11796–11893. doi:10.1021/acs.chemrev.7b00183
16. Buglioni, L.; Raymenants, F.; Slattery, A.; Zondag, S. D. A.; Noël, T. *Chem. Rev.* **2022,** *122,* 2752–2906. doi:10.1021/acs.chemrev.1c00332
17. Nagaki, A.; Kim, H.; Yoshida, J. *Angew. Chem., Int. Ed.* **2008,** *47,* 7833–7836. doi:10.1002/anie.200803205
18. Kim, H.; Min, K.-I.; Inoue, K.; Im, D. J.; Kim, D.-P.; Yoshida, J. *Science* **2016,** *352,* 691–694. doi:10.1126/science.aaf1389
19. Seo, H.; Katcher, M. H.; Jamison, T. F. *Nat. Chem.* **2017,** *9,* 453–456. doi:10.1038/nchem.2690
20. Otake, Y.; Nakamura, H.; Fuse, S. *Angew. Chem., Int. Ed.* **2018,** *57,* 11389–11393. doi:10.1002/anie.201803549
21. Nagaki, A.; Yamashita, H.; Hirose, K.; Tsuchihashi, Y.; Yoshida, J. *Angew. Chem., Int. Ed.* **2019,** *58,* 4027–4030. doi:10.1002/anie.201814088
22. Nagaki, A.; Ichinari, D.; Yoshida, J. *Chem. Commun.* **2013,** *49,* 3242–3244. doi:10.1039/c3cc40392k
23. Moon, S.-Y.; Jung, S.-H.; Bin Kim, U.; Kim, W.-S. *RSC Adv.* **2015,** *5,* 79385–79390. doi:10.1039/c5ra14890a
24. Degennaro, L.; Maggiulli, D.; Carlucci, C.; Fanelli, F.; Romanazzi, G.; Luisi, R. *Chem. Commun.* **2016,** *52,* 9554–9557. doi:10.1039/c6cc04588j
25. Nauth, A. M.; Lipp, A.; Lipp, B.; Opatz, T. *Eur. J. Org. Chem.* **2017,** 2099–2103. doi:10.1002/ejoc.201601394
26. Tucker, J. W.; Zhang, Y.; Jamison, T. F.; Stephenson, C. R. J. *Angew. Chem., Int. Ed.* **2012,** *51,* 4144–4147. doi:10.1002/anie.201200961
27. Hernandez-Perez, A. C.; Collins, S. K. *Angew. Chem., Int. Ed.* **2013,** *52,* 12696–12700. doi:10.1002/anie.201306920
28. Elliott, L. D.; Knowles, J. P.; Koovits, P. J.; Maskill, K. G.; Ralph, M. J.; Lejeune, G.; Edwards, L. J.; Robinson, R. I.; Clemens, I. R.; Cox, B.; Pascoe, D. D.; Koch, G.; Eberle, M.; Berry, M. B.; Booker-Milburn, K. I. *Chem. – Eur. J.* **2014,** *20,* 15226–15232. doi:10.1002/chem.201404347
29. Talla, A.; Driessen, B.; Straathof, N. J. W.; Milroy, L.-G.; Brunsveld, L.; Hessel, V.; Noël, T. *Adv. Synth. Catal.* **2015,** *357,* 2180–2186. doi:10.1002/adsc.201401010
30. Asao, N.; Nogami, T.; Takahashi, K.; Yamamoto, Y. *J. Am. Chem. Soc.* **2002,** *124,* 764–765. doi:10.1021/ja017366b
31. Yao, T.; Zhang, X.; Larock, R. C. *J. Am. Chem. Soc.* **2004,** *126,* 11164–11165. doi:10.1021/ja0466964
32. Patil, N. T.; Yamamoto, Y. *Chem. Rev.* **2008,** *108,* 3395–3442. doi:10.1021/cr050041j
33. Rudolph, M.; Hashmi, A. S. K. *Chem. Commun.* **2011,** *47,* 6536–6544. doi:10.1039/c1cc10780a
34. Shiroodi, R. K.; Gevorgyan, V. *Chem. Soc. Rev.* **2013,** *42,* 4991–5001. doi:10.1039/c3cs35514d
35. Saito, K.; Kajiwara, Y.; Akiyama, T. *Angew. Chem., Int. Ed.* **2013,** *52,* 13284–13288. doi:10.1002/anie.201308303
36. Obradors, C.; Echavarren, A. M. *Chem. Commun.* **2014,** *50,* 16–28. doi:10.1039/c3cc45518a
37. Terada, M.; Li, F.; Toda, Y. *Angew. Chem., Int. Ed.* **2014,** *53,* 235–239. doi:10.1002/anie.201307371
38. Dorel, R.; Echavarren, A. M. *Chem. Rev.* **2015,** *115,* 9028–9072. doi:10.1021/cr500691k
39. Debrouwer, W.; Heugebaert, T. S. A.; Roman, B. I.; Stevens, C. V. *Adv. Synth. Catal.* **2015,** *357,* 2975–3006. doi:10.1002/adsc.201500520
40. Asiri, A. M.; Hashmi, A. S. K. *Chem. Soc. Rev.* **2016,** *45,* 4471–4503. doi:10.1039/c6cs00023a
41. Lauder, K.; Toscani, A.; Scalacci, N.; Castagnolo, D. *Chem. Rev.* **2017,** *117,* 14091–14200. doi:10.1021/acs.chemrev.7b00343
42. Zhang, Z.; Smal, V.; Retailleau, P.; Voituriez, A.; Frison, G.; Marinetti, A.; Guinchard, X. *J. Am. Chem. Soc.* **2020,** *142,* 3797–3805. doi:10.1021/jacs.9b11154
43. Raj, A. S. K.; Narode, A. S.; Liu, R.-S. *Org. Lett.* **2021,** *23,* 1378–1382. doi:10.1021/acs.orglett.1c00038
44. Greiner, L. C.; Arichi, N.; Inuki, S.; Ohno, H. *Angew. Chem., Int. Ed.* **2023,** *62,* e202213653. doi:10.1002/anie.202213653
45. Das, S. *Asian J. Org. Chem.* **2023,** *12,* e202300267. doi:10.1002/ajoc.202300267
46. Beatty, J. W.; Douglas, J. J.; Cole, K. P.; Stephenson, C. R. J. *Nat. Commun.* **2015,** *6,* 7919. doi:10.1038/ncomms8919
47. Nakajima, K.; Miyake, Y.; Nishibayashi, Y. *Acc. Chem. Res.* **2016,** *49,* 1946–1956. doi:10.1021/acs.accounts.6b00251

48. Ermanis, K.; Colgan, A. C.; Proctor, R. S. J.; Hadrys, B. W.; Phipps, R. J.; Goodman, J. M. *J. Am. Chem. Soc.* **2020,** *142,* 21091–21101. doi:10.1021/jacs.0c09668
49. Xiong, T.; Zhang, Q. *Chem. Soc. Rev.* **2021,** *50,* 8857–8873. doi:10.1039/d1cs00208b
50. Alfonzo, E.; Hande, S. M. *ACS Catal.* **2020,** *10,* 12590–12595. doi:10.1021/acscatal.0c03851
51. Kikuchi, J.; Kodama, S.; Terada, M. *Org. Chem. Front.* **2021,** *8,* 4153–4159. doi:10.1039/d1qo00657f
52. Schlegel, M.; Qian, S.; Nicewicz, D. A. *ACS Catal.* **2022,** *12,* 10499–10505. doi:10.1021/acscatal.2c02997
53. Takemura, N.; Sumida, Y.; Ohmiya, H. *ACS Catal.* **2022,** *12,* 7804–7810. doi:10.1021/acscatal.2c01964
54. Miura, T.; Yoritate, M.; Hirai, G. *Chem. Commun.* **2023,** *59,* 8564–8567. doi:10.1039/d3cc02361c
55. Terada, M.; Yazaki, R.; Obayashi, R.; Iwasaki, Z.; Umemiya, S.; Kikuchi, J. *Chem. Sci.* **2024,** *15,* 6115–6121. doi:10.1039/d4sc00808a
56. Prier, C. K.; Rankic, D. A.; MacMillan, D. W. C. *Chem. Rev.* **2013,** *113,* 5322–5363. doi:10.1021/cr300503r
57. Romero, N. A.; Nicewicz, D. A. *Chem. Rev.* **2016,** *116,* 10075–10166. doi:10.1021/acs.chemrev.6b00057
58. $Cu(NTf_2)_2$ which was also the effective catalyst in our batch system (ref. [55]) did not solve well in 1,2-DCE.
59. Benzyltrimethylsilane (**2a**), which was not consumed in the corresponding radical reaction, was almost completely recovered.
60. Maruyama, T.; Mizuno, Y.; Shimizu, I.; Suga, S.; Yoshida, J. *J. Am. Chem. Soc.* **2007,** *129,* 1902–1903. doi:10.1021/ja068589a
61. Montanaro, S.; Ravelli, D.; Merli, D.; Fagnoni, M.; Albini, A. *Org. Lett.* **2012,** *14,* 4218–4221. doi:10.1021/ol301900p

License and Terms

BEILSTEIN JOURNAL OF ORGANIC CHEMISTRY

Photoredox-catalyzed intramolecular nucleophilic amidation of alkenes with β-lactams

Valentina Giraldi[‡1,2], Giandomenico Magagnano[‡1], Daria Giacomini[1,2], Pier Giorgio Cozzi[1,2] and Andrea Gualandi[*1,2]

Full Research Paper

Open Access

Address:
[1]Department of Chemistry “G. Ciamician”, ALMA MATER STUDIORUM - Università di Bologna, Via Gobetti 85, 40129 Bologna, Italy and [2]Center for Chemical Catalysis - C3, ALMA MATER STUDIORUM - Università di Bologna, Via Gobetti 85, 40129 Bologna, Italy

Email:
Andrea Gualandi[*] - andrea.gualandi10@unibo.it

* Corresponding author ‡ Equal contributors

Keywords:
β-lactam; acridinium photocatalyst; alkenes; amides; intramolecular radical reaction; photoredox catalysis

Beilstein J. Org. Chem. **2024,** *20,* 2461–2468.
https://doi.org/10.3762/bjoc.20.210

Received: 23 July 2024
Accepted: 19 September 2024
Published: 01 October 2024

This article is part of the thematic issue "Photocatalysis and photochemistry in organic synthesis".

Guest Editor: T. Noël

Abstract

The direct nucleophilic addition of amides to unfunctionalized alkenes via photoredox catalysis represents a facile approach towards functionalized alkylamides. Unfortunately, the scarce nucleophilicity of amides and competitive side reactions limit the utility of this approach. Herein, we report an intramolecular photoredox cyclization of alkenes with β-lactams in the presence of an acridinium photocatalyst. The approach uses an intramolecular nucleophilic addition of the β-lactam nitrogen atom to the radical cation photogenerated in the linked alkene moiety, followed by hydrogen transfer from the hydrogen atom transfer (HAT) catalyst. This process was used to successfully prepare 2-alkylated clavam derivatives.

Introduction

Access to nitrogen radicals for the functionalization of alkenes is a field under active investigation [1-4], as it gives the possibility to directly introduce nitrogen into an alkyl chain (alkene carboamination) to obtain valuable nitrogen-containing molecules [5,6]. Among several N-centered radicals, such as aminyl, amidyl, or iminyl radicals, N-heterocyclic amidyl radicals were largely underinvestigated despite their importance as intermediates or relevant N-heterocyclic products in medicinal chemistry [7-10].

Recently, photoredox catalysis has emerged as a novel area of research [11,12], particularly focusing on innovative approaches to synthesize natural or bioactive compounds [13]. In the carboamination of alkenes, amides are used in photoredox cyclizations under proton-coupled electron transfer (PCET) conditions [14-17]. An alternative method to generate *N*-amidyl radicals uses activated N–O amide derivatives capable of generating amidyl radicals through fragmentation [18,19]. The direct formation of amidyl radicals in the presence of a carbon alkyl

chain could lead to a competitive 1,5-hydrogen atom transfer (1,5-HAT) [20-22], limiting the direct functionalization of amides with alkenes under photoredox conditions. Another viable approach for amide functionalization through photoredox catalysis involves the nucleophilic addition, in the presence of base, of an amide to a radical cation obtained by oxidation of an unfunctionalized alkene moiety (Figure 1A) [23-25]. The nucleophilic attack of the nitrogen atom on the oxidized C=C double bond results in the formation of a radical intermediate after deprotonation. This radical intermediate can proceed through various pathways (e.g., HAT, oxidation) to yield the desired final product.

In the functionalization of amides with alkenes under oxidative conditions, the oxidation potential of the alkene plays a pivotal role in the oxidation to a radical cation through photoredox catalysis [26]. Alkenes that are less functionalized possess a higher oxidation potential, necessitating the use of potent photocatalysts (PC) that act as oxidants in the excited state [27]. The direct functionalization of amides with alkenes has been a relatively underexplored area in research, as evidenced by the limited number of examples reported in the literature. An interesting observation was made by the Nicewicz group during their investigation of the hydrofunctionalization reaction of unsaturated amides and thioamides [28]. They have found that the oxygen atom of the amide group, rather than the nitrogen atom, acted as a nucleophile, leading to the formation of 2-oxazolines and 2-thiazolines. Another recent example of intramolecular nucleophilic attack induced by photocatalytic oxidation was reported by Yoon et al. with tosylamide derivatives [29]. Specifically, amides were employed in a photoredox cyclization process using a strong photooxidative acridinium catalyst such as the Fukuzumi catalyst (**I**, Figure 1B) [30,31]. Through tailored molecular design, it is possible to enhance the oxidation capability of these catalysts, enabling the utilization of less reactive alkenes and even aromatic molecules such as toluene [32].

Until now, heterocyclic amides such as β-lactam compounds have not been employed in alkene carboaminations. However, photoredox catalysis could be applied to a suitable β-lactam intermediate decorated with an alkene moiety to achieve N–H addition and cyclization to the fused bicyclic system of clavams (Figure 2A).

Clavulanic acid (**1**, Figure 2B) belongs to the family of clavam β-lactam compounds and is well known as a potent β-lactamase inhibitor [33,34]. It is produced by the filamentous bacterium *Streptomyces clavuligerus,* but in low yield. Various clavams **2**–**5** have been identified (Figure 2B), either through isolation as natural metabolites or obtained by synthetic methods [35-43]. The inhibitory activity of β-lactamases is exhibited by those congeners with a (3*R*,5*R*)-configuration, such as clavulanic acid (**1**), whereas clavams with other configurations are not lactamase inhibitors, although some of these have antifungal or antibacterial properties [35]. In the literature, oxacepham scaffolds, the 6-membered fused bicyclic analog of clavams, were prepared from appropriately substituted unfused precursors by

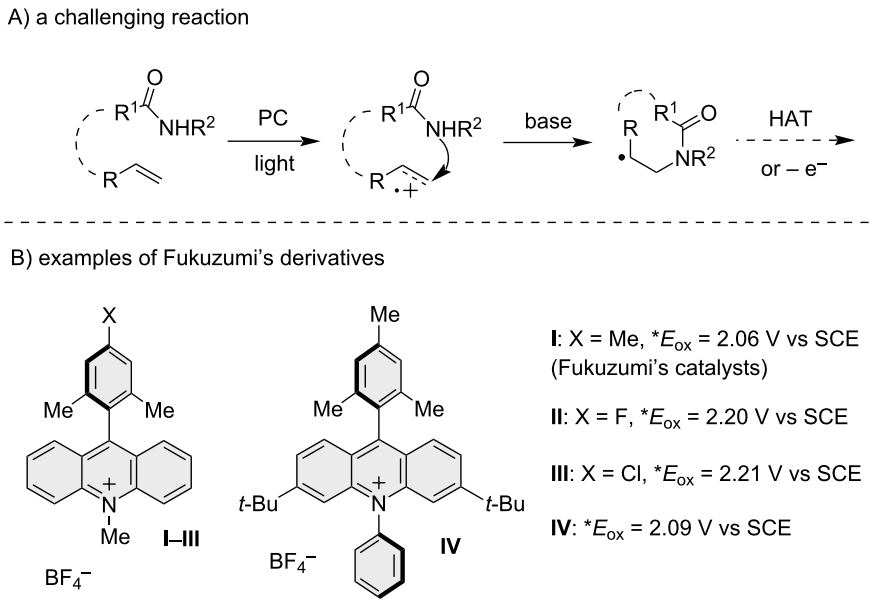

Figure 1: A) Photoredox amidocyclization reaction. B) The strongly oxidizing Fukuzumi catalyst (**I**) used in the functionalization of alkenes by amides, and more recent variants.

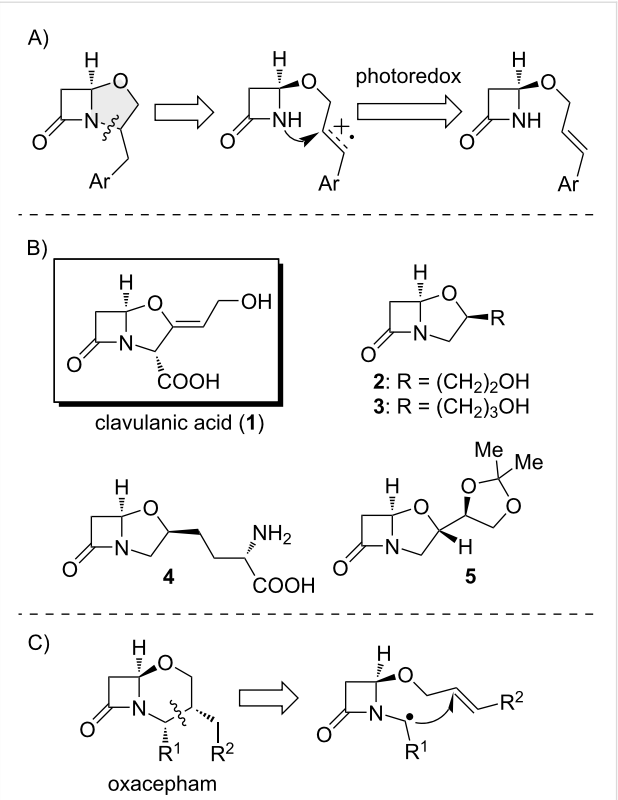

Figure 2: A) Access of clavam derivatives by intramolecular photoredox reaction of alkenes. B) Clavulanic acid and its derivatives. C) Construction of the oxacepham scaffold by radical cyclization.

intramolecular C-radical addition to alkene functionalities [44]. The utilization of radical conditions has prevented the effective nucleophilic opening of the lactams.

Notably, all reported structures have alkyl or aryl substituents in position 3 of the clavam ring. Conversely, clavams substituted with alkyl chains at the 2-position, to the best of our knowledge, have not been previously reported and are absent from common organic compound databases. To explore potential biological effects, a simple and modular approach to these molecules is thus required. Based on this, we decided to use photoredox chemistry to access 2-alkylclavams through a simplified synthetic pathway. We investigated the intramolecular nucleophilic addition of the nitrogen atom of the β-lactams to photooxidized alkenes (Figure 2A), and our findings are presented in this study.

Results and Discussion

The initial phase of our investigation involved the synthesis of suitable starting compounds for the following oxidative cyclization. For this purpose, a series of 4-alkoxy-β-lactams containing an alkene group was readily synthesized starting from commercially available 4-acetoxy-2-azetidinone (**6**) by nucleophilic displacement of the 4-acetoxy group with allylic alcohols promoted by $Zn(OAc)_2$ (see compounds **8a**–**h**, Scheme 1) [45]. Similarly, enantiopure derivatives **10c**–**f** were synthesized from the commercially available β-lactam **9**, a key intermediate for the industrial preparation of carbapenems.

Starting from the reaction conditions reported by Nicewicz and Morse [28], we optimized the conditions with compound **8c** as the model substrate for the photoredox cyclization (Table 1). The reaction was carried out in DCM with acridinium PC **IV** (5 mol %), 50 mol % of PhSSPh as HAT catalyst, and lutidine (50 mol %) as the base.

Upon 72 hours of irradiation with a blue light at 456 nm, the product **11c** was obtained in a satisfactory yield as a mixture of diastereoisomers in a 1.4:1 ratio (Table 1, entry 1). Assignment of the relative configurations as *cis* or *trans* was achieved by

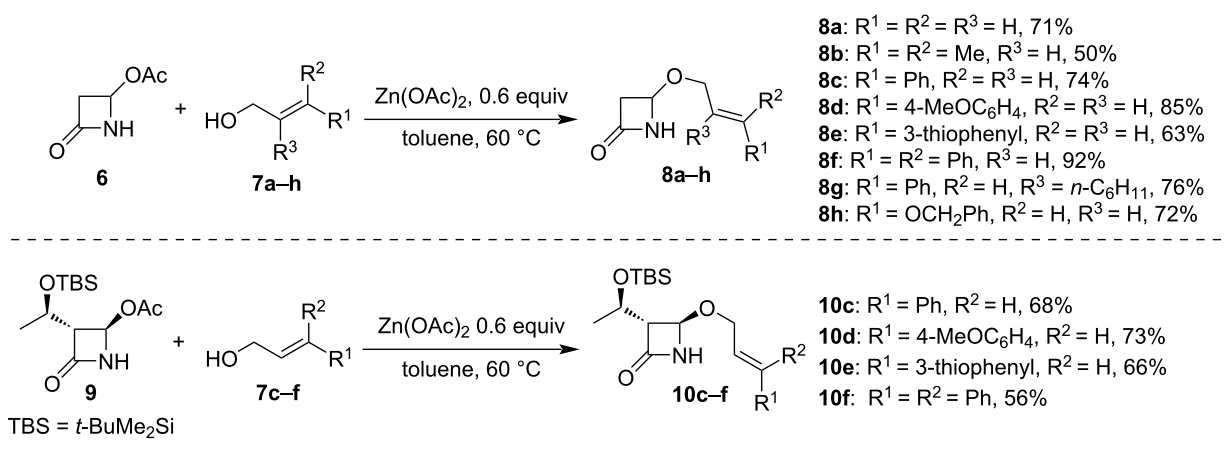

Scheme 1: Preparation of alkenyl β-lactam derivatives for the intramolecular photoredox reaction.

Table 1: Intramolecular cyclization of β-lactams induced by photoredox conditions.[a]

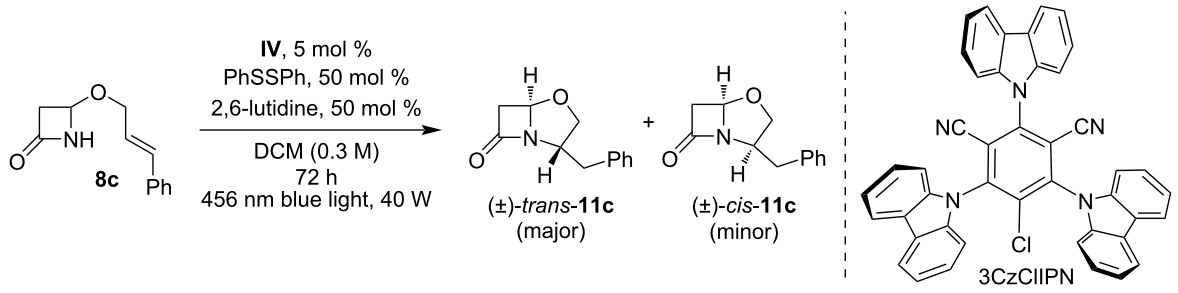

entry	deviation from standard conditions	conversion to **11c**, %[b,c]	dr[d]
1	—	72 (70)	1.4:1
2	absence of **IV**	0	—
3	absence of light	0	—
4	reaction time 14 h	traces	—
5	20 mol % PhSSPh, 20 mol % 2,6-lutidine	49	1.4:1
6	DMF solvent	0	—
7	MeCN solvent	68	1.4:1
8	DCE solvent	49	1.4:1
9	**I** instead of **IV**	60	1.4:1
10	3CzClIPN instead of **IV**	0	—

[a]The reactions were conducted under irradiation with a Kessil blue light (40 W) for 72 hours on a 0.05 mmol scale. [b]Conversion determined by ^{1}H NMR analysis of the crude reaction mixture. [c]In parentheses: isolated yield after purification by flash column chromatography. [d]*Trans*/*cis* dr determined by ^{1}H NMR analysis on the crude reaction mixture.

^{1}H NMR analysis, considering the chemical shifts of the proton in the α-position of the β-lactam nitrogen atom and the geminal protons in the benzylic position (see Supporting Information File 1). The difference in the chemical shifts of these protons in the two isomers could be attributed to the influence of the anisotropy of the neighboring carboxy group of the β-lactam and could be correlated with the configuration at the bridgehead stereocenter [46]. This analysis revealed the preferred formation of the *trans*- over the *cis*-isomer.

The optimal PC for the reaction was acridinium salt **IV** (Table 1, entry 1), while the Fukuzumi catalyst (**I**), commonly employed by Nicewicz et al., was less effective (Table 1, entry 9). 3CzClIPN, an organic dye belonging to the class of thermally activated delayed fluorescence (TADF) dyes commonly employed nowadays in photoredox catalysis [47], was tested in our reaction. This dye was chosen due to its oxidizing properties, and it ranks among the most oxidizing agents within this class of compounds ($E_{1/2}$[*PC/PC$^{\bullet-}$] = +1.56 V vs SCE) [48], but it proved ineffective in our reaction (Table 1, entry 10). The reaction was successfully conducted in various solvents, such as DCM, DCE, and MeCN (Table 1, entries 1, 7, and 8). However, DMF failed to yield the desired product (Table 1, entry 6). Shortening the reaction time to 14 hours resulted in minimal product formation (Table 1, entry 4), while reducing the amount of PhSSPh and lutidine to 20 mol % led to a lower yield (Table 1, entry 5).

With the optimized reaction conditions in hand, we submitted the previously prepared 4-alkoxy-β-lactam substrates **8a**–**h** to photoredox conditions (Scheme 1), and the salient results are reported in Scheme 2. Unfortunately, the substrates **8a**,**b** displayed low reactivity due to their significantly higher oxidation potential compared to the excited photoredox catalysts (>2.5 V vs SCE) [49]. However, other derivatives exhibited a satisfactory product yield ranging from moderate to good. Substrate **8d** exhibited an enhancement in reaction diastereoselectivity, resulting in the isolation of product **11d** with a dr of 6.7:1 in favor of the *trans*-diastereoisomer. Remarkably, the formation of a fully substituted quaternary center was possible, as observed for the product **11g**, where the *trans*-diastereoisomer was favored.

In this study, enantiopure 3-(1'-(*tert*-butyldimethylsilyl)ethyl)-β-lactams **10c**–**f** were also tested. Products **12c**–**f** were obtained with moderate to good yield, underscoring the feasibility of the methodology for the C3-substituted β-lactam moiety. The configuration at the newly formed stereocenter in the five-membered ring was attributed by ^{1}H NMR analysis for **11c**. Moreover, the configuration was also confirmed by NOE studies on

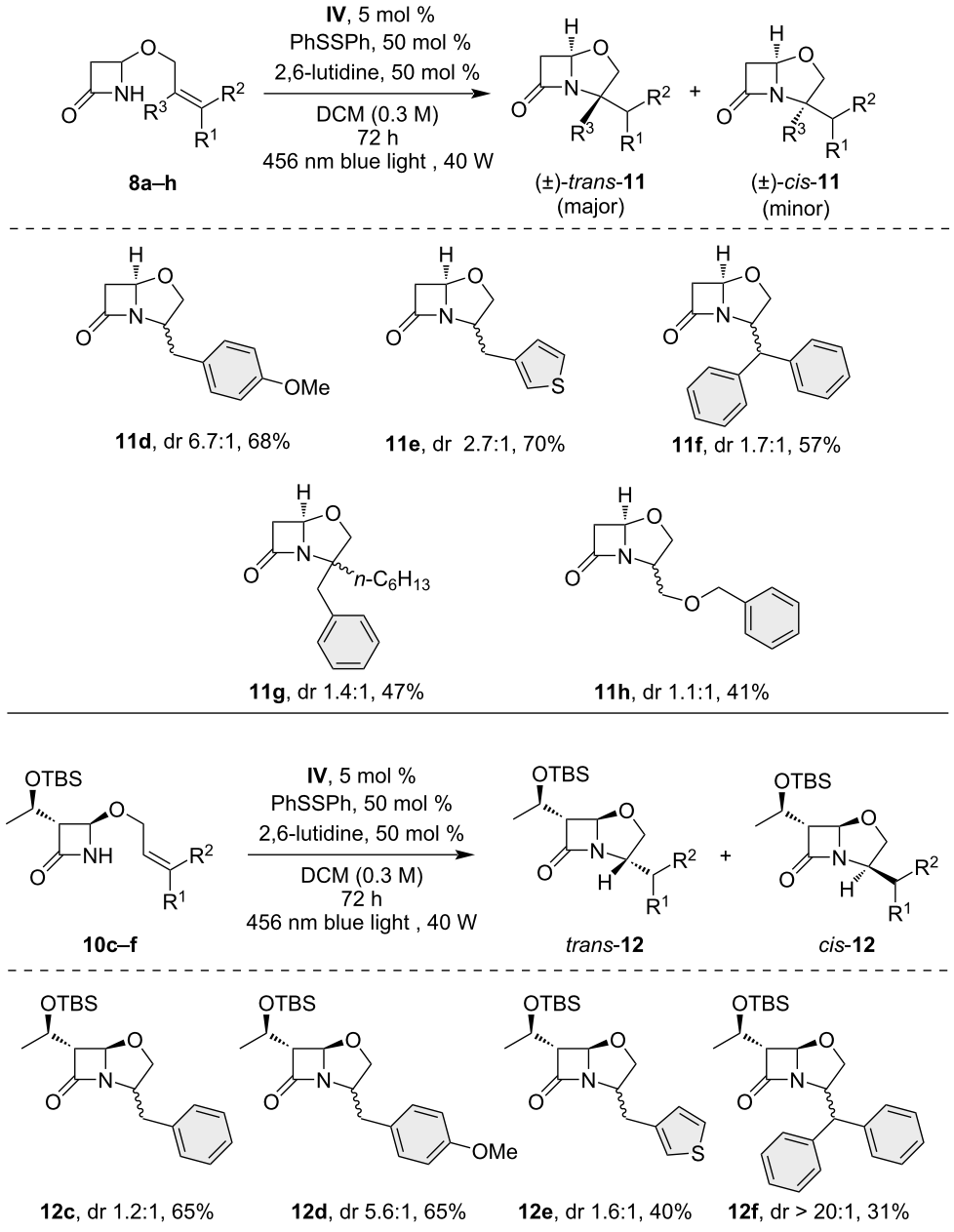

Scheme 2: Photoredox-catalyzed intramolecular N-alkylation reactions of various β-lactams. The *trans*/*cis* dr was determined by ^{1}H NMR analysis of the crude reaction mixture.

the two isolated diastereoisomers, which confirmed the preferred *trans*-isomer formation (see Supporting Information File 1).

Analysis of the dr values revealed that the diastereoselectivity of the nucleophilic attack of the β-lactam on the radical cationic intermediate was influenced by stereoelectronic factors. Compounds unsubstituted at position C-3 of the β-lactam ring, **11d**–**h**, showed modest stereoselectivity with a higher dr (6.7:1) for compound **11d**, which has an electron-donating methoxy group on the phenyl substituent. Derivatives with a 3-OTBS side chain, **12c**–**e**, displayed moderate diastereoselectivity, except for the higher diastereoselectivity achieved for **12f** (dr 20:1), probably due to steric effects, albeit at the expense of a reduced isolated yield.

Across all tested substrates, nucleophilic attack predominantly occurred at the homobenzylic position, leading to the regiose-

lective formation of clavam derivative with 2-benzylic substitution due to aryl stabilization of the radical intermediate (see mechanistic discussion below).

We briefly investigated whether this protocol could be adapted to other lactams, allowing for a practical synthesis of bicyclic structures. The resulting bicyclic lactam substrate could serve as a foundation to access pyrroloisoquinoline alkaloids [50,51]. The model substrate **14** was synthesized in a two-step process starting from succinimide (Scheme 3). Through a simple reaction in toluene at 80 °C in the presence of $Zn(OAc)_2$, the hemiaminal derivative **13** underwent substitution with cinnamyl alcohol, resulting in the isolation of **14** with a satisfactory yield. Under optimized reaction conditions, the photocatalytic cyclization occurred by producing *trans*-**15** in 35% yield as the single diastereoisomer.

For the reaction mechanism, we propose a mechanistic hypothesis according to the study by Nicewicz and Nguyen (Figure 3) [23]. The incorporation of electron-donating groups into the acridinium core, as in catalyst **IV**, enhances charge transfer by stabilizing the mesityl moiety. Conversely, the introduction of *tert*-butyl groups increases the life time of the excited state [52-56]. As a consequence, the PC **IV** is a strong oxidant in the excited state and displays unique oxidizing properties ($E_{1/2}$[*PC^+/$PC^\bullet$] = +2.09 V vs SCE) [55,56]. The *PC^+ species can oxidize the unsaturated lactam, thereby producing the corresponding radical cation intermediate **A**. The low stabilization by amide-bond resonance of the cyclic four-membered β-lactam [57,58] ensures a good nucleophilicity of the nitrogen atom to efficiently attack the radical cation **A**, giving the bicyclic radical intermediate **B**. Amide is an ambident nucleophile, and oxygen attack of radical cation **A** is also conceivable to give the corresponding imidate [28]. In our reaction, O-addition is disfavored due to the formation of an unsaturated four-membered ring as

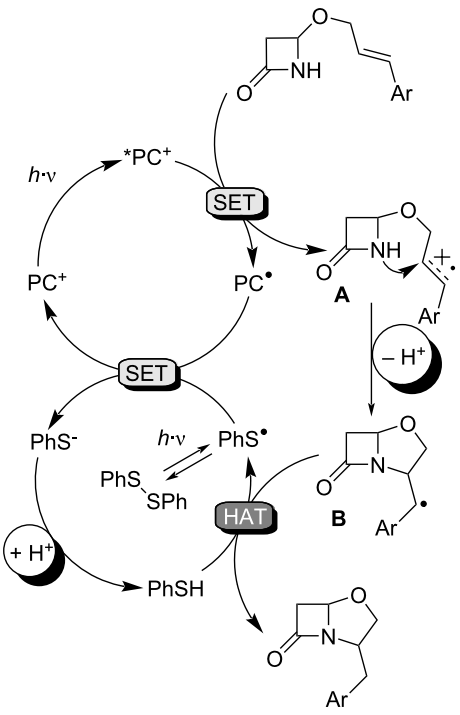

Figure 3: Tentative mechanism for the photo-cyclization reaction.

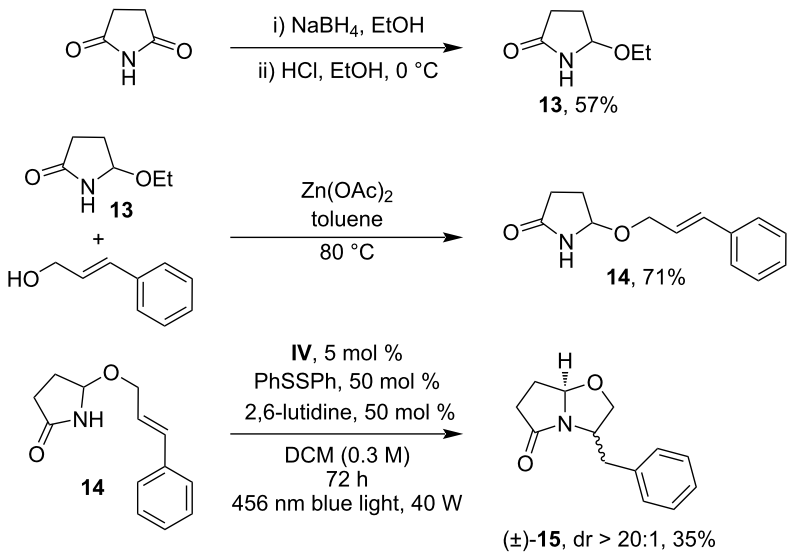

Scheme 3: Synthesis of the model substrate **14** and its photoredox-catalyzed intramolecular N-alkylation reaction. The *trans*/*cis* dr was determined by ^{1}H NMR analysis of the crude reaction mixture.

final product, characterized by significant ring strain [59]. Under light irradiation, PhSSPh is in equilibrium with the corresponding thiyl radical, which is subsequently reduced to thiophenolate by $PC^{\bullet}$, originating from the reduction of $*PC^{+}$. The reduction potential of $PhS^{-}/PhS^{\bullet}$ ($E_{p_{red}}$ = +0.45 V vs SCE) [60,61] is sufficient to oxidize the radical form of **IV** ($PC^{\bullet}/PC^{+}$ = −0.57 V vs SCE) [55,56]. Finally, PhS^{-} is protonated and HAT from thiophenol to **B** furnishes the final product, closing the HAT cycle. Additionally, lutidine acts as a proton shuttle between the lactam NH unit and thiophenolate.

Conclusion

To conclude, we have employed a photoredox methodology to access clavam and pyrrolyloxazole intermediates, showing the possibility of using the nucleophilic nitrogen atom of β-lactams under photoredox conditions. The acridinium catalyst **IV** was able to oxidize the C=C double bond present in the substrates to access the corresponding radical cation. The reaction shows high regioselectivity and good to moderate diastereoselectivity with satisfactory yield. The limitation, which will be further addressed by a more powerful catalyst, is related to the unreactivity of unsubstituted alkenes due to their higher oxidation potential. Biological studies concerning the new derivatives will also be a subject of future investigations.

Supporting Information

Supporting Information File 1

Reaction optimization studies, general experimental procedures, product isolation and characterization, spectroscopic data for new compounds, and copies of NMR spectra.
[https://www.beilstein-journals.org/bjoc/content/supplementary/1860-5397-20-210-S1.pdf]

Funding

P. G. C., D. G., and A. G. acknowledge the University of Bologna for financial support. MIUR national project (PRIN 2017 ID: 20174SYJAF) SURSUMCAT “Raising up Catalysis for Innovative Developments” and European Union’s Horizon 2020 research and innovation program under grant agreement no. 951996 are gratefully acknowledged.

ORCID® iDs

Valentina Giraldi - https://orcid.org/0000-0002-0593-1010
Giandomenico Magagnano - https://orcid.org/0000-0003-4893-4876
Daria Giacomini - https://orcid.org/0000-0001-8038-3926
Pier Giorgio Cozzi - https://orcid.org/0000-0002-2677-101X
Andrea Gualandi - https://orcid.org/0000-0003-2403-4216

Data Availability Statement

All data that supports the findings of this study is available in the published article and/or the supporting information of this article.

References

1. Kwon, K.; Simons, R. T.; Nandakumar, M.; Roizen, J. L. *Chem. Rev.* **2022,** *122,* 2353–2428. doi:10.1021/acs.chemrev.1c00444
2. Wang, P.; Zhao, Q.; Xiao, W.; Chen, J. *Green Synth. Catal.* **2020,** *1,* 42–51. doi:10.1016/j.gresc.2020.05.003
3. Pratley, C.; Fenner, S.; Murphy, J. A. *Chem. Rev.* **2022,** *122,* 8181–8260. doi:10.1021/acs.chemrev.1c00831
4. Gao, S.; Li, F. *Adv. Funct. Mater.* **2023,** *33,* 2304291. doi:10.1002/adfm.202304291
5. Kerru, N.; Gummidi, L.; Maddila, S.; Gangu, K. K.; Jonnalagadda, S. B. *Molecules* **2020,** *25,* 1909. doi:10.3390/molecules25081909
6. Lawrence, S. A. *Amines Synthesis, Properties and Applications;* Cambridge University Press: Cambridge, UK, 2006.
7. Pennington, L. D.; Collier, P. N.; Comer, E. *Med. Chem. Res.* **2023,** *32,* 1278–1293. doi:10.1007/s00044-023-03073-3
8. Heravi, M. M.; Zadsirjan, V. *RSC Adv.* **2020,** *10,* 44247–44311. doi:10.1039/d0ra09198g
9. Pennington, L. D.; Moustakas, D. T. *J. Med. Chem.* **2017,** *60,* 3552–3579. doi:10.1021/acs.jmedchem.6b01807
10. Vitaku, E.; Smith, D. T.; Njardarson, J. T. *J. Med. Chem.* **2014,** *57,* 10257–10274. doi:10.1021/jm501100b
11. Crisenza, G. E. M.; Melchiorre, P. *Nat. Commun.* **2020,** *11,* 803. doi:10.1038/s41467-019-13887-8
12. McAtee, R. C.; McClain, E. J.; Stephenson, C. R. J. *Trends Chem.* **2019,** *1,* 111–125. doi:10.1016/j.trechm.2019.01.008
13. Pitre, S. P.; Overman, L. E. *Chem. Rev.* **2022,** *122,* 1717–1751. doi:10.1021/acs.chemrev.1c00247
14. Choi, G. J.; Knowles, R. R. *J. Am. Chem. Soc.* **2015,** *137,* 9226–9229. doi:10.1021/jacs.5b05377
15. Miller, D. C.; Choi, G. J.; Orbe, H. S.; Knowles, R. R. *J. Am. Chem. Soc.* **2015,** *137,* 13492–13495. doi:10.1021/jacs.5b09671
16. Roos, C. B.; Demaerel, J.; Graff, D. E.; Knowles, R. R. *J. Am. Chem. Soc.* **2020,** *142,* 5974–5979. doi:10.1021/jacs.0c01332
17. Nguyen, L. Q.; Knowles, R. R. *ACS Catal.* **2016,** *6,* 2894–2903. doi:10.1021/acscatal.6b00486
18. Davies, J.; Svejstrup, T. D.; Fernandez Reina, D.; Sheikh, N. S.; Leonori, D. *J. Am. Chem. Soc.* **2016,** *138,* 8092–8095. doi:10.1021/jacs.6b04920
19. Ren, X.; Guo, Q.; Chen, J.; Xie, H.; Xu, Q.; Lu, Z. *Chem. – Eur. J.* **2016,** *22,* 18695–18699. doi:10.1002/chem.201603977
20. Galeotti, M.; Trasatti, C.; Sisti, S.; Salamone, M.; Bietti, M. *J. Org. Chem.* **2022,** *87,* 7456–7463. doi:10.1021/acs.joc.2c00955
21. Guo, W.; Wang, Q.; Zhu, J. *Chem. Soc. Rev.* **2021,** *50,* 7359–7377. doi:10.1039/d0cs00774a
22. Chu, J. C. K.; Rovis, T. *Nature* **2016,** *539,* 272–275. doi:10.1038/nature19810
23. Nguyen, T. M.; Nicewicz, D. A. *J. Am. Chem. Soc.* **2013,** *135,* 9588–9591. doi:10.1021/ja4031616
24. Nguyen, T. M.; Manohar, N.; Nicewicz, D. A. *Angew. Chem., Int. Ed.* **2014,** *53,* 6198–6201. doi:10.1002/anie.201402443
25. Gesmundo, N. J.; Grandjean, J.-M. M.; Nicewicz, D. A. *Org. Lett.* **2015,** *17,* 1316–1319. doi:10.1021/acs.orglett.5b00316
26. Roth, H. G.; Romero, N. A.; Nicewicz, D. A. *Synlett* **2016,** *27,* 714–723. doi:10.1055/s-0035-1561297

27. Xiong, L.; Tang, J. *Adv. Energy Mater.* **2021,** *11,* 2003216. doi:10.1002/aenm.202003216
28. Morse, P. D.; Nicewicz, D. A. *Chem. Sci.* **2015,** *6,* 270–274. doi:10.1039/c4sc02331e
29. Reed, N. L.; Lutovsky, G. A.; Yoon, T. P. *J. Am. Chem. Soc.* **2021,** *143,* 6065–6070. doi:10.1021/jacs.1c02747
30. Tlili, A.; Lakhdar, S. *Angew. Chem., Int. Ed.* **2021,** *60,* 19526–19549. doi:10.1002/anie.202102262
31. Joshi-Pangu, A.; Lévesque, F.; Roth, H. G.; Oliver, S. F.; Campeau, L.-C.; Nicewicz, D.; DiRocco, D. A. *J. Org. Chem.* **2016,** *81,* 7244–7249. doi:10.1021/acs.joc.6b01240
32. Ohkubo, K.; Matsumoto, S.; Asahara, H.; Fukuzumi, S. *ACS Catal.* **2024,** *14,* 2671–2684. doi:10.1021/acscatal.3c06111
33. López-Agudelo, V. A.; Gómez-Ríos, D.; Ramirez-Malule, H. *Antibiotics (Basel, Switz.)* **2021,** *10,* 84. doi:10.3390/antibiotics10010084
34. Saudagar, P. S.; Survase, S. A.; Singhal, R. S. *Biotechnol. Adv.* **2008,** *26,* 335–351. doi:10.1016/j.biotechadv.2008.03.002
35. Brown, A. G.; Butterworth, D.; Cole, M.; Hanscomb, G.; Hood, J. D.; Reading, C.; Rolinson, G. N. *J. Antibiot.* **1976,** *29,* 668–669. doi:10.7164/antibiotics.29.668
36. Brown, A. G.; Corbett, D. F.; Goodacre, J.; Harbridge, J. B.; Howarth, T. T.; Ponsford, R. J.; Stirling, I.; King, T. J. *J. Chem. Soc., Perkin Trans. 1* **1984,** 635–650. doi:10.1039/p19840000635
37. Brown, D.; Evans, J. R.; Fletton, R. A. *J. Chem. Soc., Chem. Commun.* **1979,** 282–283. doi:10.1039/c39790000282
38. Wanning, M.; Zähner, H.; Krone, B.; Zeeck, A. *Tetrahedron Lett.* **1981,** *22,* 2539–2540. doi:10.1016/s0040-4039(01)90514-3
39. Pruess, D. L.; Kellett, M. *J. Antibiot.* **1983,** *36,* 208–212. doi:10.7164/antibiotics.36.208
40. Evans, R. H., Jr.; Ax, H.; Jacoby, A.; Williams, T. H.; Jenkins, E.; Scannell, J. P. *J. Antibiot.* **1983,** *36,* 213–216. doi:10.7164/antibiotics.36.213
41. King, H. D.; Langhärig, J.; Sanglier, J. J. *J. Antibiot.* **1986,** *39,* 510–515. doi:10.7164/antibiotics.39.510
42. Naegeli, H. V.; Loosli, H.-R.; Nussbaumer, A. *J. Antibiot.* **1986,** *39,* 516–524. doi:10.7164/antibiotics.39.516
43. Hoppe, D.; Hilpert, T. *Tetrahedron* **1987,** *43,* 2467–2474. doi:10.1016/s0040-4020(01)81652-5
44. Bachi, M. D.; Frolow, F.; Hoornaert, C. *J. Org. Chem.* **1983,** *48,* 1841–1849. doi:10.1021/jo00159a010
45. Barrett, A. G. M.; Baugh, S. P. D.; Gibson, V. C.; Giles, M. R.; Marshall, E. L.; Procopiou, P. A. *Chem. Commun.* **1997,** 155–156. doi:10.1039/a607308e
46. Staszewska-Krajewska, O.; Bocian, W.; Maciejko, M.; Szcześniak, P.; Szymczak, K.; Chmielewski, M.; Furman, B. *ARKIVOC* **2014,** No. iii, 143–153. doi:10.3998/ark.5550190.p008.450
47. Bryden, M. A.; Zysman-Colman, E. *Chem. Soc. Rev.* **2021,** *50,* 7587–7680. doi:10.1039/d1cs00198a
48. Speckmeier, E.; Fischer, T. G.; Zeitler, K. *J. Am. Chem. Soc.* **2018,** *140,* 15353–15365. doi:10.1021/jacs.8b08933
49. Schepp, N. P.; Johnston, L. J. *J. Am. Chem. Soc.* **1996,** *118,* 2872–2881. doi:10.1021/ja9535468
50. Allin, S. M.; James, S. L.; Martin, W. P.; Smith, T. A. D. *Tetrahedron Lett.* **2001,** *42,* 3943–3946. doi:10.1016/s0040-4039(01)00613-x
51. Allin, S. M.; James, S. L.; Martin, W. P.; Smith, T. A. D.; Elsegood, M. R. J. *J. Chem. Soc., Perkin Trans. 1* **2001,** 3029–3036. doi:10.1039/b105402n
52. Brasholz, M. Acridinium Dyes and Quinones in Photocatalysis. In *Photocatalysis in Organic Synthesis;* König, B., Ed.; Science of Synthesis, Vol. 2018/6; Thieme: Stuttgart, Germany, 2018; pp 371–390. doi:10.1055/sos-sd-229-00224
53. Fukuzumi, S.; Ohkubo, K.; Suenobu, T. *Acc. Chem. Res.* **2014,** *47,* 1455–1464. doi:10.1021/ar400200u
54. Tsudaka, T.; Kotani, H.; Ohkubo, K.; Nakagawa, T.; Tkachenko, N. V.; Lemmetyinen, H.; Fukuzumi, S. *Chem. – Eur. J.* **2017,** *23,* 1306–1317. doi:10.1002/chem.201604527
55. Zilate, B.; Fischer, C.; Sparr, C. *Chem. Commun.* **2020,** *56,* 1767–1775. doi:10.1039/c9cc08524f
56. White, A. R.; Wang, L.; Nicewicz, D. A. *Synlett* **2019,** *30,* 827–832. doi:10.1055/s-0037-1611744
57. Glover, S. A.; Rosser, A. A. *J. Org. Chem.* **2012,** *77,* 5492–5502. doi:10.1021/jo300347k
58. Mucsi, Z.; Tsai, A.; Szori, M.; Chass, G. A.; Viskolcz, B.; Csizmadia, I. G. *J. Phys. Chem. A* **2007,** *111,* 13245–13254. doi:10.1021/jp0759325
59. Didier, D.; Baumann, A. N.; Eisold, M. *Tetrahedron Lett.* **2018,** *59,* 3975–3987. doi:10.1016/j.tetlet.2018.09.055
60. Fukuzumi, S.; Kotani, H.; Ohkubo, K.; Ogo, S.; Tkachenko, N. V.; Lemmetyinen, H. *J. Am. Chem. Soc.* **2004,** *126,* 1600–1601. doi:10.1021/ja038656q
61. Ohkubo, K.; Mizushima, K.; Iwata, R.; Souma, K.; Suzuki, N.; Fukuzumi, S. *Chem. Commun.* **2010,** *46,* 601–603. doi:10.1039/b920606j

License and Terms

BEILSTEIN JOURNAL OF ORGANIC CHEMISTRY

Giese-type alkylation of dehydroalanine derivatives via silane-mediated alkyl bromide activation

Perry van der Heide‡[1,2], Michele Retini‡[3], Fabiola Fanini[3], Giovanni Piersanti[3], Francesco Secci[1], Daniele Mazzarella[4,5], Timothy Noël[2] and Alberto Luridiana*[1]

Letter

Open Access

Address:
[1]Department of Chemical and Geological Sciences, University of Cagliari, S.S. 554, bivio per Sestu, 09042 Monserrato (CA), Italy, [2]Flow Chemistry Group, Van 't Hoff Institute for Molecular Sciences (HIMS), University of Amsterdam Science Park 904, 1098 XH Amsterdam, The Netherlands, [3]Department of Biomolecular Sciences, University of Urbino "Carlo Bo", Piazza Rinascimento 6, 61029 Urbino, Italy, [4]Department of Chemical Sciences and Technologies, University of Rome "Tor Vergata" Via della Ricerca Scientifica, 1, 00133 Rome, Italy, and [5]Department of Chemical Sciences, University of Padova Institution, Via Francesco Marzolo, 1, 35131 Padova, Italy

Email:
Alberto Luridiana* - alberto.luridiana@unica.it

* Corresponding author ‡ Equal contributors

Keywords:
dehydroalanine; Giese-type reaction; hydroalkylation; photocatalysis; water

Beilstein J. Org. Chem. **2024,** *20,* 3274–3280.
https://doi.org/10.3762/bjoc.20.271

Received: 09 October 2024
Accepted: 26 November 2024
Published: 17 December 2024

This article is part of the thematic issue "Photocatalysis and photochemistry in organic synthesis".

Associate Editor: C. Stephenson

Abstract

The rising popularity of bioconjugate therapeutics has led to growing interest in late-stage functionalization (LSF) of peptide scaffolds. α,β-Unsaturated amino acids like dehydroalanine (Dha) derivatives have emerged as particularly useful structures, as the electron-deficient olefin moiety can engage in late-stage functionalization reactions, like a Giese-type reaction. Cheap and widely available building blocks like organohalides can be converted into alkyl radicals by means of photoinduced silane-mediated halogen-atom transfer (XAT) to offer a mild and straightforward methodology of alkylation. In this research, we present a metal-free strategy for the photochemical alkylation of dehydroalanine derivatives. Upon abstraction of a hydride from tris(trimethylsilyl)silane (TTMS) by an excited benzophenone derivative, the formed silane radical can undergo a XAT with an alkyl bromide to generate an alkyl radical. Consequently, the alkyl radical undergoes a Giese-type reaction with the Dha derivative, forming a new $C(sp^3)$–$C(sp^3)$ bond. The reaction can be performed in a phosphate-buffered saline (PBS) solution and shows post-functionalization prospects through pathways involving classical peptide chemistry.

Introduction

The construction of $C(sp^3)$–$C(sp^3)$ bonds is a highly important target in synthetic organic chemistry. Historically, polar conjugate additions have been a benchmark method for constructing these bonds by functionalizing an electron-deficient olefin [1-3]. Recently, however, radical-based approaches have also gained widespread attention for their unique advantages in these

transformations [4]. Radical chemistry often exhibits complementary reactivity to two-electron pathways and can be performed with high selectivity, atom economy, and functional group tolerance [5]. A well-known radical pathway for the functionalization of an electron-deficient olefin is the Giese reaction (Figure 1) [6,7]. This reaction involves the hydroalkylation of the olefin via radical addition (RA), followed by either hydrogen-atom transfer (HAT) or single-electron transfer (SET) and protonation.

Traditionally, alkyl radicals have been produced from alkyl halides, using azobisisobutyronitrile (AIBN) as initiator, promoting a tin-mediated XAT (Figure 1a) [8,9]. However, tin-based compounds are highly toxic and require harsh conditions for the initiation event.

Fortunately, a renaissance in the field of photochemistry has introduced new ways of generating radicals like photoredox catalysis and via electron donor–acceptor (EDA) complexes [10-13]. These advances, coupled with modern electrochemical methods, chemical reactor engineering and light emitting diodes (LED), have eliminated the need for thermal radical activation, resulting in milder and safer reaction conditions [14-16]. Given the toxicity of tin-based compounds, there has been significant interest in developing alternative halogen-atom-transfer reagents. Borane, alkylamine, and silane compounds have emerged as effective XAT reagents upon photocatalytic activation (Figure 1b) [17-21]. A photocatalytic HAT or SET generates the corresponding boryl, α-amino or silyl radical, which can abstract a halogen atom from alkyl halides to form the corresponding alkyl radical.

However, the use of TTMS as a XAT reagent had already been established by Chatgilialoglu et al. [22] under non-photoredox conditions, MacMillan et al. [23] sparked renewed interest in silanes as XAT reagents by generating a tris(trimethylsilyl)silyl radical through photoredox catalysis for arylation reactions [22,23]. In 2018, Balsells et al. [24] reported a similar strategy to generate alkyl radicals and explored the feasibility of a Giese-type reaction (Figure 1c). More recently, Gaunt et al. [25] showed that irradiation of alkyl iodides combined with TTMS leads to the formation of an alkyl radical, which can be used in a Giese-type reaction without the need of a photocatalyst (Figure 1d) [25]. Noël et al. [26] have further extended this approach to include alkyl bromides (Figure 1e) [26]. Despite the effectiveness of the photolysis, benzophenone derivatives have also been shown to enhance the productivity of silane-mediated conjugate additions, using alkyl halides [27].

Amid the growing popularity of biomolecular drug candidates, the late-stage modification of peptide scaffolds has gained significant importance [28]. A particularly interesting class of amino acids for late-stage diversification consists of dehydroamino acids (Dha). Dha derivatives have shown modifica-

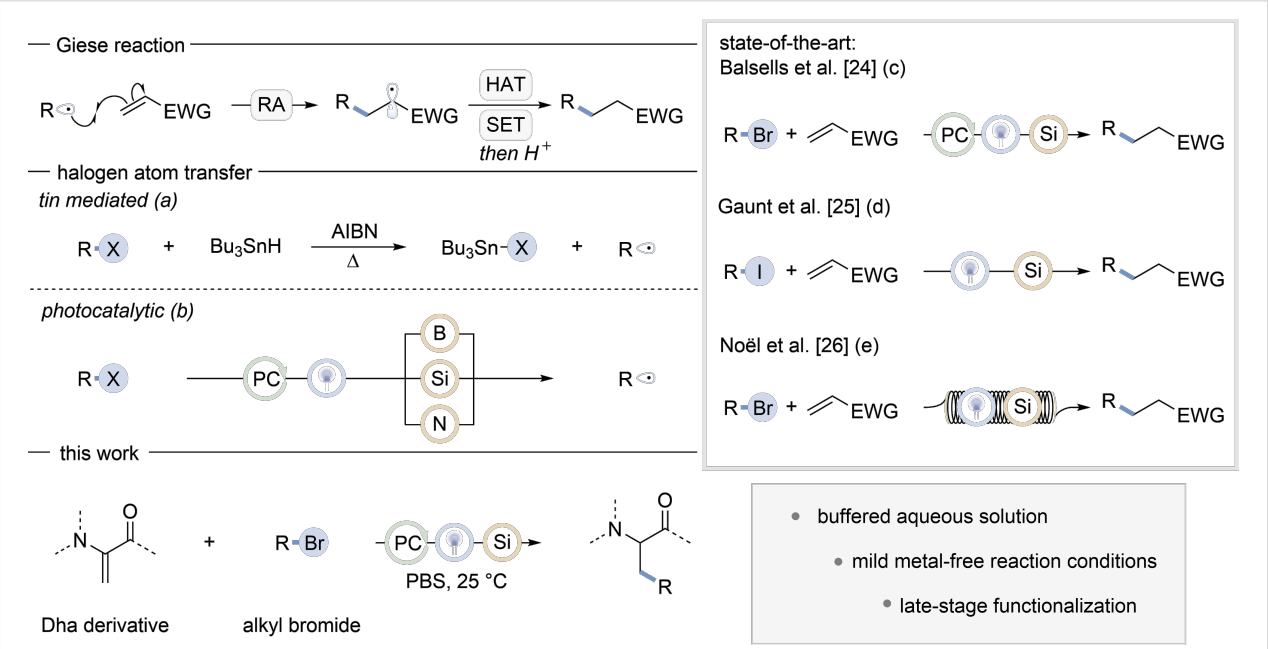

Figure 1: Giese reaction: Radical addition on olefins with an electron-withdrawing group (EWG) followed by a HAT or SET and protonation; halogen-atom transfer: (a) tin-mediated XAT, (b) XAT initiated by a photocatalyst (PC) and mediated by boranes (B), silanes (Si) or alkylamines (N); state-of-the-art: (c) silane-mediated alkylation initiated by a photocatalyst, (d) silane-mediated alkylation initiated by photolysis of alkyl iodides, (e) silane-mediated alkylation initiated by photolysis of alkyl bromides in flow; this work: silane-mediated alkylation of Dha derivatives initiated by a photocatalyst.

tion potential by means of polar, metal-, or organo-catalyzed and radical additions [29-36]. As such, Dha derivatives make an excellent candidate for exploring a photochemical Giese-type reaction [37]. To foster a physiological reaction environment, reactions can be conducted in aqueous solution, meeting important requirements with regard to bioorthogonal chemistry [38].

Considering previous research that demonstrated photochemical hydrogen atom abstraction by benzophenone derivatives from trialkylsilyl hydrides [27], as well as advances in alkyl radical formation using these hydrides, we sought to combine these findings. Herein, we report a photochemical alkylation methodology targeting the olefin moiety of Dha derivatives, conducted in an aqueous solution for the aforementioned bioorthogonal advantages.

Results and Discussion

Inspired by previously conducted research concerning benzophenone hydrogen-atom transfer and silane-mediated activation of alkyl bromides to perform a photochemical Giese reaction, methyl 2-(1,3-dioxoisoindolin-2-yl)acrylate (**1**) and bromocyclohexane (**2**) were dissolved in CH_3CN (0.1 M) together with a stoichiometric amount of tris(trimethylsilyl)silane and a substoichiometric amount of (4-methoxyphenyl)(4-(trifluoromethyl)phenyl)methanone (BP **I**) (Table 1) [26,27].

The reaction was performed in batch, using a 390 nm Kessil UV-A lamp, stirring at 600 rpm overnight at 25 °C (see Supporting Information File 1 for a more detailed optimization).

The initial reaction, using CH_3CN as solvent, led to formation of methyl 3-cyclohexyl-2-(1,3-dioxoisoindolin-2-yl)propanoate (**3**, 51% yield, 85% conv.; Table 1, entry 1). To demonstrate the importance of the photocatalyst, BP **I** was excluded (Table 1, entry 2), resulting in a slightly higher conversion and a decrease in product formation (38% yield, 90% conv.), meaning BP **I** increases the productivity of the reaction. Having established that the reaction works in CH_3CN, we evaluated its compatibility with water. To our delight, the reaction in water provided full conversion and a higher yield than the one observed in CH_3CN (58% yield, 100% conv.; Table 1, entry 3). These conditions were further refined by adding of phosphate-buffered saline and decreasing the amount of $(TMS)_3SiH$ to 1.1 equiv, as no further increase in yield was noticed during the optimization. Similar to the reaction in deionized water, all entries with PBS solution reached a full conversion. While the yield of the reaction with a 0.1 M PBS solution was slightly lower than that of the reaction in deionized water (44% yield, 100% conv.; Table 1, entry 4), a 0.2 M PBS solution resulted in an increased yield (60% yield, 100% conv.; Table 1, entry 5). Upon increasing the concentration of the PBS solution to 0.4 M,

Table 1: Methyl 2-(1,3-dioxoisoindolin-2-yl)acrylate (**1**, 0.5 mmol), bromocyclohexane (**2**, 1.25 mmol), tris(trimethylsilyl)silane (0.55 mmol), (4-methoxyphenyl)(4-(trifluoromethyl)phenyl)methanone (0.1 mmol), PBS 0.2 M solution (2.5 mL), λ = 390 nm, 25 °C, overnight. The yield of **3** was calculated by ^1H NMR with 1,1,2-trichloroethene as external standard.

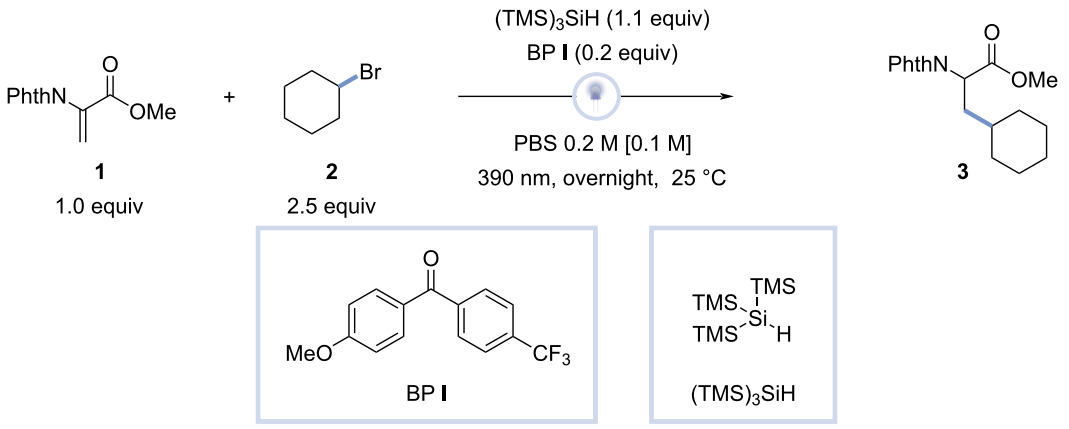

Entry	Deviation from the reaction conditions	Conversion **1** (%)	NMR yield **3** (%)
1	CH_3CN instead of PBS 0.2 M; 1.5 equiv $(TMS)_3SiH$	85	51
2	CH_3CN instead of PBS 0.2 M; no BP **I**; 1.5 equiv $(TMS)_3SiH$	90	38
3	H_2O instead of PBS 0.2 M; 1.5 equiv $(TMS)_3SiH$	100	58
4	PBS 0.1 M instead of PBS 0.2 M	100	44
5	none	100	60
6	PBS 0.4 M instead of PBS 0.2 M	100	60
7	**3 hours**	**100**	**67**

no change in yield was observed (60% yield, 100% conv.; Table 1, entry 6). Lastly, the optimal reaction time was determined to be 3 hours (67% yield, 100% conv.; Table 1, entry 7). Having optimized the reaction conditions, a scope of primary, secondary, and tertiary alkyl bromides and different Dha derivatives was investigated (Figure 2).

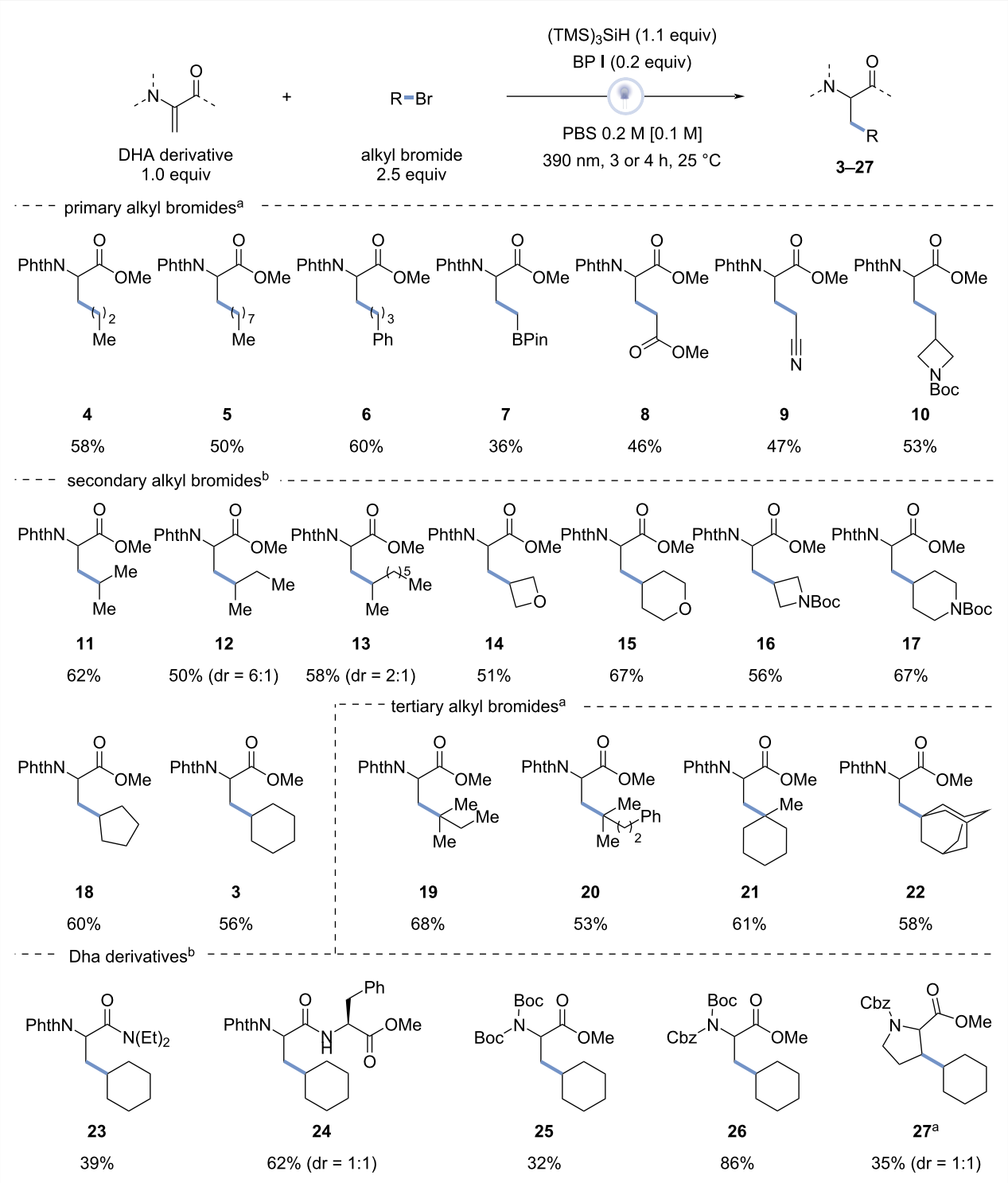

Figure 2: Alkyl bromide and Dha derivative scope. Reaction conditions: Dha derivative (0.5 mmol), alkyl bromide (1.25 mmol), tris(trimethylsilyl)silane (0.55 mmol), (4-methoxyphenyl)(4-(trifluoromethyl)phenyl)methanone (0.1 mmol), PBS 0.2 M solution (2.5 mL), λ = 390 nm, 25 °C. [a]4 hours of reaction time, [b]3 hours of reaction time. The isolated product yields are reported.

A slight modification of the reaction protocol was used in regard to primary and tertiary alkyl bromides, requiring a longer reaction time (4 hours instead of 3 hours) to achieve full conversion.

The reaction worked well with aliphatic primary bromides (**4**–**10**). However, a longer chain length slightly decreased the yield, comparing compound **4** (58%) to compound **5** (50%). The reaction was not influenced by the presence of phenyl rings, as the yield of compound **6** (60%) was comparable to the yield of **4**. Besides, the introduction of a boronic pinacol ester group, useful for subsequent post-functionalization, compound **7** was achieved in a relatively lower yield of 36%. Interestingly, the reaction also worked adequately for primary alkyl bromides with electron-withdrawing groups as demonstrated in compounds **8** (46%) and **9** (47%). Moreover, primary alkyl bromides like bromomethylazetidines as used in compound **10** (53%) also resulted in decent yields. Acyclic secondary alkyl substrates all resulted in good yields (**11**–**13**, 50–62%). For the secondary alkyl substrates, a higher yield was notably obtained for compound **13** with a longer chain length than for **12**. Similarly, the secondary cyclic alkyl substrates used in compound **18** (60%) and **3** (56%) worked well for this reaction. Besides, oxygen-containing compounds **14** and **15** were obtained in yields of 51% and 67% and medicinally interesting groups like the azetidine in compound **16** (56%) and the piperidine in compound **17** (67%) also resulted in good yields. Concerning tertiary alkyl substrates, acyclic alkyl substrates used in compound **19** (68%) and **20** (53%) as well as cyclic alkyl substrates like bromomethylcyclohexane used in compound **21** (61%) and bromoadamantane in compound **22** (58%) were obtained in satisfactory yields.

Subsequently, different Dha derivatives were subjected to the optimized reaction conditions, using bromocyclohexane (**2**) as the alkyl bromide. In order to explore the effect of the presence of an amide moiety in the Dha derivatives, a tertiary amide was firstly used to exclude selectivity issues arising from the hydrogen atoms of the amide functionality, yielding compound **23** in synthetically useful yield (39%). Interestingly, a secondary amide was formed in a higher yield of compound **24** (62%) compared to a Dha with a tertiary amide on the same position. Alternatively, the use of a double Boc-protected Dha resulted in a rather low yield of compound **25** (32%), while varying one Boc-protecting group with a Cbz-protecting group increased the yield substantially to 86% for compound **26**. In addition, the use of a cyclic, *N*-Cbz-protected Michael acceptor, derived from proline, allowed for preparation of compound **27** with a 35% yield in 4 hours without control of diastereoselectivity (dr = 1:1).

Finally, to prove that the optimized reaction also works at a larger scale, the model reaction was carried out on a 2.2 mmol scale (Figure 3), obtaining a slightly elevated yield (67%) compared to compound **3**, which was previously formed at a 0.5 mmol scale.

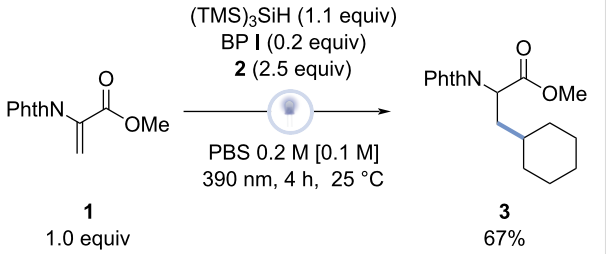

Figure 3: Scaled-up reaction. Reaction conditions: Dha derivative (2.2 mmol), alkyl bromide (5.4 mmol), tris(trimethylsilyl)silane (2.4 mmol), (4-methoxyphenyl)(4-(trifluoromethyl)phenyl)methanone (0.4 mmol), PBS 0.2 M solution (10.8 mL), λ = 390 nm, 25 °C, 4 hours, isolated product yield.

Conclusion

In conclusion, a photochemical methodology to promote the metal-free alkylation of dehydroalanine derivatives was developed, by means of silane-mediated alkyl bromide activation. The biocompatibility of the reaction enabled by the PBS solution and the mild photochemical reaction conditions makes the transformation useful for late-stage functionalization under physiological conditions. Besides, the reaction was successfully scaled up by roughly four times, leading to a slight increase in chemical yield.

Supporting Information

Supporting Information File 1

^{1}H NMR, ^{13}C NMR, and HRMS spectra of all the synthesized compounds.
[https://www.beilstein-journals.org/bjoc/content/supplementary/1860-5397-20-271-S1.pdf]

Acknowledgements

We are grateful to University Research Services Center (CeSAR)-UniCA for the analysis service.

Funding

P. H. thanks the Erasmus+ traineeship program. The research contract (63-G-19602-1) of M.R. is co-financed by the European Union "FSE-REACT-EU, PON Research and innovation 2014-2020 DM 1062/2021" (CUP H31B21009610007). A.L.

thanks the MUR for a Young Researchers Seal of Excellence fellowship (PlaDisPho) SOE_0000091 (PNRR).

ORCID® iDs

Perry van der Heide - https://orcid.org/0009-0006-3138-4379
Michele Retini - https://orcid.org/0000-0003-0218-8505
Giovanni Piersanti - https://orcid.org/0000-0003-0418-7143
Francesco Secci - https://orcid.org/0000-0003-0443-2890
Alberto Luridiana - https://orcid.org/0000-0002-7828-9866

Data Availability Statement

All data that supports the findings of this study is available in the published article and/or the supporting information of this article.

References

1. Yang, L.; Huang, H. *Chem. Rev.* **2015,** *115,* 3468–3517. doi:10.1021/cr500610p
2. Csákÿ, A. G.; de La Herrán, G.; Murcia, M. C. *Chem. Soc. Rev.* **2010,** *39,* 4080–4102. doi:10.1039/b924486g
3. Ballini, R.; Bosica, G.; Fiorini, D.; Palmieri, A.; Petrini, M. *Chem. Rev.* **2005,** *105,* 933–972. doi:10.1021/cr040602r
4. Renaud, P.; Sibi, M. P., Eds. *Radicals in Organic Synthesis;* Wiley-VCH: Weinheim, Germany, 2001. doi:10.1002/9783527618293
5. Castellino, N. J.; Montgomery, A. P.; Danon, J. J.; Kassiou, M. *Chem. Rev.* **2023,** *123,* 8127–8153. doi:10.1021/acs.chemrev.2c00797
6. Giese, B.; Meister, J. *Angew. Chem., Int. Ed. Engl.* **1977,** *16,* 178–179. doi:10.1002/anie.197701781
7. Kitcatt, D. M.; Nicolle, S.; Lee, A.-L. *Chem. Soc. Rev.* **2022,** *51,* 1415–1453. doi:10.1039/d1cs01168e
8. Kuivila, H. G.; Menapace, L. W. *J. Org. Chem.* **1963,** *28,* 2165–2167. doi:10.1021/jo01044a001
9. Giese, B.; Dupuis, J. *Angew. Chem., Int. Ed. Engl.* **1983,** *22,* 622–623. doi:10.1002/anie.198306221
10. Shaw, M. H.; Twilton, J.; MacMillan, D. W. C. *J. Org. Chem.* **2016,** *81,* 6898–6926. doi:10.1021/acs.joc.6b01449
11. Crisenza, G. E. M.; Mazzarella, D.; Melchiorre, P. *J. Am. Chem. Soc.* **2020,** *142,* 5461–5476. doi:10.1021/jacs.0c01416
12. McClain, E. J.; Monos, T. M.; Mori, M.; Beatty, J. W.; Stephenson, C. R. J. *ACS Catal.* **2020,** *10,* 12636–12641. doi:10.1021/acscatal.0c03837
13. Wortman, A. K.; Stephenson, C. R. J. *Chem* **2023,** *9,* 2390–2415. doi:10.1016/j.chempr.2023.06.013
14. Yuan, Y.; Yang, J.; Lei, A. *Chem. Soc. Rev.* **2021,** *50,* 10058–10086. doi:10.1039/d1cs00150g
15. Buglioni, L.; Raymenants, F.; Slattery, A.; Zondag, S. D. A.; Noël, T. *Chem. Rev.* **2022,** *122,* 2752–2906. doi:10.1021/acs.chemrev.1c00332
16. Wan, T.; Wen, Z.; Laudadio, G.; Capaldo, L.; Lammers, R.; Rincón, J. A.; García-Losada, P.; Mateos, C.; Frederick, M. O.; Broersma, R.; Noël, T. *ACS Cent. Sci.* **2022,** *8,* 51–56. doi:10.1021/acscentsci.1c01109
17. Chatgilialoglu, C.; Ferreri, C.; Landais, Y.; Timokhin, V. I. *Chem. Rev.* **2018,** *118,* 6516–6572. doi:10.1021/acs.chemrev.8b00109
18. Zhang, Z.; Tilby, M. J.; Leonori, D. *Nat. Synth.* **2024,** *3,* 1221–1230. doi:10.1038/s44160-024-00587-5
19. Constantin, T.; Zanini, M.; Regni, A.; Sheikh, N. S.; Juliá, F.; Leonori, D. *Science* **2020,** *367,* 1021–1026. doi:10.1126/science.aba2419
20. Wan, T.; Capaldo, L.; Ravelli, D.; Vitullo, W.; de Zwart, F. J.; de Bruin, B.; Noël, T. *J. Am. Chem. Soc.* **2023,** *145,* 991–999. doi:10.1021/jacs.2c10444
21. Poletti, L.; Massi, A.; Ragno, D.; Droghetti, F.; Natali, M.; De Risi, C.; Bortolini, O.; Di Carmine, G. *Org. Lett.* **2023,** *25,* 4862–4867. doi:10.1021/acs.orglett.3c01660
22. Chatgilialoglu, C.; Griller, D.; Lesage, M. *J. Org. Chem.* **1988,** *53,* 3641–3642. doi:10.1021/jo00250a051
23. Zhang, P.; Le, C. C.; MacMillan, D. W. C. *J. Am. Chem. Soc.* **2016,** *138,* 8084–8087. doi:10.1021/jacs.6b04818
24. ElMarrouni, A.; Ritts, C. B.; Balsells, J. *Chem. Sci.* **2018,** *9,* 6639–6646. doi:10.1039/c8sc02253d
25. Mistry, S.; Kumar, R.; Lister, A.; Gaunt, M. J. *Chem. Sci.* **2022,** *13,* 13241–13247. doi:10.1039/d2sc03516b
26. Fanini, F.; Luridiana, A.; Mazzarella, D.; Alfano, A. I.; van der Heide, P.; Rincón, J. A.; García-Losada, P.; Mateos, C.; Frederick, M. O.; Nuño, M.; Noël, T. *Tetrahedron Lett.* **2023,** *117,* 154380. doi:10.1016/j.tetlet.2023.154380
27. Luridiana, A.; Mazzarella, D.; Capaldo, L.; Rincón, J. A.; García-Losada, P.; Mateos, C.; Frederick, M. O.; Nuño, M.; Jan Buma, W.; Noël, T. *ACS Catal.* **2022,** *12,* 11216–11225. doi:10.1021/acscatal.2c03805
28. Wang, L.; Wang, N.; Zhang, W.; Cheng, X.; Yan, Z.; Shao, G.; Wang, X.; Wang, R.; Fu, C. *Signal Transduction Targeted Ther.* **2022,** *7,* 48. doi:10.1038/s41392-022-00904-4
29. Bogart, J. W.; Bowers, A. A. *Org. Biomol. Chem.* **2019,** *17,* 3653–3669. doi:10.1039/c8ob03155j
30. Jousseaume, T.; Wurz, N. E.; Glorius, F. *Angew. Chem., Int. Ed.* **2011,** *50,* 1410–1414. doi:10.1002/anie.201006548
31. Key, H. M.; Miller, S. J. *J. Am. Chem. Soc.* **2017,** *139,* 15460–15466. doi:10.1021/jacs.7b08775
32. Retini, M.; Bartolucci, S.; Bartoccini, F.; Piersanti, G. *Chem. – Eur. J.* **2022,** *28,* e202201994. doi:10.1002/chem.202201994
33. Kaplaneris, N.; Akdeniz, M.; Fillols, M.; Arrighi, F.; Raymenants, F.; Sanil, G.; Gryko, D. T.; Noël, T. *Angew. Chem., Int. Ed.* **2024,** *63,* e202403271. doi:10.1002/anie.202403271
34. Aycock, R. A.; Pratt, C. J.; Jui, N. T. *ACS Catal.* **2018,** *8,* 9115–9119. doi:10.1021/acscatal.8b03031
35. Sim, J.; Campbell, M. W.; Molander, G. A. *ACS Catal.* **2019,** *9,* 1558–1563. doi:10.1021/acscatal.8b04284
36. Gu, X.; Zhang, Y.-A.; Zhang, S.; Wang, L.; Ye, X.; Occhialini, G.; Barbour, J.; Pentelute, B. L.; Wendlandt, A. E. *Nature* **2024,** *634,* 352–358. doi:10.1038/s41586-024-07988-8
37. Peng, X.; Xu, K.; Zhang, Q.; Liu, L.; Tan, J. *Trends Chem.* **2022,** *4,* 643–657. doi:10.1016/j.trechm.2022.04.008
38. Lim, R. K. V.; Lin, Q. *Chem. Commun.* **2010,** *46,* 1589. doi:10.1039/b925931g

License and Terms

BEILSTEIN JOURNAL OF ORGANIC CHEMISTRY

Red light excitation: illuminating photocatalysis in a new spectrum

Lucas Fortier[1], Corentin Lefebvre[*2] and Norbert Hoffmann[*3]

Review

Open Access

Address:
[1]Unité de Catalyse et de Chimie du Solide (UCCS), University of Lille, CNRS, University of Artois UMR 8181, Avenue Mendeleiev, 59655 Villeneuve d'Ascq CEDEX, France, [2]Laboratory of Glycochemistry and Agroressources of Amiens (LG2A), University of Picardie Jules Verne UR 7378, 10 rue Baudelocque, 80000 Amiens, France and [3]Institute of Physics and Chemistry of Materials of Strasbourg (IPCMS), University of Strasbourg UMR 7504, 23 rue du Loess, BP 43, 67034 Strasbourg CEDEX 2, France

Email:
Corentin Lefebvre[*] - corentin.lefebvre@u-picardie.fr;
Norbert Hoffmann[*] - norbert.hoffmann@ipcms.unistra.fr

* Corresponding author

Keywords:
green chemistry; medicinal chemistry; organic photochemistry; photocatalysis; red-light mediated transformations

Beilstein J. Org. Chem. **2025,** *21,* 296–326.
https://doi.org/10.3762/bjoc.21.22

Received: 05 November 2024
Accepted: 31 January 2025
Published: 07 February 2025

This article is part of the thematic issue "Photocatalysis and photochemistry in organic synthesis".

Guest Editor: T. Noël

Abstract

Red-light-activated photocatalysis has become a powerful approach for achieving sustainable chemical transformations, combining high efficiency with energy-saving, mild conditions. By harnessing the deeper penetration and selectivity of red and near-infrared light, this method minimizes the side reactions typical of higher-energy sources, making it particularly suited for large-scale applications. Recent advances highlight the unique advantages of both metal-based and metal-free catalysts under red-light irradiation, broadening the range of possible reactions, from selective oxidations to complex polymerizations. In biological contexts, red-light photocatalysis enables innovative applications in phototherapy and controlled drug release, exploiting its tissue penetration and low cytotoxicity. Together, these developments underscore the versatility and impact of red-light photocatalysis, positioning it as a cornerstone of green organic chemistry with significant potential in synthetic and biomedical fields.

Introduction

Red-light-activated photocatalysis has recently gained significant interest as a tool for driving chemical transformations under mild and efficient conditions. The use of red and near-infrared light enables deeper penetration into reaction media, reducing the high-energy side reactions commonly triggered by UV or blue light. These features make red-light photocatalysis particularly advantageous for large-scale applications, offering enhanced safety and operational simplicity. Traditionally, research in this field has focused on metal-based photocatalysts, particularly those based on transition metals like ruthenium and

osmium due to their intrinsic photophysical properties. However, with growing concerns around environmental sustainability, there is increasing interest in developing photocatalysts that are more accessible, tunable, and eco-friendly. Each section of this document discusses a specific approach to red-light photocatalysis, reflecting the field's evolution and exploring diverse catalyst types and applications. The first section is dedicated to metal-based photocatalysts. Complexes involving metals such as osmium and ruthenium, have dominated red-light photoredox catalysis because of their ability to absorb low-energy photons and sustain redox cycles via stable excited states. In this section, the document highlights applications of these complexes in reactions like ring-closing metathesis and polymerization, where red light's deeper penetration enhances yields and efficiency, particularly for large-scale reactions. The second section broadens the focus to explore organic photocatalysts. Unlike metal-based systems, organic photocatalysts such as phthalocyanins, squaraines and cyanins, offer effective electron and energy transfer under red-light irradiation without relying on transition metals. This shift towards organic catalysts opens new possibilities for sustainable photocatalysis, with applications ranging from selective oxidation to cross-dehydrogenative coupling. These organic systems are valued for their reduced environmental impact, their wide availability, and tunability, making them viable alternatives to traditional metal-based catalysts for red-light-driven transformations. The final section examines applications of red-light photocatalysis within biological and medicinal fields. The capacity of red light to penetrate biological tissues enables processes that are challenging or even impossible under UV or blue light. This section discusses different photocatalysts, such as helical carbenium ions and advanced nitrobenzofuran derivatives for applications in phototherapy and controlled drug release, underscoring the potential of red-light photocatalysis in biomedicine.

Review

Red-light photocatalysis with metal-based complexes

Metal-based complexes naturally own a large span of colors depending on the nature of the metal and the ligands but also on the various oxidation states these compounds can attain. This property results on the absorption of a visible-light photon complementary to the observed color and has been extensively exploited in photoredox catalysis in recent years not only with heavy metals such as ruthenium and iridium [1-5], but also with lighter elements [6-8]. This field of light-mediated organic transformations relies on the use of a photocatalyst to promote radical reactions through electron transfer between this former and a given substrate or a sacrificial species. In the case of the metal-based complexes, the absorption band associated to the metal-to-ligand charge transfer (MLCT) is generally addressed even though other types of excitations like ligand-to-metal charge transfer, ligand- and metal-based excitation have been proven to be efficient in photoredox catalysis [9-12]. Actually, MLCT enables a charge separation for which the ligand-based electron can trigger a chemical reduction while the metal-centered hole, a chemical oxidation. This type of excitation is particularly enhanced in heavy metals, where the low-lying excited state often corresponds to the metal-to-ligand charge transfer (MLCT) transition. As the atomic number increases, relativistic effects become more pronounced, leading to the contraction of s and p orbitals while the d and f orbitals expand and become more diffuse. While these effects play a role in reducing the energy of the d orbitals and improving their overlap with the ligand orbitals, thereby facilitating electron transfer, the occurrence of metal-to-ligand charge transfer (MLCT) is also strongly influenced by other factors. Specifically, MLCT competes with metal-centered excitations (MC), which are governed by the ligand field splitting, an effect that increases for larger and more diffuse orbitals, and by the energy of the ligand's π^* orbitals. This interplay between relativistic effects, ligand field strength, and ligand orbital energy ultimately determines the absorption of lower-energy photons in second- and third-row transition metals compared to their first-row counterparts [13]. These phenomena are specifically improved when potent π-acceptor ligands are used due to their low-energy π^* antibonding orbitals resulting in a bathochromic shift of the MLCT absorption band. These combined effects can be illustrated in the case of the $[M(phen)_3]^{2+}$ set with iron, ruthenium, and osmium (Figure 1). For a same phenanthroline ligand, these three complexes show an MLCT absorption band at different wavelengths, i.e., 522 nm for $[Fe(phen)_3]^{2+}$ [14], 449 nm for $[Ru(phen)_3]^{2+}$ and 660 nm for $[Os(phen)_3]^{2+}$ [15].

In a same way, spin–orbit coupling, stemming from the relativistic effects, can be exploited in photoredox-catalyzed reaction [16]. Spin–orbit coupling promotes intersystem crossing (ISC) between the singlet and triplet excited states, and even allows for direct excitation to the triplet state from the ground state S_0. This effect mitigates rapid back-electron transfer from the singlet excited state to the ground state, extending the excited-state lifetime of the photocatalyst. Since the $T_1 \rightarrow S_0$ transition is spin-forbidden, the process increases the overall efficiency of photoredox-catalyzed reactions.

Absorption in the red region opens up innovative opportunities for photochemical transformations. First, the employed photon has the lowest energy in the electromagnetic spectrum of visible light, which allows for safer laboratory conditions in terms of irradiation apparatus, e.g., UV radiation sources. Secondly, from a synthetic perspective, a broader range of substrates and

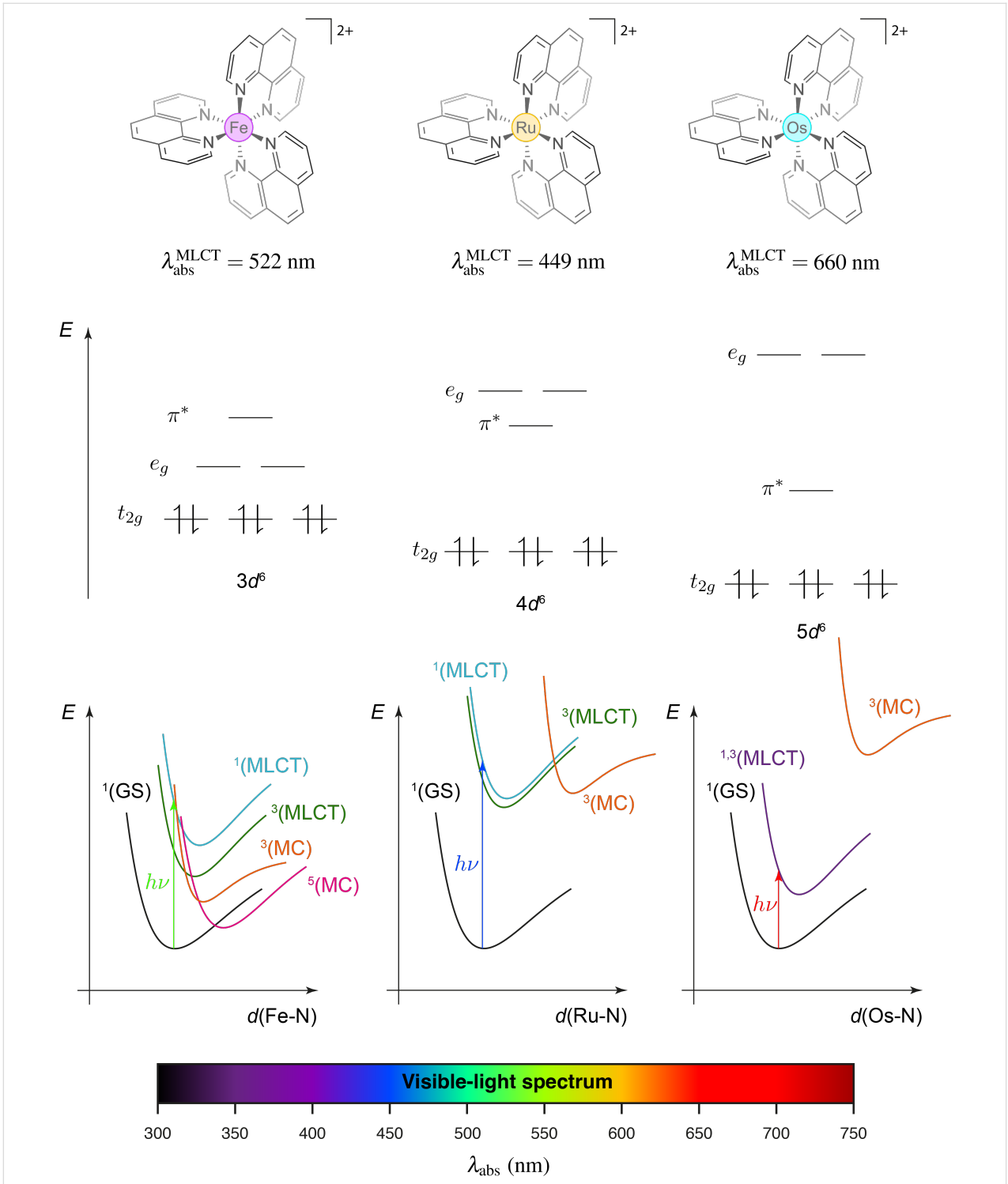

Figure 1: Influence of the metal center M (Fe, Ru, Os) on the position of the MLCT and MC (metal-centered) absorption band in the case of $[M(phen)_3]^{2+}$-type complexes (GS = ground-state).

catalysts can be considered as in most cases, they are incapable of absorbing red light and, consequently, cannot initiate a photocatalytic transformation, thereby minimizing the risk of side reactions. This latter advantage has been notably exploited in the case of ring-closing olefin metathesis reactions, where Weizmann et al. utilized the photothermal response of plasmons from gold nanoparticles to activate the catalyst [17]. This approach contrasts with the work of Rovis et al. who employed

a ruthenium(II) complex **1** activated through photoinduced electron transfer. The latter is pre-activated by the osmium complex shown in Scheme 1 after irradiation in the red region [18]. According to the mechanism proposed by the authors, the reaction is facilitated when conducted in acetone, allowing the pre-activation of the ruthenium complex with the successive release of an *N*-heterocyclic carbene ligand and a chlorine atom, which are replaced by two acetone molecules to form compound **2**. Simultaneously, excitation of the osmium(II) complex in the red region (660 nm) decreases its reduction potential to −0.97 V vs SCE, a value low enough to reduce the ruthenium complex **2**, whose potential is estimated at −0.89 V vs SCE, thereby yielding **3**, the active species for the metathesis reaction. The catalytic cycle is closed by the reduction of the resulting osmium(III) complex, regenerating the ruthenium(I) complex **2**.

In this study, T. Rovis et al. demonstrated a third advantage of working with red light: its penetrating power. To this end, a polymerization reaction of dicyclopentadiene **4** was investigated through various materials such as amber glass, white paper, a solution of hemoglobin, and silicon by selectively irradiating a specific area of the reaction medium with red light (660 nm) or blue light (456 nm), respectively (Scheme 2).

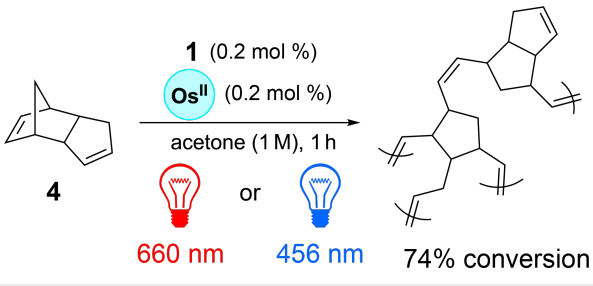

Scheme 2: Photocatalyzed polymerization of dicylopentadiene mediated with red or blue light.

The authors have demonstrated that this polymerization reaction proceeded much more efficiently under red light irradia-

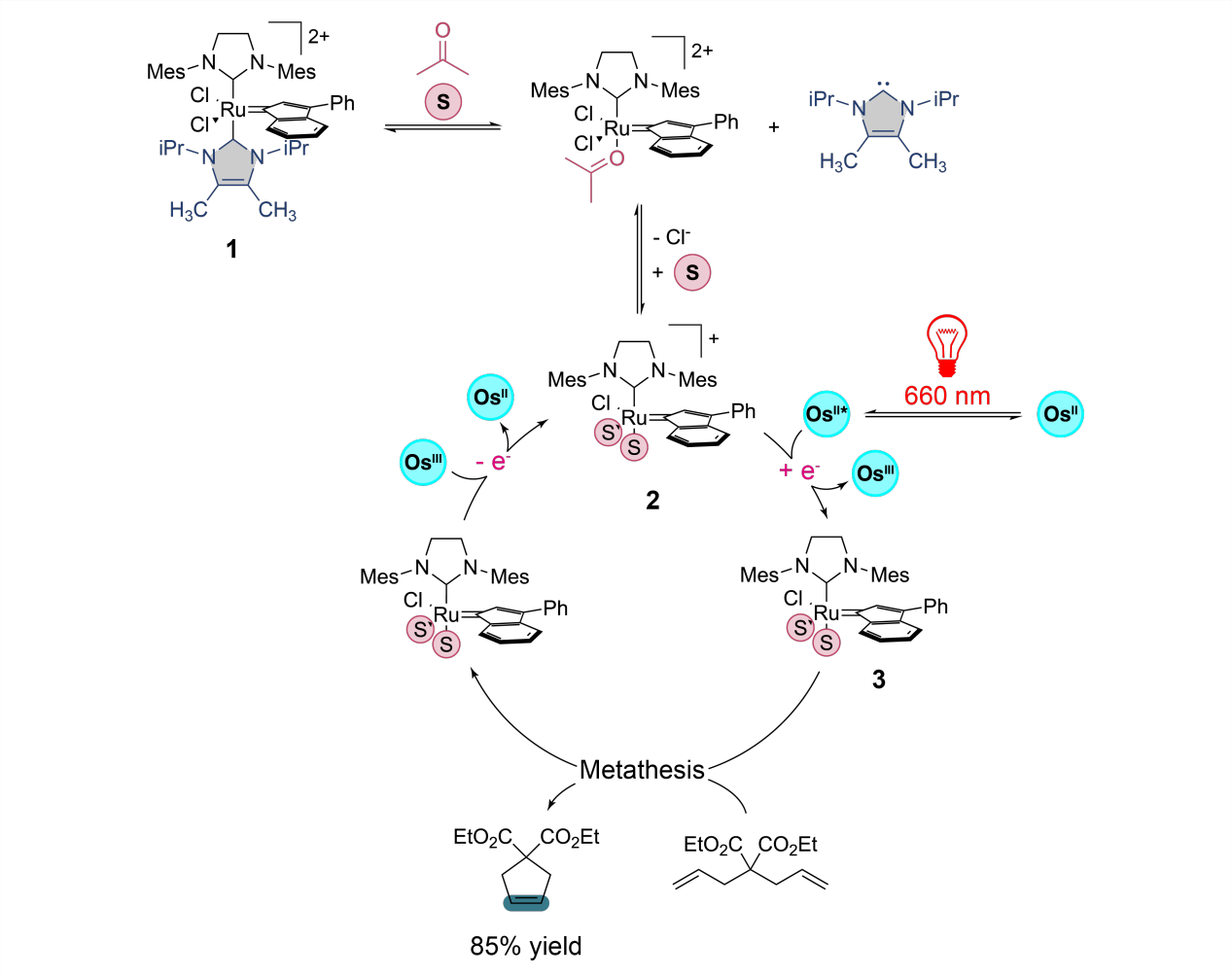

Scheme 1: Red-light-mediated ring-closing metathesis through activation of a ruthenium catalyst by an osmium photocatalyst.

tion. Indeed, red light can penetrate all the used materials and can initiate the reaction through the core of the reaction medium as the polymer forms, unlike blue light. This penetrating power of red light was also characterized by comparing the ruthenium complex $[Ru(bpy)_3]^{2+}$ absorbing at 450 nm with the osmium complex $[Os(tpy)_2]^{2+}$ absorbing at 740 nm in a the photocatalyzed trifluoromethylation reaction of **5** into **8** proposed by the same authors (Figure 2) [19]. These latter have shown the benefits of using their system based on an irradiation with red-light and the osmium complex over the ruthenium one with blue-light in a large-scale reaction. One of the most significant advantages is the superior light penetration of near-infrared light, which can reach deeper into the reaction mixture than blue light. In larger reaction volumes, where photon distribution becomes a limiting factor, near-infrared light penetrates approximately 23 times deeper than blue light when comparing the two molar extinction coefficients of $[Os(tpy)_2]^{2+}$ at 450 and 740 nm for a same concentration according to the Beer–Lambert law, hence ensuring more uniform photon exposure and an improved reaction efficiency. This enhanced light penetration is reflected in the reaction yields as a function of the reaction-scale. As this latter increases, the obtained yields using $[Ru(bpy)_3]^{2+}$ under blue light decrease significantly to reach a yield loss of 31.6% at a 250× scale, while those using $[Os(tpy)_2]^{2+}$ under near-infrared light remain constant or even increase up to a yield gain of 27.5% at the same reaction scale. T. Rovis et al. emphasize this result has profound implications for industrial applications. The ability of red light to penetrate deeply and to maintain high efficiency without requiring specialized flow reactors or high-powered light sources makes the $[Os(tpy)_2]^{2+}$/red-light irradiation system well-suited for large-scale manufacturing. In this way, the authors have also tested different osmium complexes in various well-established photocatalyzed reactions such as copper, palladium, cobalt, and nickel metallophotoredox couplings using red light, thereupon highlighting potential for broad applications in photoredox catalysis on an industrial scale.

In this context, T. Rovis et al. have studied a C–N cross-coupling Buchwald–Hartwig-like reaction using dual nickel and osmium catalysis under red-light activation, addressing common challenges such as poor light penetration, side reactions, and scalability related to traditional blue-light-driven metallophotoredox reactions. By switching from blue light (460 nm) to red light (660 nm) and osmium complex $[Os(phen)_3]^{2+}$ instead of an iridium complex, the authors have

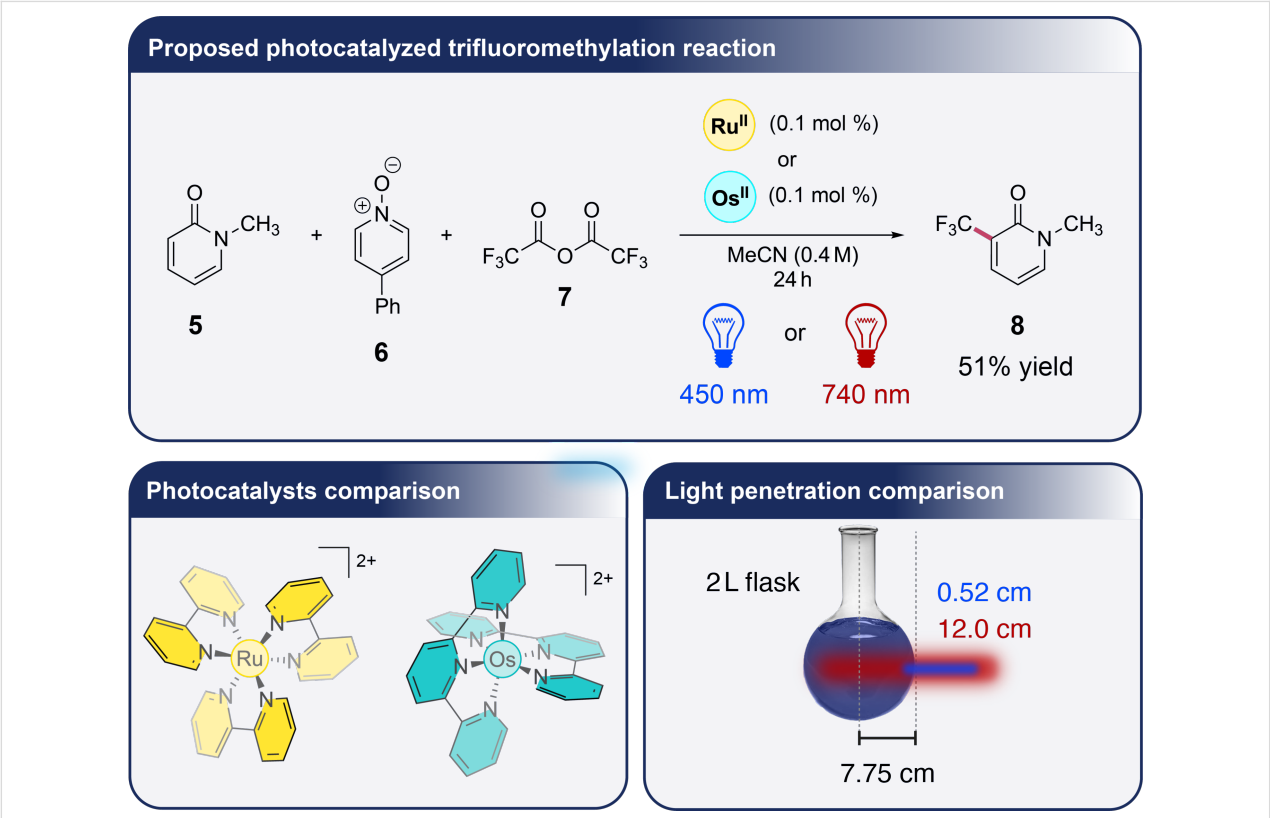

Figure 2: Comparison between $[Ru(bpy)_3]^{2+}$ and $[Os(tpy)_2]^{2+}$ in a photocatalyzed trifluoromethylation reaction: influence of the light source on the medium penetration. The flask in Figure 2 is taken from https://www.brusheezy.com, Free Photoshop Brushes by Brusheezy! This content is not subject to CC BY 4.0.

been able to significantly enhance the scope and efficiency of these reactions. Specifically, they demonstrate that red light can suppress unwanted side reactions, such as hydrodehalogenation (compounds **12**, Scheme 3a), a common issue in high-energy light systems where aryl–Ni bonds are cleaved, leading to undesirable byproducts. The study found that by using $[Os(phen)_3]^{2+}$ as the photocatalyst and 660 nm red light, the reaction exhibited greater functional group tolerance, handling a variety of electron-deficient, neutral and rich (hetero)aryl bromides **9** and primary and secondary amine-based nucleophiles **10** with minimal degradation or side reactivity in a scope of around 50 examples with yields ranging from 27 to 97 % compared to the

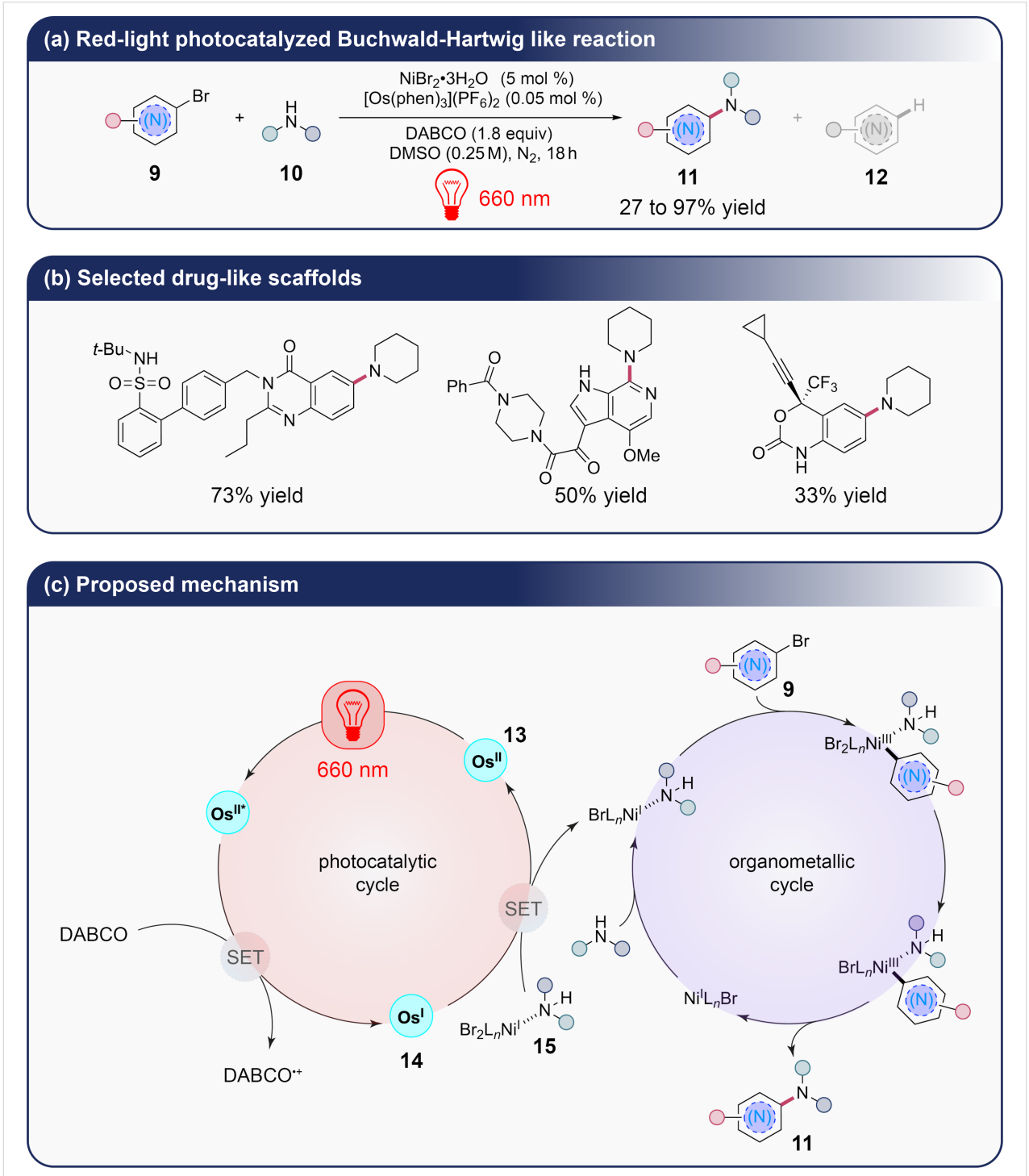

Scheme 3: Red-light photocatalyzed C–N cross-coupling reaction by T. Rovis et al. (SET = single-electron transfer).

use of blue-light (Scheme 3a) [20]. In this way, T. Rovis et al. have exploited their photocatalytic system on the functionalization of drug-like scaffolds with moderate to good yields (Scheme 3b). The mechanism of the reaction presented by the authors involves two different catalytic cycles as presented in Scheme 3c. After excitation of the osmium complex **13**, this latter is reduced via the use of a tertiary amine to give the active species **14** able to oxidize the formed nickel complex **15** in the reaction mixture. This step allows the oxidative addition of nickel on the aryl bromide **9** followed by the reductive elimination giving the desired product **11**. Besides the innovative synthetic results obtained in this study, the authors underline a major advantage to switch to red light as it enables a deeper penetration through the reaction media, making the method highly scalable. In a batch reaction, the authors have successfully scaled up the synthesis by two orders of magnitude, achieving comparable yields without the need for complex flow reactors.

The successful implementation of osmium complexes in large-scale photoredox reactions highlights the broader applicability of transition metals in facilitating challenging chemical transformations. Moving beyond the d-block, the exploration of main-group elements offers a new frontier in the use of more affordable and available photocatalysts. While transition metals such as copper, palladium, cobalt, and nickel are well-established in catalyzed cross-coupling reactions, J. Cornella et al. have highlighted the reactivity of main-group elements like bismuth, which can mimic transition-metal behavior through oxidative addition. In their recent study, the authors have developed a complementary ground-state- and excited-state-driven aryl oxidative addition platform based on an *N*,*C*,*N*-bismuthinidene complex, showing the unique capacity of this main-group element to engage in reactivity typically associated with d-block metals [21]. The study explores how this bismuth(I) complex undergoes oxidative addition with a variety of aryl electrophiles, including diazonium salts, iodonium salts, and challenging aryl iodides and aryl thianthrenium salts, typically requiring transition-metal catalysts (Figure 3). The reactivity of the *N*,*C*,*N*-bismuthinidene complex is made possible through both ground-state and photoexcited-state processes, where bismuth's ability to access multiple oxidation states facilitates the formation of stable aryl–bismuthonium complexes. Notably, the authors have demonstrated that by harnessing low-energy red light, the *N*,*C*,*N*-bismuthinidene complex can drive formal oxidative addition even with substrates that exhibit high reduction potentials such as aryl iodides and aryl thianthrenium salts, thereby expanding the scope of aryl electrophiles that can be subjected to oxidative addition. This mechanistic advancement, combined with the ability to operate under low-energy light

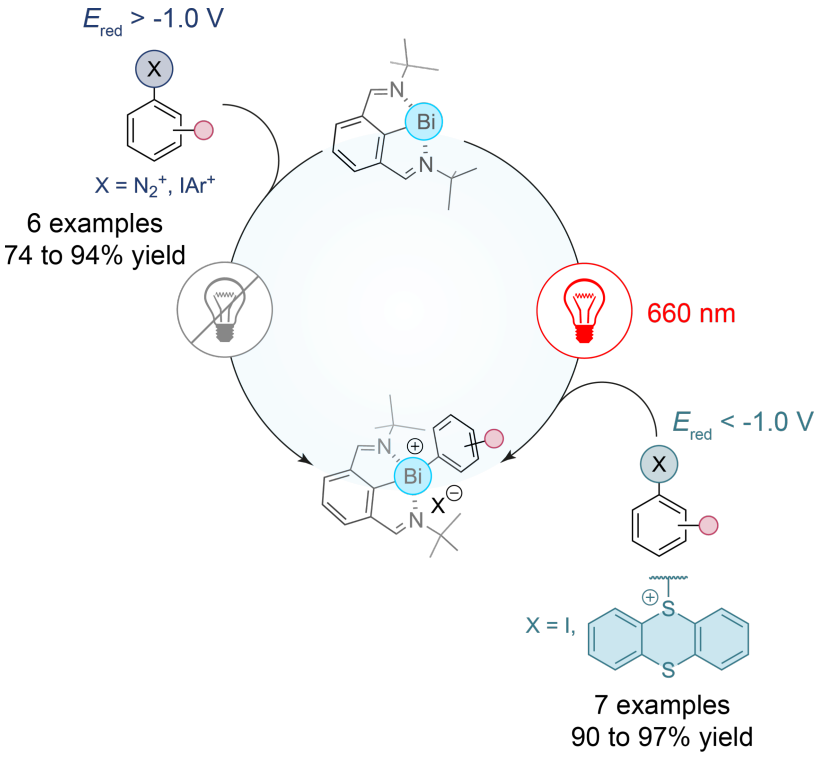

Figure 3: Red-light-mediated aryl oxidative addition with a bismuthinidene complex.

conditions, opens up new avenues for main-group redox catalysis in organic synthesis. By leveraging light excitation to enhance the reducing power of the bismuth complex, the study showcases the potential of main-group photoredox systems to complement traditional transition-metal catalysis. As the use of osmium catalysts has already demonstrated scalability in industrial applications [22], the introduction of bismuthinidene complexes presents another step forward in expanding the photoredox catalysis toolkit, potentially paving the way for more sustainable and efficient catalytic processes.

In the same way, recent advances in red-light photoredox catalysis have expanded the utility of first-row transition metals in a domain traditionally dominated by second- and third-row elements. A prime example of this evolution is the development of a dual photoredox strategy, which exploits the properties of red-light excitation while addressing the energy constraints posed by low-energy photons. Whereas multiple works addressing the upconversion phenomenon involving heavy metals like palladium, platinum [23,24] or osmium [25], grafted ruthenium complexes over ytterbium and thulium nanoparticles [26] and the use of a molybdenum-centered [27] and tungsten-centered complexes have been described in the literature [28]. The work by O. S. Wenger et al. introduces a system that mimics the Z-scheme of photosynthesis, utilizing a copper(I) bis(α-diimine) complex in combination with 9,10-dicyanoanthracene radical anion ($DCA^{\bullet-}$) [29]. This system effectively drives photoredox-mediated reduction and C–C cross-coupling reactions under mild red-light conditions with various aryl halides, an aliphatic iodide, and *O*- and *N*-tosylated substrates (Scheme 4a). The authors discuss two plausible mechanisms: a photoinduced electron transfer (PET) between the ^{3}MLCT state of the copper complex and DCA or a triplet–triplet energy transfer (TTET) between the ^{3}MLCT state of the copper complex and DCA. In both of these mechanisms, the involvement of a doublet excited-state of the radical anion of the DCA, photodegraded species issued from DCA or $DCA^{\bullet-}$/substract donor–acceptor complex is debated (Scheme 4b). Nevertheless, the authors underline that the key feature of these transformations is going through the consecutive absorption of two red-light photons which enhances the photoredox process by converting these latter into a higher-energy excited state (Scheme 4c) unlike what has been done until now with various described systems already discussed in the literature and emission of blue-light in the case of the triplet–triplet annihilation upconversion phenomenon among others (Scheme 4d) [30].

In a continuation of this trend, a recent study by O. S. Wenger et al. further expands the frontiers of red-light photoredox catalysis with first-row transition metals by introducing Cr(0) luminophores that exhibit photophysical properties competitive with Ru(II) and Os(II) complexes [31]. These new isoelectronic tris(diisocyanide)Cr(0) complexes, $[Cr(L^{Mes})_3]$ (Mes = mesityl) and $[Cr(L^{Pyr})_3]$ (Pyr = pyrenyl), display remarkably high metal-to-ligand charge transfer (MLCT) lifetimes of up to 47 ns and photoluminescence quantum yields as high as 1.04%. This surpasses previously reported first-row d^6 metal complexes such as Fe(II) complexes and positions Cr(0) as a promising alternative in photoredox applications under low-energy red-light conditions. The enhanced performance of these Cr(0) complexes is attributed to their strong ligand field, provided by the isocyanide ligands, which raises the energy of metal-centered states and minimizes non-radiative decay pathways. This design results in prolonged MLCT excited states, making these complexes suitable for challenging triplet–triplet energy transfer (TTET) and photoredox catalysis reactions such as hydrodehalogenation of aryl iodides, bromides and even chlorides **16** into **17** (Scheme 5).

This shift towards sustainable photocatalysis with first-row transition metals has been further emphasized by the work of O. S. Wenger et al. who has introduced another isoelectronic Cr(0) d^6 metal complex capable of sensitized triplet–triplet annihilation upconversion. This system achieves red-to-blue upconversion under red-light irradiation, rivaling the performance of traditional heavy-metal systems such as Os(II) complexes. By employing a Cr(0) photosensitizer combined with a silylacetylene-decorated anthracene annihilator, the authors have reported an upconversion efficiency of 1.8% and have demonstrated its utility in initiating blue light-dependent polymerization reactions under red-light conditions [32].

Beyond the position of transition metals in the periodic table, ligand design plays a crucial role in determining the photophysical properties of metal complexes. Phthalocyanins, porphyrins, and their derivatives exemplify this, as their rigid macrocyclic structures enable strong absorption in the visible to NIR regions, making them appealing for photoredox catalysis applications. For instance, ruthenium phthalocyanin complexes have emerged as potent catalysts for red-light-mediated photoreactions. Furuyama et al. demonstrated that a ruthenium phthalocyanin complex could catalyze trifluoromethylation reactions of styrene derivatives **18** with either CF_3SO_2Cl or Umemoto's reagent **19** under red-light irradiation without the need for sacrificial reducing agents (Scheme 6), contrasting with traditional blue-light photocatalysis which led to substrate decomposition [33,34]. The axial ligands on the ruthenium phthalocyanin complex, particularly electron-deficient pyridyl groups, were found to influence the catalytic activity by stabilizing the excited states and promoting metal-to-ligand charge transfer (MLCT) pathways, which is critical for efficient photoreactivity.

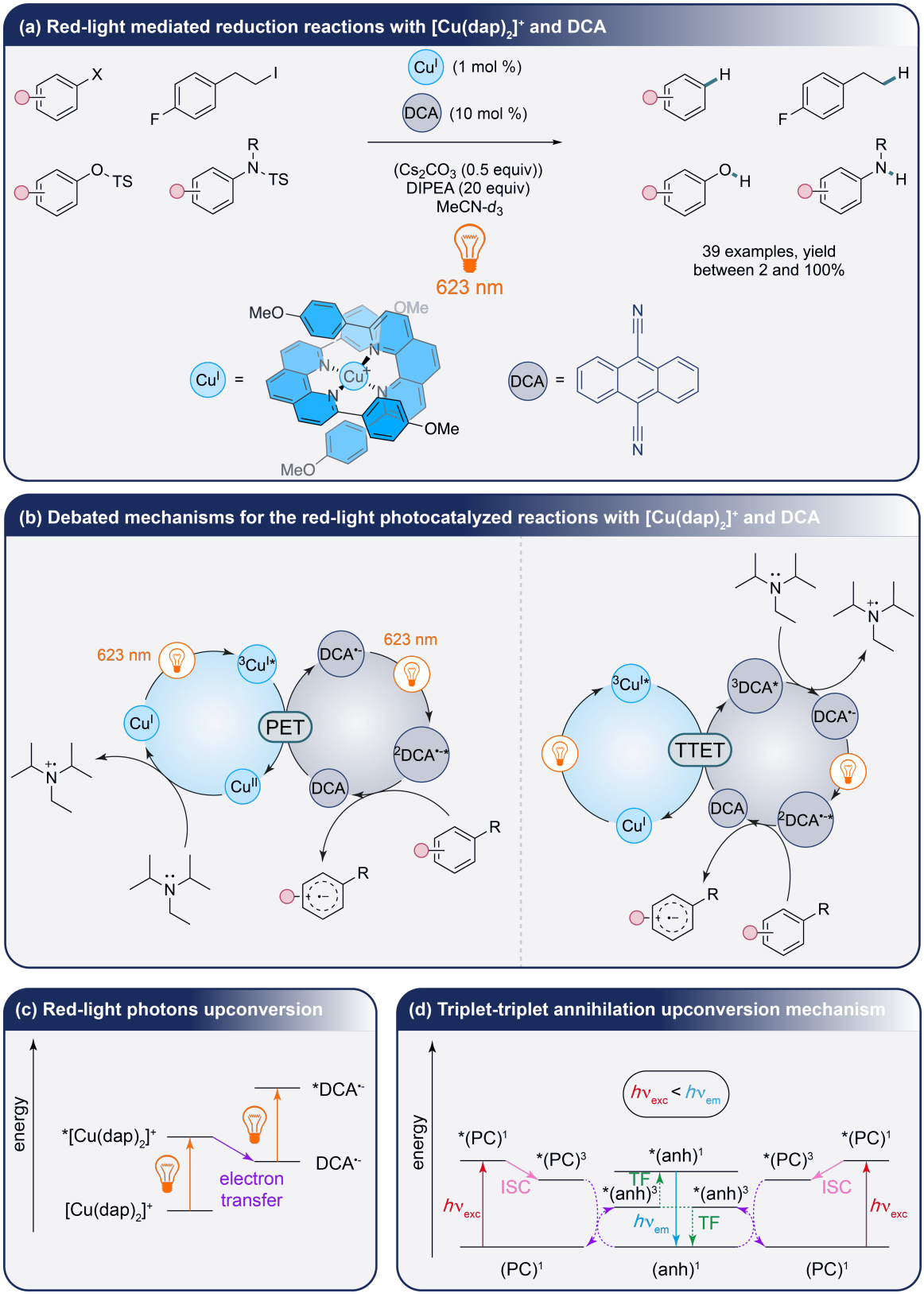

Scheme 4: Red-light-mediated reduction of aryl derivatives by O. S. Wenger et al. (PC = photocatalyst, anh = annihilator, ISC = intersystem crossing, and TF = triplet fusion).

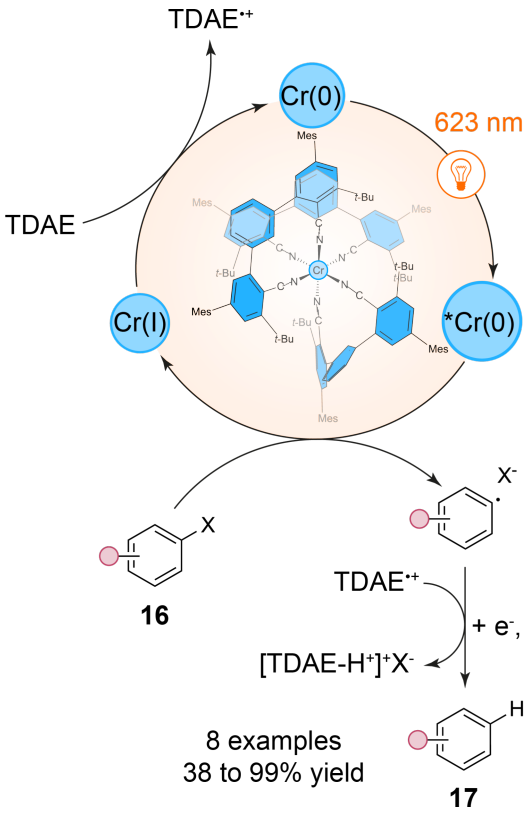

Scheme 5: Red-light-mediated aryl halides reduction with an isoelectronic chromium complex (TDAE = tetrakis(dimethylamino)ethylene).

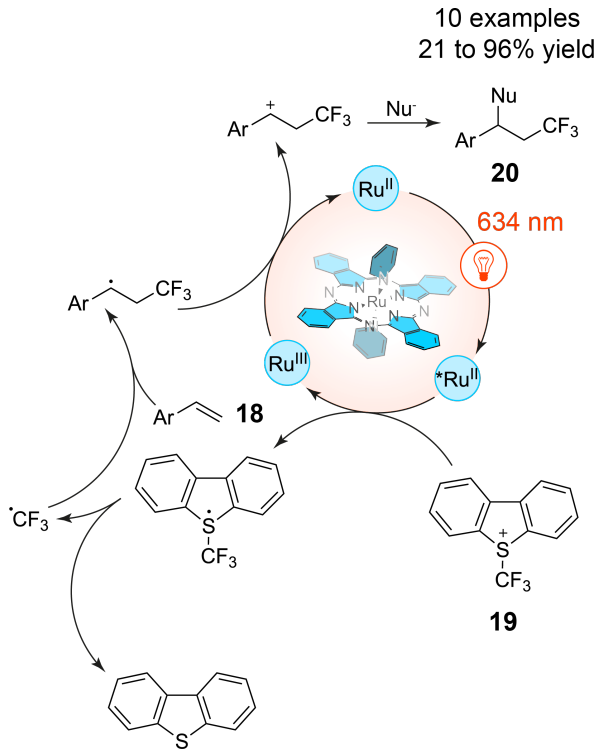

Scheme 6: Red-light-photocatalyzed trifluoromethylation of styrene derivatives with Umemoto's reagent and a phthalocyanin ruthenium complex.

Interestingly, phthalocyanin ligands are not only effective with precious metals but also exhibit catalytic performance when coordinated with first-row transition metals such as zinc as proposed by Furuyama et al. [35]. In this way, the authors have developed a series of phthalocyanin zinc complexes with electron-rich sulfur atoms at the non-peripheral positions of the phthalocyanin ring. This functionalization allows the destabilization of the highest occupied molecular orbital (HOMO), thereby shifting the absorption of the complexes into the NIR region (around 810 nm). The authors have demonstrated the efficiency of their photocatalyst in cross-dehydrogenative coupling reactions with *N*-phenyltetrahydroisoquinoline **21** and diverse nucleophiles (Scheme 7). Their photocatalyst has shown superior yields compared to free-base and other phthalocyanin first-row transition-metal complexes, such as nickel. The choice of solvent was also critical for optimizing the reaction efficiency: a mixture of pyridine and methanol not only improved the yield but also has helped to suppress side reactions. The cross-dehydrogenative coupling reactions, under near-infrared irradiation, was found to proceed via an energy-transfer mechanism involving singlet oxygen generation rather than the typical electron-transfer pathway observed in the presented visible-light-mediated reactions in this review hitherto. This singlet oxygen is generated by the energy transfer from the excited state of the phthalocyanin zinc complexes to molecular oxygen, allowing the oxidation of the *N*-phenyltetrahydroisoquinoline **21** into a reactive iminium intermediate that subsequently couples with nucleophiles to give **22**.

In a same manner, Opatz et al. have shown that zinc phthalocyanins can catalyze oxidative cyanation reactions of tertiary amines **23**, yielding α-aminonitriles **24** under continuous-flow conditions [36]. This reaction proceeds through the excitation of zinc phthalocyanin by near-infrared light (λ = 750 nm), followed by triplet energy transfer to molecular oxygen, generating singlet oxygen as the active species. Similarly as in the case of the Furuyama et al. study, the singlet oxygen subsequently oxidizes the amine substrate to an iminium ion, which reacts with a cyanide nucleophile to form the desired α-aminonitrile (Scheme 8). Notably, the authors have optimized the reaction conditions to achieve high yields across a wide substrate scope with more than 15 examples, including the cyanation of aliphatic amines such as tributylamine and sterically hindered substrates, which demonstrated the broad applicability of this photocatalytic system.

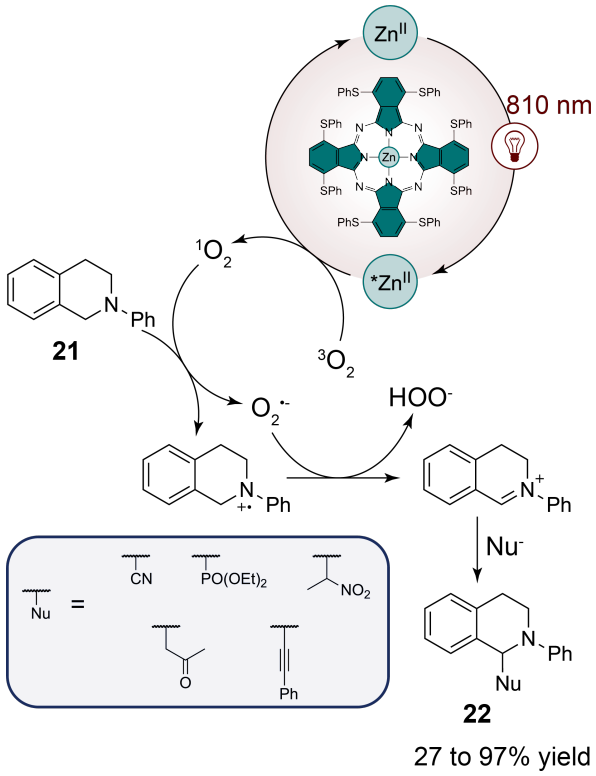

Scheme 7: Red-light-mediated energy transfer for the cross-dehydrogenative coupling of *N*-phenyltetrahydroisoquinoline with nucleophiles.

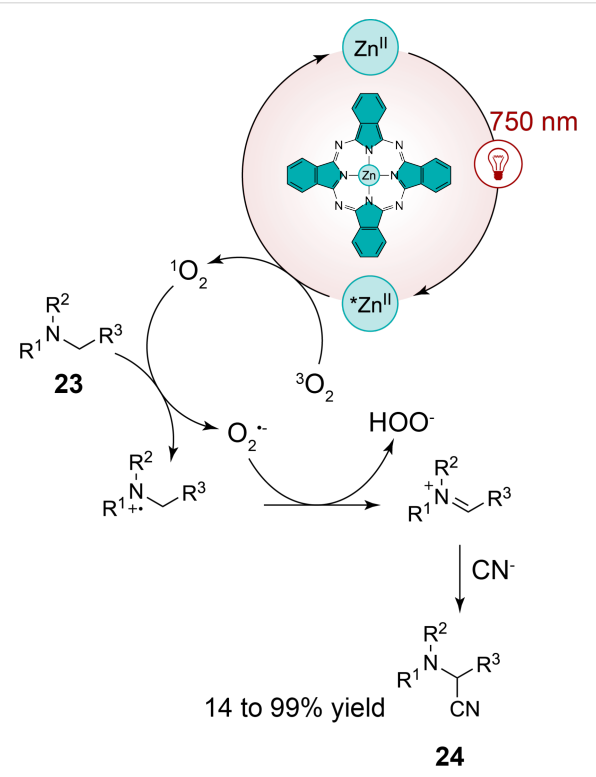

Scheme 8: Red-light-mediated oxidative cyanation of tertiary amines with a phthalocyanin zinc complex.

It has to be noted that zinc-based photocatalysts with phthalocyanin ligands are not limited to energy-transfer pathways involving singlet oxygen generation. A recent work by Yoshimitsu et al. has shown that zinc(II)-based porphyrin complexes can engage in electron-transfer mechanisms to enable radical cascade reactions under red-light irradiation (Scheme 9) [37]. These zinc(II)-based porphyrin catalysts operate via an oxidative quenching cycle, directly facilitating the transfer of an electron from the excited state of the porphyrin to the substrate, an activated ester **25**, subsequently generating carbon-centered radicals without the need for sacrificial electron donors via a decarboxylation process. In reacting with electron-deficient alkenes or alkynes **26**, these radicals further yield tetralin and dialin moieties **27**, respectively. Among their scope of 26 examples with yields ranging from 7 to 99%, the authors have shown that the use of dimethyl fumarate as a radicophile yielded the desired tetralin in 99% yield, while other radicophiles such as ethyl propiolate also furnished dialin products in high yields mainly superior to 70%.

Beyond their coordination with transition metals, phthalocyanin ligands also exhibit remarkable photoreactivity in supporting non-metallic central elements. Recent work by Amara et al. highlights the efficiency of silicon-based phthalocyanin complexes in red-light-driven photooxidation processes, marking a shift away from the reliance on traditional heavy-metal catalysts [38]. By utilizing silicon as a cheap, non-toxic, and abundantly available element, silicon-based phthalocyanin complex derivatives represent a more sustainable alternative to precious metal-based photocatalysts such as ruthenium or palladium complexes. The authors have focused on the photooxidation of β-citronellol (**28**), a key step in the production of industrial compounds like rose oxide (Scheme 10). Remarkably, the silicon phthalocyanins demonstrated exceptional stability under red-light irradiation, achieving up to 87% conversion in continuous-flow conditions. This performance is particularly notable given that the reaction was carried out using sub-part-per-million loadings of the catalyst (0.003 mol %), a stark contrast to traditional systems, which often require higher concentrations of heavy metals. Unlike classical transition-metal-based photosensitizers acting by triplet energy transfer for which high singlet oxygen quantum yields are crucial, the silicon phthalocyanins in this study have exhibited relatively low singlet oxygen quantum yield values (around 0.27 for the silicon-based photocatalysts used in this work). Despite this, their catalytic performance was not compromised. The key to their success lies in their resistance to photobleaching, which is a common issue for metal-based photocatalysts that degrade under prolonged exposure to light. The silicon-based phthalocyanin complexes maintained their structural integrity over extended reaction times, even under high substrate concentrations and

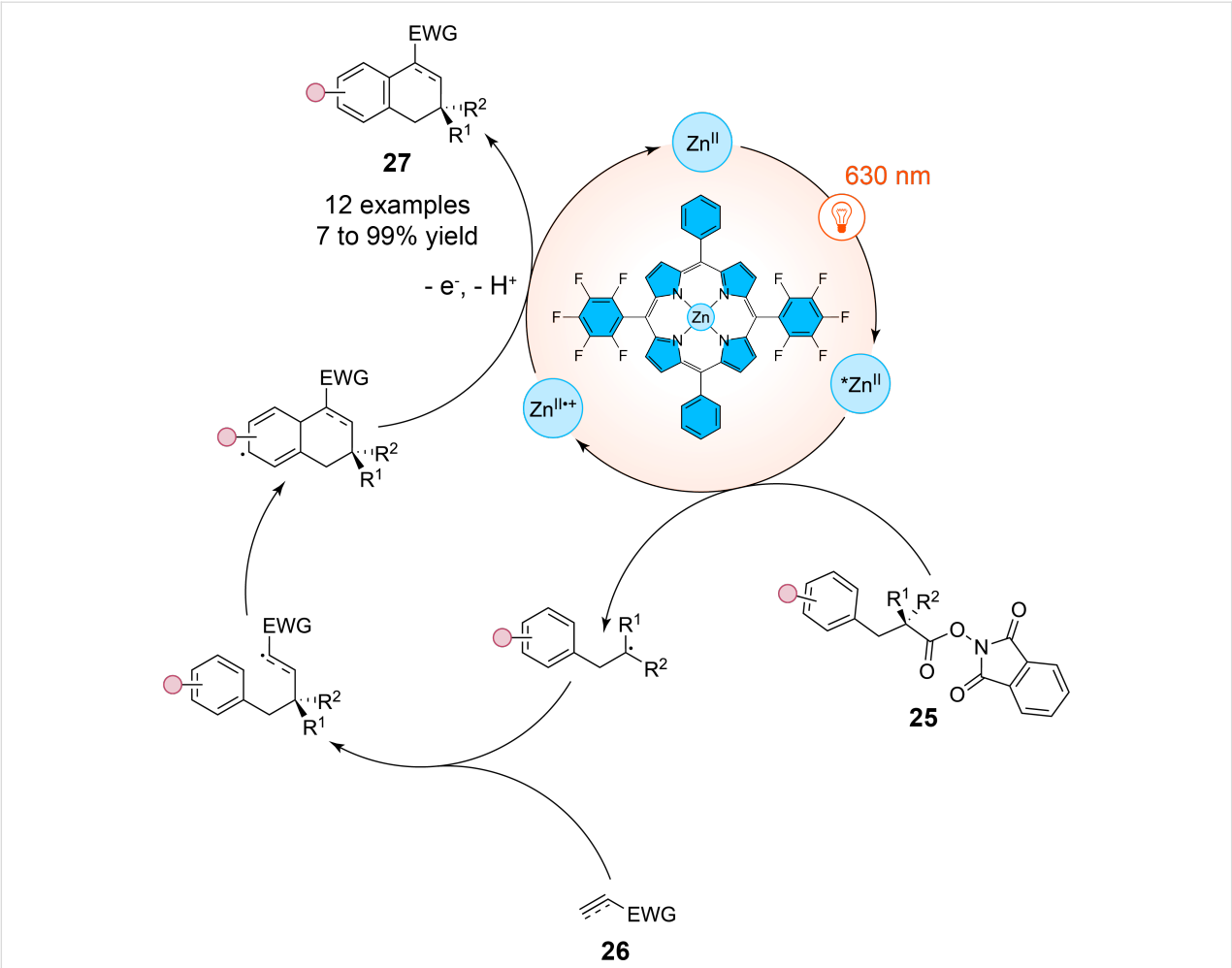

Scheme 9: Formation of dialins and tetralins via a red-light-photocatalyzed reductive decarboxylation mediated by a zinc(II) porphyrin complex.

continuous flow conditions, achieving high turnover numbers of over 50000. This stability allowed for solvent-free reactions, significantly enhancing the sustainability of the process. Additionally, the authors have explored the scalability of these systems, demonstrating their efficacy in multigram-scale photooxidations. The use of silicon-based phthalocyanin complexes in continuous-flow reactors not only increased the productivity of β-citronellol oxidation but also reduced the process mass intensity by a factor of four compared to batch processes using conventional solvents.

Recent advances have demonstrated that naturally derived photocatalysts, such as chlorophyll, a magnesium-based chlorin complex, can also efficiently drive photocatalytic transformations. In the study by Ouyang et al. chlorophyll extracted from spinach has been employed as a green and sustainable photocatalyst for the red-light-induced oxidation of organoboron compounds, a method that stands out for its environmental and operational simplicity [39]. The authors have developed a mild protocol utilizing red light to oxidize a wide range of organoboron substrates **31**, including -$B(OH)_2$, -Bpin, -BF_3K, and -Bneo (neopentyl borate) derivatives noted as "-[B]" in Scheme 11, to produce aliphatic alcohols and phenols **32** with moderate to excellent yields. The versatility of this method is highlighted by the broad substrate scope of more than 50 examples, which includes various aryl- and alkylboronates, showcasing its applicability across a range of chemical transformations. For example, phenylboronic acids with diverse substitution patterns (such as electron-donating and electron-withdrawing groups) were smoothly converted to the corresponding alcohols in yields ranging from 70% to 99%, with minimal byproducts. Even more complex substrates, like naphthalene and pyrene derivatives, underwent efficient oxidation, suggesting the method's utility in functionalizing more challenging aromatic frameworks. The mechanism of this reaction was explored in detail, and the authors have proposed that the reaction proceeds through a photoinduced electron transfer mechanism (Scheme 11). Upon red-light excitation, chlorophyll generates

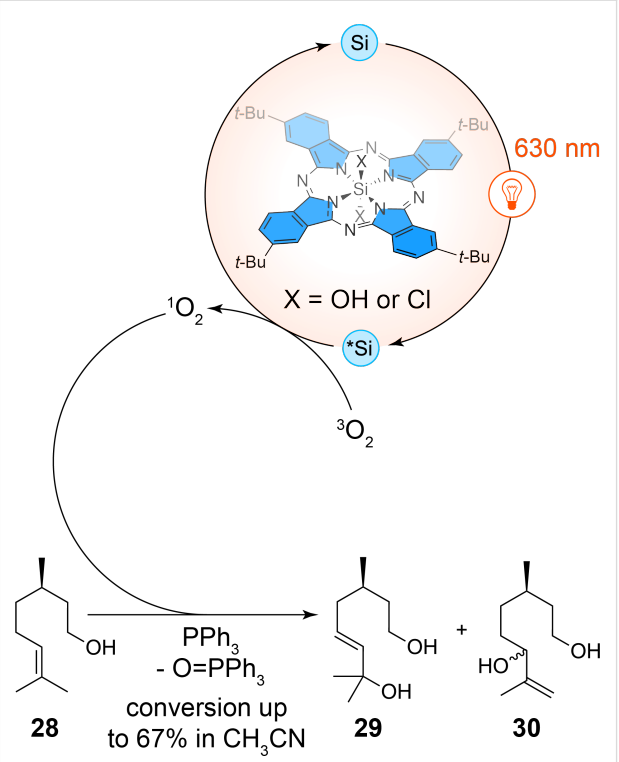

Scheme 10: Oxidation of β-citronellol (**28**) via energy transfer mediated by a red-light activable silicon phthalocyanin complex.

superoxide anion radicals ($O_2^{\bullet-}$) in the presence of oxygen, which act as the active oxidant to convert organoborons **31** to alcohols **32**. Notably, this protocol is both energy-efficient and operationally simple, with the reaction being carried out under air in ethanol, a low-toxicity solvent. Moreover, the scalability of the reaction was demonstrated with larger-scale experiments (up to 5 mmol), achieving excellent yields and minimal waste. The authors further showcased the robustness of the method by utilizing common kitchen equipment, mixing spinach extract with Baijiu (a traditional Chinese drink with a high level of ethanol) and stirring the reaction under sunlight, achieving yields as high as 60%. This demonstration underscores the practicality and accessibility of the method, even outside a laboratory setting. The green chemistry metrics analysis provided in the study confirms the environmental benefits, with high atom economy, low waste generation, minimal resource consumption, and the potential of porphyrin/phthalocyanin derivatives as ligand of high interest in red-light-mediated photocatalyzed transformations.

Red-light photocatalysis with organic molecules

While the use of metal-based porphyrin/phthalocyanin complexes has proven their efficiency in red-light-driven chemical transformations, it has to be noted that the photocatalytic efficiency of these molecules does not necessarily rely on the presence of a central metal atom. Free-base porphyrins, in particular, have demonstrated significant potential in red-light-driven transformations due to their versatile photophysical properties. These metal-free systems can function as both photooxidants and photoreductants, engaging in either energy-transfer or electron-transfer processes with high efficiency [40]. Notably, D. Gryko et al. demonstrated their application in activating diazoalkanes through red-light-mediated photosensitization and photoredox catalysis for carbene transfer reactions and radical-based functionalizations [41]. In another study by Derksen et

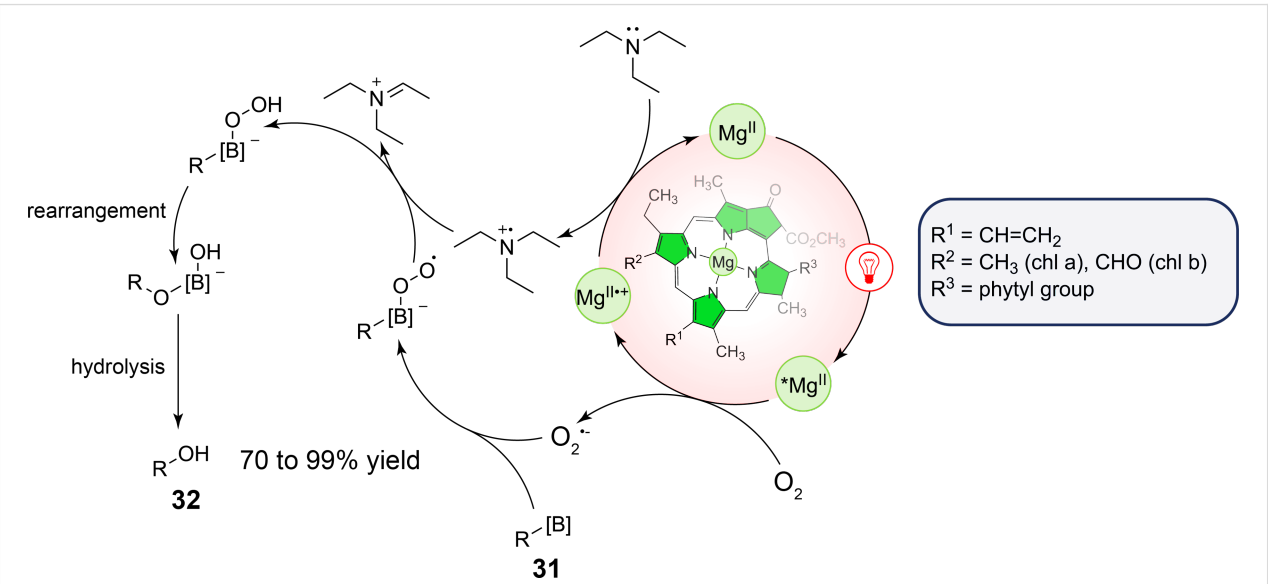

Scheme 11: Formation of alcohol derivatives **32** from boron compounds **31** using chlorophyll (chl) as a red-light-absorbing photocatalyst.

al., thiaporphyrins were introduced as highly effective catalysts for red-light-mediated photoreductive dehalogenation [42]. These thiophene-modified porphyrins exhibit excellent absorption properties beyond 645 nm, providing access to low-energy red-light-driven chemical transformations. The catalysts have successfully facilitated the dehalogenation of 18 different α-halo ketones **33** with minimal catalyst loading (0.1 mol %) and high yields under mild conditions. For instance, bromoacetophenone has been quantitatively reduced to the corresponding methyl ketone within one hour under red-light irradiation. The optimized reaction conditions proposed by the authors have demonstrated the superiority of thiaporphyrins over conventional metal-based systems like $Ru(bpy)_3Cl_2$. When tested, one of the thiaporphyrins has achieved significantly higher yields (75%) compared to the Ru-based photocatalyst, which has only afforded a modest 18% yield under similar conditions. This enhanced reactivity was attributed to the strong reduction potential of the thiaporphyrin catalysts and their ability to participate in hydrogen-atom-transfer mechanisms with a Hantzsch ester **34** as presented in Scheme 12. Moreover, the study has explored the impact of substrate steric hindrance and halogen bond strength on catalytic efficiency, revealing that bromo- and iodo-substrates react more efficiently, while chloro-substrates exhibit slower conversion rates.

In a similar way, recent advances have shown that synthetic bacteriochlorins, inspired by natural photosynthetic pigments, can also serve as effective photocatalysts under even longer wavelengths. In particular, Zhang et al. have explored the application of a man-made bacteriochlorin for photoinduced electron transfer-reversible addition-fragmentation chain transfer (PET-RAFT) polymerization under far-red light (Figure 4) [43]. This synthetic bacteriochlorin, structurally modified from tetraphenylporphyrin with two reduced pyrrole rings, exhibits strong absorption in the far-red region, providing excellent control over molecular weight and polydispersity in the polymerization of various monomers, including methyl acrylate. The authors highlight that under red-light irradiation, the bacteriochlorin catalyst has achieved 89% monomer conversion in just 12 hours, with molecular weights closely matching theoretical predictions and low polydispersity indexes. Even with reduced catalyst loadings (down to 10 ppm), the polymerization process has remained efficient, maintaining high monomer conversions and well-controlled molecular weights. What makes this approach particularly innovative is its ability to operate in the presence of oxygen, overcoming a common limitation in radical polymerization, and its demonstrated efficacy in penetrating biological tissues up to 7 mm thick.

Beyond the phthalocyanin/porphyrin family, other kinds of traditional organic photocatalysts have been extensively studied in the literature such as bridged Eosin Y **37** [44], BODIPY **38** [45], and dibenzothiazole **39** (Figure 5) [46]. Indeed, organic dyes, with their inherent advantages of low toxicity, environ-

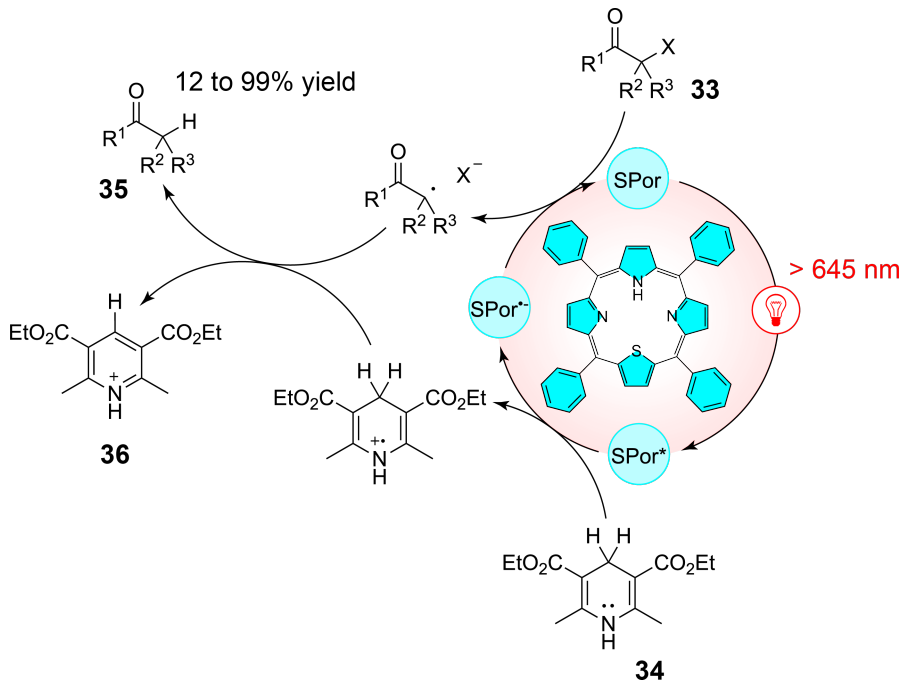

Scheme 12: Red-light-driven reductive dehalogenation of α-halo ketones mediated by a thiaporphyrin photocatalyst.

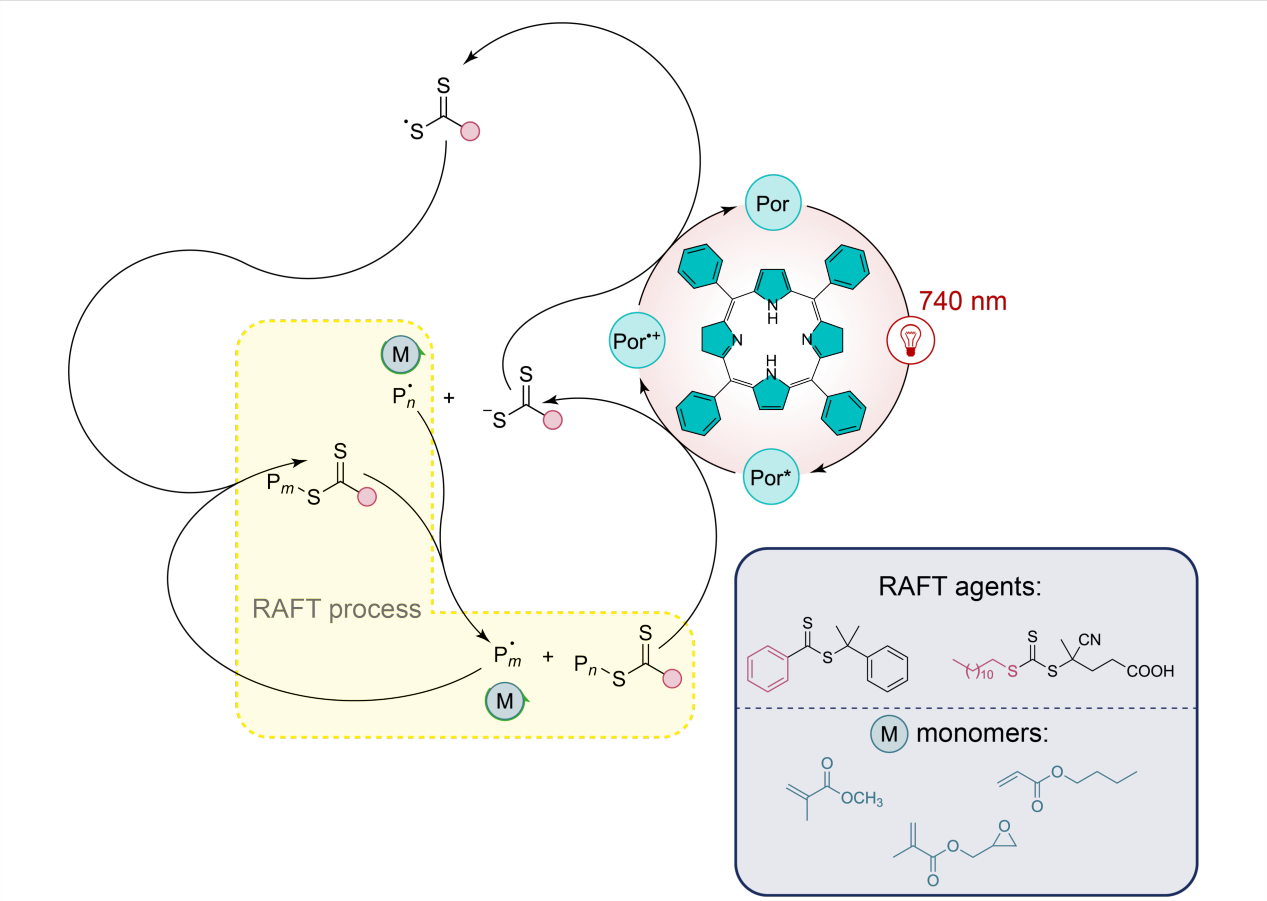

Figure 4: Photoinduced electron transfer-reversible addition-fragmentation chain transfer polymerization mediated by a red-light absorbing reduced tetraphenylporphyrin.

mental friendliness, and tunable optical properties, represent a promising alternative for red-light-mediated reactions. In particular, the versatility of these catalysts offers new avenues for facilitating red-light-driven chemical transformations with greater selectivity and efficiency.

Recently, the squaraine family, a class of organic compounds characterized by a four-membered unsaturated ring structure derived from squaric acid [47], has attracted attention due to its ability to promote single-electron transfer [48]. These compounds exhibit significant NIR fluorescence, making them valuable in applications such as biomolecule probing. Additionally, squaraine derivatives are well-established for their use in organic photovoltaic cells and as efficient photosensitizers for singlet oxygen generation. In 2022, Goddard et al. have reported the groundbreaking use of squaraine derivatives as novel organic NIR photocatalysts for various chemical transformations, marking the first application of these compounds in the field of photocatalysis [49]. The study has included a detailed mechanistic investigation to differentiate between competing single-electron transfer and energy transfer pathways. Through both experimental measurements and theoretical calculations, the authors have determined the redox potentials of several squaraine derivatives (**40**, **41**, **42**, and **43** presented in Figure 6a) which exhibit oxidation potentials at the excited state ranging from −1.22 V to −1.58 V vs SCE and reduction potentials at the excited-state between 0.84 V and 1.22 V vs SCE. In particular, derivative **40** has been proven to be the most efficient photocatalyst, promoting key transformations such as the aza-Henry reaction with **44** to give **45** under NIR light irradiation (Figure 6b). The reaction was found to critically depend on the presence of oxygen in the air for it to proceed. Through optimization and mechanistic investigations of the near-IR-photocatalyzed aza-Henry reaction, the authors have proposed either a single-electron transfer or an energy transfer mechanism. Additionally, the reaction displayed an unexpected sensitivity to the light wavelength used. Employing a higher-energy light source at 660 nm led to a reduction in the isolated yield from 70% to 56%. Despite the full conversion of the starting material, the overall efficiency was hindered by the formation of side-products. Furthermore, various nucleophiles were found to be compatible with this transformation.

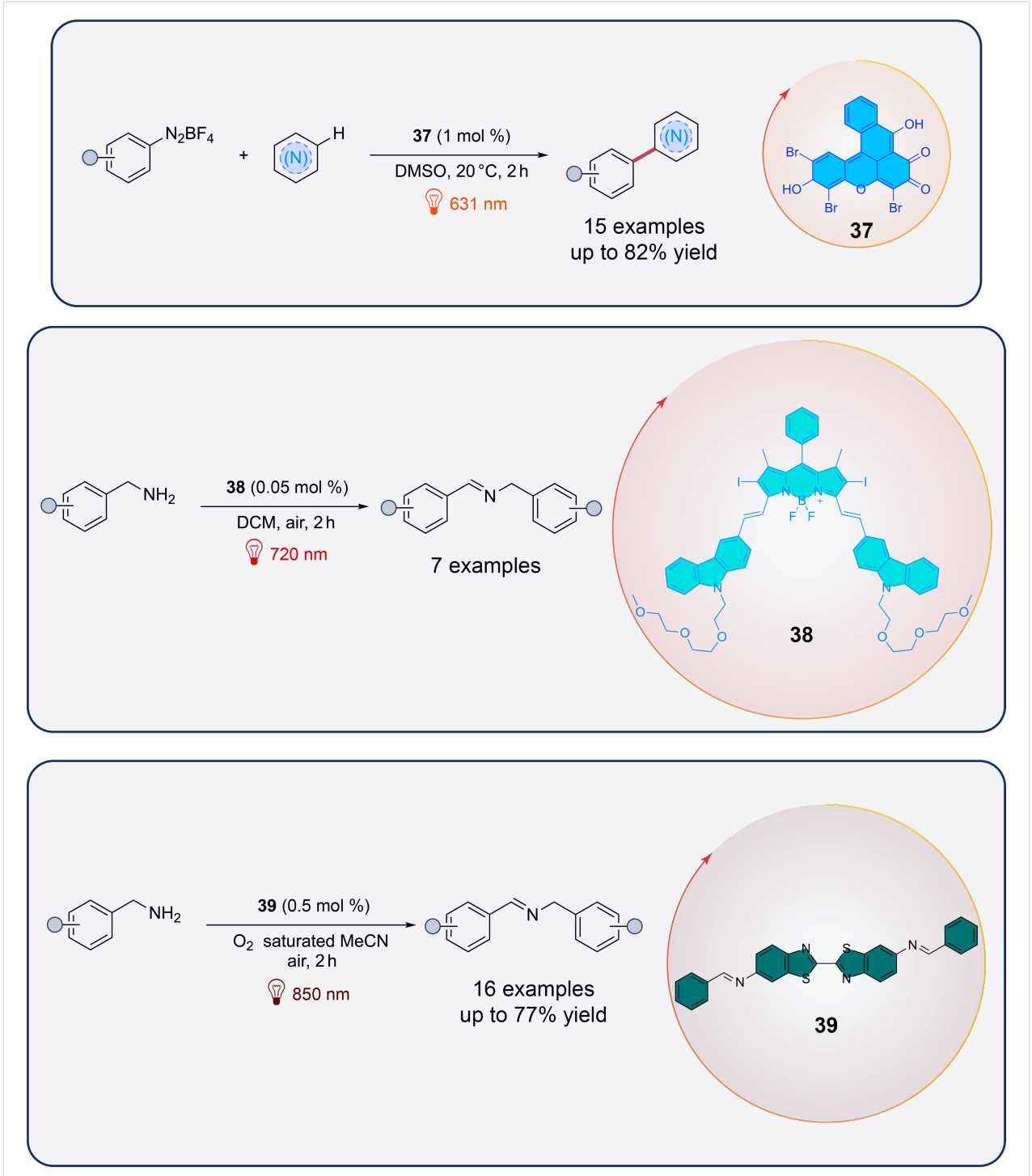

Figure 5: Recent examples of red-light-mediated photocatalytic reactions with traditional organic dyes.

In parallel the same team further proposed various infrared-mediated reactions catalyzed by **40** as presented in Figure 7.

It has to be noted that other squaraine derivatives have also been explored as innovative photoinitiators and photosensitizers for initiating the free radical polymerization (FRP) of methacrylates under near-infrared light exposure (Figure 8). Photopolymerization in this case is initiated by reduction of iodonium salts [50].

Following the exploration of squaraine derivatives and their applications in NIR-mediated photocatalysis, another class of

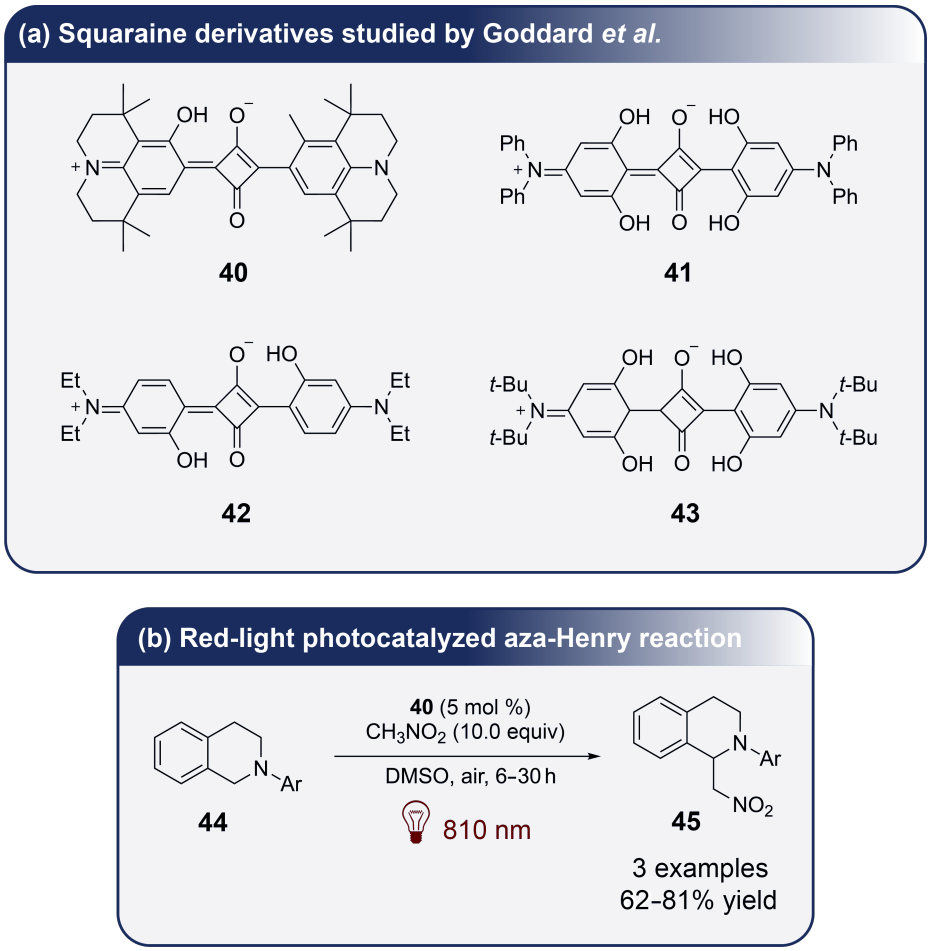

Figure 6: Squaraine photocatalysts used by Goddard et al. and aza-Henry reaction with squaraine-based photocatalyst **40**. Mechanism based on single-electron transfer and energy transfer.

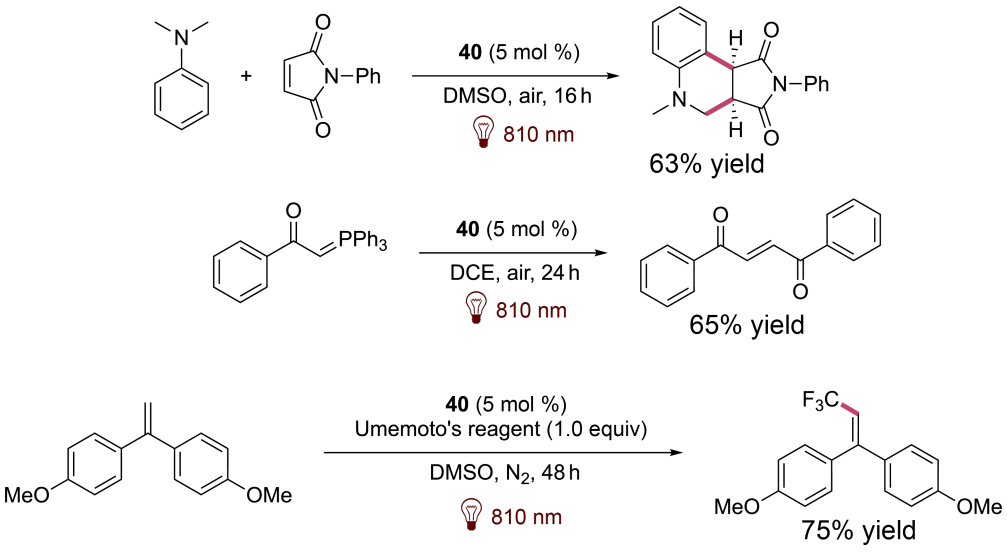

Figure 7: Reactions described by Goddard et al. involving **40** as the photocatalyst.

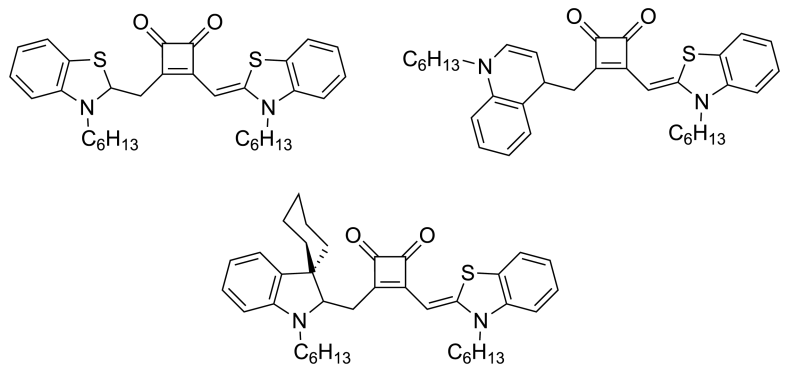

Figure 8: Various structures of squaraine derivatives used to initiate photopolymerizations.

compounds, cyanin molecules, has recently gained significant attention for their unique photophysical characteristics and versatility in NIR-driven reactions [51]. Cyanins consist of nitrogen-containing heterocycles connected by a polymethin chain [52,53], whose synthesis and modifications have been widely explored [54-56]. Such compounds exhibit remarkable redox versatility, enabling them to participate in both oxidation and reduction reactions and few of them are naturally occurring such as Betanin and Musca-Aurin II (Figure 9). Their relatively stable excited states, combined with their low toxicity and ease of chemical modification, make them a highly effective platform for improving reaction efficiencies. These molecules can facilitate single-electron transfer or energy transfer under mild conditions, and their structural diversity allows for fine-tuning of their redox potentials and light absorption characteristics. This adaptability makes cyanins ideal for a variety of synthetic applications, such as polymerization and radical-mediated reactions, often difficult for catalysts operating under visible light.

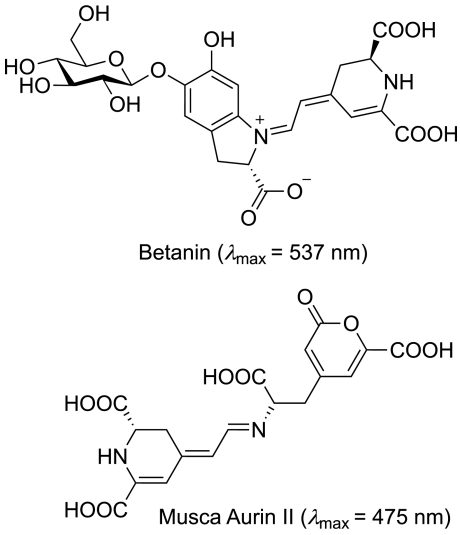

Figure 9: Naturally occurring cyanins.

Cyanin compounds can be categorized based on their structural motifs, such as closed-chain cyanins, streptocyanins, and merocyanins. These groups are distinguished by their terminal structures, which can range from heterocyclic to non-heterocyclic rings or even amino and carbonyl groups. Furthermore, cyanins can also be classified by the number of methine units in their polymethine chains, including monomethin, trimethin, pentamethin, and heptamethin derivatives. The length of the polymethin chain has a pronounced effect on their absorption properties, with the addition of each conjugated carbon–carbon double bond causing a red shift of about 100 nm in the absorption spectrum. The formation of *J*-aggregates allows cyanin compounds to narrow both absorption and emission peaks, along with a bathochromic shift in their spectra. Heptamethin cyanins, in particular, are highly relevant for NIR applications, making them valuable in photochemistry. Additionally, their solubilities, redox and photophysical properties can be fine-tuned through specific chemical modifications, further enhancing their versatility for a range of synthetic and photophysical applications as well as preventing their photodegradation (Figure 10) [57-60].

The use of cyanins as near-infrared photosensitizers was first introduced in photopolymerization processes. Cyanins have been shown to effectively initiate radical polymerization under visible light through mechanisms such as borate oxidation [61] and 1,3,5-triazine reduction [62]. More recently, cyanin dyes have enabled the reduction of iodonium salts under NIR excitation [63,64]. These preliminary findings suggest that cyanins, specifically tailored to absorb in the NIR region, exhibit promising redox properties for applications in organic synthesis. A recent work by Goddard et al. has demonstrated that compound **46** is highly effective in various photoredox transformations, such as aza-Henry reactions with nucleophiles like malonates, cyanides, and phosphites. The study further revealed that the

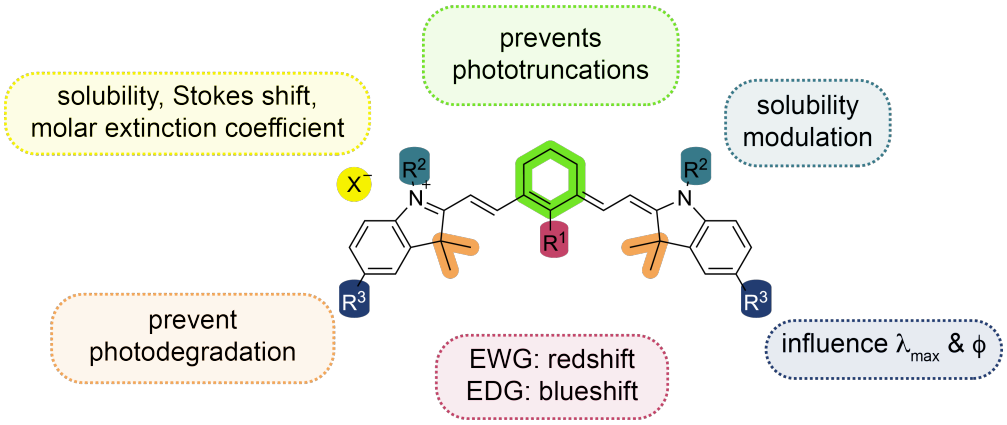

Figure 10: Influence of the structure on the photophysical properties of a cyanin dye.

radicals generated from these processes can be successfully utilized in dual catalysis with copper, yielding a variety of alkynylated products (Figure 11) [65].

Compound **46** has been shown to exhibit redox properties similar to those of squaraine derivatives, enabling key transformations such as the cyclization of anilines with maleimides and the reduction of Umemoto salts for trifluoromethylation of alkenes. With an excited-state reduction potential around 0.80 V, **46** demonstrates the capability to oxidize boronic acids such as **47**, producing the corresponding alcohols **48** via a single-electron-transfer mechanism that leverages atmospheric oxygen (Scheme 13).

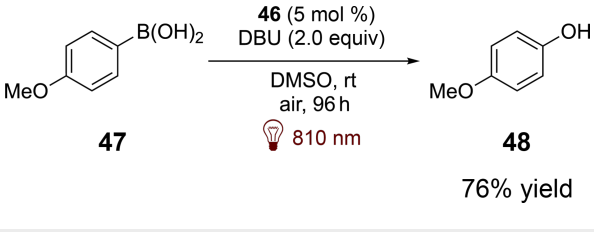

Scheme 13: Photocatalyzed arylboronic acids oxidation by **46**.

While the initial photocatalytic results using NIR-irradiated **46** were promising, the overall reaction kinetics were relatively slow. In response, Goddard et al. have developed a second generation of cyanin dyes. For example, in the case of the photocatalyzed trifluoromethylation of alkenes, it has been shown that the stability of the photocatalyst was crucial for achieving efficient and faster conversion. In their study, the authors have reported the synthesis and characterization of over 20 new cyanins, reporting their synthetic applications and both calculated and measured their photophysical properties and redox

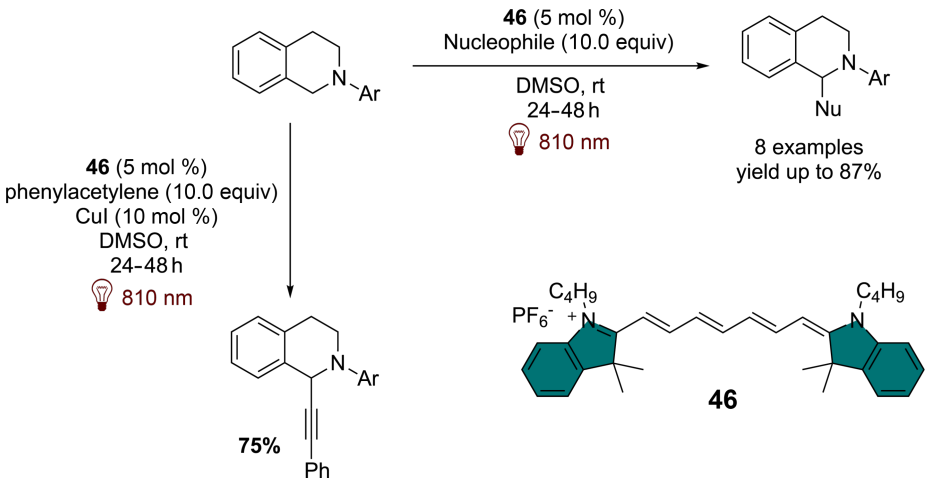

Figure 11: NIR-light-mediated aza-Henry reaction photocatalyzed by **46**.

potentials [66]. The study shows that substituents at the central position of the polymethin chain significantly affect their redox properties (Figure 12). Cyanins with electron-donating groups (e.g., **49** and **50**) are less oxidizing, with cathodically shifted reduction potentials compared to the unsubstituted **46**. In contrast, cyanins with electron-withdrawing groups (e.g., **51** and **52**) show anodically shifted reduction peaks, making them more oxidizing. Extended conjugation in cyanins (e.g., **53** and **54**) further increases their oxidizing nature at the ground state. Overall, both central substitution and extended conjugation play crucial roles in determining the redox behavior of these dyes. Cyanins with an amino group on the heptamethin chain have been proven to be the most effective photocatalysts for accelerating the aza-Henry reaction. The differing reaction kinetics and tests with 9,10-dimethylanthracene suggest that a cooperative mechanism involving both single-electron transfer and singlet oxygen generation via energy transfer likely drives the product formation. In a related study on the reduction of Umemoto salts for trifluoromethylation of alkenes, most photocatalysts showed instability under the experimental conditions. However, **54** has emerged as the most stable and efficient NIR photocatalyst, facilitating the trifluoromethylation even under low-energy irradiation at 940 nm.

Another emerging class of catalysts that has garnered attention for its applications in NIR photocatalysis is helical carbenium

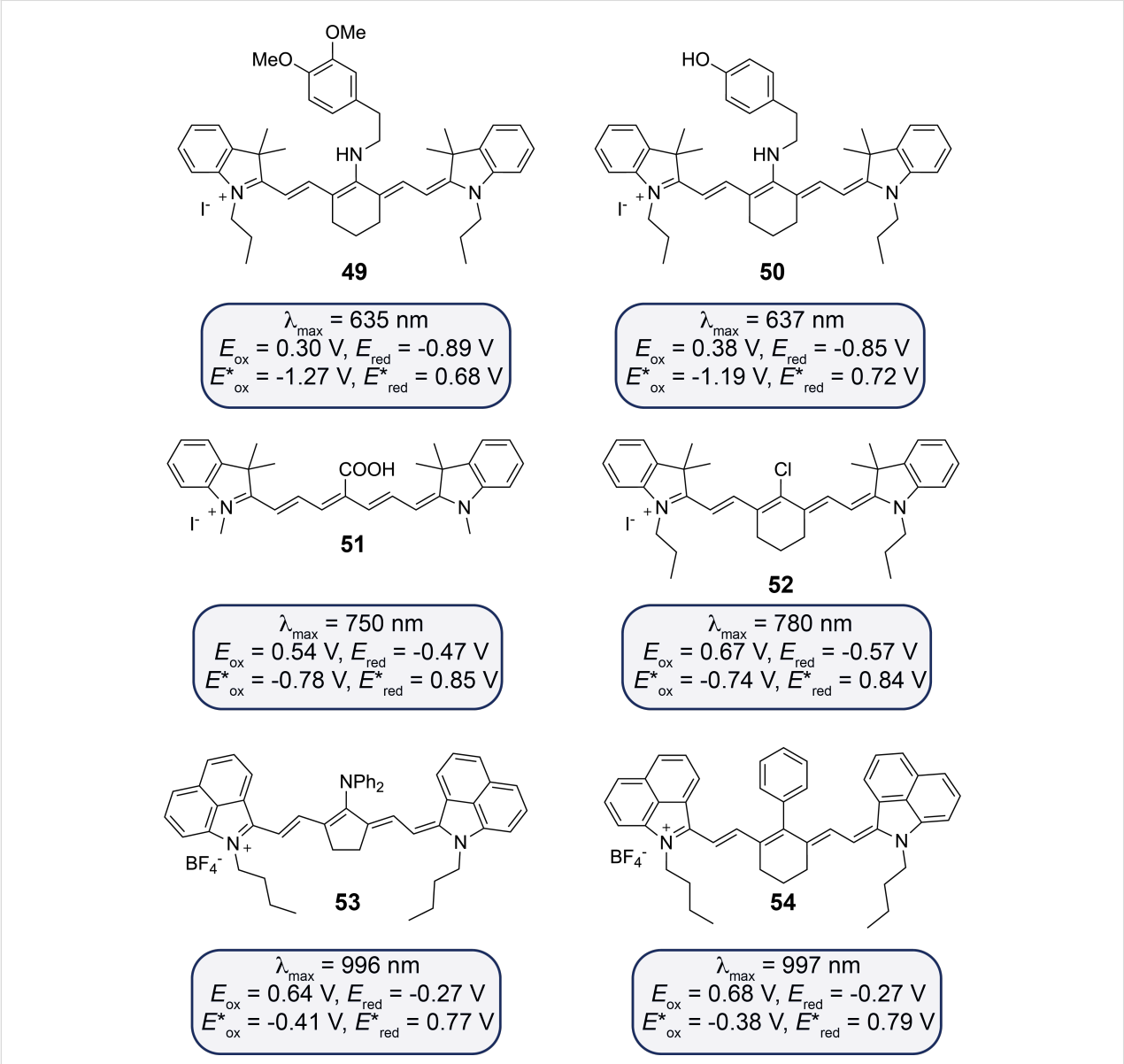

Figure 12: Cyanin structures synthetized and characterized by Goddard et al. (redox potentials given against saturated-calomel electrode (SCE)).

ion-based systems. These systems, characterized by their distinct helical structures and robust redox behavior, represent a novel approach to harnessing NIR light for challenging chemical transformations. The helical carbenium ion, dimethoxyquinacridinium ($DMQA^+$) and its synthesis, has been extensively studied for its photophysics, making it a subject of significant interest in the field of photocatalysis [67,68]. Based on previously observed results, Gianetti et al. have speculated that *N*,*N*′-di-*n*-propyl-1,13-dimethoxyquinacridinium (**55**, DMQA) tetrafluoroborate could serve as a versatile NIR organic photocatalyst [69]. Redox potentials of this photocatalyst engaged in both oxidative quenching and reductive quenching cycles have been calculated and have indicated that this latter could be a viable candidate for use in photoredox catalysis. Additionally, its measured excited-state lifetime (τ = 5.5 ns) is similar to those of other widely used organic photocatalysts, such as carbazole derivatives, further supporting its potential applicability [70]. Values are given in Figure 13.

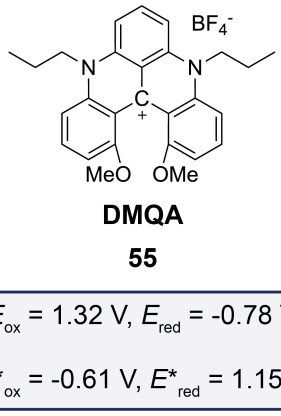

Figure 13: *N*,*N*′-Di-*n*-propyl-1,13-dimethoxyquinacridinium (**55**) with its redox potentials at its ground state and excited state (values given against saturated-calomel electrode (SCE)).

The first results obtained in organic synthesis have consisted in the dual Pd/DMQA-catalyzed C(sp^2)–H arylation with aryldiazonium such as **56** with lactam derivative **57**, which have leaded to similar results as the traditionnal use of $Ru(bpy)_3^{2+}$ with the formation of **58** in 95% yield (Scheme 14).

Similarly, the photoinduced aerobic oxidative hydroxylation of arylboronic acids **59** has been successfully accomplished. Since

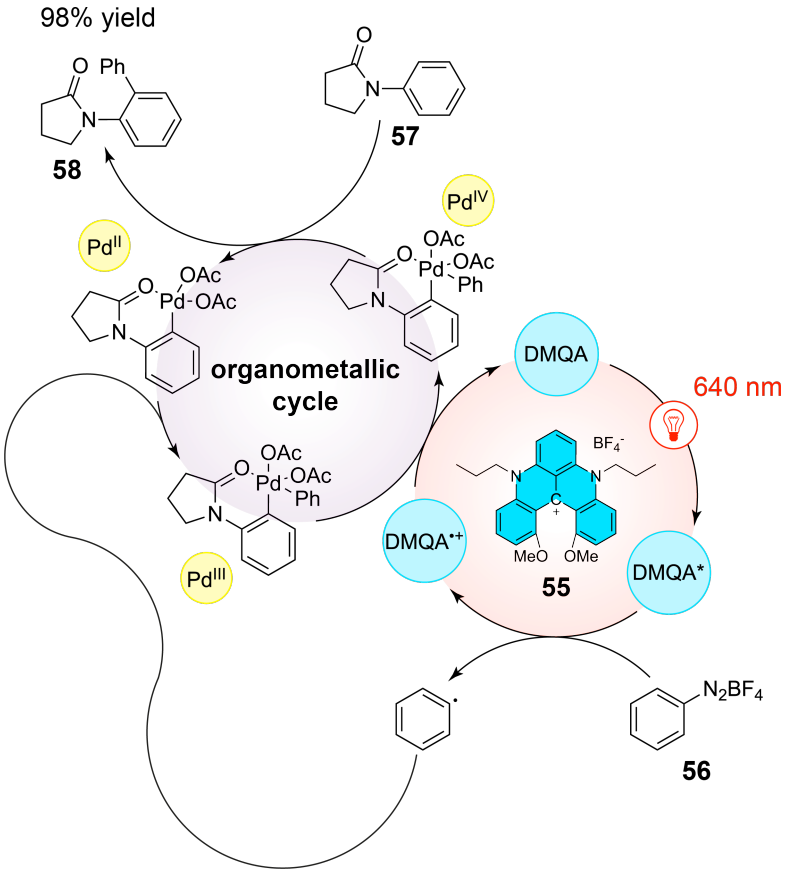

Scheme 14: Dual catalyzed C(sp^2)–H arylation of **57** using DMQA **55** as the red-light-absorbing photocatalyst.

this reaction does not depend on the presence of singlet oxygen, it confirmed the electron-transfer capability of the DMQA catalyst, which operates through a reductive quenching mechanism. A suitable reaction pathway was established, leading to moderate to excellent yields of the corresponding phenols **60** (Scheme 15). The reaction primarily involves the oxidation of iPr_2NEt (DIPEA) by the excited photocatalyst **55** to generate the radical cation $iPr^2NEt^{\bullet+}$ ($iPr_2NEt/iPr^2NEt^{\bullet+}$ = +0.72 V vs SCE) and the reduction of O_2 by the reduced photocatalyst, forming the superoxide radical anion $O_2^{\bullet-}$ ($O_2/O_2^{\bullet-}$ = −0.57 V vs SCE). This latter can then react with arylboronic acids **59** to give, after hydrolysis, phenol derivatives **60**.

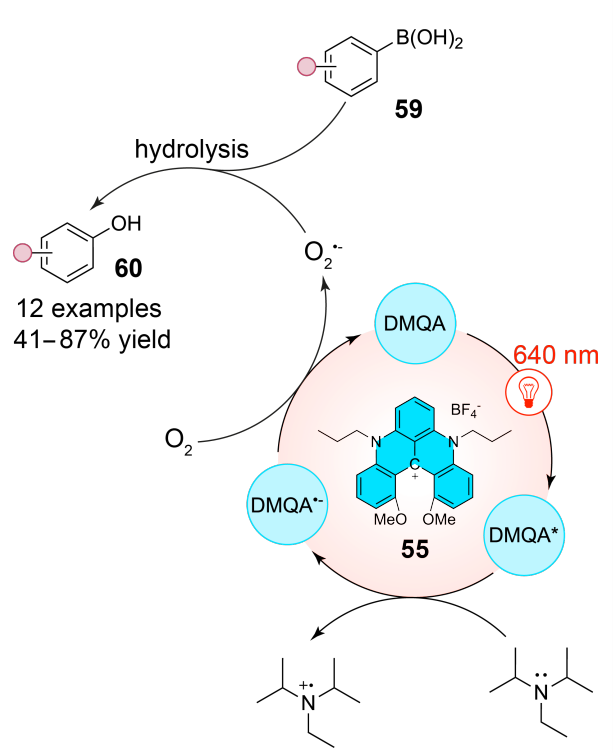

Scheme 15: Red-light-mediated aerobic oxidation of arylboronic acids **59** into phenols **60** via the use of DMQA as the photocatalyst.

Other transformations have been addressed by Gianetti et al. such as C(sp^3)–H oxidation, intermolecular atom transfer radical addition and C(sp)–H arylation using red light and DMQA (Figure 14), hence showing the great versatility of this photocatalyst.

Red-light photocatalysis in biological systems

Photochemical reactions are of high interest for being applied in biological or medicinal domains. However, the weak light penetration of biological tissues limits the application to surface processes. The penetration of NIR light is considerably better [71]. Consequently, many photochemical processes are currently

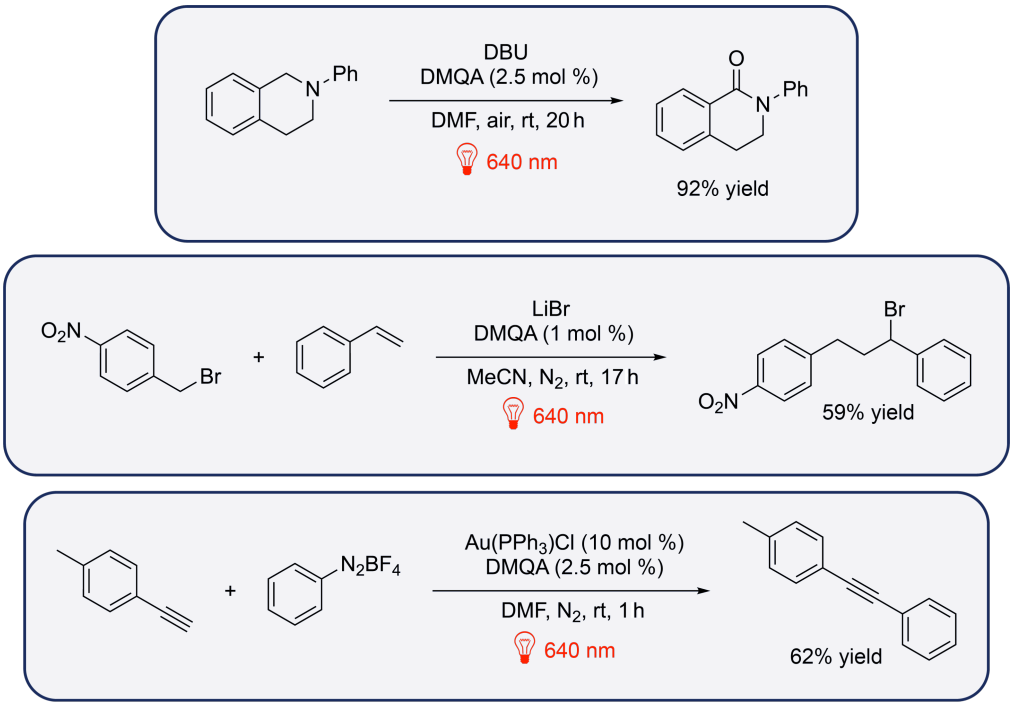

Figure 14: Red-light-photocatalyzed reactions proposed by Gianetti et al. using DMQA as the photocatalyst.

studied using NIR light [72]. This approach considerably enlarges the application of photochemical reactions to medicine.

The peroxynitrite anion ($ONOO^-$) plays an important role in many diseases such as diabetes, neurodegenerative disorders, or inflammatory diseases [73]. In order to study the mechanisms of the biological activity and to find biomedical applications, different releasing systems of this anion are developed. The peroxynitrite anion is formed by coupling of nitric oxide (NO) and the superoxide ($O_2^{\bullet -}$). An efficient system has been developed to realize this reaction (Scheme 16) [74]. In a photocatalytic reaction, NO is released from the corresponding com-

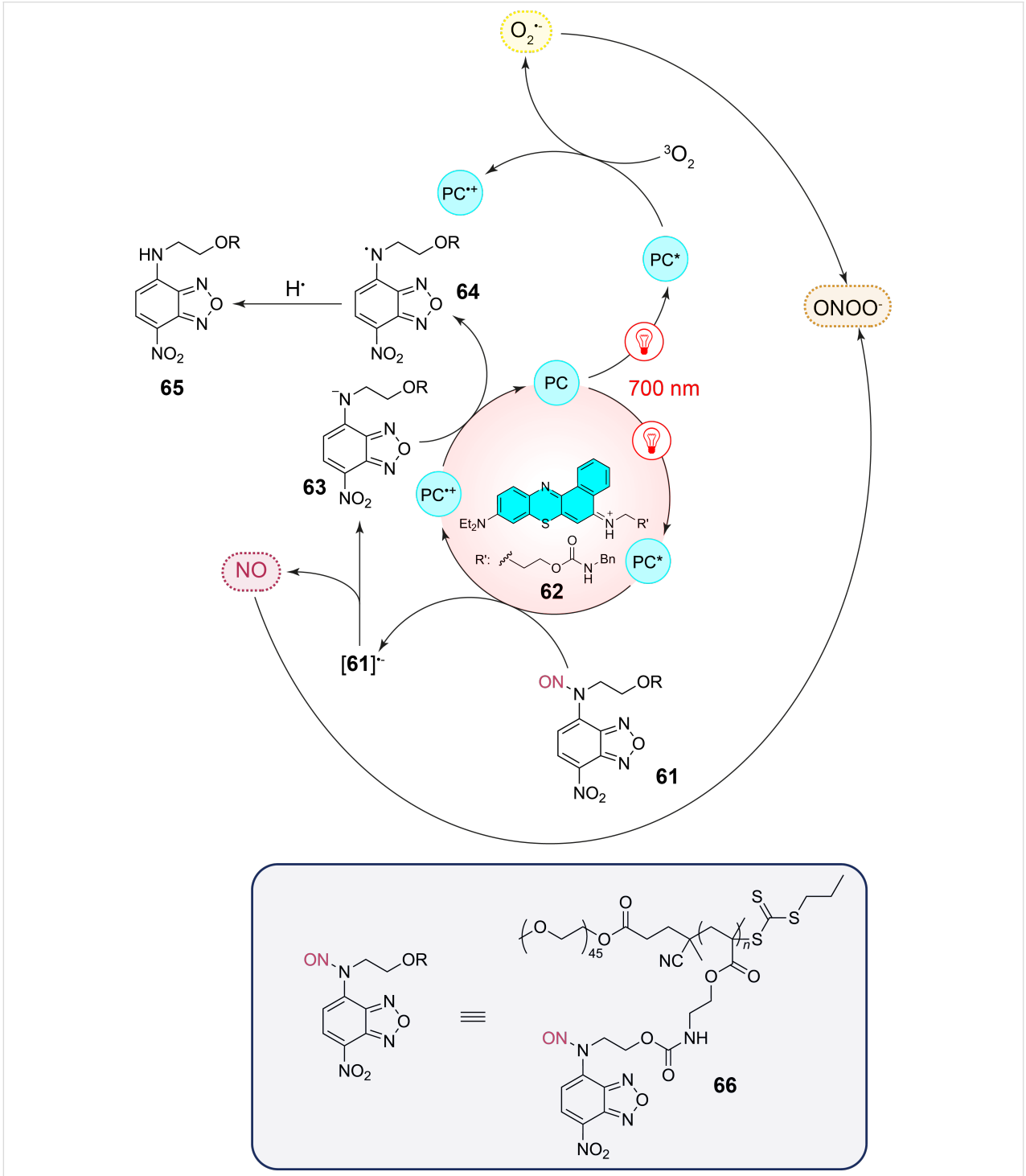

Scheme 16: Simultaneous release of NO and production of superoxide ($O_2^{\bullet -}$) and their combination yielding the peroxynitrite anion ($ONOO^-$).

pound **61**. Nile blue **62** is used as photocatalyst (**PC**). After photochemical excitation with NIR light (λ = 700 nm), electron transfer occurs from the catalyst to compound **61**. This step is most probably favored by the formation of a precursor complex involving π–π-stacking [75]. The resulting radical anion releases NO also yielding the anion **63**. Electron transfer to the radical cation of the photocatalyst regenerates it. In this step, the neutral radical **64** is also formed. Hydrogen abstraction (hydrogen atom transfer, HAT) yields compound **65**. NO and the superoxide ($O_2^{\bullet-}$) are simultaneously produced by the same photocatalytic system. In order to favor their combination leading to the peroxynitrite anion ($ONOO^-$), the NO-releasing structure is incorporated in a polymeric structure **66** which generates micellar nanoparticles. The substituent R' in the photocatalyst **62** favors its incorporation in the nanoparticles. Thus, both reaction partners are approached.

A similar photocatalytic system has been developed for the release of nitric oxide (Figure 15) [76]. Meanwhile, numerous applications of the NO release to medicine have been studied [77]. In the present case a palladium porphyrin complex is used as photocatalyst and a coumarin derivative is used as NO donor when the irradiation is carried out at λ = 630 nm. NO is released in a photoredox catalytic process and both reaction partners are covalently bound in a block copolymer which forms micelles. This method has been developed in the context of the treatment of intervertebral disc degeneration caused by bacterial infection. It also inhibits the inflammatory response and osteoclast differentiation in the intervertebral disc tissues. The present coumarin derivative is also capable of releasing nitric oxide by direct UV light absorption. However, this method, although simpler, is not suitable for the present medicinal application.

The space and time-controlled release of bioactive compounds is an important tool in bio- and medicinal chemistry to study biochemical mechanisms or to develop new therapeutic methods [78-80]. Such reactions can be performed at particular locations such as DNA or tubulin, when the photocatalyst is placed via a tethered ligand (Scheme 17) [81]. In the present case, the triarylmethine dye **67** was used as sensitizer. It is in equilibrium with the lactone form **68** and can bind either to tubulin or DNA depending on the conjugate R. The lactone form enables cell-permeability. The bioactive compound **69** causes microtubule depolymerization and it is caged in the dihydrotetrazine derivative **70**. Upon photocatalyzed oxidation, the corresponding tetrazine compound **71** is formed. This reaction only occurs close to the photocatalyst or sensitizer fixed at the intracellular target, for example at tubulin. An intramolecular Diels–Alder reaction followed by nitrogen extrusion generates the intermediate **72**. In the following uncaging step, the

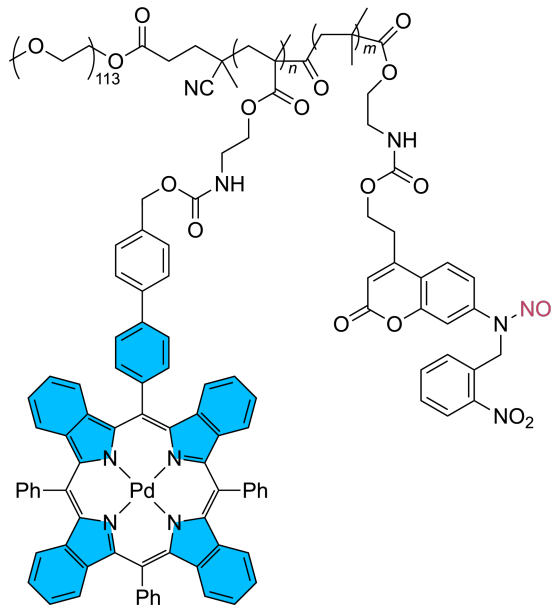

Figure 15: Palladium porphyrin complex as the photoredox catalyst and the NO releasing substrate are linked in the same block copolymer.

active compound **69** is released and aromaticity is regenerated in the pyrazine derivative **73**. An extracellular reaction of the system is quenched by ascorbate (low permeability) thus inhibiting the photooxidation of **70**.

Systematic uncaging of drugs is an important topic in medicinal chemistry and general methods for this purpose are of high interest. Phenyl radicals **74** can be produced from the corresponding arylboronic acid precursors **75** (Scheme 18) and the addition of oxygen leads to the hydroperoxide **76** [82]. The latter undergoes fragmentation releasing the drug, quinomethene **77**, and carbon dioxide. By this route baclofen, vorinostat, or AA147 were uncaged.

Near IR irradiation (λ = 660 nm) can also be used to transform aromatic azides **78** into corresponding aminyl radicals **79** in a photoredox catalytic process (Scheme 19) [83]. In this case, a tin chlorin e6 complex [Sn(IV)] is used as photoredox catalyst, which, after photochemical excitation, is easily reduced to [Sn(III)]. Among the investigated compounds for this purpose, NADH was the best reductant. The tin(III) species reduces the azide **78** and the resulting radical anion **80** yields aminyl radicals **79** after protonation and release of nitrogen. These radicals have been added to enzymes such as carbonic anhydrase which in this way was labeled in vitro with biotin. In a cellular context, the tin chlorin e6 complex [Sn(IV)] was also conjugated to antibodies and thus transferred to epidermal growth receptor (EGFR), a cell surface receptor tyrosine kinase. Under

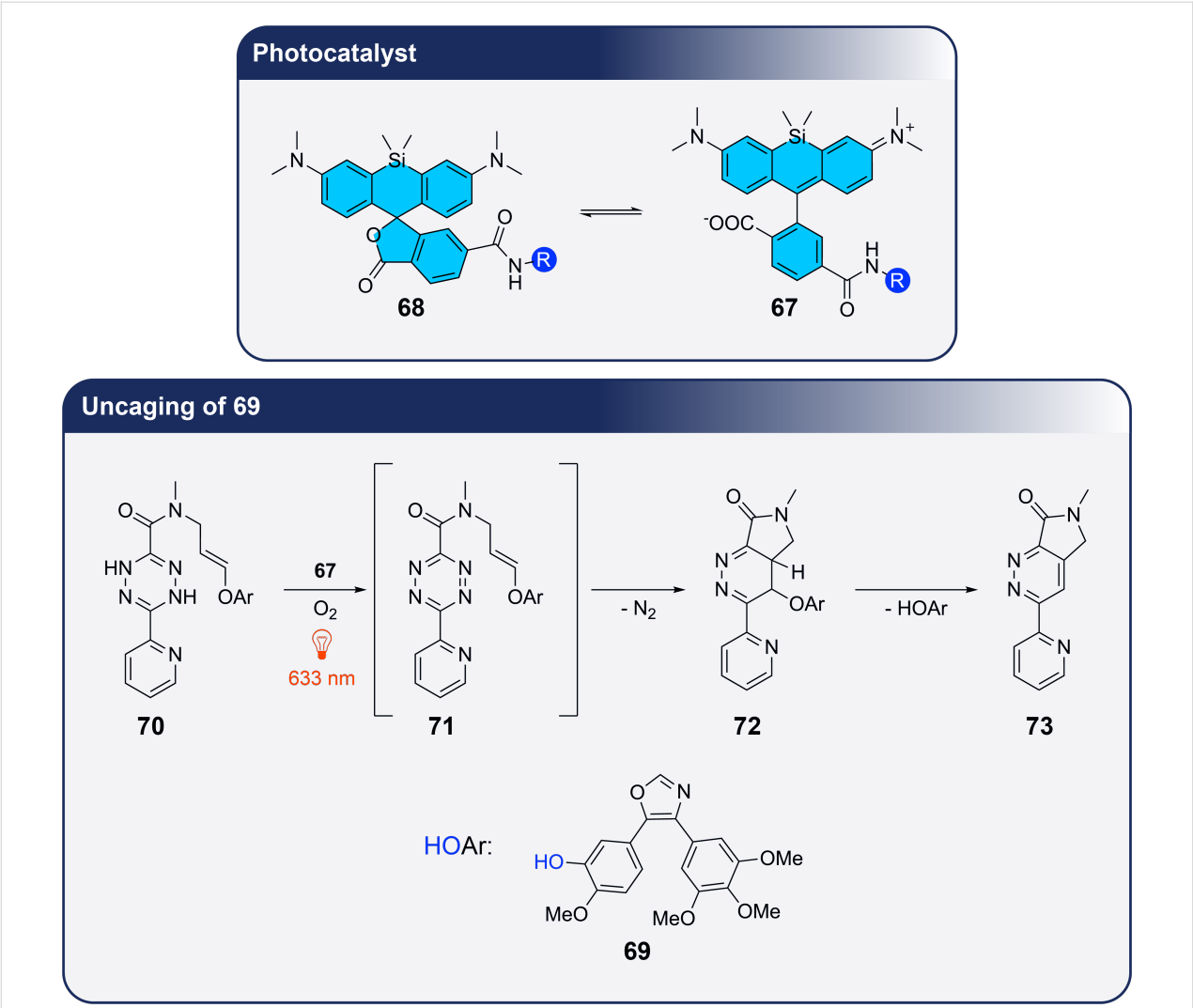

Scheme 17: Uncaging of compound **69** which is a microtubule depolymerizing agent using near IR irradiation. The sensitizer is attached to tubulin with the docetaxel conjugate (R).

these conditions, biotinylation was carried out only at the cell surface close to the sensitizer marked antibodies. The technique was also applied to the labeling at the erythrocyte surface. The method was studied as well with more conventional iridium-based photoredox catalysts absorbing light in the range of $390 < \lambda < 470$ nm. However, tissue penetration of light of these wavelengths is only 1–2 mm while the tissue penetration of light of $\lambda = 660$ nm is > 6 mm. Consequently, these conditions were significantly less efficient. A similar study has been published using osmium-based photosensitizers also absorbing light in the near infrared domain [84].

Fluoroalkyl radicals are electrophilic and thus easily reacted with aromatic, especially heteroaromatic compounds [85]. Using 5,10,15,20-tetrakis(4-trimethylammoniophenyl)porphyrin tetra(*p*-toluenesulfonate) (TTMAPP, **81**, 1 mol %) or helical *N*′-di-*n*-propyl-1,13-dimethoxyquinacridinium tetrafluoroborate (*n*-Pr-DMQA$^+$, **55**, 2.5 mol %) fluoroalkyl radicals are produced from the corresponding precursors **82** (Scheme 20) [86]. They have been added to a variety of tryptophan-containing peptides **83** and the resulting products **84** have been obtained with yields up to 74%. Using a corresponding terminal diiodide, two tryptophan moieties have been connected by a fluorinated linker. Linear peptides with two tryptophan units can be cyclized using similar diiodofluoroalkyl linkers. The fluoroalkyl iodides **85** carrying a biotin moiety have been used in this reaction to label enzymes such as carbonic anhydrase, albumin, phosphorylase, or bovine serum albumin. Biotinylation with this method was also carried out in living cells.

Two-photon absorption is a very elegant method to use near infrared light for electronic excitation of molecules absorbing

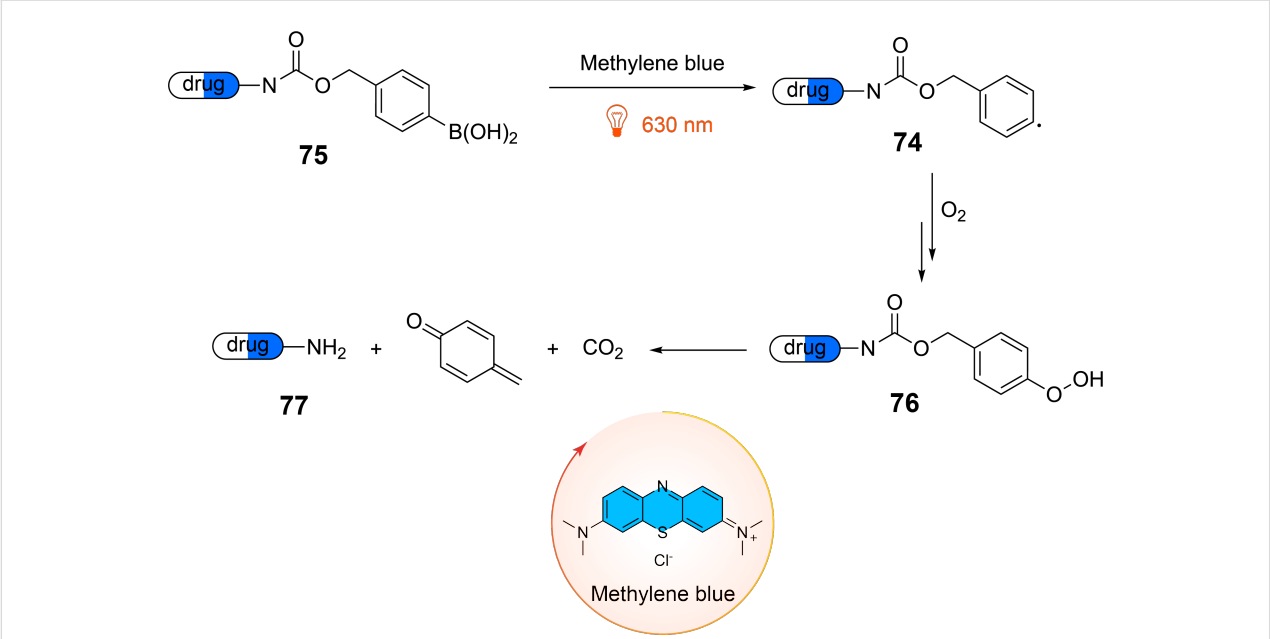

Scheme 18: Photochemical uncaging of drugs protected with a phenylboronic acid derivative using near IR irradiation.

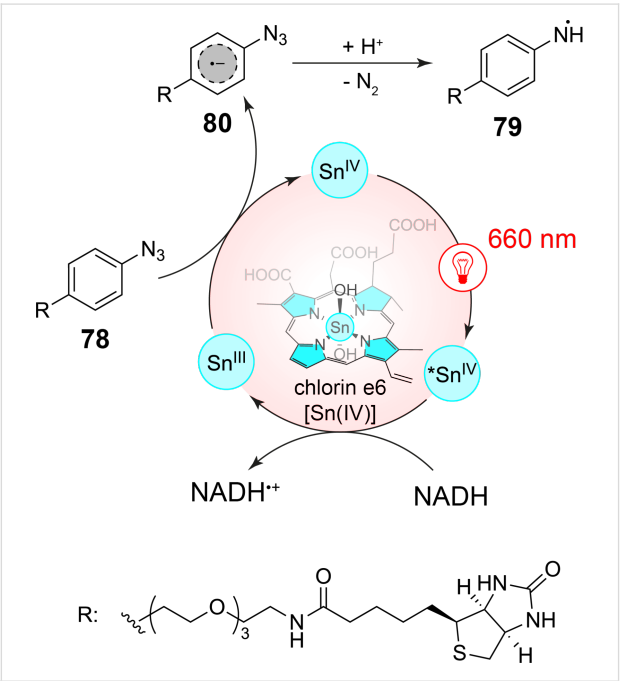

Scheme 19: Photoredox catalytical generation of aminyl radicals with near IR irradiation for the transfer of biotin to biological structures.

single photons in the visible domain of the light spectrum (Figure 16). The efficiency of such an excitation depends on the symmetry properties of the chromophore [87,88]. A two-photon excitation is carried out with corresponding lasers. This technique enables the usage of a larger variety of chromophores in medicinal and biochemistry and related domains while conserving the property of a relatively high tissue penetration [89,90]. Electronic excitation by two-photon absorption in tissues can be highly localized as it occurs only in the focal point of lensing. Thus, even a single cell in a tissue can be selectively addressed [91].

Calcium ions play an important role in many biological phenomena, for example in neurotransmission. Calcium ions can efficiently be caged by ethylene glycol tetraacetic acid (EGTA) derivatives [92]. The cage was bound to a nitrophenyl benzofuran chromophore **86** (Scheme 21) [93]. This chromophore is considered as styrene derivative and such compounds possess a relatively high cross section for two-photon absorption. After absorption of two near infrared photons, the benzyl ether bond is cleaved and the cage is split into two fragments **87** and **88**, thus releasing Ca^{2+} ions. The cross section for this fragmentation is 20.7 GM at λ = 740 nm determined with the corresponding esters **89**. The cage was applied to whole-cell-clamped neurons as derivative **90**. By releasing the carboxylic acid protecting group, Ca^{2+} is complexed (**86**). The presynaptic terminals were stimulated by the uncaging two-photon absorption process and the influence on the postsynaptic currents was measured.

Conclusion

Red-light photocatalysis has emerged as a powerful tool in both synthetic chemistry and biological applications, owing to its unique ability to drive reactions under mild, energy-efficient conditions. In synthetic chemistry, metal-based photocatalysts,

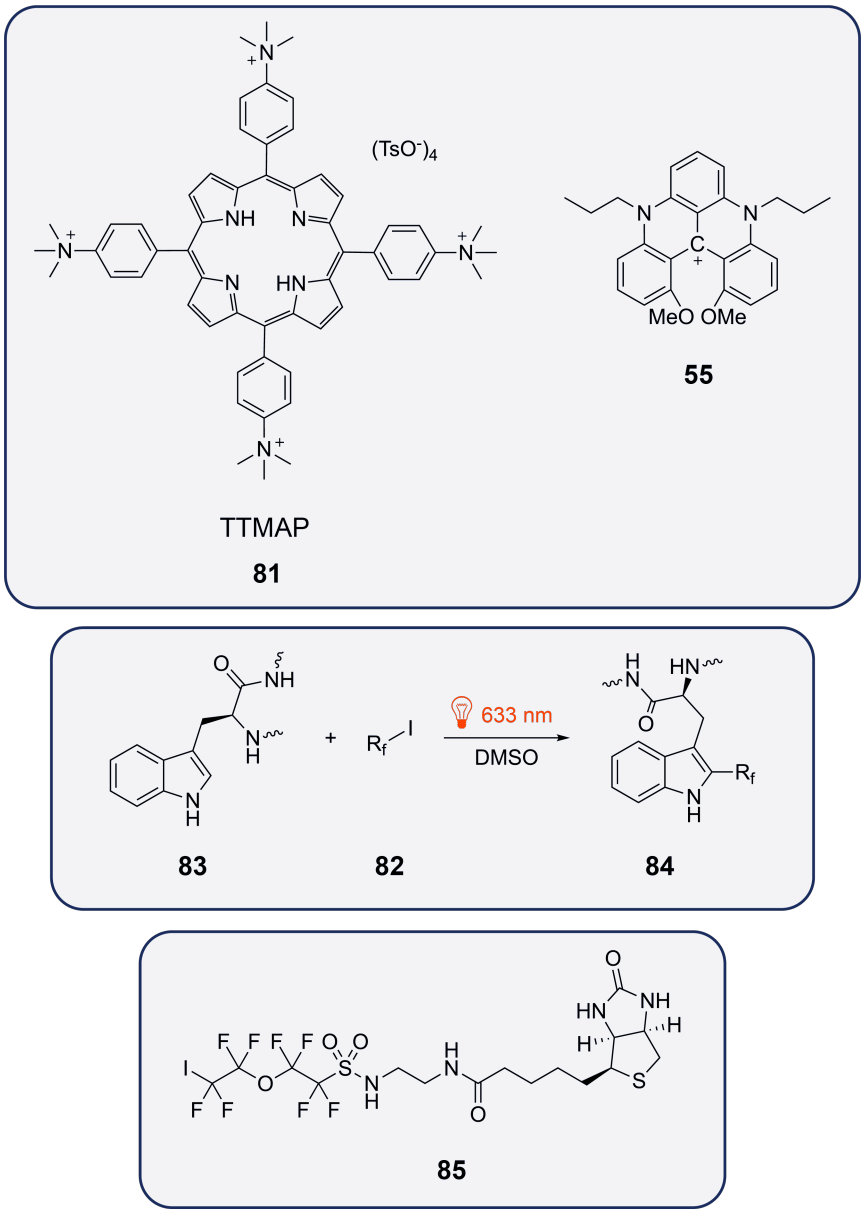

Scheme 20: Photoredox catalytical fluoroalkylation of tryptophan moieties.

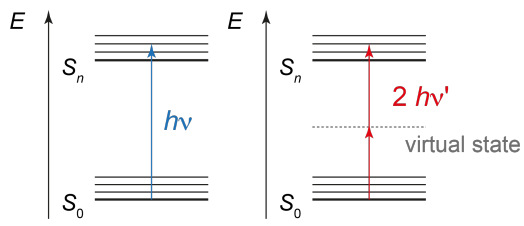

Figure 16: Simultaneous absorption of two photons of infrared light of low energy enables electronic excitation of compounds absorbing single photons in the visible spectrum domain.

particularly those involving heavy metals like ruthenium and osmium, have been instrumental in expanding the scope of red-light-driven photoredox transformations. These complexes are valued for their exceptional photophysical properties which have facilitated a range of efficient and scalable transformations. At the same time, the use of ligands such as phthalocyanines has opened new avenues by enabling the application of more abundant metals, such as zinc, copper, and cobalt, thereby promoting the development of more sustainable photocatalytic systems. In parallel, organic photocatalysts such as squaraines and cyanins have gained prominence as versatile and

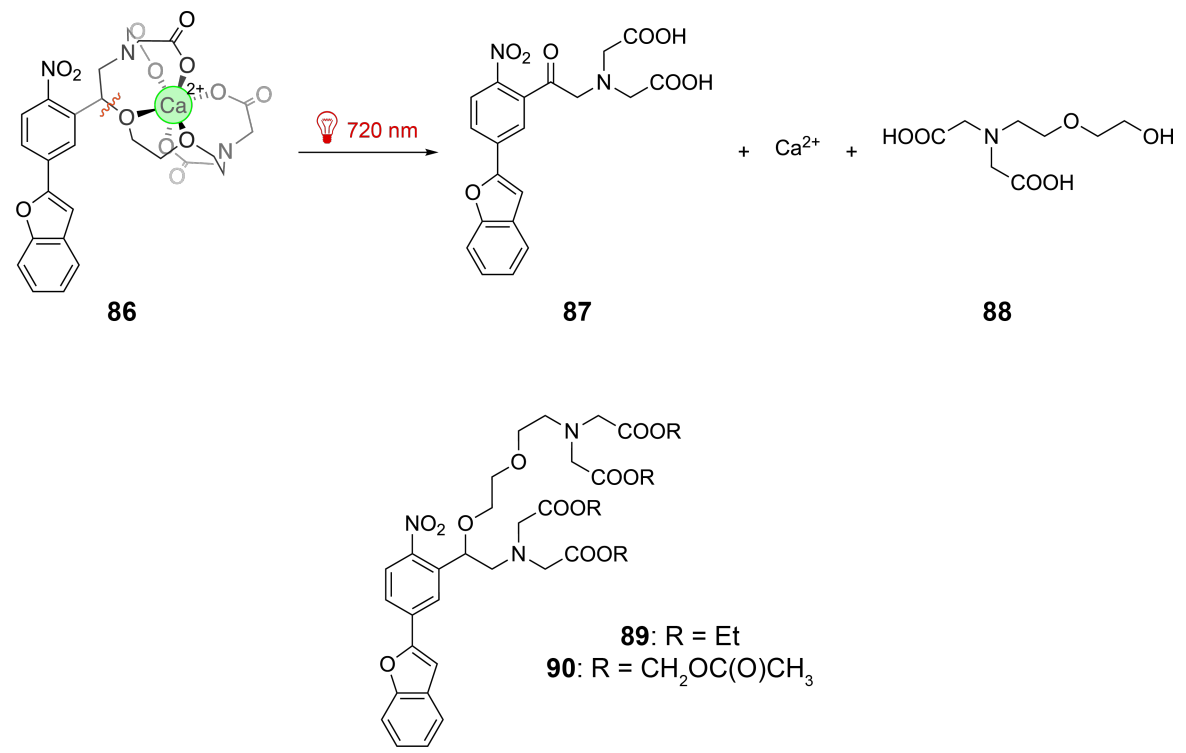

Scheme 21: Uncaging Ca^{2+} ions using two-photon excitation with near infrared light.

sustainable alternatives. These systems offer unique advantages in terms of tunability and environmental impact. Their strong absorption in the red and near-infrared (NIR) regions, combined with their ability to mediate both energy- and electron-transfer processes, underscores their potential for diverse synthetic applications. In biological contexts, the deep tissue penetration of red and NIR light enables precise and localized processes that are challenging under shorter wavelengths. Applications such as drug uncaging, the controlled release of nitric oxide, and the targeted generation of bioactive species highlight the transformative potential of red-light photocatalysis in medicine and biochemistry. However, significant challenges remain to fully exploit the potential of red-light photocatalysis. The design of photocatalysts with both high oxidation and reduction potentials in their excited states, as well as longer excited-state lifetimes, is critical for broadening the substrate scope and achieving greater efficiency. These advancements would enable access to more complex transformations and functionalization of substrates currently out of reach. Looking ahead, the coupling of red-light photocatalysis with organic electrochemistry through electrophotocatalysis offers exciting new perspectives. This innovative strategy could facilitate the generation of novel red-light-absorbing species with enhanced redox properties, enabling transformations that are inaccessible to either technique alone.

Acknowledgements

The flask in the graphical abstract is taken from https://www.brusheezy.com, Free Photoshop Brushes by Brusheezy! This content is not subject to CC BY 4.0.

Author Contributions

Lucas Fortier: writing – original draft; writing – review & editing. Corentin Lefebvre: writing – original draft; writing – review & editing. Norbert Hoffmann: writing – original draft; writing – review & editing.

ORCID® iDs

Corentin Lefebvre - https://orcid.org/0000-0001-5358-102X
Norbert Hoffmann - https://orcid.org/0000-0002-8615-7476

Data Availability Statement

Data sharing is not applicable as no new data was generated or analyzed in this study.

References

1. Hoffmann, N. *ChemSusChem* **2012,** *5,* 352–371. doi:10.1002/cssc.201100286
2. Prier, C. K.; Rankic, D. A.; MacMillan, D. W. C. *Chem. Rev.* **2013,** *113,* 5322–5363. doi:10.1021/cr300503r

3. Teegardin, K.; Day, J. I.; Chan, J.; Weaver, J. *Org. Process Res. Dev.* **2016,** *20,* 1156–1163. doi:10.1021/acs.oprd.6b00101
4. Bell, J. D.; Murphy, J. A. *Chem. Soc. Rev.* **2021,** *50,* 9540–9685. doi:10.1039/d1cs00311a
5. Prieto, A.; Jaroschik, F. *Curr. Org. Chem.* **2022,** *26,* 6–41. doi:10.2174/1385272825666211126123928
6. Larsen, C. B.; Wenger, O. S. *Chem. – Eur. J.* **2018,** *24,* 2039–2058. doi:10.1002/chem.201703602
7. Wenger, O. S. *J. Am. Chem. Soc.* **2018,** *140,* 13522–13533. doi:10.1021/jacs.8b08822
8. Hockin, B. M.; Li, C.; Robertson, N.; Zysman-Colman, E. *Catal. Sci. Technol.* **2019,** *9,* 889–915. doi:10.1039/c8cy02336k
9. Yu, D.; To, W.-P.; Tong, G. S. M.; Wu, L.-L.; Chan, K.-T.; Du, L.; Phillips, D. L.; Liu, Y.; Che, C.-M. *Chem. Sci.* **2020,** *11,* 6370–6382. doi:10.1039/d0sc01340d
10. Ting, S. I.; Garakyaraghi, S.; Taliaferro, C. M.; Shields, B. J.; Scholes, G. D.; Castellano, F. N.; Doyle, A. G. *J. Am. Chem. Soc.* **2020,** *142,* 5800–5810. doi:10.1021/jacs.0c00781
11. Juliá, F. *ChemCatChem* **2022,** *14,* e202200916. doi:10.1002/cctc.202200916
12. May, A. M.; Dempsey, J. L. *Chem. Sci.* **2024,** *15,* 6661–6678. doi:10.1039/d3sc05268k
13. Yam, V. W.-W.; Chan, A. K.-W.; Hong, E. Y.-H. *Nat. Rev. Chem.* **2020,** *4,* 528–541. doi:10.1038/s41570-020-0199-7
14. Braterman, P. S.; Song, J.-I.; Peacock, R. D. *Inorg. Chem.* **1992,** *31,* 555–559. doi:10.1021/ic00030a006
15. Shillito, G. E.; Bodman, S. E.; Mapley, J. I.; Fitchett, C. M.; Gordon, K. C. *Inorg. Chem.* **2020,** *59,* 16967–16975. doi:10.1021/acs.inorgchem.0c02102
16. Nakajima, M.; Nagasawa, S.; Matsumoto, K.; Kuribara, T.; Muranaka, A.; Uchiyama, M.; Nemoto, T. *Angew. Chem., Int. Ed.* **2020,** *59,* 6847–6852. doi:10.1002/anie.201915181
17. Lemcoff, N.; Nechmad, N. B.; Eivgi, O.; Yehezkel, E.; Shelonchik, O.; Phatake, R. S.; Yesodi, D.; Vaisman, A.; Biswas, A.; Lemcoff, N. G.; Weizmann, Y. *Nat. Chem.* **2023,** *15,* 475–482. doi:10.1038/s41557-022-01124-7
18. Cabanero, D. C.; Nguyen, J. A.; Cazin, C. S. J.; Nolan, S. P.; Rovis, T. *ACS Catal.* **2023,** *13,* 4384–4390. doi:10.1021/acscatal.3c00473
19. Ravetz, B. D.; Tay, N. E. S.; Joe, C. L.; Sezen-Edmonds, M.; Schmidt, M. A.; Tan, Y.; Janey, J. M.; Eastgate, M. D.; Rovis, T. *ACS Cent. Sci.* **2020,** *6,* 2053–2059. doi:10.1021/acscentsci.0c00948
20. Goldschmid, S. L.; Soon Tay, N. E.; Joe, C. L.; Lainhart, B. C.; Sherwood, T. C.; Simmons, E. M.; Sezen-Edmonds, M.; Rovis, T. *J. Am. Chem. Soc.* **2022,** *144,* 22409–22415. doi:10.1021/jacs.2c09745
21. Mato, M.; Bruzzese, P. C.; Takahashi, F.; Leutzsch, M.; Reijerse, E. J.; Schnegg, A.; Cornella, J. *J. Am. Chem. Soc.* **2023,** *145,* 18742–18747. doi:10.1021/jacs.3c06651
22. Breuer, M.; Ditrich, K.; Habicher, T.; Hauer, B.; Keßeler, M.; Stürmer, R.; Zelinski, T. *Angew. Chem., Int. Ed.* **2004,** *43,* 788–824. doi:10.1002/anie.200300599
23. Ravetz, B. D.; Pun, A. B.; Churchill, E. M.; Congreve, D. N.; Rovis, T.; Campos, L. M. *Nature* **2019,** *565,* 343–346. doi:10.1038/s41586-018-0835-2
24. Zeng, L.; Huang, L.; Lin, W.; Jiang, L.-H.; Han, G. *Nat. Commun.* **2023,** *14,* 1102. doi:10.1038/s41467-023-36679-7
25. Glaser, F.; Wenger, O. S. *Chem. Sci.* **2023,** *14,* 149–161. doi:10.1039/d2sc05229f
26. Freitag, M.; Möller, N.; Rühling, A.; Strassert, C. A.; Ravoo, B. J.; Glorius, F. *ChemPhotoChem* **2019,** *3,* 24–27. doi:10.1002/cptc.201800212
27. Bilger, J. B.; Kerzig, C.; Larsen, C. B.; Wenger, O. S. *J. Am. Chem. Soc.* **2021,** *143,* 1651–1663. doi:10.1021/jacs.0c12805
28. Fajardo, J., Jr.; Barth, A. T.; Morales, M.; Takase, M. K.; Winkler, J. R.; Gray, H. B. *J. Am. Chem. Soc.* **2021,** *143,* 19389–19398. doi:10.1021/jacs.1c07617
29. Glaser, F.; Wenger, O. S. *JACS Au* **2022,** *2,* 1488–1503. doi:10.1021/jacsau.2c00265
30. Sellet, N.; Cormier, M.; Goddard, J.-P. *Org. Chem. Front.* **2021,** *8,* 6783–6790. doi:10.1039/d1qo01476e
See for selected examples.
31. Sinha, N.; Wegeberg, C.; Häussinger, D.; Prescimone, A.; Wenger, O. S. *Nat. Chem.* **2023,** *15,* 1730–1736. doi:10.1038/s41557-023-01297-9
32. Wang, C.; Wegeberg, C.; Wenger, O. S. *Angew. Chem., Int. Ed.* **2023,** *62,* e202311470. doi:10.1002/anie.202311470
33. Ishikawa, Y.; Kameyama, T.; Torimoto, T.; Maeda, H.; Segi, M.; Furuyama, T. *Chem. Commun.* **2021,** *57,* 13594–13597. doi:10.1039/d1cc06307c
34. Kai, U.; Katsurayama, Y.; Nishida, R.; Kameyama, T.; Torimoto, T.; Furuyama, T. *J. Org. Chem.* **2024,** *89,* 8178–8184. doi:10.1021/acs.joc.4c00889
35. Katsurayama, Y.; Ikabata, Y.; Maeda, H.; Segi, M.; Nakai, H.; Furuyama, T. *Chem. – Eur. J.* **2022,** *28,* e202103223. doi:10.1002/chem.202103223
36. Grundke, C.; Silva, R. C.; Kitzmann, W. R.; Heinze, K.; de Oliveira, K. T.; Opatz, T. *J. Org. Chem.* **2022,** *87,* 5630–5642. doi:10.1021/acs.joc.1c03101
37. Okanishi, Y.; Takemoto, O.; Kawahara, S.; Hayashi, S.; Takanami, T.; Yoshimitsu, T. *Org. Lett.* **2024,** *26,* 3929–3934. doi:10.1021/acs.orglett.4c01112
38. Lancel, M.; Golisano, T.; Monnereau, C.; Gomez, C.; Port, M.; Amara, Z. *ACS Sustainable Chem. Eng.* **2023,** *11,* 15674–15684. doi:10.1021/acssuschemeng.3c04688
39. Yan, P.; Zeng, R.; Bao, B.; Yang, X.-M.; Zhu, L.; Pan, B.; Niu, S.-L.; Qi, X.-W.; Li, Y.-L.; Ouyang, Q. *Green Chem.* **2022,** *24,* 9263–9268. doi:10.1039/d2gc03055a
40. Rybicka-Jasińska, K.; Wdowik, T.; Łuczak, K.; Wierzba, A. J.; Drapała, O.; Gryko, D. *ACS Org. Inorg. Au* **2022,** *2,* 422–426. doi:10.1021/acsorginorgau.2c00025
See for selected examples.
41. Orłowska, K.; Łuczak, K.; Krajewski, P.; Santiago, J. V.; Rybicka-Jasińska, K.; Gryko, D. *Chem. Commun.* **2023,** *59,* 14649–14652. doi:10.1039/d3cc05174a
42. Lee, J.; Papatzimas, J. W.; Bromby, A. D.; Gorobets, E.; Derksen, D. J. *RSC Adv.* **2016,** *6,* 59269–59272. doi:10.1039/c6ra11374e
43. Cao, H.; Wang, G.; Xue, Y.; Yang, G.; Tian, J.; Liu, F.; Zhang, W. *ACS Macro Lett.* **2019,** *8,* 616–622. doi:10.1021/acsmacrolett.9b00320
44. Tanioka, M.; Kuromiya, A.; Ueda, R.; Obata, T.; Muranaka, A.; Uchiyama, M.; Kamino, S. *Chem. Commun.* **2022,** *58,* 7825–7828. doi:10.1039/d2cc02907c
45. Zeng, L.; Wang, Z.; Zhang, T.; Duan, C. *Molecules* **2022,** *27,* 4047. doi:10.3390/molecules27134047
46. Kundu, B. K.; Han, G.; Sun, Y. *J. Am. Chem. Soc.* **2023,** *145,* 3535–3542. doi:10.1021/jacs.2c12244
47. Bonnett, R.; Motevalli, M.; Siu, J. *Tetrahedron* **2004,** *60,* 8913–8918. doi:10.1016/j.tet.2004.07.023

48. Xia, G.; Wang, H. *J. Photochem. Photobiol., C* **2017,** *31,* 84–113. doi:10.1016/j.jphotochemrev.2017.03.001
49. Sellet, N.; Sebbat, M.; Elhabiri, M.; Cormier, M.; Goddard, J.-P. *Chem. Commun.* **2022,** *58,* 13759–13762. doi:10.1039/d2cc04707a
50. Bonardi, A.; Bonardi, F.; Noirbent, G.; Dumur, F.; Dietlin, C.; Gigmes, D.; Fouassier, J.-P.; Lalevée, J. *Polym. Chem.* **2019,** *10,* 6505–6514. doi:10.1039/c9py01447k
51. Gopika, G. S.; Prasad, P. M. H.; Lekshmi, A. G.; Lekshmypriya, S.; Sreesaila, S.; Arunima, C.; Kumar, M. S.; Anil, A.; Sreekumar, A.; Pillai, Z. S. *Mater. Today: Proc.* **2021,** *46,* 3102–3108. doi:10.1016/j.matpr.2021.02.622
52. Lange, N.; Szlasa, W.; Saczko, J.; Chwiłkowska, A. *Pharmaceutics* **2021,** *13,* 818. doi:10.3390/pharmaceutics13060818
53. Sun, W.; Guo, S.; Hu, C.; Fan, J.; Peng, X. *Chem. Rev.* **2016,** *116,* 7768–7817. doi:10.1021/acs.chemrev.6b00001
54. Shindy, H. A. *Dyes Pigm.* **2017,** *145,* 505–513. doi:10.1016/j.dyepig.2017.06.029
55. Mason, S. J.; Hake, J. L.; Nairne, J.; Cummins, W. J.; Balasubramanian, S. *J. Org. Chem.* **2005,** *70,* 2939–2949. doi:10.1021/jo0479415
56. Maller, C.; Schedel, F.; Köhn, M. *J. Org. Chem.* **2024,** *89,* 3844–3856. doi:10.1021/acs.joc.3c02673
57. Gayton, J. N.; Autry, S.; Fortenberry, R. C.; Hammer, N. I.; Delcamp, J. H. *Molecules* **2018,** *23,* 3051. doi:10.3390/molecules23123051
58. Kulinich, A. V.; Derevyanko, N. A.; Ishchenko, A. A.; Gusyak, N. B.; Kobasa, I. M.; Romańczyk, P. P.; Kurek, S. S. *Dyes Pigm.* **2019,** *161,* 24–33. doi:10.1016/j.dyepig.2018.09.031
59. Schwechheimer, C.; Rönicke, F.; Schepers, U.; Wagenknecht, H.-A. *Chem. Sci.* **2018,** *9,* 6557–6563. doi:10.1039/c8sc01574k
60. Matikonda, S. S.; Helmerich, D. A.; Meub, M.; Beliu, G.; Kollmannsberger, P.; Greer, A.; Sauer, M.; Schnermann, M. J. *ACS Cent. Sci.* **2021,** *7,* 1144–1155. doi:10.1021/acscentsci.1c00483
61. Jędrzejewska, B.; Pietrzak, M.; Rafiński, Z. *Polymer* **2011,** *52,* 2110–2119. doi:10.1016/j.polymer.2011.03.035
62. Kabatc, J.; Zasada, M.; Pączkowski, J. *J. Polym. Sci., Part A: Polym. Chem.* **2007,** *45,* 3626–3636. doi:10.1002/pola.22112
63. Bonardi, A.-H.; Bonardi, F.; Morlet-Savary, F.; Dietlin, C.; Noirbent, G.; Grant, T. M.; Fouassier, J.-P.; Dumur, F.; Lessard, B. H.; Gigmes, D.; Lalevée, J. *Macromolecules* **2018,** *51,* 8808–8820. doi:10.1021/acs.macromol.8b01741
64. Wang, Q.; Popov, S.; Feilen, A.; Strehmel, V.; Strehmel, B. *Angew. Chem., Int. Ed.* **2021,** *60,* 26855–26865. doi:10.1002/anie.202108713
65. Obah Kosso, A. R.; Sellet, N.; Baralle, A.; Cormier, M.; Goddard, J.-P. *Chem. Sci.* **2021,** *12,* 6964–6968. doi:10.1039/d1sc00998b
66. Sellet, N.; Clement-Comoy, L.; Elhabiri, M.; Cormier, M.; Goddard, J.-P. *Chem. – Eur. J.* **2023,** *29,* e202302353. doi:10.1002/chem.202302353
67. Laursen, B. W.; Krebs, F. C. *Angew. Chem., Int. Ed.* **2000,** *39,* 3432–3434. doi:10.1002/1521-3773(20001002)39:19<3432::aid-anie3432>3.0.co;2-s
68. Bosson, J.; Gouin, J.; Lacour, J. *Chem. Soc. Rev.* **2014,** *43,* 2824–2840. doi:10.1039/c3cs60461f
69. Mei, L.; Veleta, J. M.; Gianetti, T. L. *J. Am. Chem. Soc.* **2020,** *142,* 12056–12061. doi:10.1021/jacs.0c05507
70. Romero, N. A.; Nicewicz, D. A. *Chem. Rev.* **2016,** *116,* 10075–10166. doi:10.1021/acs.chemrev.6b00057
71. Ash, C.; Dubec, M.; Donne, K.; Bashford, T. *Lasers Med. Sci.* **2017,** *32,* 1909–1918. doi:10.1007/s10103-017-2317-4
72. Jiang, W.; Lin, L.; Wu, P.; Lin, H.; Sui, J. *Chem. – Eur. J.* **2024,** *30,* e202400816. doi:10.1002/chem.202400816
73. Szabó, C.; Ischiropoulos, H.; Radi, R. *Nat. Rev. Drug Discovery* **2007,** *6,* 662–680. doi:10.1038/nrd2222
74. Shen, Z.; Zheng, S.; Fang, Y.; Zhang, G.; Zhu, C.; Liu, S.; Hu, J. *Angew. Chem., Int. Ed.* **2023,** *62,* e202219153. doi:10.1002/anie.202219153
75. Kochi, J. K. *Angew. Chem., Int. Ed. Engl.* **1988,** *27,* 1227–1266. doi:10.1002/anie.198812273
76. Tao, S.; Shen, Z.; Chen, J.; Shan, Z.; Huang, B.; Zhang, X.; Zheng, L.; Liu, J.; You, T.; Zhao, F.; Hu, J. *ACS Nano* **2022,** *16,* 20376–20388. doi:10.1021/acsnano.2c06328
77. Carpenter, A. W.; Schoenfisch, M. H. *Chem. Soc. Rev.* **2012,** *41,* 3742–3752. doi:10.1039/c2cs15273h
78. Klán, P.; Šolomek, T.; Bochet, C. G.; Blanc, A.; Givens, R.; Rubina, M.; Popik, V.; Kostikov, A.; Wirz, J. *Chem. Rev.* **2013,** *113,* 119–191. doi:10.1021/cr300177k
79. Goeldner, M.; Givens, R. S., Eds. *Dynamic Studies in Biology: Phototriggers, Photoswitches and Caged Biomolecules;* Wiley-VCH: Weinheim, Germany, 2005. doi:10.1002/3527605592
80. Štacko, P.; Šolomek, T. *Chimia* **2021,** *75,* 873–881. doi:10.2533/chimia.2021.873
81. Rosenberger, J. E.; Xie, Y.; Fang, Y.; Lyu, X.; Trout, W. S.; Dmitrenko, O.; Fox, J. M. *J. Am. Chem. Soc.* **2023,** *145,* 6067–6078. doi:10.1021/jacs.2c10655
82. Liu, M.; Luo, Y.; Yan, J.; Xiong, X.; Xing, X.; Kim, J. S.; Zou, T. *J. Am. Chem. Soc.* **2023,** *145,* 10082–10091. doi:10.1021/jacs.3c00254
83. Buksh, B. F.; Knutson, S. D.; Oakley, J. V.; Bissonnette, N. B.; Oblinsky, D. G.; Schwoerer, M. P.; Seath, C. P.; Geri, J. B.; Rodriguez-Rivera, F. P.; Parker, D. L.; Scholes, G. D.; Ploss, A.; MacMillan, D. W. C. *J. Am. Chem. Soc.* **2022,** *144,* 6154–6162. doi:10.1021/jacs.2c01384
84. Tay, N. E. S.; Ryu, K. A.; Weber, J. L.; Olow, A. K.; Cabanero, D. C.; Reichman, D. R.; Oslund, R. C.; Fadeyi, O. O.; Rovis, T. *Nat. Chem.* **2023,** *15,* 101–109. doi:10.1038/s41557-022-01057-1
85. Yerien, D. E.; Cooke, M. V.; García Vior, M. C.; Barata-Vallejo, S.; Postigo, A. *Org. Biomol. Chem.* **2019,** *17,* 3741–3746. doi:10.1039/c9ob00486f
86. Ryu, K. A.; Reyes-Robles, T.; Wyche, T. P.; Bechtel, T. J.; Bertoch, J. M.; Zhuang, J.; May, C.; Scandore, C.; Dephoure, N.; Wilhelm, S.; Quasem, I.; Yau, A.; Ingale, S.; Szendrey, A.; Duich, M.; Oslund, R. C.; Fadeyi, O. O. *ACS Catal.* **2024,** *14,* 3482–3491. doi:10.1021/acscatal.4c00447
87. Pawlicki, M.; Collins, H. A.; Denning, R. G.; Anderson, H. L. *Angew. Chem., Int. Ed.* **2009,** *48,* 3244–3266. doi:10.1002/anie.200805257
88. Fillaut, J.-L. *Coord. Chem. Rev.* **2024,** *518,* 216050. doi:10.1016/j.ccr.2024.216050
89. Dyer, J.; Jockusch, S.; Balsanek, V.; Sames, D.; Turro, N. J. *J. Org. Chem.* **2005,** *70,* 2143–2147. doi:10.1021/jo048053c
90. Nguyen, L. T. B.; Abe, M. *Bull. Chem. Soc. Jpn.* **2023,** *96,* 899–906. doi:10.1246/bcsj.20230140
91. Boca, S. C.; Four, M.; Bonne, A.; van der Sanden, B.; Astilean, S.; Baldeck, P. L.; Lemercier, G. *Chem. Commun.* **2009,** 4590–4592. doi:10.1039/b907143a
92. Ellis-Davies, G. C. R. *Chem. Rev.* **2008,** *108,* 1603–1613. doi:10.1021/cr078210i

93. Jakkampudi, S.; Abe, M.; Komori, N.; Takagi, R.; Furukawa, K.; Katan, C.; Sawada, W.; Takahashi, N.; Kasai, H. *ACS Omega* **2016,** *1,* 193–201. doi:10.1021/acsomega.6b00119

License and Terms

BEILSTEIN JOURNAL OF ORGANIC CHEMISTRY

Photomechanochemistry: harnessing mechanical forces to enhance photochemical reactions

Francesco Mele[‡1], Ana M. Constantin[‡1], Andrea Porcheddu[2], Raimondo Maggi[1,3], Giovanni Maestri[3,4], Nicola Della Ca'[1,3] and Luca Capaldo[*1,3]

Perspective

Open Access

Address:
[1]SynCat Lab, Department of Chemistry, Life Sciences and Environmental Sustainability, University of Parma, Parco Area delle Scienze 17/A, 43124 Parma, Italy, [2]Dipartimento di Scienze Chimiche e Geologiche, Università degli Studi di Cagliari, Cittadella Universitaria, SS554 bivio per Sestu, 09042-Monserrato (CA), Italy, [3]CIRCC (Interuniversity Consortium Chemical Reactivity and Catalysis), via Celso Ulpiani 27, 70126 Bari, Italy and [4]Department of Chemistry, Life Sciences and Environmental Sustainability, University of Parma, Parco Area delle Scienze 17/A, 43124 Parma, Italy

Email:
Luca Capaldo[*] - luca.capaldo@unipr.it

* Corresponding author ‡ Equal contributors

Keywords:
light-mediated synthesis; mechanochemistry; photomechanochemistry

Beilstein J. Org. Chem. **2025,** *21,* 458–472.
https://doi.org/10.3762/bjoc.21.33

Received: 04 December 2024
Accepted: 11 February 2025
Published: 03 March 2025

This article is part of the thematic issue "Photocatalysis and photochemistry in organic synthesis".

Guest Editor: T. Noël

Abstract

Photomechanochemistry, i.e., the merger of light energy and mechanical forces, is emerging as a new trend in organic synthesis, enabling unique reactivities of fleeting excited states under solvent-minimized conditions. Despite its transformative potential, the field faces significant technological challenges that must be addressed to unlock its full capabilities. In this Perspective, we analyze selected examples to showcase the available technologies to combine light and mechanical forces, including manual grinding, vortex and shaker mixing, rod milling, and ball milling. By examining the advantages and limitations of each approach, we aim to provide an overview of the current state of synthetic photomechanochemistry to identify opportunities for future advancements in this rapidly evolving area of research.

Introduction

Light-mediated synthetic methodologies have significantly transformed contemporary organic chemistry by enabling a broad array of previously unattainable transformations [1]. In fact, the absorption of a photon by a molecule causes the reorganization of the electron density around the atoms and unlocks unique reactivity modes [2,3]. In photochemical methods, light is directly absorbed by a functional group embedded in the substrate and can be exploited for example to cleave bonds or trigger rearrangements. Most organic molecules are colorless and, in fact, do not absorb visible light: highly energetic UV ir-

radiation is typically needed. A milder approach is offered by photocatalytic approaches. Here, a photocatalyst is added to the reaction mixture to convert light energy into chemical potential to transform molecules. Intriguingly, photocatalysts typically absorb harmless visible light and can be chosen *ad hoc* to trigger the desired chemistry. Indeed, the photocatalyst–substrate interaction can occur via energy transfer [4-8], single-electron transfer [9-12], or hydrogen-atom transfer [13-15].

Regardless of the mechanistic details of the activation manifold, all photochemical reactions obey two laws: the Grotthuss–Draper and the Einstein–Stark laws [16]. The Grotthuss–Draper law dictates that only absorbed light can induce photochemical transformations within a system. In his own words, "independently on its chemical nature, each body reacts more strongly to the color that is complementary to that it shows in the normal state" [17]. While this concept may appear self-evident to contemporary photochemists, it served as an early cautionary note to consistently measure the absorption spectrum of reagents and ensure that the emission spectrum of the light source used overlaps (at least to some extent) with it (Figure 1). The Stark–Einstein law, sometimes referred to as the law of photochemical equivalence, asserts that the absorption of light is a quantum process involving one photon per absorbing molecule (or atom) [18]. It should be stressed that one photon might trigger a chain of events leading to the formation of multiple molecules of product (Figure 1). The Grotthuss–Draper and Einstein–Stark laws mainly predict the feasibility of a light-mediated transformation from a conceptual standpoint.

Another fundamental law in photochemistry is the Beer–Lambert law, which describes a negative exponential correlation between the transmittance of a solution containing chromophores (i.e., a light-absorbing species) and the optical path length (Figure 1). In essence, as a beam of light traverses through a solution, photons are quickly absorbed, resulting in abrupt reduction in light intensity. Thr Beer–Lambert law imposes the most stringent constraints from a practical point of view, mainly in terms of scalability. This requires highly diluted solutions, which in turn demands large volumes of solvents, negatively impacting the sustainability of light-mediated synthesis as it transitions from academic curiosity to industrial application. Moreover, since the solvent is the reaction component with the highest concentration, competitive side-reactions such as hydrogen-atom transfer or solvolysis are often observed.

A technological solution to cope with the Beer–Lambert law was offered by flow chemistry [19-21] by employing microreactors with reduced optical paths to enhance irradiation efficiency [22-24]. Photon-limited reactions, whose efficiency is primarily constrained by the availability of photons in the reaction mixture, particularly benefit from this approach. Paradoxically, flow chemistry is a convenient technology to increase the productivity of photochemical reactions via numbering-up and sizing-up approaches [25], but it is highly dependent on solvents. In fact, high concentrations of reagents or products can lead to precipitation, causing undesired clogging of the reactor and potentially disastrous consequences for the intended transformation. It is important to mention that specific solutions for handling slurries in flow have been developed, where additional energy is applied to increase mixing such as pulsation [26-28], ultrasound energy [29], segmented flow [30], or mechanical stirring [31].

In line with the recent emphasis on Green Chemistry principles [32,33], alternatives have been developed in order to reduce the amount of organic solvents [34] required for light-mediated

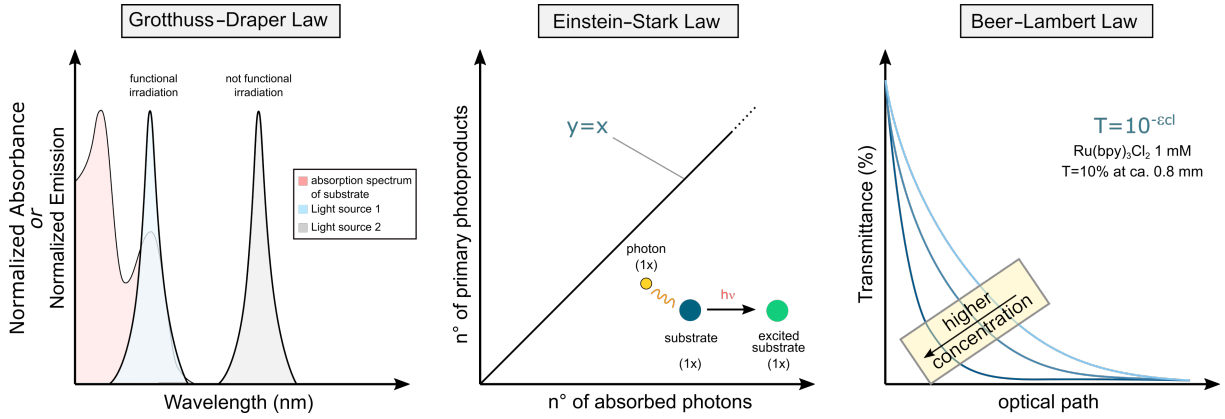

Figure 1: The Grotthuss–Draper, Einstein–Stark, and Beer–Lambert laws. *T*: transmittance; ε: molar attenuation coefficient; *c*: concentration; *l*: optical path.

transformations including on- and in-water approaches [35-37], the use of supercritical CO_2 as solvent [38], and the melting point depression strategy [39]. However, a more drastic option would be to remove the solvent: no solvent is the best solvent.

Mechanochemical synthesis, particularly through ball milling, has emerged as a powerful and sustainable technique that offers numerous advantages over traditional solution-phase methods [40-42]. By often eliminating the need for solvents, mechanochemistry reduces environmental impact and simplifies experimental procedures. Moreover, it often leads to shorter reaction times [43,44] and can overcome solubility limitations [45]. Similar to the effect of photons in light-mediated synthesis, mechanical forces generated during ball milling can induce unconventional reaction pathways [46] enabling the synthesis of novel compounds and materials. While the mechanisms underlying mechanochemical reactions are still under investigation [47-50], the increasing body of research demonstrates the potential of this technique to revolutionize synthetic chemistry.

Combining photochemistry with mechanochemistry holds potential for unique opportunities for substrate activation while adopting an environmentally benign emerging technology (Figure 2, top). For example, it is well known that molecules in the solid state (or in very high concentration) often exhibit photophysical behaviors distinct from those observed in dilute solutions because of the formation of aggregates perturbing electronic transitions [51-53]. Moreover, at high concentrations, the formation of electron donor–acceptor (EDA) complexes [54] or exciplexes is expected to be favored, and the effect of mechanical forces on these is worth being thoroughly investigated. However, to benefit from these unique opportunities, the scientific community must resolve both conceptual and practical challenges. On one side, light penetration is penalized by the absence of the solvent, especially in the case of non-transparent solids. On the other side, typical reactors used for classical mechanochemical synthesis are made of non-transparent materials such as stainless steel (SS), zirconia, or polytetrafluoroethylene (PTFE), making the use of photons operationally difficult.

In this Perspective, we gathered selected examples to showcase how light energy and mechanical forces have been integrated through the years, either in a combined or sequential manner. Our goal is not to provide an exhaustive review on photomechanochemistry [34,42,55], nor a detailed explanation of solid-state photochemistry [56,57], but rather to capture a snapshot of the current technological advancement in the field. This Perspective is organized into four sections based on the adopted setup for photomechanochemistry: manual grinding, vortex

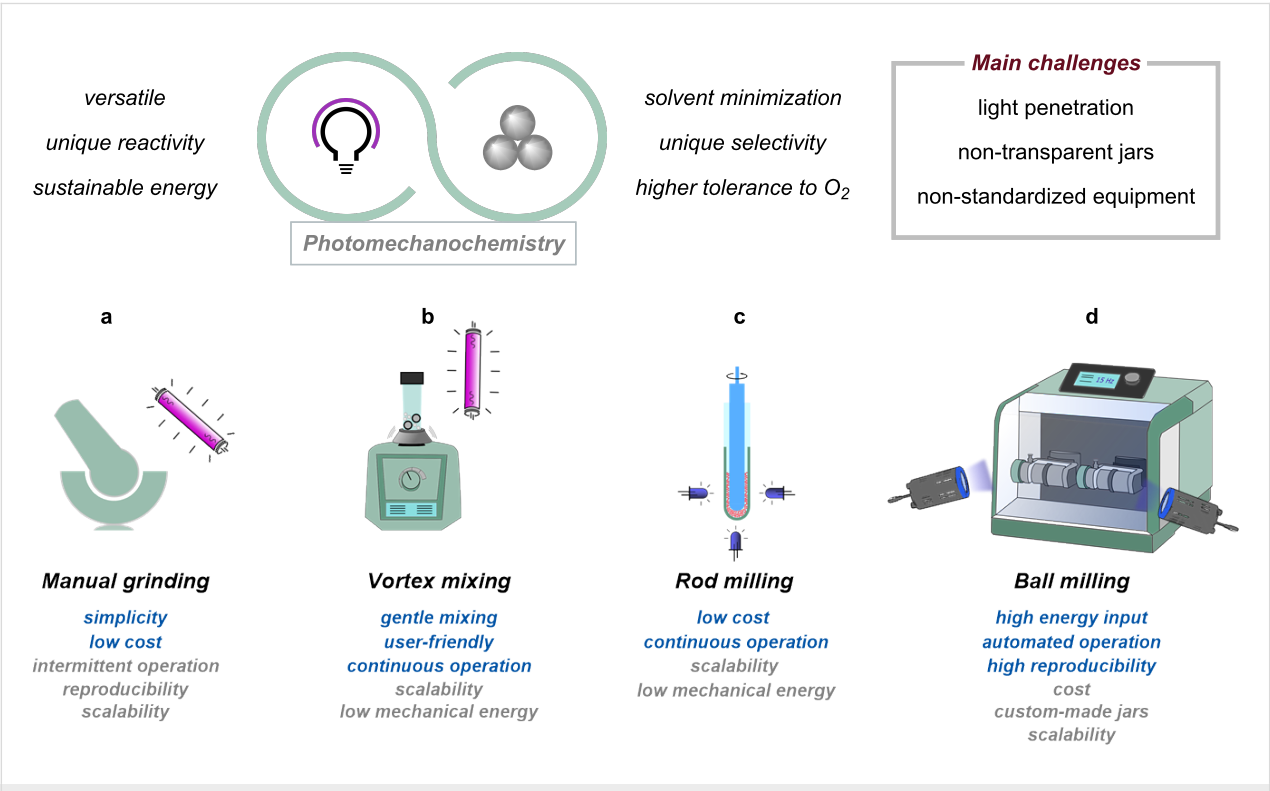

Figure 2: The benefits of merging photochemistry with mechanochemical setups (top). Most common setups for photomechanochemistry (bottom): a) manual grinding, b) vortex mixing, c) rod milling, and d) ball milling.

mixing, rod milling methods, and ball milling (Figure 2, bottom).

One final note is about the solvent adopted: in some examples described below, minimal amounts of solvent are used to homogenize the reaction mixture. This approach is called liquid-assisted grinding (LAG) and it is commonly accepted as a mechanochemical approach [58].· Throughout the text, we adopted the term photomechanochemistry to include both photochemical and photocatalytic methods [59], while others have used "mechanophotocatalysis" or "mechanophotochemistry" for greater specificity.

Discussion

Experimental setups for photomechanochemistry

As mentioned above, the goal of the present perspective article is to put the spotlight on the technological advancement in the emerging field of photomechanochemistry, starting from simple manual grinding to more modern ball-milling techniques.

Manual grinding (Figure 2a) with a pestle and mortar is the simplest and most cost-effective technique for photomechanochemistry, relying on hand-applied forces to maximize the surface area of the solids and, therefore, irradiation efficiency. UV lamps (e.g., medium-pressure Hg lamps) are typically used for irradiation, thus requiring specialized safety equipment. While it offers some control over pressure and duration, manual grinding suffers from inconsistencies due to operator variability, limited throughput (and, hence, scalability), and challenges in reproducibility. This approach is not operated in continuo: grinding and irradiation occur sequentially and not simultaneously.

Vortex shakers (Figure 2b), which provide circular motion for mixing, are cheap, user-friendly and available in most laboratories. However, they have limited energy input, making them less effective for high-energy reactions, and are typically used for small-scale experiments. Also in this case, the integration of light sources requires specialized setups (vide infra). Automated vortex milling for photomechanochemistry is possible.

Rod milling (Figure 2c) involves the use of a glass rod inserted into a transparent glass test tube containing the reaction mixture. As the rod rotates, it generates the mechanochemical forces required to drive the reaction while continuously exposing fresh surface area to light. This setup allows the reaction mixture to be irradiated efficiently using inexpensive and energy-saving light-emitting diodes (LEDs). Importantly, this apparatus can be operated in continuo, providing opportunity for limiting human intervention.

Ball milling (Figure 2d) stands out for its high-energy input, automated operation, and reproducibility, making it ideal for larger-scale and more force-intensive reactions. Both LED strips and LED lamps are used as light sources in combination with transparent jars in PMMA, glass, or epoxy resins. It can achieve consistent results but comes with higher costs, more complex operation, and challenges in effectively integrating light sources for photomechanochemical reactions.

Manual grinding

Manual grinding was predominantly used in the early days of photomechanochemistry, when [2 + 2] photochemical cycloadditions were extensively studied to get insights into the impact of light energy onto crystals [60,61]. In the following, we describe selected examples with an emphasis on the role of manual grinding in improving irradiation.

Mechanochemistry is a linchpin in topochemical solid-state reactions, where the correct molecular alignment within the crystal drives the reaction. For example, in 2008, Vittal et al. [62] designed a mechanochemical strategy to align the C=C bonds of 4,4'-bipyridylethylene (bpe, **1.1**) molecules to drive efficient [2 + 2] cycloaddition and give the corresponding cyclobutanes (**1.2**). This approach relied on zinc cations to align **1.1** through the formation of hydrogen-bonded coordination complexes. Thus, when a single crystal of the $[Zn(bpe)_2(H_2O)_4](NO_3)_2{\cdot}8/3H_2O{\cdot}2/3bpe$ complex was exposed to UV irradiation (dark blue phosphor lamps, λ = 350 nm) for 25 h, only 46% conversion to **1.2** was observed via ^{1}H NMR spectroscopy (Scheme 1). During the reaction progress, the C=C bonds of bpe ligands undergo pedal-like motion prior to photodimerization [63]. For the single-crystal irradiation, the slow reactivity can be attributed to the hindered pedal motion in the single crystals, likely due to the presence of coordinative bonds on one side and hydrogen bonds on the other. Surprisingly, when the crystals were manually ground for 5 min before irradiation, the conversion to dimer **1.2** remarkably increased to 88% in only 4 h of UV irradiation time. Overall, the role of manual grinding was not only to increase the surface area exposed to light but also to allow the motions within the crystal.

In another instance, MacGillivray and colleagues reported the synthesis of *rctt*-tetrakis(4-pyridyl)cyclobutane (**2.3**) via [2 + 2] photodimerization of *trans*-1,2-bis(4-pyridyl)ethylene (**2.1**) via supramolecular catalysis by 4,6-dichloro-resorcinol (**2.2**) in the solid state (Scheme 2) [64]. The authors noticed that single crystals of **2.1**·**2.2** (1:1 stoichiometry) produced by mortar-and-pestle grinding undergo a single-crystal-to-single-crystal

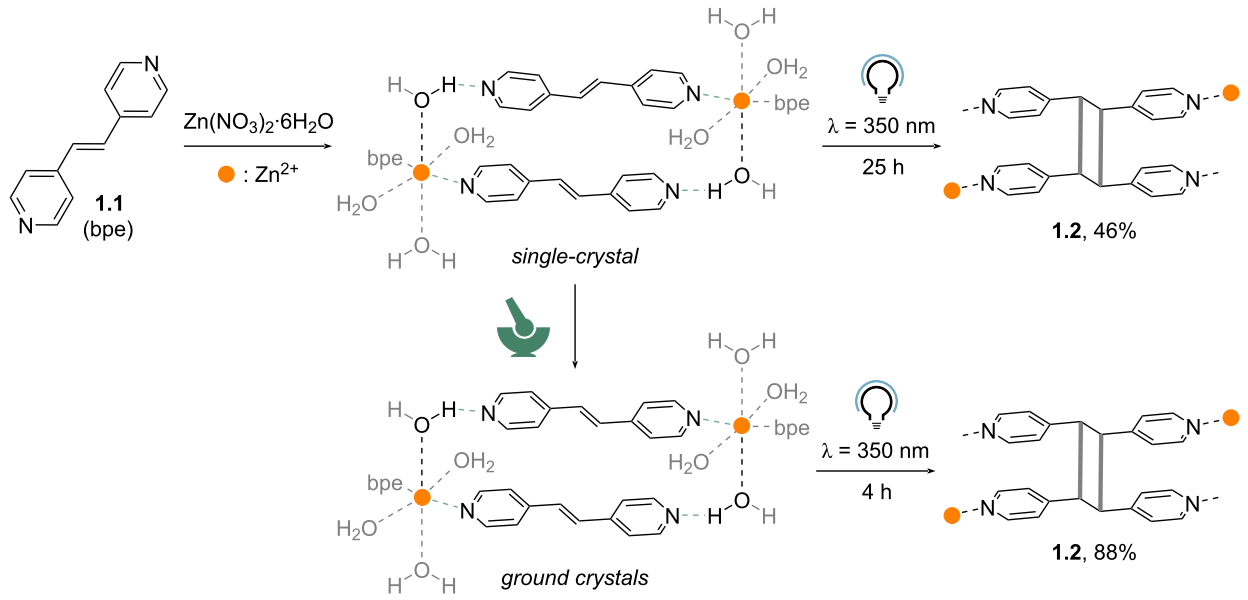

Scheme 1: Mechanochemically triggered pedal-like motion in solid-state [2 + 2] photochemical cycloaddition for the formation of cyclobutanes [62].

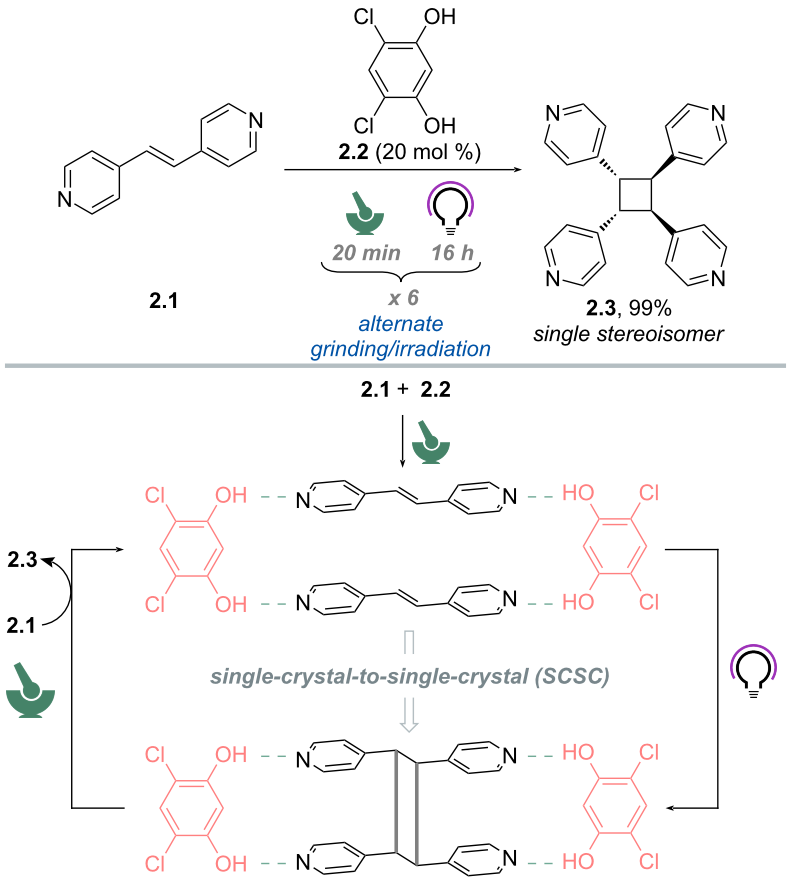

Scheme 2: Mechanically promoted [2 + 2] photodimerization of *trans*-1,2-bis(4-pyridyl)ethylene (**2.1**) via supramolecular catalysis by 4,6-dichlororesorcinol (**2.2**) in the solid state [64].

(SCSC) transformation when exposed to UV light (medium-pressure Hg lamp). The cyclobutane **2.3** was obtained as a single stereoisomer and in quantitative yield after 80 h of irradiation. The role of **2.2** is to create a close-packed environment via hydrogen-bond interactions where the [2 + 2] photodimerization can occur stereoselectively. Next, the authors evaluated the possibility of using the template agent **2.2** in a sub-stoichiometric fashion (20 mol %). However, even upon prolonged exposure, the yield of **2.3** did not exceed 20% (by ^{1}H NMR spectroscopy). To achieve turnover, the photoreacted solid was subjected to a second grinding and exposed again to UV irradiation for an additional 16 h, which resulted in 40% yield. Alternating grinding and irradiation, the authors managed to obtain quantitative conversion of **2.1** to **2.3**. Overall, in this work, mechanochemistry worked akin to agitation provided by stirring or heating in solution. In fact, ^{1}H NMR spectroscopy, XRD and DFT analyses showed that grinding serves to dissociate the more loosely bound **2.3** from **2.2**, where a release of strain energy and formation of a more thermodynamically stable **2.1**·**2.2** complex for a subsequent turnover are favored.

The first preparative example of photomechanochemistry via manual grinding was reported by Wang and co-workers in 2022. They reported the photo-thermo-mechanochemical approach for the synthesis of quinolines from sulfoxonium ylides and 2-vinylanilines promoted by an iron(II) phthalocyanine ($Fe^{II}Pc$) photocatalyst (Scheme 3) [65]. First, a mixture of 2-(1-phenylvinyl)aniline (**3.1**), sulfoxonium ylide **3.2**, and Na_2CO_3 was ground in a mortar at room temperature for 3–5 min. Second, the reaction mixture was transferred into a quartz tube, heated to 50 °C (heating mantle) for 18 h, while being irradiated with blue LEDs under air-equilibrated conditions. In these conditions, product **3.3** was isolated in excellent yield (94%). The reaction remained efficient across a variety of substrates, as shown in Scheme 3. The authors noted that, if the mixture was not ground before irradiation, product **3.3** was obtained in just 46% yield after isolation. Thus, the role of mechanochemistry was to achieve optimal mixing of the starting materials. The authors also noted that the reaction proceeds in the dark upon vigorous heating (120 °C). The reaction could be performed on a gram scale as well, leading to the formation of **3.3** in 92% yield.

The examples described above demonstrate that manual grinding offers simplicity and low cost for photomechanochemical reactions. However, its primary limitation lies in the manual operation and the separation of the grinding and photoreaction steps. This approach affects the reproducibility of the reaction, as it depends on the energy applied by the operator. Moreover, it is time-consuming and impractical.

Shaking and vortex grinding

To overcome the limits of manual grinding, mechanochemists have introduced automated shaking (e.g., vortex grinding) to enable the simultaneous application of mechanical forces and photon exposure.

In an early example, Toda et al. discovered that shaking a 1:1 mixture of chalcone (**4.1**) and 1,1,6,6-tetraphenylhexa-2,4-diyne-1,6-diol (**4.2**) with a test-tube shaker under irradiation with a high-pressure Hg lamp, the [2 + 2] *syn*-head-to-tail dimer product **4.3** was obtained selectively in 80% yield after 10 h (Scheme 4) [66]. In detail, **4.2** works as a host to direct the photodimerization of **4.1** in a stereoselective fashion. The authors noted that, in stark contrast, the irradiation of **4.1** alone in a crystalline state yielded a mixture of isomers of **4.3** in low

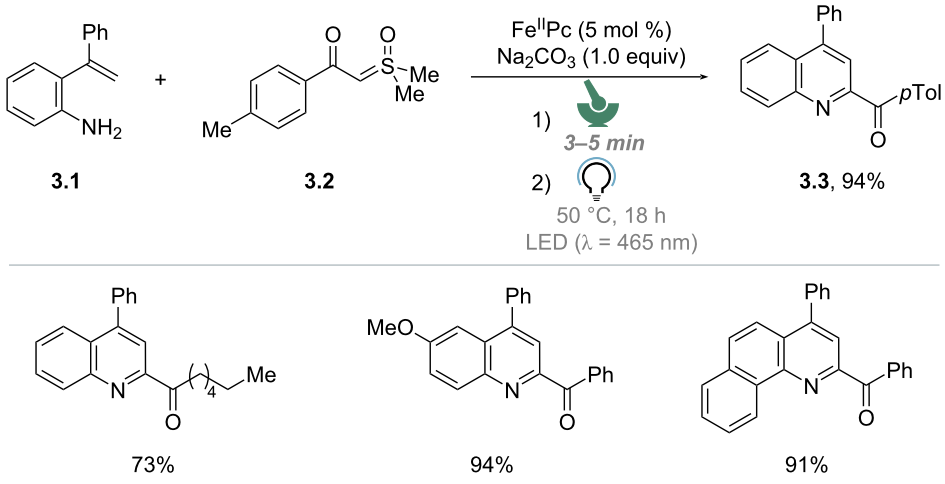

Scheme 3: Photo-thermo-mechanosynthesis of quinolines [65].

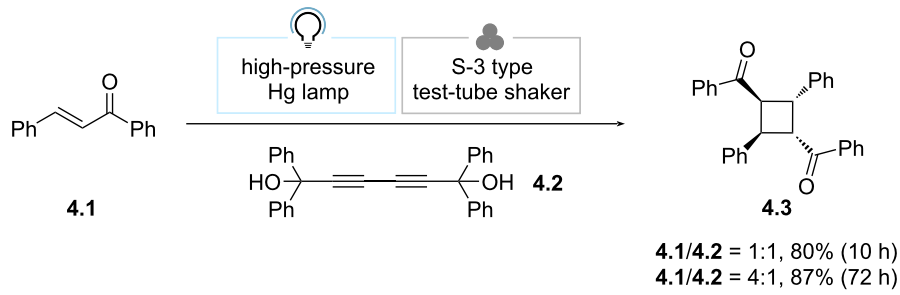

Scheme 4: Study of the mechanically assisted [2 + 2] photodimerization of chalcone [66].

yield. Intriguingly, when a 4:1 ratio of **4.1** and **4.2** was used, **4.3** was obtained in 87% yield, albeit after 72 h of irradiation. This experiment proved that **4.2** can be used in a sub-stoichiometric way, in fact acting as a catalyst.

More recently, based on their previous approach via manual grinding (Scheme 2) [64], MacGillivray and co-workers adopted the vortex grinding method to enable automated and continuous mixing during irradiation, thus increasing the reproducibility and convenience of the process [67]. In particular, the authors found that the simultaneous irradiation using a low-pressure Hg lamp and grinding led to 97% ^{1}H NMR yield of **2.3** in 24 h starting from **2.1** and **2.2**, which corresponds to a 4-fold improvement on reaction rates compared to manual grinding [64]. The authors proposed that continuous mechanical stress results in an increase of nucleation sites and allows catalysis to be accelerated with respect to manual grinding. Moreover, continued mechanical stress imparted by the adopted Zn-plated steel balls could also relieve any stress that builds up in the solid as a result of the photoreaction.

In 2014, the MacGillivray group resorted to liquid-assisted vortex grinding (LAVG) to broaden the applicability of vortex grinding (Scheme 5) [68]. The authors reported that when a 1:1 mixture of *p*-di[2-(4-pyridyl)ethenyl]benzene (**5.1**) and 4-benzylresorcinol (**5.2**) was ground with a mortar and pestle (1 h) and then irradiated with a low-pressure Hg lamp (60 h), [2.2]paracyclophane (**5.3**) was formed in poor yield (35% by ^{1}H NMR spectroscopy). Dry vortex grinding did not improve the result. However, the addition of a LAG agent (MeOH, 50 μL) in the automated grinding step dramatically improved the outcome (quantitative conversion after 20 h of irradiation). Intriguingly, the simultaneous LAVG and irradiation enabled the formation of **5.3** in 97% yield upon reduced irradiation time (10 h).

Rod milling

A different approach is offered by rod milling. It employs a glass rod positioned within a transparent glass test tube that contains the reaction mixture. Through the rotation of the rod, shearing forces are gently applied to facilitate the reaction, while continuously exposing fresh material to light.

In 2016, König and co-workers exploited rod milling to develop a photomechanochemical approach for the riboflavin tetraacetate (RFTA)-catalyzed photocatalytic oxidation of alcohols to the corresponding carbonyl compounds upon irradiation with five LEDs (λ = 455 nm) [69]. As an example, the authors were able to convert 4,4'-dimethoxybenzhydrol (**6.1**) to 4,4'-dimethoxybenzophenone (**6.2**) in 74% yield after isolation using

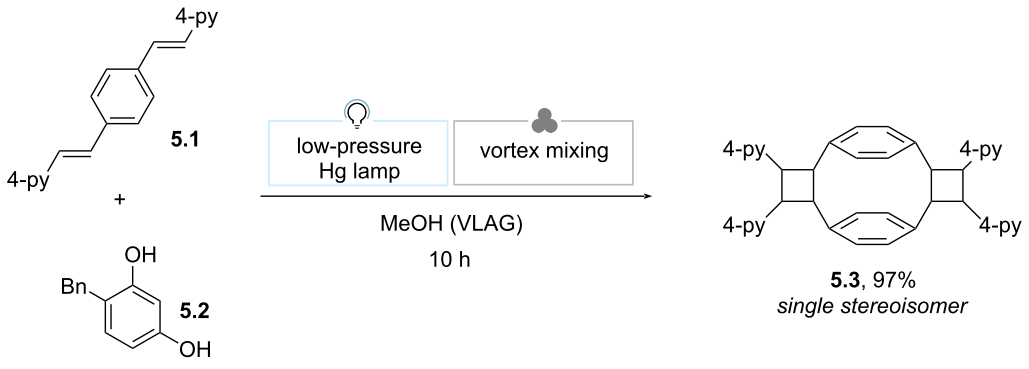

Scheme 5: Liquid-assisted vortex grinding (LAVG) for the synthesis of [2.2]paracyclophane [68].

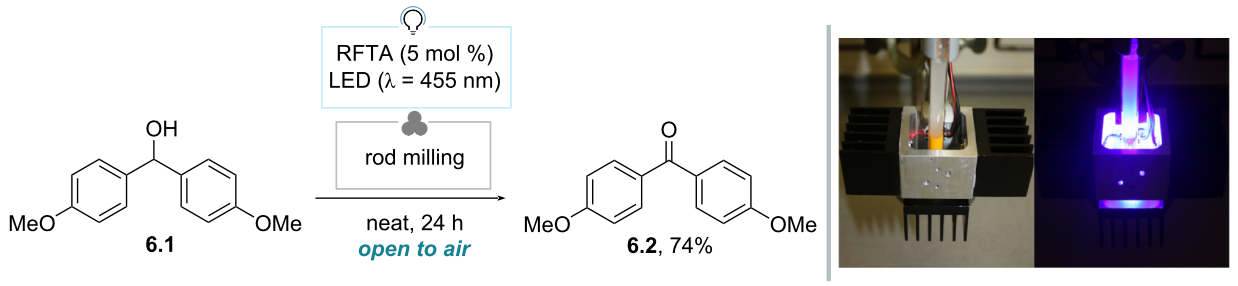

Scheme 6: Photomechanochemical approach for the riboflavin tetraacetate-catalyzed photocatalytic oxidation of alcohols. The photos in Scheme 6 were reproduced from [69] (© 2016 M. Obst et al., published by Beilstein-Institut, distributed under the terms of the Creative Commons Attribution 4.0 International License, https://creativecommons.org/licenses/by/4.0).

5 mol % RFTA under air (24 h), all performed without any additional solvent (Scheme 6). The authors noted that the reaction proceeds via a molten state, since in a control experiment without RFTA the mixture was found to liquefy. This was due to the heat generated by LEDs and not by the grinding action. Thus, light irradiation fulfils a double function: the excitation of the photocatalyst and melting of the substrate, inducing mobility of the molecules and the occurrence of the catalytic cycle. On a different note, the authors stressed that ball milling did not allow to form the expected product. This happened because light was unable to reach the photocatalyst in the latter setup, due to small amounts of solid adhering to the inner surface of the jar and the shielding effect within the milling chamber.

Ball milling

Manual and vortex grinding present certain advantages, such as a low initial investment for conducting photomechanochemistry. However, these methods face significant limitations that restrict the integration of photomechanochemistry into synthetic workflows, both in academia and industry. They are inherently low in throughput, lack standardized equipment for photochemical reactions, and suffer from poor reproducibility. In fact, it is striking that often little detail is given regarding the geometry of the setup as well as the milling conditions. Additionally, these methods are neither scalable nor typically suitable for automation. Therefore, it comes as no surprise that the examples described above bear little synthetic potential.

The substantial technological advancements within the chemical field have impacted mechanochemistry as well, leading to the introduction of ball milling, which enables precise control over energy input, operating temperatures, and offers the potential for automated, reproducible processes. As an added benefit, the use of closed reactors ensures maximum operational safety, preventing direct exposure of the operator to potentially hazardous solid mixtures. A key technological challenge in this domain is to develop methods to effectively deliver photons to the reaction mixture.

In 2017, Štrukil reported the first instance of a photochemical reaction conducted within a ball milling apparatus: the authors termed this approach “mechanochemically-assisted solid-state photocatalysis” (Scheme 7) [70]. Therein, a custom-built photoreactor was integrated into a standard laboratory ball mill apparatus. This reactor, equipped with blue LEDs, allowed for adjustable light intensity and maintained optimal temperature regulation using a fan. To overcome the challenge posed by the non-transparency of milling jars, a glass capsule was utilized.

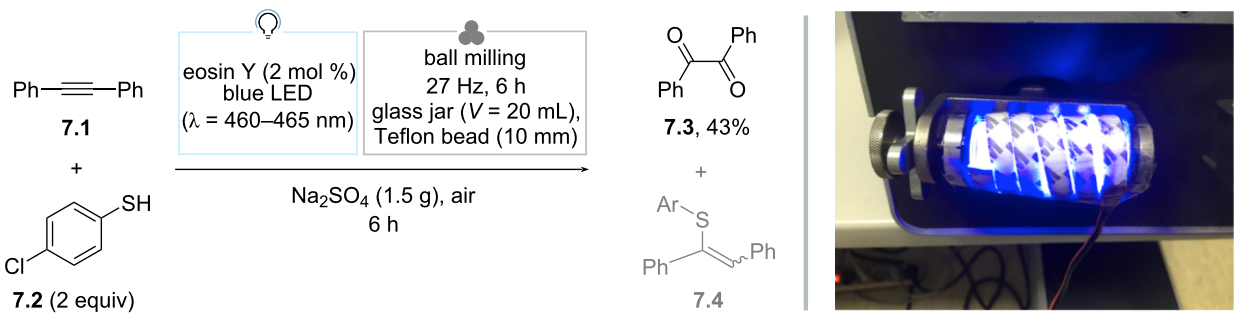

Scheme 7: Photomechanochemical oxidation of 1,2-diphenylethyne to benzil. The photo in Scheme 7 was republished with permission of The Royal Society of Chemistry, from [70] (“Mechanochemically-assisted solid-state photocatalysis (MASSPC)” by V. Štrukil et al., Chem. Commun., vol. 53, © 2017); permission conveyed through Copyright Clearance Center, Inc. This content is not subject to CC BY 4.0

Teflon balls were employed to grind the reagents, thereby minimizing wear on the milling vessel. As a benchmark reaction, they selected the photochemical oxidation of 1,2-diphenylethyne to benzil [71]. Thus, when a 1:2 mixture of **7.1** and 4-chlorothiophenol (**7.2**) was ground in the presence of eosin Y as the photocatalyst and anhydrous Na_2SO_4 as a bulking agent, benzil (**7.3**) was obtained in 43% GC yield under blue light irradiation (LED, 14.5 W). Isolation led to diminished yields (ca. 35%). When milling was conducted in the dark, only traces of **7.3** were detected and an isomeric mixture of 1-(4-chlorophenylthio)stilbene (**7.4**, *E*:*Z* 33:67) was observed. The authors demonstrated that, when **7.4** (mixture) was irradiated, it was readily converted to **7.3** (36%, 4 h). Overall, it was concluded that **7.1** and **7.2** first react to give **7.4** via a dark mechanochemical thiol–yne reaction; the latter is then converted to **7.3** by singlet oxygen generated in situ, by eosin Y. It is important to notice here that the reaction is proposed to proceed according to a different mechanistic scenario than that operating in solution [71], where photogenerated thiyl radicals proved crucial intermediates.

Parallelly, Hernández reported a photomechanochemical approach for the borylation of aryldiazonium salts in a ball milling apparatus equipped with a transparent polymethylmethacrylate (PMMA) jar (Scheme 8) [72]. As far as the irradiation source is concerned, the authors wrapped a LED strip around the jar. A solution-based precedent by the Yan group was used as a benchmark transformation [73]. Under optimized conditions, a mixture of diazonium salt **8.1**, B_2Pin_2 (1.5 equiv) and eosin Y (5 mol %) was irradiated with green light while being milled in a 25 mL PMMA milling jar with 15 ZrO_2 balls of 5 mm in diameter at 25 Hz. The expected product **8.2** was obtained in 68% yield after isolation. A comprehensive set of control experiments highlighted the essential role of mechanochemistry in enhancing the mixing efficiency and increasing the exposure of the surface of the reaction mixture to light. Additionally, the formation of compound **8.2** was associated with the observation of an initial molten state of the mixture, which could have promoted single-electron-transfer processes that are crucial for product formation. Lastly, the author noted that the inclusion of acetonitrile as a LAG agent enabled the transformation even without the presence of a photocatalyst [72,74].

In 2023, Braunschweig and co-workers reported the photomechanochemical [2 + 2] cycloaddition of acenaphthylene (**9.1**) (Scheme 9) [75]. In this case the authors used a ball-mill reactor equipped with a blue LED, and the reaction was run in a glass vial with two transparent PMMA balls. The authors noted that fluorination of the vial and the use of silica gel to adjust texture were needed to prevent reagent adhesion on the vial walls. Thus, the reactor was operated at 17.7 Hz for 20 h and the dimerization to **9.2** occurred in 96% ^{1}H NMR yield with a 6:94 *anti*/*syn* selectivity. A different selectivity was observed when crystals were first ground, and then irradiated under argon without applying forces (65% yield, 70:30 *anti*/*syn*). This indicates a unique divergent photomechanochemical reaction pathway with respect to the simple irradiation in solid state. Remarkably, no selectivity was observed in solution state (DMSO as solvent), while a completely reversed selectivity (99%, *anti*/*syn* 91:9) was obtained when using an anti-solvent (H_2O). To account for the unique outcome of photomechanochemical conditions, the authors performed a DFT study and introduced the concept of mechanosusceptibility. Briefly, they computationally applied a force along the C–C-bond-forming tensor that would result in the formation of either the *syn* or the *anti* products, and found that the bond-forming event leading to the former can occur at lower applied forces.

In the same year, Borchardt reported the first use of a ball mill with UV light for Mallory and cyclodehydrochlorination reactions (Scheme 10) [76]. The authors proposed a photomechanochemical reactor where the jar of the ball mill vibrates

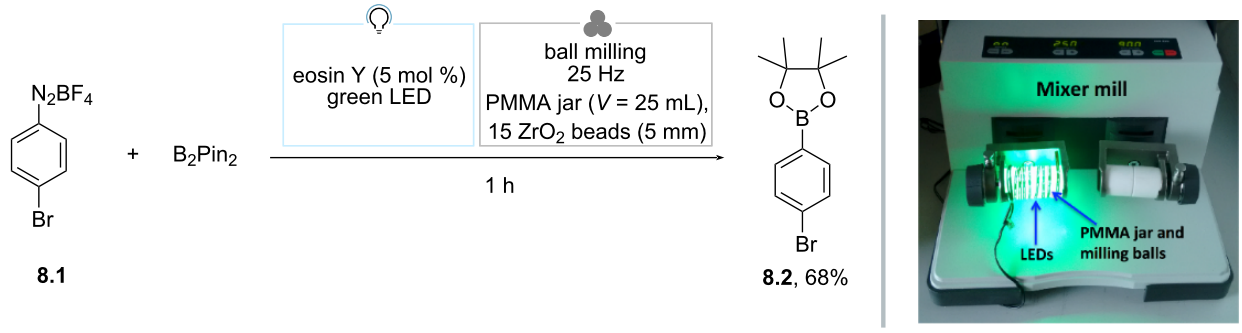

Scheme 8: Photomechanochemical borylation of aryldiazonium salts. The photo in Scheme 8 was reproduced from [72] (© 2017 J. G. Hernández et al., published by Beilstein-Institut, distributed under the terms of the Creative Commons Attribution 4.0 International License, https://creativecommons.org/licenses/by/4.0).

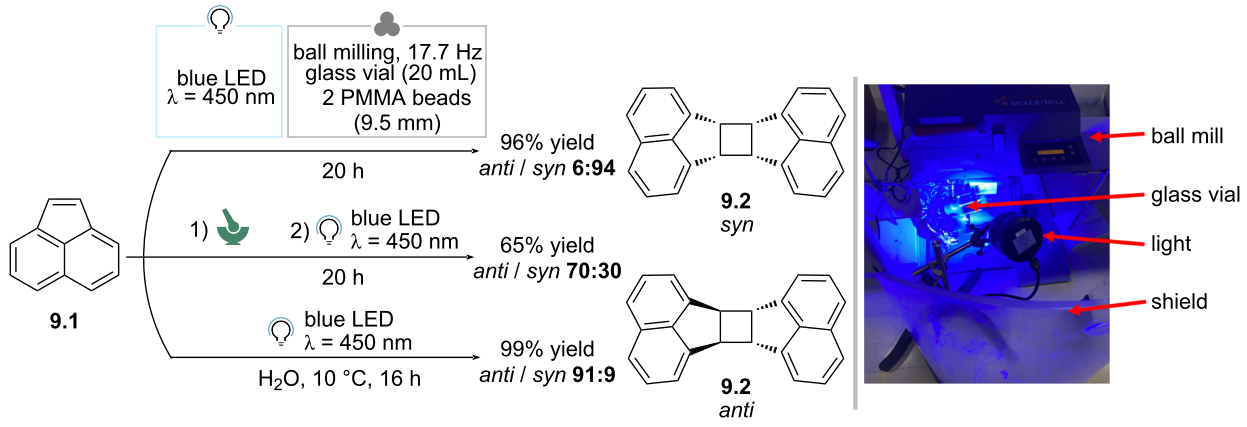

Scheme 9: Photomechanochemical control over stereoselectivity in the [2 + 2] dimerization of acenaphthylene. The photo in Scheme 9 was republished with permission of The Royal Society of Chemistry, from [75] ("Photomechanochemical control over stereoselectivity in the [2 + 2] photodimerization of acenaphthylene" by S. Biswas et al., Faraday Discuss., vol. 241, © 2023); permission conveyed through Copyright Clearance Center, Inc. This content is not subject to CC BY 4.0.

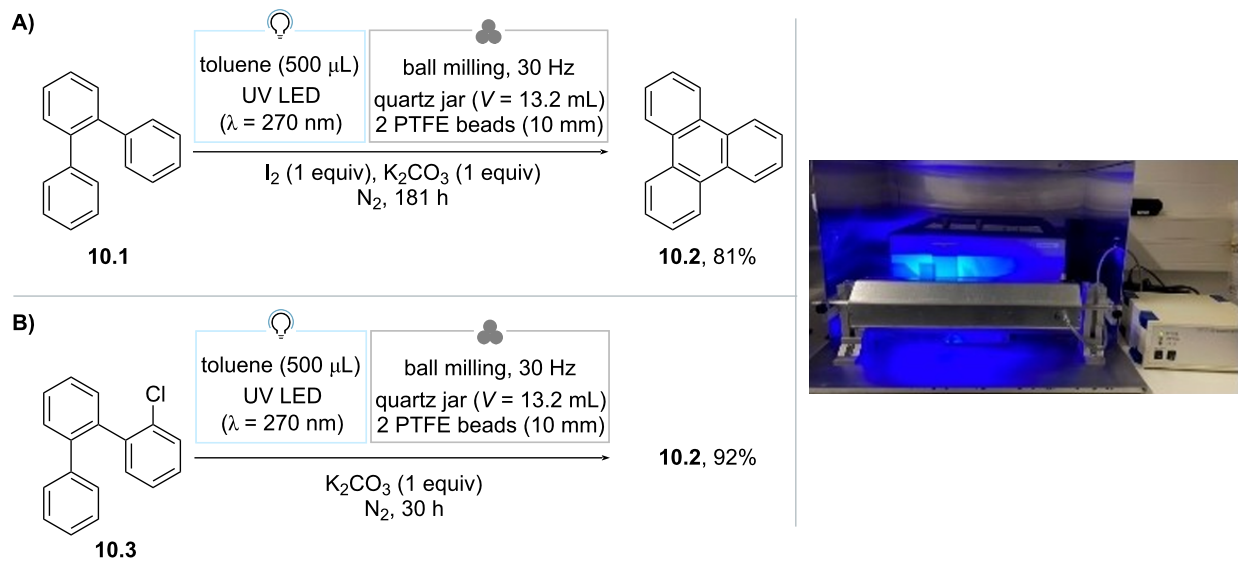

Scheme 10: Photomechanochemical synthesis of polyaromatic compounds using UV light. The photo in Scheme 10 was reproduced from [76] (© 2023 D. M. Baier et al., published by Wiley-VCH GmbH, distributed under the terms of the Creative Commons Attribution-NonCommercial 4.0 International License, https://creativecommons.org/licenses/by-nc/4.0/). This content is not subject to CC BY 4.0.

within an aluminum frame on which UV-C LEDs are mounted. The milling vessel used in this process is a cylinder of quartz glass with PFA (perfluoroalkoxyalkane) caps on both ends to absorb impacts. Thus, the Mallory reaction to get triphenylene was investigated. When *o*-terphenyl (**10.1**) was milled (30 Hz, PTFE balls) and irradiated (λ = 270 nm) in the presence of silica gel (bulking agent), I_2 (1 equiv) as an oxidant, and K_2CO_3 (1 equiv) as a base in the presence of toluene, the expected product **10.2** was obtained in 81% yield after isolation upon 181 h of irradiation. The authors claim that toluene acts as a photosensitizer since cyclohexane, which has similar solubilizing power, did not serve well as a LAG agent. The authors demonstrated that nanographenes could be obtained via cyclodehydrochlorination of **10.3** under photomechanochemical conditions as well. Also in this case, the addition of toluene was beneficial and excellent yield of the corresponding product (**10.2**) was observed in 30 h of reaction. As a comparison, the latter reaction required 48 h in solution. Intriguingly, **10.3** could in turn be synthesized via a mechanochemical Suzuki coupling, demonstrating superior performance compared to the solution-phase approach. This mechanochemical method afforded **10.3** in approximately the same yield, but significantly faster, com-

pleting the reaction in 2 h instead of 24 h. Overall, in this case, milling ensures the necessary mixing of the reactants and continuously exposes fresh surfaces of the solids to light. The authors were able to scale the conversion of **10.3** to **10.2** on a gram scale (1 g), even though with a diminished yield (48%) due to inefficient mixing.

In a recent instance, Millward and Zysman-Colman reported a comprehensive exploration of the benefits of the photomechanochemical approach in the field of synthesis [77]. Specifically, they developed photomechanochemical conditions for the atom-transfer-radical addition (ATRA) of sulfonyl chlorides to alkenes, pinacol coupling of carbonyl compounds, decarboxylative acylation, and photocatalyzed [2 + 2] cycloaddition (Scheme 11).

Regarding the experimental setup, the authors adapted a commercially available ball mill, by introducing a custom-made stainless steel safety shield to minimize unwanted light leakage. The interior surface of the shield is somewhat reflective. A hole in the milling shield above each jar holder allows for irradiation of the reaction glass vessels from above using powerful LED lamps.

First, photomechanochemistry facilitated the copper-photocatalyzed ATRA of sulfonyl chlorides and styrenes under fully aerobic conditions (Scheme 11A), a feature unattainable in traditional solution-phase synthesis. In fact, in the latter case, almost complete recovery of the starting material was observed. Second, the authors found that the replacement of diisopropylethylamine (DIPEA) with Hantzsch ester in the role of sacrificial reductant for the pinacol coupling of benzaldehyde enables solvent-free conditions for this transformation (Scheme 11B). Here, the aggregation state of the substrate and the reductant proved to be crucial to establish a fully operative protocol. The third reaction tested under mechanophotocatalytic conditions was the well-established decarboxylative acylation of electrophilic olefins (Scheme 11C). Compared to solution-phase pho-

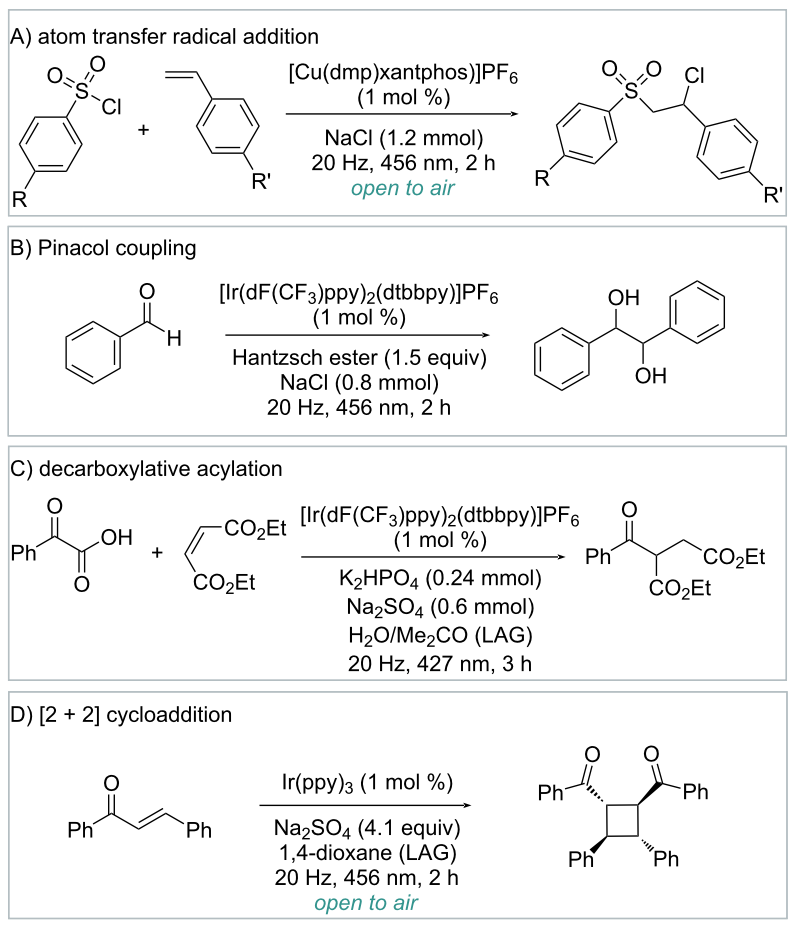

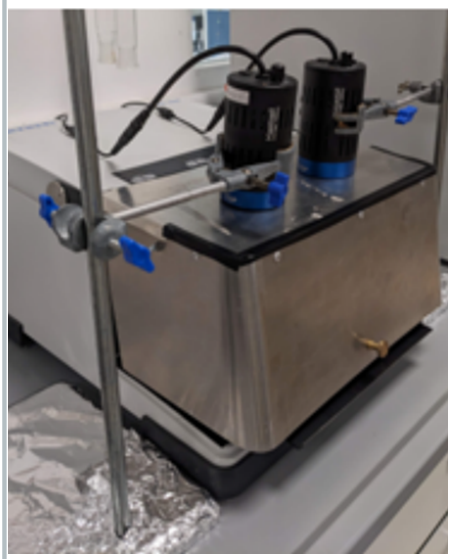

Scheme 11: Mechanically assisted photocatalytic reactions: A) atom-transfer-radical addition, B) pinacol coupling, C) decarboxylative alkylation, D) [2 + 2] cycloaddition. The photo in Scheme 11 was reproduced from [77] (© 2024 F. Millward et al., published by Wiley-VCH GmbH, distributed under the terms of the Creative Commons Attribution 4.0 International License, https://creativecommons.org/licenses/by/4.0).

tocatalysis, photomechanochemical conditions allowed to reduce the reaction time from 24 h to 3 h while maintaining comparable yields. Finally, the authors proved that photomechanochemistry contributes to the initial rate enhancement of photocatalyzed [2 + 2] cycloadditions under aerobic conditions, even though over longer irradiation times the solution-state yields are superior (Scheme 11D).

Very recently, Wu, Wang, and co-workers proposed a radically different approach to photomechanochemistry [78]. Rather than trying to interface two technologies, the authors opted to use mechanoluminescent powders to generate photons directly inside the jar. In more detail, $SrAl_2O_4:Eu^{2+}/Dy^{3+}$ (SAOED) was used as a mechanoluminescent material to drive the visible-light-mediated Hofmann–Loffler–Freytag (HLF) reaction (Scheme 12A). Thus, when using a mixture of **12.1** (0.2 mmol), NaI (1 equiv), Koser's reagent, and Na_2CO_3 (each 4 equiv), in the presence of 100 wt % of SAOED, pyrrolidine **12.2** was isolated in 90% yield. As far as the mechanochemical setup is concerned, the authors milled the reaction mixture at 30 Hz in a 5 mL stainless-steel jar equipped with twenty stainless-steel balls (Ø = 3 mm). Intriguingly, the authors noticed that multiple smaller balls, when used in a comparable total mass, outperformed a single larger ball in terms of reaction efficiency. Moreover, intermittent milling (4 × 30 min periods with 5 min breaks instead of 2 h in a row) proved beneficial to minimize heat accumulation resulting in product decomposition. Next, the authors proved the generality of mechanoluminescence by performing the sulfonylation of alkenes via EDA-complexes photochemistry (Scheme 12B). Thus, when a mixture of 1,1-diphenylethylene (**12.3**, 0.2 mmol), tosyl chloride (**12.4**, 2 equiv), and tris(4-methoxyphenyl)amine (10 mol %) was milled in the presence of 100 wt % of SAOED at 30 Hz for 3 h, sulfone **12.5** was obtained in 89% yield after isolation. The synthesis of **12.5** was scaled up to 15 mmol scale, obtaining the desired product in a yield of 79%. Scanning electron microscopy (SEM) analysis revealed the deformation and reduction in size of SAOED particles upon milling. Interestingly, carbon determination experiments revealed that SAOED is quickly poisoned by organic matter, thus hampering recyclability. This can be to some extent reversed via calcination (700 °C, 2 h).

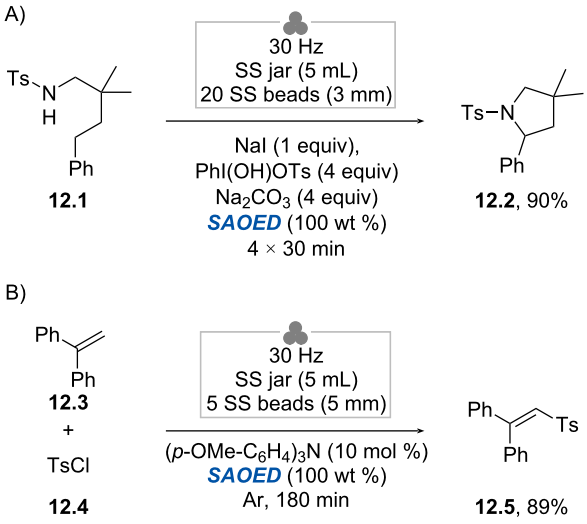

Scheme 12: Use of mechanoluminescent materials as photon sources for photomechanochemistry. SAOED: $SrAl_2O_4:Eu^{2+}/Dy^{3+}$.
A) Hofmann–Loffler–Freytag reaction; B) EDA-based photochemistry [78].

Conclusion and Future Directions

In this Perspective, we have examined how photons and impact forces have been merged so far. Although early examples of photomechanochemistry date back to the 1980s, there has been a recent surge in interest. It is important to note that photomechanochemistry remains in its early stages, with studies thus far focusing primarily on straightforward transformations, such as [2 + 2] photodimerization, and a limited number of preparative examples. In most examples, mechanochemistry is proposed to constantly expose fresh surface to light and promote mass transfer. As understanding of the methodology advances, the development of more complex synthetic strategies, including C–H, C–C, and C–heteroatom-bond formation, is expected [79]. Moreover, we anticipate that the difference in photophysical properties between organic molecules in diluted and extremely concentrated solutions will lead to unprecedented reactivity.

From a conceptual standpoint, the examples presented above effectively illustrate that each discipline offers unique benefits within this marriage. On one side, as amply discussed in the introduction, photochemistry allows to leverage reactivity modes inaccessible through traditional approaches. On the other side, mechanochemistry brings around advantages in terms of sustainability and operational efficiency. Firstly, it either eliminates the need for solvents entirely or significantly reduces their use, as in liquid-assisted grinding (LAG). This minimizes waste production compared to conventional solution-based methods. This is particularly advantageous when high-boiling point (e.g., DMSO) or noxious solvents (e.g., DMF and halogenated ones) are required. It is worth noting, however, that in some cases the heat generated from the high-power light sources causes the reaction mixture to melt, which might not be general, but rather substrate-dependent. Secondly, mechanochemistry allows the synthesis practitioner to run reactions at maximal concentrations, accelerating reaction rates and enabling processes involving insoluble reagents and/or photocatalysts. Additionally, as discussed, the use of impact forces can lead to unique selectivity profiles compared to solution-based methods, further

enhancing its utility. Thirdly, dissolved oxygen must be often meticulously removed in solution-based methods via tedious techniques such as freeze-pump-thaw. By eliminating solvents, mechanochemistry enables the development of more practical and efficient photochemical protocols, especially at scale, where degassing large volumes is technologically and economically challenging.

From a practical standpoint, the progression from manual grinding to ball milling was a natural development, yet there is still significant potential for further advancements. The examples discussed above clearly show that mechanochemistry and light-driven synthesis have evolved at different rates, with each field capturing the interest of distinct research communities. This has led to the creation of hybrid systems – improvised combinations of commercial ball mills with transparent jars (e.g., PMMA, glass, quartz, or epoxy resin) and off-the-shelf LED lamps or strips. However, a standardized apparatus for photomechanochemistry is not available yet. Looking forward, designing specialized equipment capable of integrating both mechanical impact forces and photon input would be highly beneficial.

Moreover, a major challenge limiting the widespread adoption of mechanochemistry in industrial applications is scalability [80], a concern that also extends to photomechanochemistry. One potential solution to address this issue has been the introduction of twin-screw extruders [81]. However, it remains uncertain whether this approach can be effectively adapted for use in photomechanochemical processes. Such dedicated machinery could enable a synergistic interaction between photons and forces, streamlining the combination of mechanochemical and photochemical processes and paving the way for more efficient, sustainable, and selective transformations in organic synthesis. An unexplored opportunity is offered by resonant acoustic mixing (RAM) [82], a technology that leverages low frequency acoustic waves to deliver controlled mechanical force within a reaction vessel. In this case, cheap commercially available glass vessels present in all laboratories can be used, thus solving the issue of fabricating custom-made transparent jars. Intriguingly, RAM appears an ideal technique for high-throughput experimentation [83]. A further area of development would be the possibility of integrating options for the in-situ monitoring of reactions, such as X-ray and Raman techniques [47,48,84-87].

In conclusion, in recognizing that both photochemistry and mechanochemistry provide highly sustainable approaches for synthesis, we envision a powerful synergy between these fields. In fact, we provide a SWOT (*Strengths, Weaknesses, Opportunities, Threats*) analysis for the strategic development of this new exciting field (Figure 3). By combining their knowledge, researchers working at this interface have the potential to redefine the landscape of sustainable synthesis, with this Perspective serving as a snapshot of the current state-of-the-art.

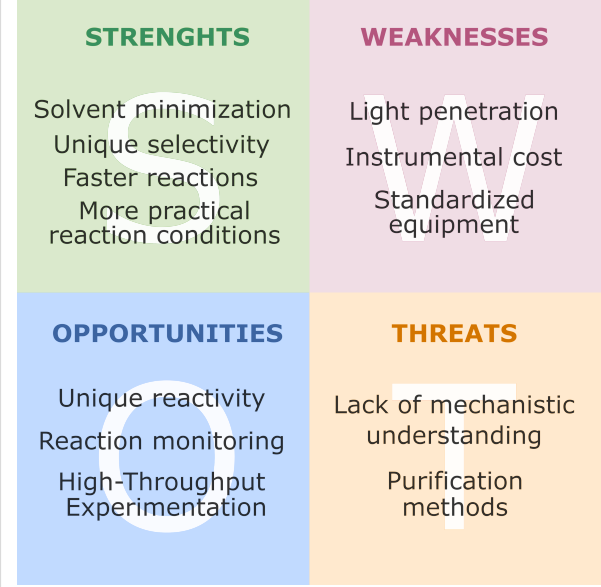

Figure 3: SWOT (strengths, weaknesses, opportunities, threats) analysis of photomechanochemistry.

Acknowledgements

L.C. acknowledges the COMP-HUB and COMP-R Initiatives, funded by the 'Departments of Excellence' programs of the Italian Ministry for University and Research (MUR, 2018–2027). We also wish to thank Chiara Armento for support in the production of the graphical abstract.

Author Contributions

Francesco Mele: conceptualization; data curation; writing – original draft; writing – review & editing. Ana M. Constantin: conceptualization; data curation; writing – original draft; writing – review & editing. Andrea Porcheddu: writing – review & editing. Raimondo Maggi: writing – review & editing. Giovanni Maestri: writing – review & editing. Nicola Della Ca': project administration; writing – review & editing. Luca Capaldo: conceptualization; data curation; project administration; supervision; writing – original draft; writing – review & editing.

ORCID® iDs

Francesco Mele - https://orcid.org/0000-0001-6921-1963
Ana M. Constantin - https://orcid.org/0000-0001-7781-2064
Andrea Porcheddu - https://orcid.org/0000-0001-7367-1102
Raimondo Maggi - https://orcid.org/0000-0003-3811-7186
Giovanni Maestri - https://orcid.org/0000-0002-0244-8605

Nicola Della Ca' - https://orcid.org/0000-0002-7853-7954
Luca Capaldo - https://orcid.org/0000-0001-7114-267X

Data Availability Statement

Data sharing is not applicable as no new data was generated or analyzed in this study.

References

1. Hammond, G. S.; Turro, N. J. *Science* **1963,** *142,* 1541–1553. doi:10.1126/science.142.3599.1541
2. Albini, A.; Fagnoni, M., Eds. *Photochemically-Generated Intermediates In Synthesis;* John Wiley & Sons: Hoboken, NJ, USA, 2013. doi:10.1002/9781118689202
3. Zimmerman, H. E. *Angew. Chem., Int. Ed. Engl.* **1969,** *8,* 1–11. doi:10.1002/anie.196900011
4. Zhao, J.; Wu, W.; Sun, J.; Guo, S. *Chem. Soc. Rev.* **2013,** *42,* 5323–5351. doi:10.1039/c3cs35531d
5. Zhou, Q.-Q.; Zou, Y.-Q.; Lu, L.-Q.; Xiao, W.-J. *Angew. Chem., Int. Ed.* **2019,** *58,* 1586–1604. doi:10.1002/anie.201803102
6. Strieth-Kalthoff, F.; James, M. J.; Teders, M.; Pitzer, L.; Glorius, F. *Chem. Soc. Rev.* **2018,** *47,* 7190–7202. doi:10.1039/c8cs00054a
7. Albini, A. *Synthesis* **1981,** 249–264. doi:10.1055/s-1981-29405
8. Strieth-Kalthoff, F.; Glorius, F. *Chem* **2020,** *6,* 1888–1903. doi:10.1016/j.chempr.2020.07.010
9. Chan, A. Y.; Perry, I. B.; Bissonnette, N. B.; Buksh, B. F.; Edwards, G. A.; Frye, L. I.; Garry, O. L.; Lavagnino, M. N.; Li, B. X.; Liang, Y.; Mao, E.; Millet, A.; Oakley, J. V.; Reed, N. L.; Sakai, H. A.; Seath, C. P.; MacMillan, D. W. C. *Chem. Rev.* **2022,** *122,* 1485–1542. doi:10.1021/acs.chemrev.1c00383
10. Shaw, M. H.; Twilton, J.; MacMillan, D. W. C. *J. Org. Chem.* **2016,** *81,* 6898–6926. doi:10.1021/acs.joc.6b01449
11. McAtee, R. C.; McClain, E. J.; Stephenson, C. R. J. *Trends Chem.* **2019,** *1,* 111–125. doi:10.1016/j.trechm.2019.01.008
12. Romero, N. A.; Nicewicz, D. A. *Chem. Rev.* **2016,** *116,* 10075–10166. doi:10.1021/acs.chemrev.6b00057
13. Capaldo, L.; Ravelli, D.; Fagnoni, M. *Chem. Rev.* **2022,** *122,* 1875–1924. doi:10.1021/acs.chemrev.1c00263
14. Cao, H.; Tang, X.; Tang, H.; Yuan, Y.; Wu, J. *Chem Catal.* **2021,** *1,* 523–598. doi:10.1016/j.checat.2021.04.008
15. Ye, Z.; Lin, Y.-M.; Gong, L. *Eur. J. Org. Chem.* **2021,** 5545–5556. doi:10.1002/ejoc.202101036
16. Albini, A. *Photochemistry;* Springer: Berlin, Heidelberg, 2016. doi:10.1007/978-3-662-47977-3
17. von Grothuss, T. *Abhandlungen über Elektrizität und Licht;* W. Engelmann: Leipzig, Germany, 1906.
18. Einstein, A. *Ann. Phys. (Berlin, Ger.)* **1912,** *342,* 832–838. doi:10.1002/andp.19123420413
19. Plutschack, M. B.; Pieber, B.; Gilmore, K.; Seeberger, P. H. *Chem. Rev.* **2017,** *117,* 11796–11893. doi:10.1021/acs.chemrev.7b00183
20. Capaldo, L.; Wen, Z.; Noël, T. *Chem. Sci.* **2023,** *14,* 4230–4247. doi:10.1039/d3sc00992k
21. Wang, Q.; Yin, R.; Wang, Z.; Zhang, Y.; Wu, J. *J. Flow Chem.* **2024,** *14,* 97–107. doi:10.1007/s41981-023-00302-z
22. Cambié, D.; Bottecchia, C.; Straathof, N. J. W.; Hessel, V.; Noël, T. *Chem. Rev.* **2016,** *116,* 10276–10341. doi:10.1021/acs.chemrev.5b00707
23. Sambiagio, C.; Noël, T. *Trends Chem.* **2020,** *2,* 92–106. doi:10.1016/j.trechm.2019.09.003
24. Zondag, S. D. A.; Mazzarella, D.; Noël, T. *Annu. Rev. Chem. Biomol. Eng.* **2023,** *14,* 283–300. doi:10.1146/annurev-chembioeng-101121-074313
25. Dong, Z.; Wen, Z.; Zhao, F.; Kuhn, S.; Noël, T. *Chem. Eng. Sci.: X* **2021,** *10,* 100097. doi:10.1016/j.cesx.2021.100097
26. Bianchi, P.; Williams, J. D.; Kappe, C. O. *J. Flow Chem.* **2020,** *10,* 475–490. doi:10.1007/s41981-020-00105-6
27. Debrouwer, W.; Kimpe, W.; Dangreau, R.; Huvaere, K.; Gemoets, H. P. L.; Mottaghi, M.; Kuhn, S.; Van Aken, K. *Org. Process Res. Dev.* **2020,** *24,* 2319–2325. doi:10.1021/acs.oprd.0c00150
28. Vandekerckhove, B.; Ruttens, B.; Metten, B.; Stevens, C. V.; Heugebaert, T. S. A. *React. Chem. Eng.* **2024,** *9,* 1784–1795. doi:10.1039/d4re00058g
29. Dong, Z.; Zondag, S. D. A.; Schmid, M.; Wen, Z.; Noël, T. *Chem. Eng. J.* **2022,** *428,* 130968. doi:10.1016/j.cej.2021.130968
30. Pieber, B.; Shalom, M.; Antonietti, M.; Seeberger, P. H.; Gilmore, K. *Angew. Chem., Int. Ed.* **2018,** *57,* 9976–9979. doi:10.1002/anie.201712568
31. Pomberger, A.; Mo, Y.; Nandiwale, K. Y.; Schultz, V. L.; Duvadie, R.; Robinson, R. I.; Altinoglu, E. I.; Jensen, K. F. *Org. Process Res. Dev.* **2019,** *23,* 2699–2706. doi:10.1021/acs.oprd.9b00378
32. Anastas, P.; Eghbali, N. *Chem. Soc. Rev.* **2010,** *39,* 301–312. doi:10.1039/b918763b
33. Erythropel, H. C.; Zimmerman, J. B.; de Winter, T. M.; Petitjean, L.; Melnikov, F.; Lam, C. H.; Lounsbury, A. W.; Mellor, K. E.; Janković, N. Z.; Tu, Q.; Pincus, L. N.; Falinski, M. M.; Shi, W.; Coish, P.; Plata, D. L.; Anastas, P. T. *Green Chem.* **2018,** *20,* 1929–1961. doi:10.1039/c8gc00482j
34. Obst, M.; Kõnig, B. *Eur. J. Org. Chem.* **2018,** 4213–4232. doi:10.1002/ejoc.201800556
35. Dou, Q.; Zeng, H. *Curr. Opin. Green Sustainable Chem.* **2023,** *40,* 100766. doi:10.1016/j.cogsc.2023.100766
36. Russo, C.; Brunelli, F.; Tron, G. C.; Giustiniano, M. *J. Org. Chem.* **2023,** *88,* 6284–6293. doi:10.1021/acs.joc.2c00805
37. Cortes-Clerget, M.; Yu, J.; Kincaid, J. R. A.; Walde, P.; Gallou, F.; Lipshutz, B. H. *Chem. Sci.* **2021,** *12,* 4237–4266. doi:10.1039/d0sc06000c
38. Han, X.; Poliakoff, M. *Chem. Soc. Rev.* **2012,** *41,* 1428–1436. doi:10.1039/c2cs15314a
39. Tian, Y.-M.; Silva, W.; Gschwind, R. M.; König, B. *Science* **2024,** *383,* 750–756. doi:10.1126/science.adl3092
40. Howard, J. L.; Cao, Q.; Browne, D. L. *Chem. Sci.* **2018,** *9,* 3080–3094. doi:10.1039/c7sc05371a
41. Cuccu, F.; De Luca, L.; Delogu, F.; Colacino, E.; Solin, N.; Mocci, R.; Porcheddu, A. *ChemSusChem* **2022,** *15,* e202200362. doi:10.1002/cssc.202200362
42. Friščić, T.; Mottillo, C.; Titi, H. M. *Angew. Chem., Int. Ed.* **2020,** *59,* 1018–1029. doi:10.1002/anie.201906755
43. Gao, Y.; Kubota, K.; Ito, H. *Angew. Chem., Int. Ed.* **2023,** *62,* e202217723. doi:10.1002/anie.202217723
44. Templ, J.; Schnurch, M. *Angew. Chem., Int. Ed.* **2024,** *63,* e202411536. doi:10.1002/anie.202411536
45. Seo, T.; Toyoshima, N.; Kubota, K.; Ito, H. *J. Am. Chem. Soc.* **2021,** *143,* 6165–6175. doi:10.1021/jacs.1c00906
46. Leitch, J. A.; Browne, D. L. *Chem. – Eur. J.* **2021,** *27,* 9721–9726. doi:10.1002/chem.202100348

47. Friščić, T.; Halasz, I.; Beldon, P. J.; Belenguer, A. M.; Adams, F.; Kimber, S. A. J.; Honkimäki, V.; Dinnebier, R. E. *Nat. Chem.* **2013,** *5,* 66–73. doi:10.1038/nchem.1505
48. Užarević, K.; Halasz, I.; Friščić, T. *J. Phys. Chem. Lett.* **2015,** *6,* 4129–4140. doi:10.1021/acs.jpclett.5b01837
49. Michalchuk, A. A. L.; Emmerling, F. *Angew. Chem., Int. Ed.* **2022,** *61,* e202117270. doi:10.1002/anie.202117270
50. Hutchings, B. P.; Crawford, D. E.; Gao, L.; Hu, P.; James, S. L. *Angew. Chem., Int. Ed.* **2017,** *56,* 15252–15256. doi:10.1002/anie.201706723
51. Kim, J. H.; Matsuoka, M.; Fukunishi, K. *Dyes Pigm.* **1996,** *31,* 263–272. doi:10.1016/0143-7208(96)00015-0
52. Holmes, W. C. *Ind. Eng. Chem.* **1924,** *16,* 35–40. doi:10.1021/ie50169a014
53. Lavorel, J. *J. Phys. Chem.* **1957,** *61,* 1600–1605. doi:10.1021/j150558a006
54. Crisenza, G. E. M.; Mazzarella, D.; Melchiorre, P. *J. Am. Chem. Soc.* **2020,** *142,* 5461–5476. doi:10.1021/jacs.0c01416
55. Martinez, V.; Stolar, T.; Karadeniz, B.; Brekalo, I.; Užarević, K. *Nat. Rev. Chem.* **2022,** *7,* 51–65. doi:10.1038/s41570-022-00442-1
56. Cohen, M. D. *Angew. Chem., Int. Ed. Engl.* **1975,** *14,* 386–393. doi:10.1002/anie.197503861
57. Cohen, M. D. *Tetrahedron* **1987,** *43,* 1211–1224. doi:10.1016/s0040-4020(01)90244-3
58. Ying, P.; Yu, J.; Su, W. *Adv. Synth. Catal.* **2021,** *363,* 1246–1271. doi:10.1002/adsc.202001245
59. Capaldo, L.; Ravelli, D. *Eur. J. Org. Chem.* **2020,** 2783–2806. doi:10.1002/ejoc.202000144
60. Vittal, J. J. *J. Photochem. Photobiol., C* **2023,** *57,* 100636. doi:10.1016/j.jphotochemrev.2023.100636
61. Ardila-Fierro, K. J.; Hernández, J. G. *Angew. Chem., Int. Ed.* **2024,** *63,* e202317638. doi:10.1002/anie.202317638
62. Peedikakkal, A. M. P.; Vittal, J. J. *Chem. – Eur. J.* **2008,** *14,* 5329–5334. doi:10.1002/chem.200701494
63. Harada, J.; Ogawa, K. *Chem. Soc. Rev.* **2009,** *38,* 2244–2252. doi:10.1039/b813850h
64. Sokolov, A. N.; Bučar, D.-K.; Baltrusaitis, J.; Gu, S. X.; MacGillivray, L. R. *Angew. Chem., Int. Ed.* **2010,** *49,* 4273–4277. doi:10.1002/anie.201000874
65. Liu, L.; Lin, J.; Pang, M.; Jin, H.; Yu, X.; Wang, S. *Org. Lett.* **2022,** *24,* 1146–1151. doi:10.1021/acs.orglett.1c04220
66. Toda, F.; Tanaka, K.; Sekikawa, A. *J. Chem. Soc., Chem. Commun.* **1987,** 279–280. doi:10.1039/c39870000279
67. Stojaković, J.; Farris, B. S.; MacGillivray, L. R. *Chem. Commun.* **2012,** *48,* 7958–7960. doi:10.1039/c2cc33227b
68. Stojaković, J.; Farris, B. S.; MacGillivray, L. R. *Faraday Discuss.* **2014,** *170,* 35–40. doi:10.1039/c4fd00006d
69. Obst, M.; König, B. *Beilstein J. Org. Chem.* **2016,** *12,* 2358–2363. doi:10.3762/bjoc.12.229
70. Štrukil, V.; Sajko, I. *Chem. Commun.* **2017,** *53,* 9101–9104. doi:10.1039/c7cc03510a
71. Liu, X.; Cong, T.; Liu, P.; Sun, P. *J. Org. Chem.* **2016,** *81,* 7256–7261. doi:10.1021/acs.joc.6b00097
72. Hernández, J. G. *Beilstein J. Org. Chem.* **2017,** *13,* 1463–1469. doi:10.3762/bjoc.13.144
73. Yu, J.; Zhang, L.; Yan, G. *Adv. Synth. Catal.* **2012,** *354,* 2625–2628. doi:10.1002/adsc.201200416
74. Majek, M.; Jacobi von Wangelin, A. *Acc. Chem. Res.* **2016,** *49,* 2316–2327. doi:10.1021/acs.accounts.6b00293
75. Biswas, S.; Banerjee, S.; Shlain, M. A.; Bardin, A. A.; Ulijn, R. V.; Nannenga, B. L.; Rappe, A. M.; Braunschweig, A. B. *Faraday Discuss.* **2023,** *241,* 266–277. doi:10.1039/d2fd00122e
76. Baier, D. M.; Spula, C.; Fanenstich, S.; Grätz, S.; Borchardt, L. *Angew. Chem., Int. Ed.* **2023,** *62,* e202218719. doi:10.1002/anie.202218719
77. Millward, F.; Zysman-Colman, E. *Angew. Chem., Int. Ed.* **2024,** *63,* e202316169. doi:10.1002/anie.202316169
78. Xin, X.; Geng, J.; Zhang, D.; Ang, H. T.; Wang, H.; Cheng, Y.; Liu, Y.; Toh, R. W.; Wu, J.; Wang, H. *Nat. Synth.* **2025,** *4,* 177–187. doi:10.1038/s44160-024-00681-8
79. Luttringer, F.; Lavayssiere, M.; Rastoder, E.; Salov, N.; Gravelet, T.; Quintin, F.; Pinaud, J.; Lamaty, F.; Bantreil, X. *RSC Mechanochem.* **2025,** *2,* 108–115. doi:10.1039/d4mr00112e
80. Reynes, J. F.; Isoni, V.; García, F. *Angew. Chem., Int. Ed.* **2023,** *62,* e202300819. doi:10.1002/anie.202300819
81. Bolt, R. R. A.; Leitch, J. A.; Jones, A. C.; Nicholson, W. I.; Browne, D. L. *Chem. Soc. Rev.* **2022,** *51,* 4243–4260. doi:10.1039/d1cs00657f
82. Effaty, F.; Gonnet, L.; Koenig, S. G.; Nagapudi, K.; Ottenwaelder, X.; Friščić, T. *Chem. Commun.* **2023,** *59,* 1010–1013. doi:10.1039/d2cc06013b
83. Nanni, A.; Kong, D.; Zhu, C.; Rueping, M. *Green Chem.* **2024,** *26,* 8341–8347. doi:10.1039/d4gc01790k
84. Batzdorf, L.; Fischer, F.; Wilke, M.; Wenzel, K.-J.; Emmerling, F. *Angew. Chem., Int. Ed.* **2015,** *54,* 1799–1802. doi:10.1002/anie.201409834
85. Gracin, D.; Štrukil, V.; Friščić, T.; Halasz, I.; Užarević, K. *Angew. Chem., Int. Ed.* **2014,** *53,* 6193–6197. doi:10.1002/anie.201402334
86. Gugin, N. Y.; Yusenko, K. V.; King, A.; Meyer, K.; Al-Sabbagh, D.; Villajos, J. A.; Emmerling, F. *Chem* **2024,** *10,* 3459–3473. doi:10.1016/j.chempr.2024.07.033
87. Lampronti, G. I.; Michalchuk, A. A. L.; Mazzeo, P. P.; Belenguer, A. M.; Sanders, J. K. M.; Bacchi, A.; Emmerling, F. *Nat. Commun.* **2021,** *12,* 6134. doi:10.1038/s41467-021-26264-1

License and Terms

BEILSTEIN JOURNAL OF ORGANIC CHEMISTRY

Photocatalyzed elaboration of antibody-based bioconjugates

Marine Le Stum‡, Eugénie Romero*,‡ and Gary A. Molander*,‡

Perspective

Open Access

Address:
Université Paris-Saclay, CEA, INRAE, Département Médicaments et Technologies pour la Santé (DMTS), SCBM, 91191 Gif-Sur-Yvette, France

Email:
Eugénie Romero* - eugenie.romero@cea.fr; Gary A. Molander* - gmolandr@sas.upenn.edu

* Corresponding author ‡ Equal contributors

Keywords:
antibodies; bioconjugation; bioorthogonality; chemoselectivity; late-stage functionalization; photochemistry

Beilstein J. Org. Chem. **2025,** *21,* 616–629.
https://doi.org/10.3762/bjoc.21.49

Received: 21 December 2024
Accepted: 05 March 2025
Published: 18 March 2025

This article is part of the thematic issue "Photocatalysis and photochemistry in organic synthesis".

Guest Editor: T. Noël

Abstract

Antibody–drug conjugates (ADCs) represent a promising class of targeted therapeutics, combining the specificity of antibodies with the potency of cytotoxic drugs to enhance therapeutic efficacy while minimizing off-target effects. The development of new chemical methods for bioconjugation is essential to generate ADCs and to optimize their stability, efficacy, and safety. Traditional conjugation methods often face challenges related to site-selectivity and heterogeneous product mixtures, highlighting the need to develop new, innovative chemical strategies. Photoredox chemistry emerges as a powerful tool in this context, enabling precise, mild, and selective modifications of peptides and proteins. By harnessing light to drive chemical transformations, photoredox techniques can facilitate the synthesis of antibody bioconjugates. This perspective will discuss the drive to develop and empower photoredox methods applied to antibody functionalization.

Introduction

Antibodies represent increasingly important tools in several groundbreaking approaches to medical innovation, including basic biomedical research and therapy. One of the most critical requirements for the application of antibodies in disease detection and treatment is that they are adorned with functional units (e.g., fluorophores, radionuclides, toxic payloads) that must be efficiently and selectively installed through compatible synthetic methods.

Dozens of ADCs have been approved for clinical uses, and to date all are designed in the context of cancer therapy [1], which combines the precision targeting of monoclonal antibodies (mAbs) with the therapeutic effects of cytotoxic drugs [2]. The ADCs are thus designed to deliver potent cytotoxic agents selectively and directly to cancer cells while minimizing damage to healthy tissues. Notably, ADCs have started to enter clinical trials for non-oncology applications as well [3].

The importance and value of ADCs are several fold:

- Precise targeting: ADCs specifically recognize their target cells because of their antibody component. This

minimizes collateral damage to healthy tissues, reducing side effects compared to traditional chemotherapy.
- Enhanced potency: By delivering cytotoxic payloads directly to tumor or other target cells, ADCs achieve higher drug concentrations at the site of action. This potency enhances therapeutic efficacy.
- Treatment of refractory diseases: ADCs have shown remarkable success in treatment of highly refractory diseases. Their ability to overcome resistance makes them valuable options for patients who previously had limited treatment choices.

ADCs consist of three main components (Figure 1): (1) Monoclonal antibody (mAb): The antibody specifically recognizes and binds to surface antigens present on tumor or other targeted cells. (2) Linker: the linker connects the antibody to the payload. The nature of the moiety linking the drug/radiolabel/imaging agent to the antibody plays a crucial role in the pharmacokinetic properties [4,5], therapeutic index, selectivity, and overall success of the ADC. The linker will ideally be stable in plasma for an extended period before the intended target can be reached, and after internalization, linkers play a key role in the drug-releasing event. Importantly, some exceptions exist. For example, in trodelvy, used in a treatment for patients with triple-negative breast cancer, the linker may release the drug prior to internalization. (3) Payload: The payload may be a subunit used in cellular tracking, imaging, or most commonly toxic drug therapeutics. The overall goal of ADCs is to deliver the payload directly to target cells via the antibody without affecting normal, healthy tissue.

Importantly, the use of antibodies in modern medicine is not restricted solely to ADCs and cancer therapy. For example, mABs now find routine use in the context of radionuclide (PET) imaging agents, informing therapeutic decision-making [6,7]. Antibody–oligonucleotide conjugates, antibody–enzyme conjugates, antibody–polymer conjugates, antibody–nanomaterial conjugates, antibody–catalyst conjugates, and antibodies involved in protein degradation also play critical roles in biomedical research and therapies [2].

In whatever capacity, the use of antibodies applied to medicine is critically dependent on the ability to anchor them to operative payloads in a highly precise manner [8-10]. Many researchers are tackling the challenge of new strategies for chemoselective synthetic modifications of biomolecules, including antibodies [11]. In the case of ADCs, conjugation of the linker/payload to the antibody must not drastically alter the pharmacokinetics or physicochemical properties of the antibody [12,13]. Typically, zero to eight payloads are attached to the antibody. Heterogeneous ADCs may thus be a mix of both unconjugated and “overloaded” antibodies. Unconjugated antibodies compete with antibodies containing payloads for binding, which can diminish the effectiveness of the antibody-payload materials. On the other hand, excessive loading of the antibody can lead to antibody aggregation, increased toxicity, decreased stability, and/or a shorter ADC half-life [14]. Optimization of the drug/antibody ratio (DAR) and payload distribution/location thus becomes significant for ideal ADC design.

Given the complexity of biological macromolecules, there are inherent limitations in terms of the types of reactions that can be used to modify them. Reactions must be carried out at or near ambient temperatures and near-neutral pH. Aqueous media is often required to solubilize the substrates and/or to prevent denaturation, and reactions are normally carried out under very dilute (micromolar) conditions. As importantly, the highly functionalized nature of polypeptides/proteins demands exquisite selectivity to target specific sites on the macromolecule of interest. In addition to the requisite features of the chemical

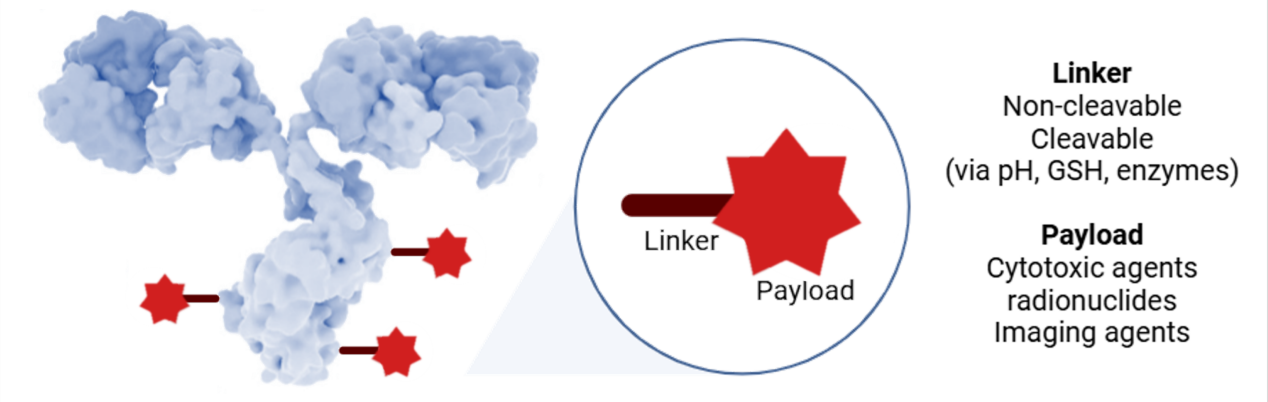

Figure 1: Representation of an antibody–drug conjugate. The antibody shown in this figure is from https://www.gettyimages.de/detail/illustration/monoclonal-antibody-igg2a-lizenfreie-illustration/585105259?searchscope=image%2Cfilm&adppopup=true; ALFRED PASIEKA/SCIENCE PHOTO LIBRARY, No. 585105259. This content is not subject to CC BY 4.0.

methods outlined above, there are key requirements for synthetic methods used in ADCs, which include high site-selectivity and controlled stoichiometry (DAR). Additionally, the methods should be synthetically reliable, easy, and rapid to carry out, and they must tolerate diverse functional groups on the payloads/linker [15,16]. These factors conspire to set a very high bar for those processes that are amenable to covalent bioconjugation.

Effective bioconjugation has been dramatically facilitated by the development of robust bioorthogonal reactions, which has revolutionized the field of chemical biology [17]. A bioorthogonal reactive group can be introduced into proteins via direct chemical coupling on specific native amino acids, by enzymatic coupling, or by bioengineering for the incorporation of non-canonical amino acids [18,19]. In fact, incorporating non-natural amino acids significantly broadens the scope of reactions that can be used in bioconjugation. As an example, click chemistry comprises one particularly useful and important tool in which azides and other dipolar species engage with reactive alkenes and alkynes on non-canonical amino acids [20]. Transition-metal-mediated processes, including metathesis reactions, aryl cross-coupling reactions, and conjugate addition reactions with dehydroalanine derivatives round out the most predominant reactions used on non-natural amino acids. However, even though bioengineering allows the incorporation of non-canonical amino acids with astounding effectiveness and near-complete selectivity, this technology is exceedingly expensive and time-consuming, and the expertise required to carry out these transformations is constrained to a very limited number of laboratories, particularly in the field of antibodies.

Given the challenges of bioengineering antibodies with non-canonical amino acids, the direct and chemoselective modification of native antibodies is most attractive, albeit not without serious obstacles. Among native amino acids, attachment to lysine (Lys) [21] and cysteine (Cys) are the most common. Antibodies typically contain as many as 90 lysine units, many of which are at highly solvent-accessible sites [22,23]. Conjugation to Lys is thus rarely controlled and leads to a wide range of DARs that can destabilize the antibody and furthermore greatly alter the pharmacokinetics of the ADC (vide infra). Additionally, undesirable Cys and Tyr modifications may compete in some instances with the Lys conjugation.

Cysteine amino acids are less prevalent and typically more evenly distributed in antibodies than lysine but are often tied up in disulfide bridges that must be reduced prior to conjugation [24,25]. Such reductions must thus be carefully controlled to allow conjugation while ensuring the overall structural integrity of the antibody. The free sulfhydryls can be conjugated by several means, including alkylation with α-halo carbonyls (in which case Lys may compete), and Michael additions (e.g., to maleimide, which is reversible and therefore may lead to incomplete conversion). The Michael adducts also present chemical instability in plasma and additionally generate an undesirable new stereocenter [26,27].

Few methods have been developed for the functionalization of tyrosine (Tyr) and tryptophan (Trp). With a low abundance (≈3%) in proteins, Tyr modifications are widely recognized for their ability to profoundly impact protein properties and function. Their chemical modification has been developed using iminoxyl radicals [28]. Although numerous methods exist for the functionalization of Trp in proteins, their application in the elaboration of ADCs is limited [29].

Given the many challenges in antibody modification as outlined above, it is perhaps of no surprise that the recent renaissance of synthetic chemistry based on novel photochemical methods has been applied to their functionalization [30]. In the context of photochemistry applied to bioconjugation, photochemical affinity labelling (PAL) is a technique that has been used to create selective chemical reactions, often for bioconjugation, by utilizing photoaffinity reagents. These reagents are typically photoreactive molecules that can be activated by light to form covalent bonds with nearby molecules [31-33]. PAL involves using a light-activated group (often a photo-crosslinker) that can form covalent bonds when exposed to UV or visible light. These photoaffinity tags or crosslinkers are designed to bind to specific biomolecules, such as proteins, nucleic acids, or lipids, in a highly selective manner. The light irradiation triggers a chemical reaction, such as a bond formation, which allows the conjugation of two molecules. PAL is commonly used in targeted bioconjugation when the timing and location of the conjugation need to be controlled. A typical example is using azido groups or alkyne groups in conjunction with light to initiate a covalent bond between two different molecules, such as a drug and a targeting moiety. This technique has been shown to be useful in applications such as cell labeling, protein–protein interactions, and photoradiosynthesis of bioconjugates, but the most important challenge remains the lack of specificity to target one amino acid, and thus to have a better control of the selectivity and the DAR, leading to more homogeneous ADCs. In this specific context, photocatalysis (Figure 2) enables site-specific bioconjugation by generating reactive intermediates (such as radicals or electron-deficient species) that can selectively react under the agency of low-energy visible light with specific functional groups on biomolecules. This allows precise control over the conjugation process, enabling targeted modifications without affecting non-reactive sites.

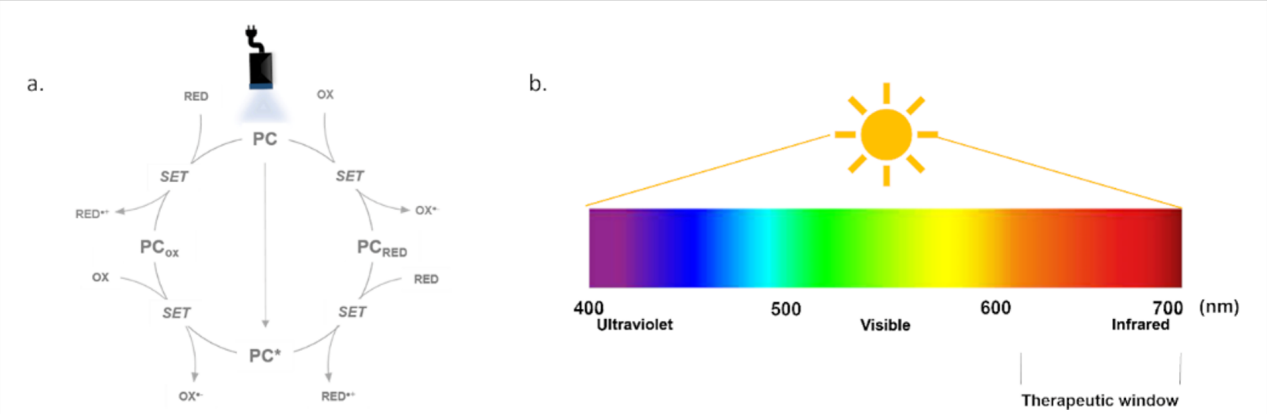

Figure 2: a. Photoredox catalytic cycles; b. absorption spectrum of photosensitizers. Therapeutic window indicates the most appropriate wavelength range to apply irradiation for biological applications.

Although previous reviews have discussed the more traditional synthetic methods applied to ADCs [34-36], the discussion below focuses on photocatalytic approaches that have been used to date to elaborate antibodies, providing insight into those methods that aim to revolutionize approaches to cancer treatment and other medical applications via the use of synthetically functionalized antibodies.

Perspective

In this perspective, how light-driven chemistry can enhance the development of innovative methods for accessing antibody–drug conjugates (ADCs) will be outlined. A brief introduction to photoredox chemistry as it relates to bioconjugation in proteins is followed by a summary of the limited photoredox approaches reported for antibodies. Finally, the potential benefits and cautionary details these chemical strategies possess for creating ADCs with well-defined DAR and enhanced selectivity are discussed.

Photocatalytic modification of proteins

Photoredox chemistry has emerged as a transformative approach in the modification of proteins, enabling researchers to achieve selective and efficient conjugation under mild conditions [37]. By utilizing visible light and transition-metal catalysts, this technique allows the generation of reactive intermediates that can facilitate various modifications, including labeling, crosslinking, and the creation of protein–drug conjugates. The incorporation of photoredox strategies has facilitated the synthesis of complex protein architectures, enabling precise control over conjugation sites and degrees of modification. The number of publications reporting photoredox bioconjugation applied to proteins over the last 20 years is significant (Figure 3).

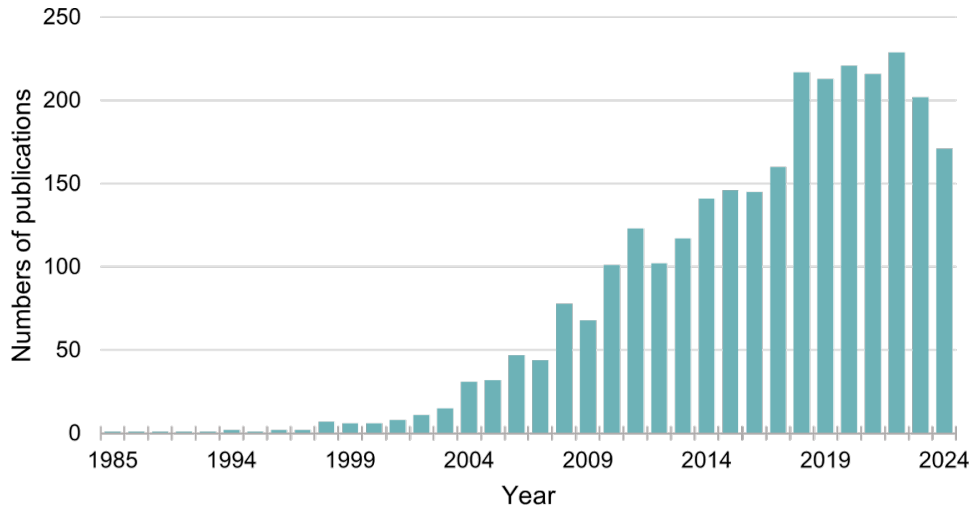

Figure 3: Graph representing the average number of publications focusing on photoredox chemistry applied to protein-based bioconjugation (source: SciFinder).

Recent reviews have highlighted advancements in this field, emphasizing methods that enable site-specific modifications of proteins with minimal disruption to their native structures [38,39].

In 2021, Bottecchia and Noël reported the utility of photoredox catalysis for the functionalization of amino acid side chains, paving the way for tailored modifications in biotherapeutics [40]. More recently, Sato et al. have reviewed photochemical strategies enabled by a range of catalysts, including photoredox catalysts, energy-transfer catalysts, and genetically encoded photocatalysts, highlighting their distinct features, mechanisms, applications, and prospects [41]. This thorough analysis showcased the promising advancements in the chemical modification of proteins.

As this field continues to expand, ongoing research efforts are focusing on optimizing reaction conditions, understanding mechanistic pathways, and exploring new catalysts to broaden the scope of photoredox applications in protein chemistry.

The integration of photoredox chemistry with protein modification has opened new avenues for designing advanced biotherapeutics, including ADCs and targeted delivery systems.

Photoinduced modification of antibodies

Although the bioconjugation of proteins via photocatalytic pathways is well-documented, the application of this method to the functionalization of antibodies remains largely unexplored. This is primarily because of the structural complexity of antibodies, which exhibit a three-dimensional architecture and numerous potential modification sites, making selective control of functionalization sites challenging. Nonetheless, photocatalytic approaches offer a unique potential to overcome these limitations, particularly by enabling modifications under mild and controlled conditions. Unlike classical methods, such as thiol chemistry [22] or widely used click reactions [33], photocatalysis could provide innovative solutions to produce ADCs, especially in terms of selectivity and the preservation of sensitive biological structures when appropriate redox potentials of photocatalysts are applied to the targeted amino acid. Additional advantages of photoinduced reactions include the ability to perform the reactions rapidly (typically <15 minutes). It was only in the late 2010s that the first publications on the subject emerged. An overview of reported photoredox approaches for the functionalization of antibodies is outlined below.

Histidine

In 2021, the group of Sato developed a selective functionalization method for histidine using an umpolung approach based on singlet oxygen [42]. Through energy transfer (EnT) from the ruthenium-based photocatalyst to triplet oxygen, singlet oxygen is produced in a targeted manner, which oxidizes histidine to an endoperoxide, significantly increasing its reactivity toward nucleophiles (Figure 4A). This strategy employs a functionalized ruthenium complex and a fragment crystallizable (Fc) ligand anchored to a magnetic bead, enabling the localized generation of singlet oxygen near antibodies (Figure 4B). The short lifetime and limited diffusion of singlet oxygen ensure exclusive reactions with proximal histidine residues. This strategy maximizes the efficiency and specificity of functionalization, representing a significant advancement in the selective modification of antibodies.

This method demonstrated an innovative mode of selectivity, even though some drawbacks remain. For example, the 1-methyl-4-arylurazole used in these transformations is a strong electrophile that can react with Tyr, for instance, if such an amino acid is located near the reactive site. In addition, command of the DAR might have some limits, as the distance between the catalyst and the mAbs is not well defined, meaning that the photoredox reaction might not give satisfactory reproducibility.

Histidine/Tyr

More recently, the same research group demonstrated the divergent functionalization of tyrosine or histidine, thanks to the use of a DNA photoswitch Ru complex, either used as a standalone system or involved in an artificial metalloenzyme (ArM). The use of the ArM significantly enhances the potential of the photocatalyst for antibody modification [43]. By inserting a $[Ru(bpy)_2dppz]^{2+}$ complex into the apo-form of riboflavin-binding protein (RFBP), a complete reversal of selectivity was achieved: the Ru complex alone enabled tyrosine modification via a photoredox reaction, whereas when embedded within the protein, the Ru-based ArM complex promoted histidine modification through an energy-transfer mechanism (Figure 5). Based on DFT calculations, this is permitted by the modification of the energy diagram of the ruthenium complex in the presence of biological and aqueous media. When applied to trastuzumab, the artificial metalloenzyme system ([Ru] ⊂ RFBP) thus yielded striking results – significantly reducing undesired tyrosine modifications on the heavy chain while enabling selective modification of histidine.

This impressive divergent method allows the same photocatalyst and electrophile to be involved in two different but selective bioconjugations of mAbs. It remains limited to reactions involving oxidative mechanistic pathways with $^1O_2$.

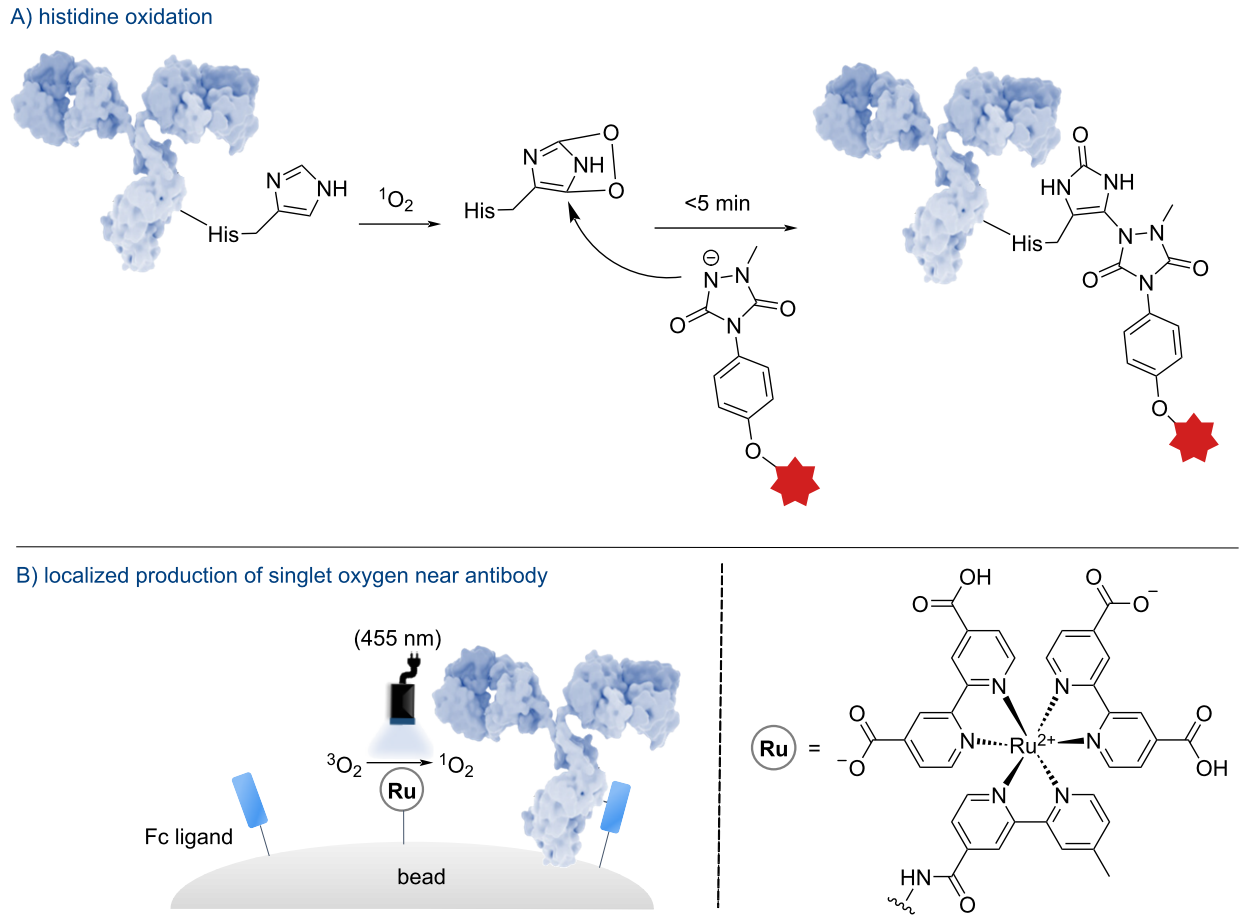

Figure 4: Schematic procedure developed by Sato et al. on histidine photoinduced modification. The antibody shown in this figure is from https://www.gettyimages.de/detail/illustration/monoclonal-antibody-igg2a-lizenfreie-illustration/585105259?searchscope=image%2Cfilm&adppopup=true; ALFRED PASIEKA/SCIENCE PHOTO LIBRARY, No. 585105259. This content is not subject to CC BY 4.0.

Cys

In 2016, Bräse et al. developed a photomediated disulfide rebridging method, exploiting the disulfide bridging sites in biomolecules to introduce specific functional groups (Figure 6) [44]. The bioconjugation reaction is based on thiol–yne coupling. Originally developed on peptides and proteins, this approach was applied to a fragment antigen-binding (Fab) antibody fragment (approximately 46 kDa) containing a single interchain disulfide bond. After 4 h of irradiation under UV wavelengths, the desired rebridged Fab fragment was obtained with around 40% conversion.

Although this method shows promise, it remains to be seen whether it is feasible for a full antibody, such as an IgG1, which typically contains four un-buried interchain disulfide bonds. Thus, rebridging allows the disulfide bonds to be reformed after conjugation, but one may question whether this could affect the long-term stability or functionality of the ADC, particularly if the new bonds do not perfectly mimic the properties of native disulfide bridges.

More recently, Lang et al. developed an approach using dual photoredox/nickel-catalyzed antibody functionalization [45], demonstrating the selective modification of Cys residues through photocatalytic methods (Figure 7). A key advantage of this strategy lies in the use of readily available and inexpensive $Ru(bpy)_3$, along with a water-soluble, air- and moisture-stable $Ni(dabpy)Br_2$ catalyst. Moreover, they demonstrated that this system works efficiently in aqueous conditions, making it highly suitable for applications involving antibodies. These characteristics make the method highly attractive for industrial applications, where both scalability and robustness are essential.

Beyond its practical advantages, the method offers notable versatility, enabling the conjugation of a wide range of aryl linkers to Cys residues. This flexibility is crucial for the devel-

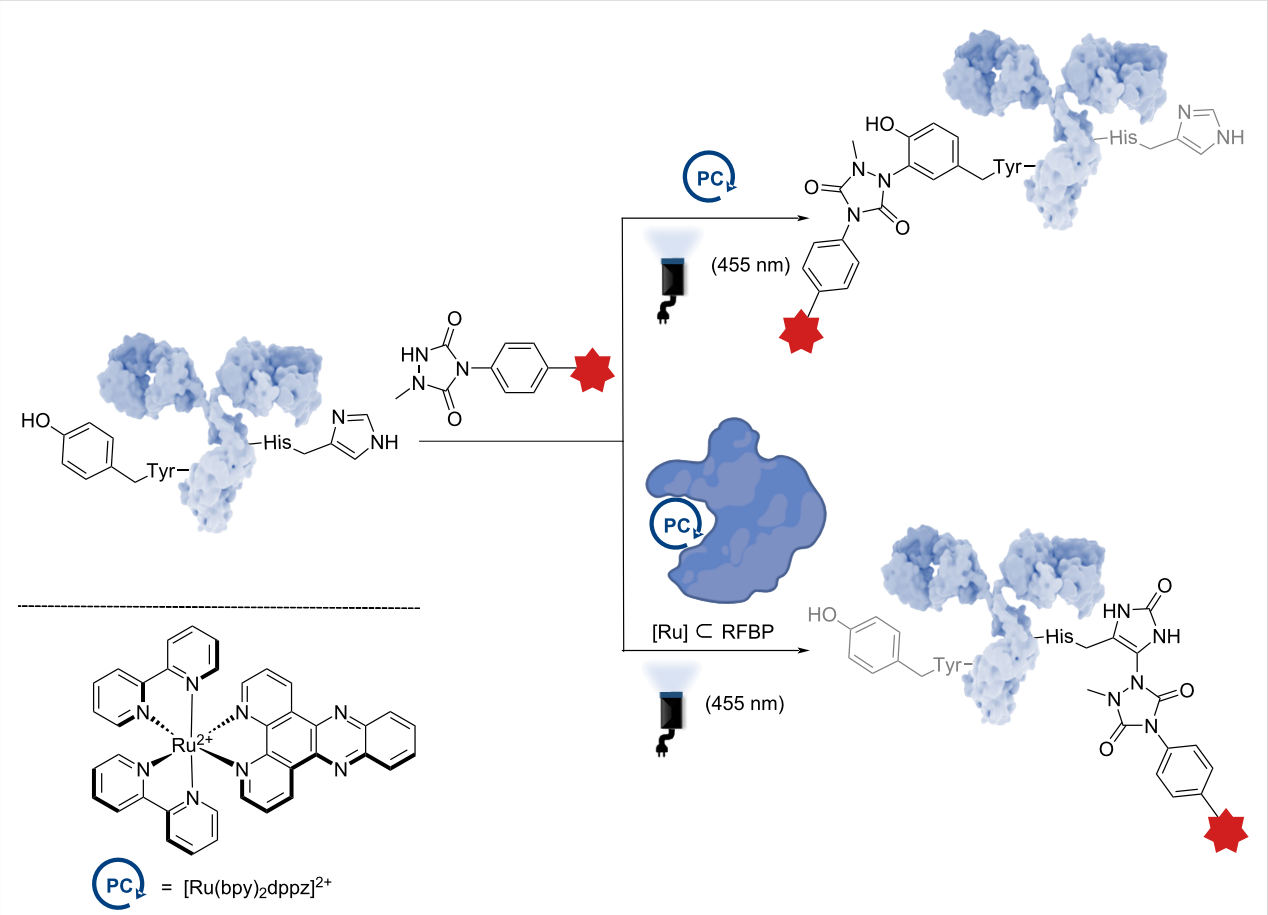

Figure 5: Schematic procedure of the divergent method developed by Sato et al. on histidine/tyrosine photoinduced modification. The antibody shown in this figure is from https://www.gettyimages.de/detail/illustration/monoclonal-antibody-igg2a-lizenfreie-illustration/585105259?searchscope=image%2Cfilm&adppopup=true; ALFRED PASIEKA/SCIENCE PHOTO LIBRARY, No. 585105259. This content is not subject to CC BY 4.0.

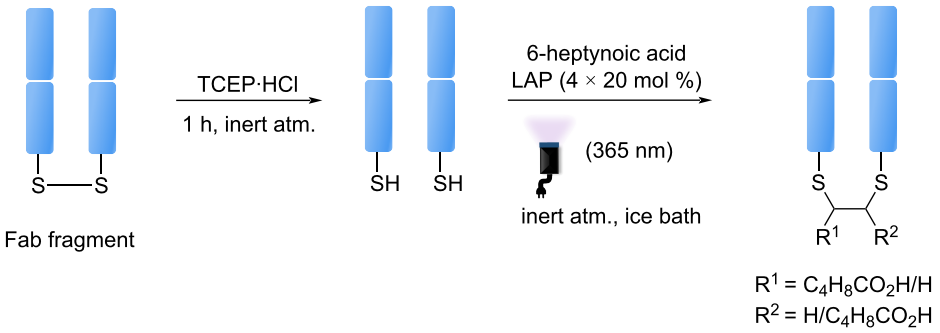

Figure 6: Schematic procedure developed by Bräse et al. on photoinduced disulfide rebridging method.

opment of ADCs, where precise control over the linker and conjugation site is vital to optimizing therapeutic efficacy and pharmacokinetics. The Lang group's approach therefore represents a significant advancement in the field of selective and scalable antibody functionalization.

Importantly, although pioneering the field of dual nickel catalysis for the functionalization of antibodies in a very elegant and practical manner, the method has been applied to Cys, which necessitates the use of a reductant to access the free form of Cys. Another consequence was the high and non-reproducible

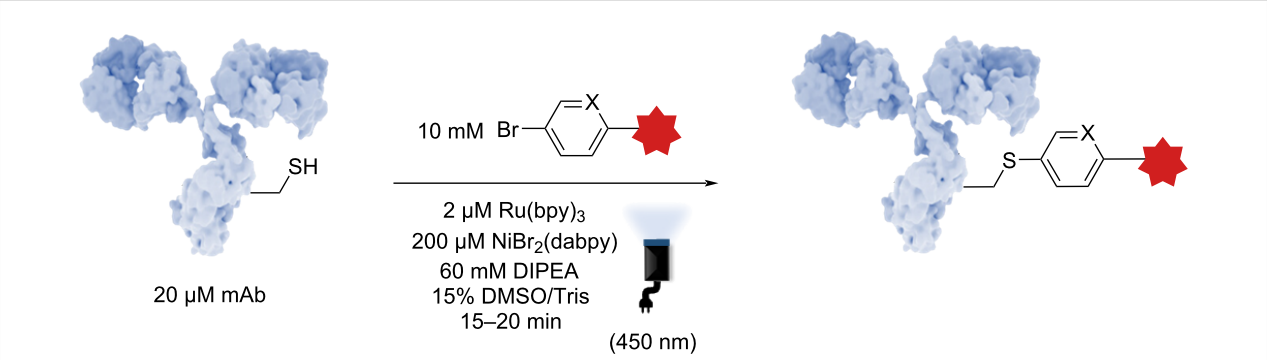

Figure 7: Schematic procedure developed by Lang et al. on a photoinduced dual nickel photoredox-catalyzed approach. The antibody shown in this figure is from https://www.gettyimages.de/detail/illustration/monoclonal-antibody-igg2a-lizenfreie-illustration/585105259?searchscope=image%2Cfilm&adppopup=true; ALFRED PASIEKA/SCIENCE PHOTO LIBRARY, No. 585105259. This content is not subject to CC BY 4.0.

DAR. The development of such methods applied to other canonical amino acids should benefit from the advantages of this approach while overcoming the encountered problems.

Glutamic acid

The Chung group explored the development of a method based on a high affinity immunoglobulin G (IgG) Fc-binding strategy to generate ADCs (Figure 8). Although such methods are generally reported with a heterogeneous DAR, the group developed a site-specific approach leading to a homogeneous DAR 2, thanks to a photoreactive Fc-binding peptide derivative (pFcBP) containing a photoleucine (pLeu) [46]. By analyzing the X-ray crystal structure of IgG, the researchers identified high-affinity binding sites for the ligand within the Fc domain. This structural analysis allowed precise determination of amino acid residue positions and orientations.

Upon photoirradiation, the pLeu within the pFcBP generated a carbene from the diazirine moiety. This transformation facilitated a site-specific covalent linkage to the antibody, resulting

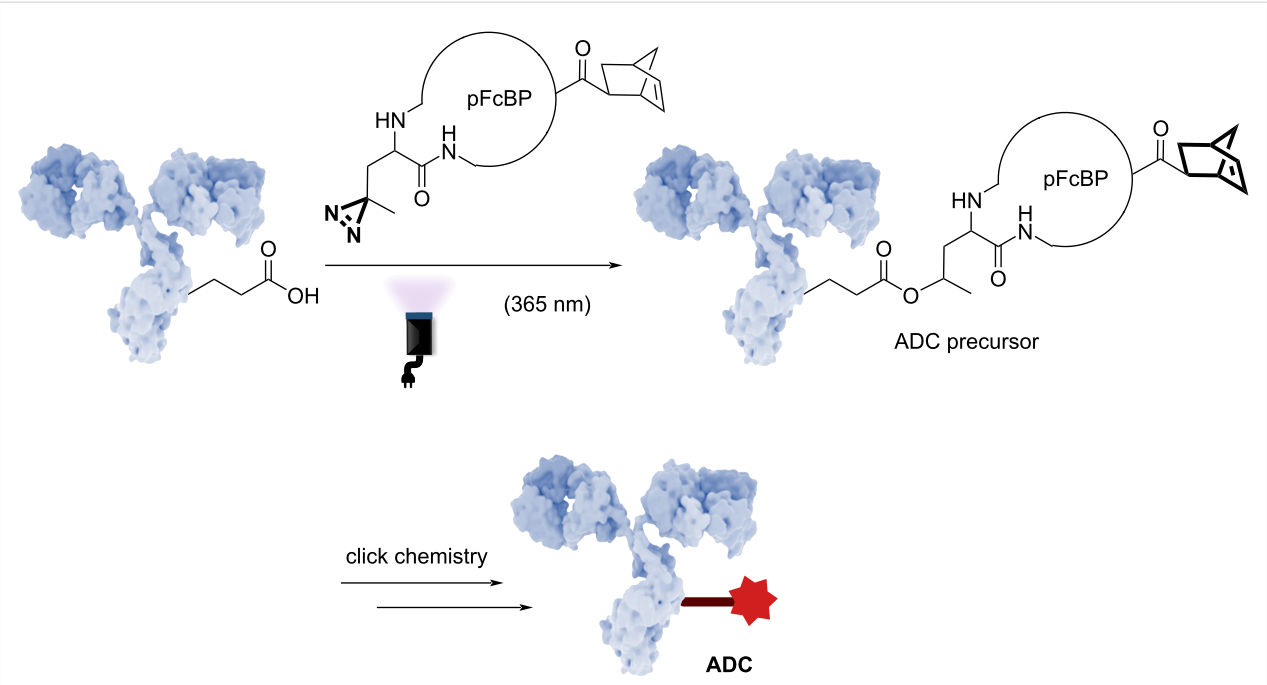

Figure 8: Schematic of the procedure developed by Chang et al. on photoinduced high affinity IgG Fc-binding strategy. The antibody shown in this figure is from https://www.gettyimages.de/detail/illustration/monoclonal-antibody-igg2a-lizenfreie-illustration/585105259?searchscope=image%2Cfilm&adppopup=true; ALFRED PASIEKA/SCIENCE PHOTO LIBRARY, No. 585105259. This content is not subject to CC BY 4.0.

in the formation of a DAR 2 ADC precursor. For their ADC design strategy, the group selected a polyethylene glycol (PEG) linker, as it enhances the water solubility of the ADC, while the payload consists of the cytotoxic agent DM1, which acts as a microtubule destabilizer. To ensure the stability and homogeneity of the final product, the design of the FcBP included a norbornene motif at the N-terminal end of the peptide sequence. The norbornene motif selectively reacts with a tetrazine located on the spacer-payload.

This study demonstrates the potency of photoinduced methods to access more homogeneous ADCs, hopefully reducing patient side effects.

In summary, photoredox modifications of antibodies have gained attention in recent years, though the field is still in its early stages because of the complexity of antibody structures. These photoinduced methods offer the potential for selective and mild functionalization, which could be particularly valuable for producing homogeneous ADCs with controlled properties. Even though very few photoredox approaches have been published in the literature when compared to proteins, highlighting the complexity of antibody architecture, new photoinduced methods for the selective modification of natural amino acids in antibodies are of high necessity.

Discussion

Tremendous inroads have already been made in the application of photochemical methods to the construction of ADCs. Highlighted below are additional aspects that photochemical transformations could, in our opinion, bring to ADCs that are not easily achieved through traditional, mostly two-electron mechanistic approaches (Figure 9).

Chemoselectivity

As mentioned in the introduction, there are exceedingly stringent requirements for the types of reactions that can be used for the elaboration of ADCs. Among the signature features of photochemical, single-electron transformations is their ability to be conducted in dilute aqueous media at room temperature and at neutral pH [47]. Additionally, the distinctive mechanistic paradigms under which photochemical reactions operate makes them uniquely tolerant of numerous unprotected functional groups [48]. Consequently, the elaboration of a variety of highly sophisticated biomolecules, including ADCs, can be carried out without protecting groups in a highly selective manner. This chemoselectivity should extend to any molecularly complex linkers and/or payloads being conjugated to the mAbs, allowing highly efficient entry to ADCs.

DAR control

A noteworthy characteristic of photochemical transformations is the ability to unambiguously start and stop reactions instantaneously using light on and light off reaction conditions (Figure 10). Aspirationally this would allow exquisite control of the drug/antibody ratio, taking advantage of the nature of photochemical transformations to occur rapidly and selectively at the kinetically most reactive sites [49,50]. Importantly, as a general

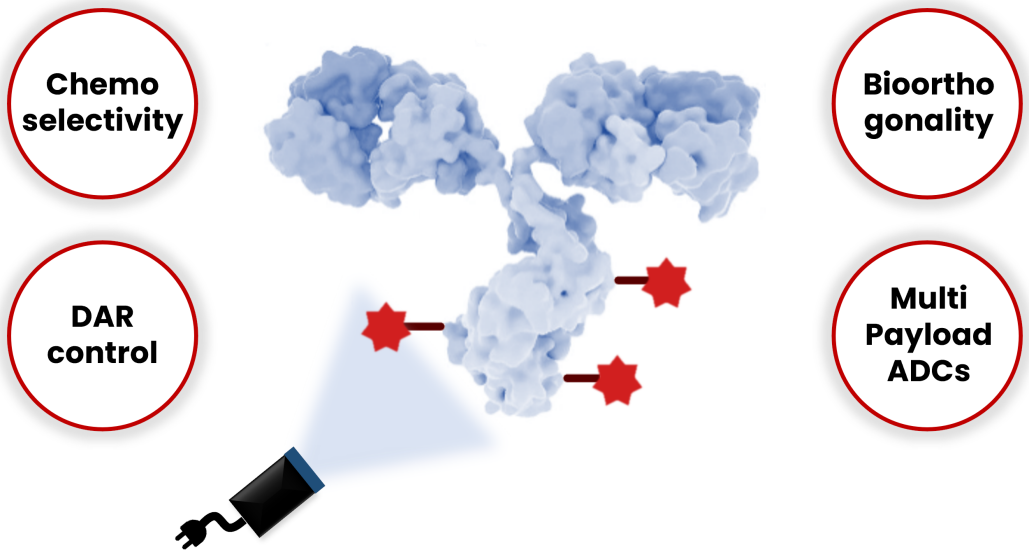

Figure 9: Potential advantages of photoredox chemistry for bioconjugation applied to antibodies. The antibody shown in this figure is from https://www.gettyimages.de/detail/illustration/monoclonal-antibody-igg2a-lizenfreie-illustration/585105259?searchscope=image%2Cfilm&adppopup=true; ALFRED PASIEKA/SCIENCE PHOTO LIBRARY, No. 585105259. This content is not subject to CC BY 4.0.

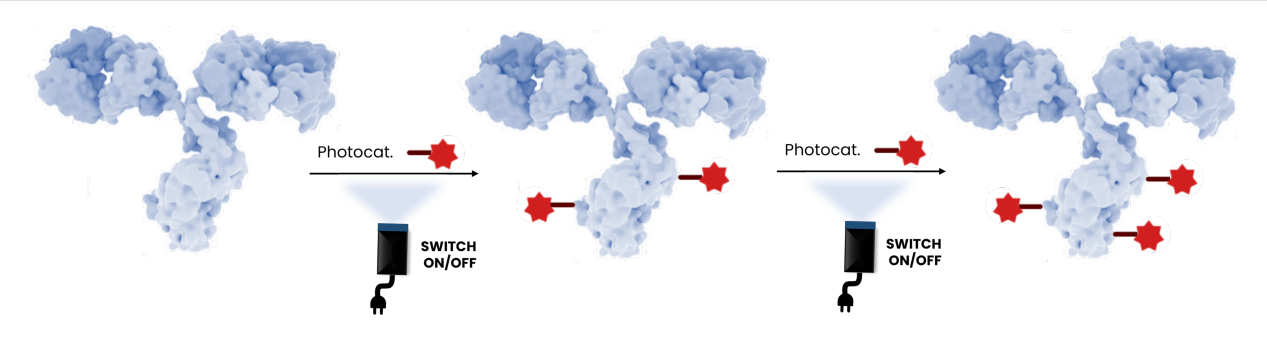

Figure 10: Representation of the photoinduced control of the DAR. The antibody shown in this figure is from https://www.gettyimages.de/detail/illustration/monoclonal-antibody-igg2a-lizenfreie-illustration/585105259?searchscope=image%2Cfilm&adppopup=true; ALFRED PASIEKA/SCIENCE PHOTO LIBRARY, No. 585105259. This content is not subject to CC BY 4.0.

comment, targeting a single class of amino acids, the most solvent-exposed would react preferentially to those buried within hydrophobic domains of the mAbs, and ideally the relative rates of their reactivity would translate directly to tightly controlled DARs. The time of irradiation, the wavelength of the light, the lamp wattage, and diverse photocatalysts or mechanisms (e.g., energy transfer, photoredox, or electron-donor/electron-acceptor photoinduced electron transfer) might all be brought to bear on controlling the DAR. In addition to the DAR, homogeneity for conjugation at specific sites using light control might also be improved using photochemical transformations. Importantly, optimization of bioconjugation reactions with technologies such as high-throughput experimentation has already been applied on antibodies [51].

Bioorthogonality

Bioorthogonal chemistry has transformed our capability to study and alter biological systems at the molecular level [52,53]. Owing to the often-unique mechanisms characterized by photocatalytically promoted reactions, reactivity patterns might be developed that allow selective reactions at amino acids that are not currently used for conjugation of linkers/payloads to the mAb. Potential access to modification of the mAbs at different amino acids has obvious ramifications for installation of the linker/payload because of the relative abundance and local environments of the amino acids, in addition to the inherent reactivity of these diverse components. In turn, this selectivity for reaction at a wider range of amino acids impacts several important features of ADCs, including site selection for the linker/payload, the DAR, and the homogeneity of the ADCs.

Multi-payload ADCs

Most clinically approved ADCs contain a single-drug payload. However, systemic cancer chemotherapies often involve combinations of drugs. Combination regimens improve treatment outcomes by producing synergistic anticancer effects and slowing the development of drug-resistant cell populations. Researchers aim to replicate combination regimens by developing techniques for attaching multiple payloads to a single antibody molecule with high homogeneity [54-56]. Generating homogeneous multi-payload ADCs is complex because of the diverse reactive functional groups on antibody surfaces. As outlined above in the discussion concerning bioorthogonality, it is conceivable that photochemical methods could be developed allowing multi-payload ADCs to be prepared effortlessly, as the single-electron mechanistic approach of such reactions is completely orthogonal to currently used methods, and even among photochemical methods that might be designed for different amino acids. The scheme below (Figure 11) represents schematically how bioorthogonal introduction of linkers/payloads on the ADCs might be carried out using photocatalyzed approaches to ADC construction. Importantly, native amino acids could be used in these processes, and thus the onerous and expensive introduction of non-canonical amino acids into the ADCs would be completely unnecessary. Photocatalyzed methods could also be used in conjunction with more traditional chemical approaches at either stage to allow biorthogonal strategies for multi-payloads ADCs.

Antibody–protein conjugates

Antibody–protein conjugates possess tremendous promise within the domains of biotechnology and biomedical research [57,58]. To date, such entities have most often been formulated from the expression of fusion proteins, although more recently post-translational protein–protein conjugation has been recognized as a means to access such structures [59]. However, methods developed to date based on traditional two-electron chemistry with canonical amino acids are extremely limited and are most effectively based on maleimide hydrolyzing methods that rely on a single amino acid (Cys) conjugation. The development of viable photochemical transformations targeted toward a variety of diverse canonical amino acids would introduce more versatility, efficiency, and convenience in the construction of these increasingly important structural units.

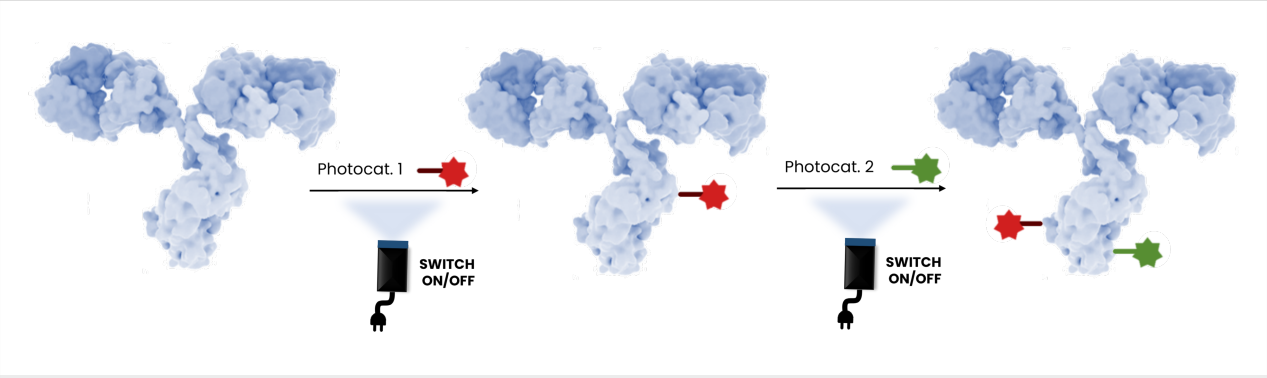

Figure 11: Representation of a photoinduced control of multi-payloads ADC strategy. The antibody shown in this figure is from https://www.gettyimages.de/detail/illustration/monoclonal-antibody-igg2a-lizenfreie-illustration/585105259?searchscope=image%2Cfilm&adppopup=true; ALFRED PASIEKA/SCIENCE PHOTO LIBRARY, No. 585105259. This content is not subject to CC BY 4.0.

Cautionary considerations

Photoredox chemistry offers a powerful approach for the targeted modification of proteins and antibodies, enabling selective covalent bond formation and functionalization under mild conditions. However, its use in biomolecule modification comes with several specific features that require consideration. Some of these are detailed below.

Photoaggregation: The possibility of photoinduced aggregation during photoconjugation reactions represents a major challenge for the stability and efficacy of conjugated antibodies [60]. Exposure of antibodies to light, particularly UV light, can trigger photoinduced reactions that compromise their structural stability. These phenomena include the oxidation of sensitive residues such as tryptophan (Trp), tyrosine (Tyr), cysteine (Cys), and histidine (His), as well as partial unfolding of the antibodies, exposing hydrophobic regions that promote nonspecific interactions and aggregate formation. Additionally, covalent cross-links may form, involving disulfide bridges or Cys–Tyr bonds, further increasing the risk of aggregation.

Photosensitive payloads, although essential for specific therapeutic or diagnostic applications, are particularly vulnerable to these photochemical reactions. Their light-induced modifications not only exacerbate aggregation but may also reduce therapeutic efficacy and increase the risk of immunogenicity. These effects are especially concerning when the DAR is high, as a higher DAR increases the overall photosensitivity of the conjugated antibody.

Therefore, it is crucial to account for these factors during photoconjugation reactions to mitigate aggregation phenomena. Strategies such as optimizing the length and nature of the linker, precisely controlling reaction conditions (light intensity, exposure time), or modifying conjugation sites to distance payloads from sensitive residues may offer effective solutions. Finally, storage and handling of conjugated antibodies require special attention to minimize exposure to ambient light, which could contribute to structural instability and promote aggregation over time.

Reaction time: Proteins and antibodies are delicate macromolecules, and prolonged exposure to light or reactive intermediates can lead to protein denaturation or aggregation [61]. Because photoredox reactions often generate highly reactive species (such as radicals or singlet oxygen), long exposure times could cause unwanted side reactions, including the degradation of 3D structure of the protein or antibody. A short reaction time minimizes this risk by allowing the reaction to proceed quickly and efficiently before damage occurs. To avoid damage caused by high energy wavelength, the use of irradiation in the red region could be considered [62-65].

Aqueous media: Developing photoredox reactions compatible with aqueous media is essential for the modification of antibodies, as these biomolecules are typically dissolved in water or aqueous buffers to maintain their stability and activity. Antibodies are sensitive to their environment, and using a non-negligible amount of organic solvents or harsh chemical conditions can lead to denaturation, aggregation, or loss of functionality. Buffers, which are commonly used to stabilize antibodies by maintaining their pH and ionic strength, must also be compatible with the photoredox process to prevent unwanted side reactions or instability.

Thus, although photoredox chemistry offers a promising method for the targeted modification of antibodies, careful consideration of factors such as photoaggregation, reaction time, and aqueous media compatibility is essential to ensure the stability, efficacy, and functionality of the conjugated biomolecules.

Conclusion

In conclusion, the development of antibody–drug conjugates (ADCs) holds great promise for advancing targeted therapeutics, particularly in the treatment of cancer and other refractory diseases. However, the challenges related to achieving selective, efficient, and stable conjugation of antibodies to their payloads remain a significant barrier to realizing the full potential of ADCs. Traditional conjugation methods often struggle with issues such as site-selectivity and heterogeneous products. Photoredox chemistry has emerged as a transformative approach, offering precise control over the modification of antibodies with the potential to enhance ADC purity, stability, and therapeutic efficacy. By utilizing light-driven chemical transformations, photoredox techniques enable selective functionalization of antibodies at specific sites, addressing the limitations of conventional methods. As research in photochemistry continues to evolve, these strategies may pave the way for the creation of more homogeneous and optimized ADCs, enhancing their therapeutic outcomes and minimizing off-target effects. This perspective highlights the exciting future of photoredox methods in the development of next-generation ADCs, ultimately contributing to the broader landscape of targeted biomedicine.

Acknowledgements

The antibody shown in the graphical abstract is from https://www.gettyimages.de/detail/illustration/monoclonal-antibody-igg2a-lizenfreie-illustration/585105259?searchscope=image%2Cfilm&adppopup=true; ALFRED PASIEKA/SCIENCE PHOTO LIBRARY, No. 585105259. This content is not subject to CC BY 4.0.

Funding

GAM acknowledges support from the Université Paris-Saclay for a Jean d'Alembert Research Fellowship.

ORCID® iDs

Marine Le Stum - https://orcid.org/0009-0001-0095-2138
Eugénie Romero - https://orcid.org/0000-0003-0484-1221
Gary A. Molander - https://orcid.org/0000-0002-9114-5584

Data Availability Statement

All data that supports the findings of this study is available in the published article and/or the supporting information of this article.

References

1. Fu, Z.; Li, S.; Han, S.; Shi, C.; Zhang, Y. *Signal Transduction Targeted Ther.* **2022,** *7,* 93. doi:10.1038/s41392-022-00947-7
2. Qian, L.; Lin, X.; Gao, X.; Khan, R. U.; Liao, J.-Y.; Du, S.; Ge, J.; Zeng, S.; Yao, S. Q. *Chem. Rev.* **2023,** *123,* 7782–7853. doi:10.1021/acs.chemrev.2c00915
3. Buttgereit, F.; Aelion, J.; Rojkovich, B.; Zubrzycka-Sienkiewicz, A.; Chen, S.; Yang, Y.; Arikan, D.; D'Cunha, R.; Pang, Y.; Kupper, H.; Radstake, T.; Amital, H. *Arthritis Rheumatol.* **2023,** *75,* 879–889. doi:10.1002/art.42415
4. Samantasinghar, A.; Sunildutt, N. P.; Ahmed, F.; Soomro, A. M.; Salih, A. R. C.; Parihar, P.; Memon, F. H.; Kim, K. H.; Choi, K. H. *Biomed. Pharmacother.* **2023,** *161,* 114408. doi:10.1016/j.biopha.2023.114408
5. Hobson, A. D.; Xu, J.; Marvin, C. C.; McPherson, M. J.; Hollmann, M.; Gattner, M.; Dzeyk, K.; Fettis, M. M.; Bischoff, A. K.; Wang, L.; Fitzgibbons, J.; Wang, L.; Salomon, P.; Hernandez, A., Jr.; Jia, Y.; Sarvaiya, H.; Goess, C. A.; Mathieu, S. L.; Santora, L. C. *J. Med. Chem.* **2023,** *66,* 9161–9173. doi:10.1021/acs.jmedchem.3c00794
6. Usama, S. M.; Thapaliya, E. R.; Luciano, M. P.; Schnermann, M. J. *Curr. Opin. Chem. Biol.* **2021,** *63,* 38–45. doi:10.1016/j.cbpa.2021.01.009
7. Lin, D.; Lechermann, L. M.; Huestis, M. P.; Marik, J.; Sap, J. B. I. *Angew. Chem., Int. Ed.* **2024,** *63,* e202317136. doi:10.1002/anie.202317136
8. Wu, K.-L.; Yu, C.; Lee, C.; Zuo, C.; Ball, Z. T.; Xiao, H. *Bioconjugate Chem.* **2021,** *32,* 1947–1959. doi:10.1021/acs.bioconjchem.1c00342
9. Park, J.; Lee, S.; Kim, Y.; Yoo, T. H. *Bioorg. Med. Chem.* **2021,** *30,* 115946. doi:10.1016/j.bmc.2020.115946
10. von Witting, E.; Hober, S.; Kanje, S. *Bioconjugate Chem.* **2021,** *32,* 1515–1524. doi:10.1021/acs.bioconjchem.1c00313
11. Walsh, S. J.; Bargh, J. D.; Dannheim, F. M.; Hanby, A. R.; Seki, H.; Counsell, A. J.; Ou, X.; Fowler, E.; Ashman, N.; Takada, Y.; Isidro-Llobet, A.; Parker, J. S.; Carroll, J. S.; Spring, D. R. *Chem. Soc. Rev.* **2021,** *50,* 1305–1353. doi:10.1039/d0cs00310g
12. Coumans, R. G. E.; Ariaans, G. J. A.; Spijker, H. J.; Renart Verkerk, P.; Beusker, P. H.; Kokke, B. P. A.; Schouten, J.; Blomenröhr, M.; van der Lee, M. M. C.; Groothuis, P. G.; Ubink, R.; Dokter, W. H. A.; Timmers, C. M. *Bioconjugate Chem.* **2020,** *31,* 2136–2146. doi:10.1021/acs.bioconjchem.0c00337
13. Garbaccio, R. M. Chemistry of Antibody–Small Molecule Drug Conjugates. In *Comprehensive Organic Synthesis,* 2nd ed.; Knochel, P., Ed.; Elsevier: Amsterdam, Netherlands, 2014; Vol. 9, pp 438–462. doi:10.1016/b978-0-08-097742-3.00942-3
14. Sochaj, A. M.; Świderska, K. W.; Otlewski, J. *Biotechnol. Adv.* **2015,** *33,* 775–784. doi:10.1016/j.biotechadv.2015.05.001
15. Kang, M. S.; Kong, T. W. S.; Khoo, J. Y. X.; Loh, T.-P. *Chem. Sci.* **2021,** *12,* 13613–13647. doi:10.1039/d1sc02973h
16. Lu, J.; Jiang, F.; Lu, A.; Zhang, G. *Int. J. Mol. Sci.* **2016,** *17,* 561. doi:10.3390/ijms17040561
17. Porte, K.; Riberaud, M.; Châtre, R.; Audisio, D.; Papot, S.; Taran, F. *ChemBioChem* **2021,** *22,* 100–113. doi:10.1002/cbic.202000525
18. Lemieux, G. A.; Bertozzi, C. R. *Trends Biotechnol.* **1998,** *16,* 506–513. doi:10.1016/s0167-7799(98)01230-x
19. Hackenberger, C. P. R.; Schwarzer, D. *Angew. Chem., Int. Ed.* **2008,** *47,* 10030–10074. doi:10.1002/anie.200801313
20. Stump, B. *ChemBioChem* **2022,** *23,* e202200016. doi:10.1002/cbic.202200016
21. Haque, M.; Forte, N.; Baker, J. R. *Chem. Commun.* **2021,** *57,* 10689–10702. doi:10.1039/d1cc03976h

22. McCombs, J. R.; Owen, S. C. *AAPS J.* **2015,** *17,* 339–351. doi:10.1208/s12248-014-9710-8
23. Jain, N.; Smith, S. W.; Ghone, S.; Tomczuk, B. *Pharm. Res.* **2015,** *32,* 3526–3540. doi:10.1007/s11095-015-1657-7
24. Yuan, D.; Zhang, Y.; Lim, K. H.; Leung, S. K. P.; Yang, X.; Liang, Y.; Lau, W. C. Y.; Chow, K. T.; Xia, J. *J. Am. Chem. Soc.* **2022,** *144,* 18494–18503. doi:10.1021/jacs.2c07594
25. Natesan, R.; Dykstra, A. B.; Banerjee, A.; Agrawal, N. J. *Antibiotics (Basel, Switz.)* **2023,** *12,* 83. doi:10.3390/antib12040083
26. Alley, S. C.; Benjamin, D. R.; Jeffrey, S. C.; Okeley, N. M.; Meyer, D. L.; Sanderson, R. J.; Senter, P. D. *Bioconjugate Chem.* **2008,** *19,* 759–765. doi:10.1021/bc7004329
27. Shen, B.-Q.; Xu, K.; Liu, L.; Raab, H.; Bhakta, S.; Kenrick, M.; Parsons-Reponte, K. L.; Tien, J.; Yu, S.-F.; Mai, E.; Li, D.; Tibbitts, J.; Baudys, J.; Saad, O. M.; Scales, S. J.; McDonald, P. J.; Hass, P. E.; Eigenbrot, C.; Nguyen, T.; Solis, W. A.; Fuji, R. N.; Flagella, K. M.; Patel, D.; Spencer, S. D.; Khawli, L. A.; Ebens, A.; Wong, W. L.; Vandlen, R.; Kaur, S.; Sliwkowski, M. X.; Scheller, R. H.; Polakis, P.; Junutula, J. R. *Nat. Biotechnol.* **2012,** *30,* 184–189. doi:10.1038/nbt.2108
28. Maruyama, K.; Ishiyama, T.; Seki, Y.; Sakai, K.; Togo, T.; Oisaki, K.; Kanai, M. *J. Am. Chem. Soc.* **2021,** *143,* 19844–19855. doi:10.1021/jacs.1c09066
29. Xie, X.; Moon, P. J.; Crossley, S. W. M.; Bischoff, A. J.; He, D.; Li, G.; Dao, N.; Gonzalez-Valero, A.; Reeves, A. G.; McKenna, J. M.; Elledge, S. K.; Wells, J. A.; Toste, F. D.; Chang, C. J. *Nature* **2024,** *627,* 680–687. doi:10.1038/s41586-024-07140-6
30. Zhang, Y.; Tan, J.; Chen, Y. *Chem. Commun.* **2023,** *59,* 2413–2420. doi:10.1039/d2cc06987c
31. Holland, J. P.; Gut, M.; Klingler, S.; Fay, R.; Guillou, A. *Chem. – Eur. J.* **2020,** *26,* 33–48. doi:10.1002/chem.201904059
32. Lechner, V. M.; Nappi, M.; Deneny, P. J.; Folliet, S.; Chu, J. C. K.; Gaunt, M. J. *Chem. Rev.* **2022,** *122,* 1752–1829. doi:10.1021/acs.chemrev.1c00357
33. Aguilar Troyano, F. J.; Merkens, K.; Anwar, K.; Gómez-Suárez, A. *Angew. Chem., Int. Ed.* **2021,** *60,* 1098–1115. doi:10.1002/anie.202010157
34. Kostova, V.; Désos, P.; Starck, J.-B.; Kotschy, A. *Pharmaceuticals* **2021,** *14,* 442. doi:10.3390/ph14050442
35. Hobson, A. D. *RSC Med. Chem.* **2024,** *15,* 809–831. doi:10.1039/d3md00674c
36. Dudchak, R.; Podolak, M.; Holota, S.; Szewczyk-Roszczenko, O.; Roszczenko, P.; Bielawska, A.; Lesyk, R.; Bielawski, K. *Bioorg. Chem.* **2024,** *143,* 106982. doi:10.1016/j.bioorg.2023.106982
37. Ryu, K. A.; Kaszuba, C. M.; Bissonnette, N. B.; Oslund, R. C.; Fadeyi, O. O. *Nat. Rev. Chem.* **2021,** *5,* 322–337. doi:10.1038/s41570-021-00265-6
38. Li, P.; Terrett, J. A.; Zbieg, J. R. *ACS Med. Chem. Lett.* **2020,** *11,* 2120–2130. doi:10.1021/acsmedchemlett.0c00436
39. Liu, J.-Q.; Shatskiy, A.; Matsuura, B. S.; Kärkäs, M. D. *Synthesis* **2019,** *51,* 2759–2791. doi:10.1055/s-0037-1611852
40. Bottecchia, C.; Noël, T. *Chem. – Eur. J.* **2019,** *25,* 26–42. doi:10.1002/chem.201803074
41. Liu, Z.; Okamoto, Y.; Sato, S. *ChemCatChem* **2024,** *16,* e202301424. doi:10.1002/cctc.202301424
42. Nakane, K.; Sato, S.; Niwa, T.; Tsushima, M.; Tomoshige, S.; Taguchi, H.; Ishikawa, M.; Nakamura, H. *J. Am. Chem. Soc.* **2021,** *143,* 7726–7731. doi:10.1021/jacs.1c01626
43. Okamoto, Y.; Mabuchi, T.; Nakane, K.; Ueno, A.; Sato, S. *ACS Catal.* **2023,** *13,* 4134–4141. doi:10.1021/acscatal.2c05946
44. Griebenow, N.; Dilmaç, A. M.; Greven, S.; Bräse, S. *Bioconjugate Chem.* **2016,** *27,* 911–917. doi:10.1021/acs.bioconjchem.5b00682
45. Bacauanu, V.; Merz, Z. N.; Hua, Z. L.; Lang, S. B. *J. Am. Chem. Soc.* **2023,** *145,* 25842–25849. doi:10.1021/jacs.3c10185
46. Lee, T.; Kim, J. H.; Kwon, S. J.; Park, S. H.; Kim, J.; Kang, H. J.; Chung, S. J. *Org. Lett.* **2020,** *22,* 8419–8423. doi:10.1021/acs.orglett.0c03049
47. Russo, C.; Brunelli, F.; Tron, G. C.; Giustiniano, M. *J. Org. Chem.* **2023,** *88,* 6284–6293. doi:10.1021/acs.joc.2c00805
48. Shaw, M. H.; Twilton, J.; MacMillan, D. W. C. *J. Org. Chem.* **2016,** *81,* 6898–6926. doi:10.1021/acs.joc.6b01449
49. Tower, S. J.; Hetcher, W. J.; Myers, T. E.; Kuehl, N. J.; Taylor, M. T. *J. Am. Chem. Soc.* **2020,** *142,* 9112–9118. doi:10.1021/jacs.0c03039
50. Kim, J.; Li, B. X.; Huang, R. Y.-C.; Qiao, J. X.; Ewing, W. R.; MacMillan, D. W. C. *J. Am. Chem. Soc.* **2020,** *142,* 21260–21266. doi:10.1021/jacs.0c09926
51. Emmert, M. H.; Yang, C.; Kwan, E. E.; Chmielowski, R.; Kilgore, B.; VanAernum, Z. L.; Bottecchia, C.; Barrientos, R. C.; Haley, M.; Raymond, K.; Rauscher, M.; Dunn, Z. D.; Desai, J. *Org. Process Res. Dev.* **2025,** *29,* 79–91. doi:10.1021/acs.oprd.4c00343
52. Kim, J.; Xu, Y.; Lim, J. H.; Lee, J. Y.; Li, M.; Fox, J. M.; Vendrell, M.; Kim, J. S. *J. Am. Chem. Soc.* **2025,** *147,* 701–712. doi:10.1021/jacs.4c13131
53. Mato, M.; Fernández-González, X.; D'Avino, C.; Tomás-Gamasa, M.; Mascareñas, J. L. *Angew. Chem., Int. Ed.* **2024,** *63,* e202413506. doi:10.1002/anie.202413506
54. Journeaux, T.; Bernardes, G. J. L. *Nat. Chem.* **2024,** *16,* 854–870. doi:10.1038/s41557-024-01507-y
55. Tsuchikama, K.; Anami, Y.; Ha, S. Y. Y.; Yamazaki, C. M. *Nat. Rev. Clin. Oncol.* **2024,** *21,* 203–223. doi:10.1038/s41571-023-00850-2
56. Journeaux, T.; Geeson, M. B.; Murray, T. V.; Papworth, M. A.; Gothard, M.; Kettle, J. G.; Vasco, A. V.; Bernardes, G. J. L. *Angew. Chem., Int. Ed.* **2025,** *64,* e202417620. doi:10.1002/anie.202417620
57. Bell, M. R.; Engleka, M. J.; Malik, A.; Strickler, J. E. *Protein Sci.* **2013,** *22,* 1466–1477. doi:10.1002/pro.2356
58. Mahmood, T.; Shahbaz, A.; Hussain, N.; Ali, R.; Bashir, H.; Rizwan, K. *Int. J. Biol. Macromol.* **2023,** *230,* 123161. doi:10.1016/j.ijbiomac.2023.123161
59. Vasco, A. V.; Taylor, R. J.; Méndez, Y.; Bernardes, G. J. L. *J. Am. Chem. Soc.* **2024,** *146,* 20709–20719. doi:10.1021/jacs.4c03721
60. Cockrell, G. M.; Wolfe, M. S.; Wolfe, J. L.; Schöneich, C. *Mol. Pharmaceutics* **2015,** *12,* 1784–1797. doi:10.1021/mp5006799
61. Pattison, D. I.; Davies, M. J. Actions of ultraviolet light on cellular structures. *Cancer: Cell Structures, Carcinogens and Genomic Instability;* Experientia Supplementum, Vol. 96; Birkhäuser-Verlag: Basel, Switzerland, 2006; pp 131–157. doi:10.1007/3-7643-7378-4_6
62. Sellet, N.; Cormier, M.; Goddard, J.-P. *Org. Chem. Front.* **2021,** *8,* 6783–6790. doi:10.1039/d1qo01476e
63. Connell, T. U. *Dalton Trans.* **2022,** *51,* 13176–13188. doi:10.1039/d2dt01491b
64. Linsley, C. S.; Quach, V. Y.; Agrawal, G.; Hartnett, E.; Wu, B. M. *Drug Delivery Transl. Res.* **2015,** *5,* 611–624. doi:10.1007/s13346-015-0260-0

65. Ravetz, B. D.; Tay, N. E. S.; Joe, C. L.; Sezen-Edmonds, M.; Schmidt, M. A.; Tan, Y.; Janey, J. M.; Eastgate, M. D.; Rovis, T. *ACS Cent. Sci.* **2020,** *6,* 2053–2059. doi:10.1021/acscentsci.0c00948

License and Terms

BEILSTEIN JOURNAL OF ORGANIC CHEMISTRY

Light-enabled intramolecular [2 + 2] cycloaddition via photoactivation of simple alkenylboronic esters

Lewis McGhie[1,2], Hannah M. Kortman[1,2], Jenna Rumpf[1,2], Peter H. Seeberger[1,2] and John J. Molloy[*1]

Letter

Open Access

Address:
[1]Biomolecular Systems Department, Max Planck Institute of Colloids and Interfaces, Am Mühlenberg 1, 14476 Potsdam, Germany and [2]Department of Chemistry and Biochemistry, Freie Universität Berlin, Arnimallee 22, 14195 Berlin, Germany

Email:
John J. Molloy[*] - john.molloy@mpikg.mpg.de

* Corresponding author

Keywords:
boron; catalysis; [2 + 2] cycloaddition; energy transfer; photochemistry

Beilstein J. Org. Chem. **2025,** *21,* 854–863.
https://doi.org/10.3762/bjoc.21.69

Received: 29 January 2025
Accepted: 16 April 2025
Published: 30 April 2025

This article is part of the thematic issue "Photocatalysis and photochemistry in organic synthesis".

Guest Editor: T. Noël

Abstract

The photoactivation of organic molecules via energy transfer (EnT) catalysis is often limited to conjugated systems that have low-energy triplet excited states, with simple alkenes remaining an intractable challenge. The ability to address this limitation, using high energy sensitizers, would represent an attractive platform for future reaction design. Here, we disclose the photoactivation of simple alkenylboronic esters established using alkene scrambling as a rapid reaction probe to identify a suitable catalyst and boron motif. Cyclic voltammetry, UV–vis analysis, and control reactions support sensitization, enabling an intramolecular [2 + 2] cycloaddition to be realized accessing 3D bicyclic fragments containing a boron handle.

Introduction

The strategic use of a photon to activate organic molecules has had a profound impact on contemporary synthesis, enabling the practitioner to strategically construct molecules that are higher in energy from simple feedstock commodities [1-5]. Indeed, the unique ability to access high energy intermediates leveraging light, has facilitated landmark organic transformations, such as the venerable Paternò–Büchi [6-8], Norrish–Yang [9-11], and enone–alkene cycloadditions [12-14], that proceed via the generation of a singlet or triplet diradical through the activation of an unsaturated bond [2,14]. While these seminal contributions have enabled the efficient activation of carbonyl and alkene moieties, the inability of most organic molecules to efficiently absorb photons at longer wavelengths often preclude their use in direct excitation strategies, requiring unique experimental set ups and light sources that are prohibitively high in energy for selective reactivity [5].

The inception of energy transfer catalysis (EnT) has expedited discoveries concerning the photoactivation of organic molecules [15-17], enabling direct access to the triplet excited state through the use of a photocatalyst (Figure 1A, top). Pioneering studies have leveraged this platform with great effect, typically

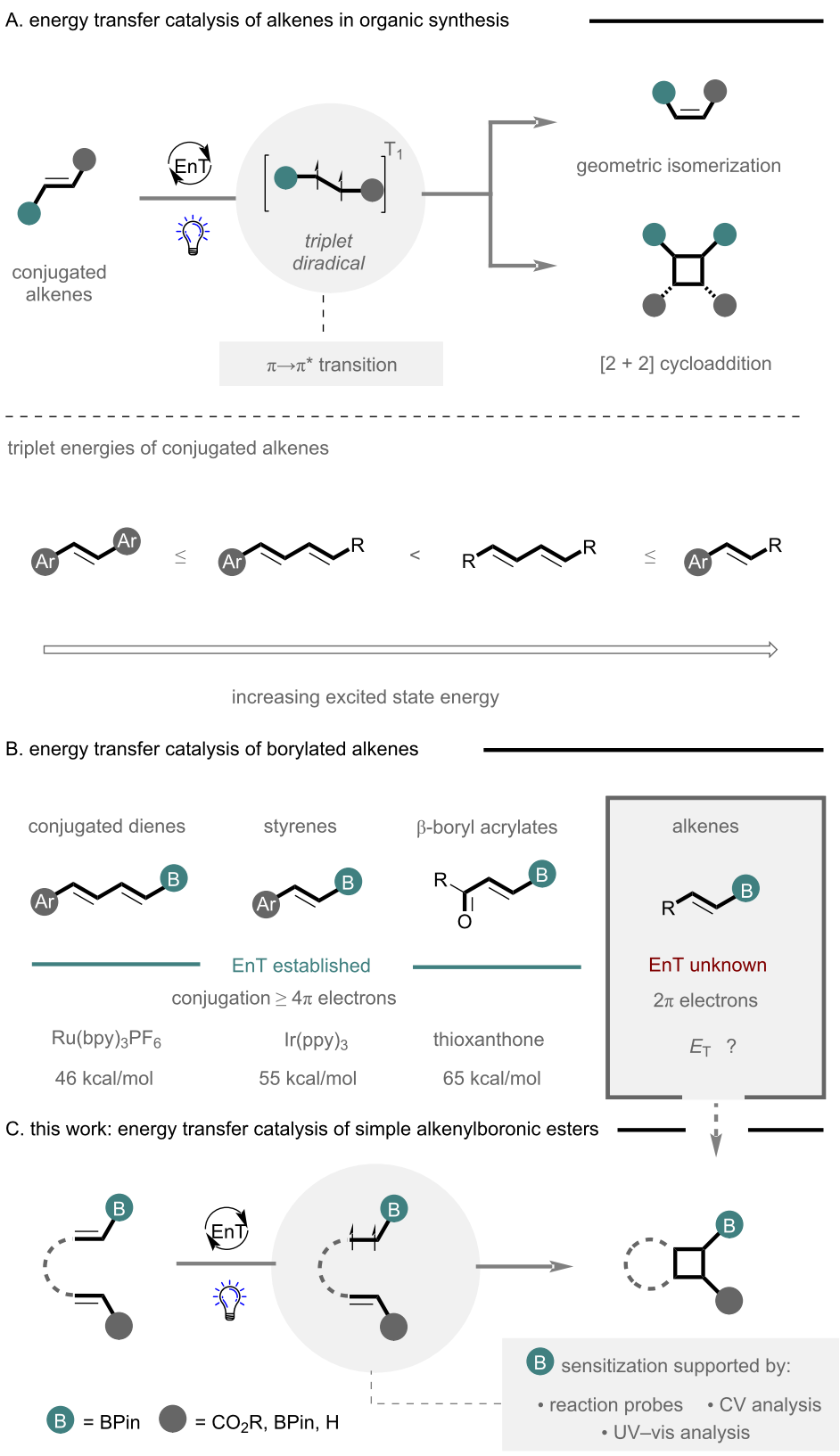

Figure 1: A) Energy transfer catalysis of alkenes in organic synthesis. B) Energy transfer catalysis of conjugated borylated alkenes. C) Energy transfer catalysis of simple alkenylboronic esters.

invoking π→π* transitions of conjugated alkenes to lower the bond order and generate a triplet diradical, primed for further reactivity. This key intermediate is pivotal in a plenum of synthetic transformations including geometric isomerization of alkenes [18,19], [2 + 2] cycloadditions [20-24], and dearomative [4 + 2] cycloadditions [25-27]. When considering conjugated alkenes, the triplet excited state energy and excited state lifetime are intrinsically linked to the degree of conjugation and substitution of a scaffold (Figure 1A, bottom), with increasing excited state energy moving from stilbenes and conjugated dienes to simple dienes, styrenes and enones (not shown) [28]. Consequently, small truncated chromophores, such as simple alkenes remain an intractable challenge for efficient EnT due to prohibitively high excited state energies and short lifetimes [29]. However, with notable strides in catalyst design, leading to catalysts with high excited state energies [30-33], in combination with concomitant advances in machine learning excited state predictions [34], it is anticipated that perhaps even the most challenging of substrates can be realized in future endeavors.

Given the dexterity of organoboron handles, both as exit vectors for the exploration of chemical space [35-38], and as covalent binders to target biomolecules [39-41], it serves as no great surprise that their reactivity in EnT catalysis has also been intensively pursued (Figure 1B). The controlled geometric isomerization of boron-containing conjugated dienes [42], styrenes [43-45] and β-boryl acrylates [46,47] has been established with great effect, while elegant [2 + 2] cycloaddition strategies to readily translate 2D to 3D chemical space have also been explored [48-52]. Here, efficient excitation, via EnT catalysis, is typically contingent on extended chromophores ≥ 4π electrons, with less conjugated systems requiring more powerful catalysts. A recent elegant example by Masarwa and co-workers demonstrated the efficient sensitization of an alkene-containing four boron substituents using $Ir(ppy)_3$ as a suitable sensitizer in the presence of styrene, indicating a prominent role of the adjacent p-orbital [51]. While simple alkenylboronic esters have been employed as triplet diradical quenchers to facilitate the synthesis of boron-containing cyclobutanes [53-55], excitation of these motifs to form a triplet diradical, and its application in a synthetic process, is conspicuously underexplored, presumably due to unreachable excited states and poor lifetimes when limited to a single boron unit.

Herein, we demonstrate the sensitization of alkenylboronates to enable efficient intramolecular [2 + 2] cycloaddition using high energy photosensitizers (Figure 1C). Sensitization was quickly established and explored through the use of alkene scrambling (geometrical isomerization) reaction probes, to identify a suitable catalyst and boron residue, while control reactions and mechanistic studies support the proposed sensitization. The platform enables direct access to mono- and vicinal cyclobutylboronic esters that could be effectively derivatized to demonstrate their potential in synthesis.

Results and Discussion

To validate the proposed sensitization of alkenylboronic esters, we initiated our study probing the geometric isomerization of easily accessible substrate (*E*)-**1a** under photocatalysis conditions (Table 1). It is pertinent to note, while the core substrate (*E*)-**1a** lacks the necessary non-covalent interactions to achieve

Table 1: Probing EnT catalysis of alkenylboronic ester **1a** via alkene scrambling.[a]

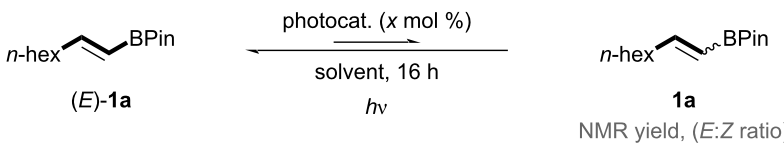

(*E*)-**1a** — **1a**

NMR yield, (*E*:*Z* ratio)

Entry	Catalyst	E_T (kcal/mol)[b]	λ (nm)	Solvent	Yield (%)[c]	*E*/*Z*[c]
1	$Ir(ppy)_3$	55	450	MeCN	92	>95:5
2	$(Ir[dF(CF_3)ppy]_2(dtbpy))PF_6$	60	450	MeCN	92	>95:5
3[d]	thioxanthone	65	400	MeCN	81	89:11
4[d]	xanthone	74	365	MeCN	83	73:27
5[d]	xanthone	74	365	DCM	80	75:25
6[d]	xanthone	74	365	THF	86	>95:5
7[d]	xanthone	74	365	DMF	86	>95:5
8	–	–	365	MeCN	92	>95:5

[a]Standard conditions: (*E*)-**1a** (0.1 mmol), cat. (1 mol %), solvent (0.03 M), under light irradiation (1 W), rt, 16 h; [b]see [28]; [c]determined by ^1H NMR spectroscopy against a known internal standard (1,3,5-trimethoxybenzene); [d]5 mol % catalyst loading.

directionality ($E \rightarrow Z$), synonymous with conventional photocatalyzed isomerization processes [19], it serves as a rapid reaction probe to support sensitization via the generation of a photostationary state equilibrium. The use of $Ir(ppy)_3$ (Table 1, entry 1), an efficient sensitizer for the activation of polyboronated alkenes [51] and β-borylstyrenes [43,48], was ineffective and no reactivity was observed. Implementing a higher energy iridium sensitizer (≈60 kcal/mol) was also unsuccessful (Table 1, entry 2), however, employing thioxanthone (65 kcal/mol) demonstrated efficient activation of the alkene leading to the generation of an 89:11 (*E*/*Z*) mixture of geometrical isomers (Table 1, entry 3). The use of xanthone (74 kcal/mol), a highly powerful organic photocatalyst, enabled enhanced reactivity producing a photostationary state of 73:27 after 16 hours (Table 1, entry 4). Varying solvent had a profound effect on reactivity with more Lewis-basic solvents suppressing reactivity (Table 1, entries 4 and 5 vs entries 6 and 7), indicating p-orbital availability plays a prominent role [56,57]. A control reaction (Table 1, entry 8), in combination with UV–vis absorption studies (see Supporting Information File 1 for full details), demonstrate that catalysis is operational.

Having established xanthone as a suitable high energy sensitizer for the efficient activation of simple alkenylboronic esters, we next set out to determine the role of the boron unit and hybridization state (Figure 2A). Efficient EnT catalysis could be

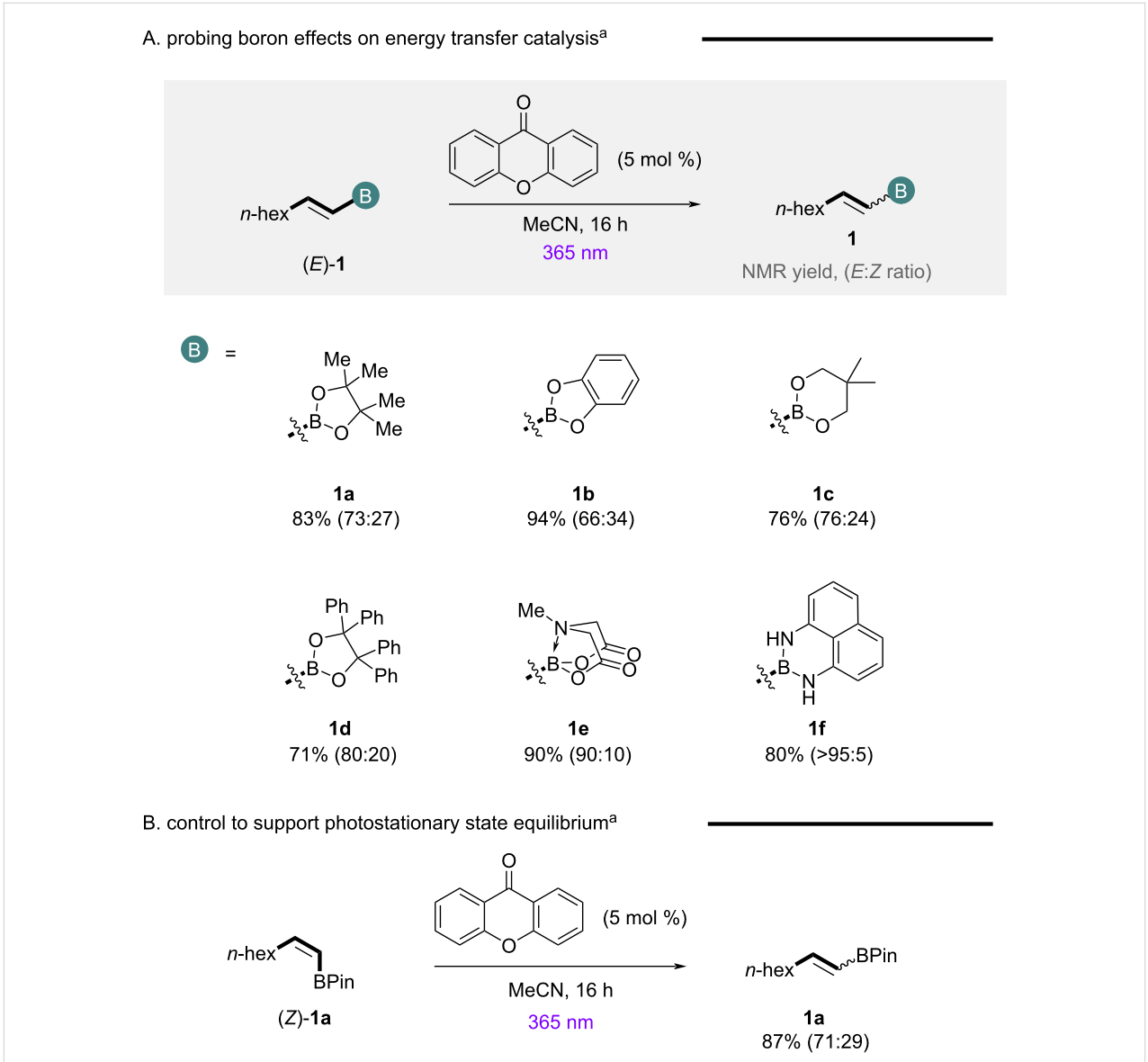

Figure 2: Probing boron effects on reactivity (A) and confirming the generation of a photostationary state equilibrium (B). Standard reaction conditions: (*E*)-**1** (0.1 mmol), xanthone (5 mol %), MeCN (0.03 M), rt, 16 h.

achieved with neutral trigonal planar systems **1a**–**d**, while BMIDA substrate **1e** was also effective presumably due to the proposed hemilabile nature of the MIDA protecting group in acetonitrile [58]. More electron-donating ligands such as 1,8-diaminonaphthalene (BDAN, **1f**) were detrimental to reactivity leading to substrate degradation. Given the ease of access and enhanced stability of pinacol esters to column chromatography, this motif was advanced for further reaction design. Cyclic voltammetry analysis of **1a** indicates that single-electron-transfer processes with the excited state catalyst are not operational (see Supporting Information File 1 for full details), providing support for an EnT mechanism, while exposing the *Z*-isomer (*Z*)-**1a** to the model reaction conditions, led to the generation of a similar photostationary state equilibrium of isomers, characteristic of an EnT process (Figure 2B) [19].

In a bid to translate sensitization reaction probes to meaningful synthetic transformations, conventional intermolecular [2 + 2] cycloaddition reactions were initially trialled (Figure 3A). Preliminary reactions using styrene or methyl acrylate were unsuccessful, with no [2 + 2] cycloaddition observed, despite the use of higher catalyst loadings. The efficient isomerization of **1a** during these reactions indicated that substrate lifetime for efficient intermolecular reactivity may be problematic. While substrate-tethered reactivity, developed by Brown and co-workers was unsuccessful [49], the strategic incorporation of an alkene tether, bringing both alkenes spatially proximal, facilitated a [2 + 2] cycloaddition to generate bicyclic product **4a** as a 1:1 mixture of diastereoisomers in low yield. This provides an exciting proof of principle that it is possible to efficiently quench the generated triplet diradical in an intramolecular system.

To further assess the properties relevant for intramolecular reactivity, substrate **3b** was designed (see Supporting Information File 1 for full details), given that non-activated α,β-unsaturated systems are also comparatively underexplored via EnT activation (Table 2) [59,60]. As anticipated, guided by alkene scrambling reaction probes (Table 1), iridium sensitizers were unsuccessful (Table 2, entries 1 and 2). Thioxanthone provided the cyclobutyl product **4b** in 10% yield (Table 2, entry 3), indicating catalysis with poor overlap between the catalyst

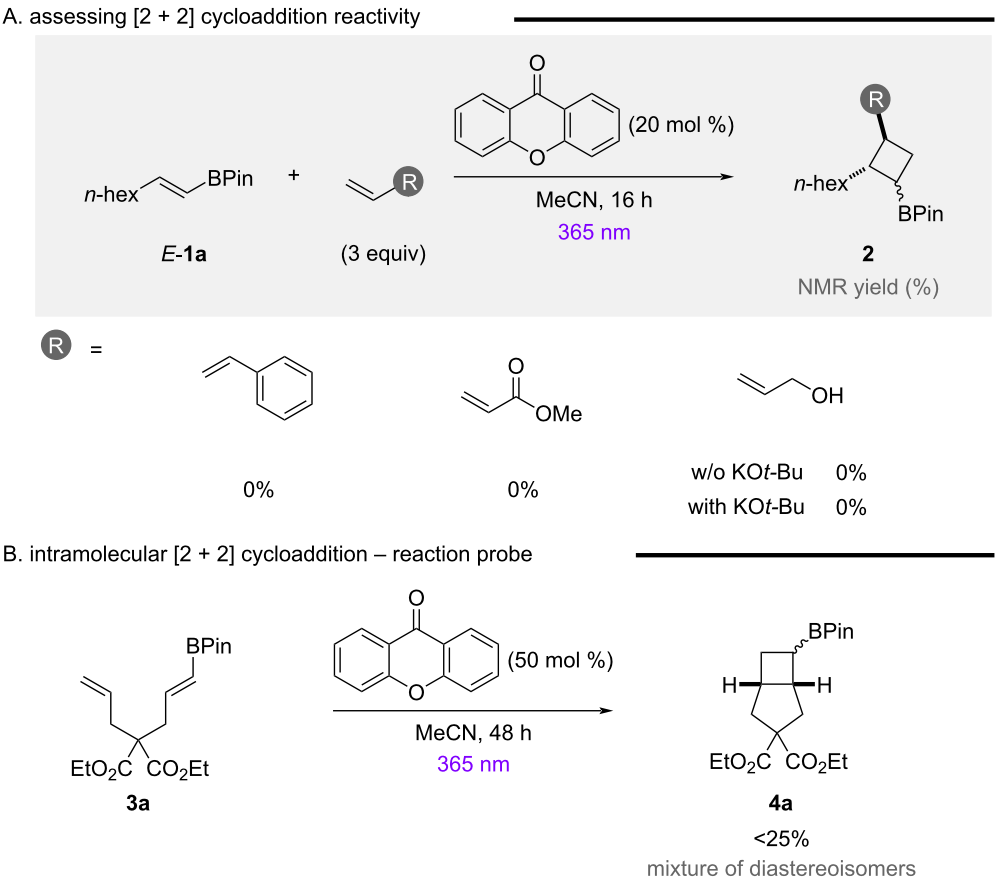

Figure 3: Probing EnT catalysis enabled [2 + 2] cycloaddition of simple alkenylboronic esters.

Table 2: Reaction optimization of intramolecular [2 + 2] cycloaddition.[a]

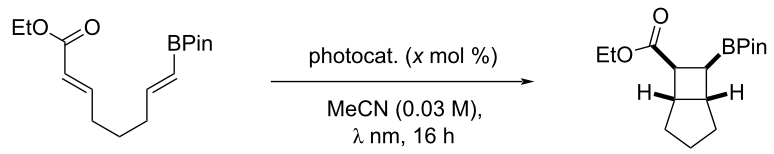

3b **4b**

Entry	Catalyst	mol %	E_T (kcal/mol)	λ (nm)	Yield (%)[b]	dr[b]
1	Ir(p-CF_3)$_3$	1	56	450	0	–
2	(Ir[dF(CF_3)ppy]$_2$(dtbpy))PF_6	1	60	450	0	–
3	thioxanthone	5	65	390	10	–
4	xanthone	5	74	365	35	6:1
5	**xanthone**	**20**	**74**	**365**	**76**	**5:1**

[a]Standard conditions: **3b** (0.1 mmol), cat. (*x* mol %), MeCN (0.03 M), under light irradiation (1 W), rt, 16 h; [b]determined by ^{1}H NMR spectroscopy against a known internal standard (1,3,5-trimethoxybenzene).

(65 kcal/mol) and substrate. The use of xanthone demonstrated clean translation to product favouring *syn* diastereoselectivity [61,62] (Table 2, entry 4), with additional catalyst increasing yield during the 16 h reaction time (Table 2, entry 5).

With a general set of reaction conditions for the [2 + 2] cycloaddition established, the scope and pivotal properties of the core structure was assessed (Scheme 1). Single point modifications of the tethered backbone were tolerated, enabling access to small 3D bicyclic scaffolds **4b**, **4c**, and **4d** containing both a boron and ester handle. Consciously aware that α,β-unsaturated esters could potentially also undergo energy transfer in the presence of high energy sensitizers [59,60], the system **4e** with two ester components was also designed. The reaction proceeded cleanly to the cycloadduct, indicating sensitization of the acrylate is also operational. Access to *vicinal* boron scaffolds **4f** and **4g** provided conclusive evidence that sensitization of alkenylboronic esters is achievable using xanthone, with in situ oxidation enabling direct access to otherwise challenging to synthesize cyclobutyldiols. The lower observed diastereoselectivity may reflect differences in stereoelectronic stabilization of the transient 1,4-biradical intermediate on changing substituent ($CO_2R \rightarrow BPin$) [63-65]. It is pertinent to note that increased catalyst loading and reaction times were necessary for efficient reactivity with alkenylboronic esters, suggesting acrylates are more efficiently sensitized (lower T_1 excited state) than their alkenylboronic ester counterparts. This is unsurprising given their enhanced conjugation (4π electrons vs 2π electrons and p-orbital). To probe the efficiency of trisubstituted alkenes, *vicinal* boron precursor **3h** was designed (Scheme 1, bottom). Despite the additional substituent, the reaction was tolerated, albeit with decreased diastereoselectivity in comparison to previous alkenylboronic ester examples **4b**–**d**.

To demonstrate the synthetic utility of the generated small 3D fragments and complement existing [2 + 2] strategies via direct excitation [66,67], product derivatization was explored (Scheme 2A). While initial efforts for oxidation proved challenging, due to a competing retro-aldol ring-opening reaction, employing a buffered system enabled access to β-alcohol **5**. Given the previous power of trifluoroborates in cross-coupling strategies for cyclobutyl scaffolds [53-55], products **6** and **7** could be synthesized via mild conditions [68].

Inspired by recent advances by Nolan and co-workers demonstrating the synthetic power of gold catalysts in EnT catalysis [31,69-72], we probed the reactivity of [Au(SIPr)(Cbz)] in our model system given the excited state energy (67 kcal/mol) is between both active catalysts thioxanthone (65 kcal/mol) and xanthone (74 kcal/mol). While a higher catalyst loading than conventional systems was required for efficient reactivity (Scheme 2B), the [2 + 2] cycloaddition could be readily achieved. It is pertinent to note the enhanced levels of diastereoselectivity obtained for this reaction further underscore the potential of gold catalysts for future EnT reactions. Control reactions indicate selective activation of the α,β-unsaturated ester (see Supporting Information File 1 for full details).

Conclusion

In summary, photoactivation of simple alkenylboronic esters was established using alkene scrambling as a rapid reaction probe to determine the catalyst and boron moiety for sensitization. The use of cyclic voltammetry, UV–vis analysis, and control reaction probes support sensitization as an operational mechanism. While intermolecular alkene quenching to enable [2 + 2] cycloaddition was inefficient, presumably due to poor

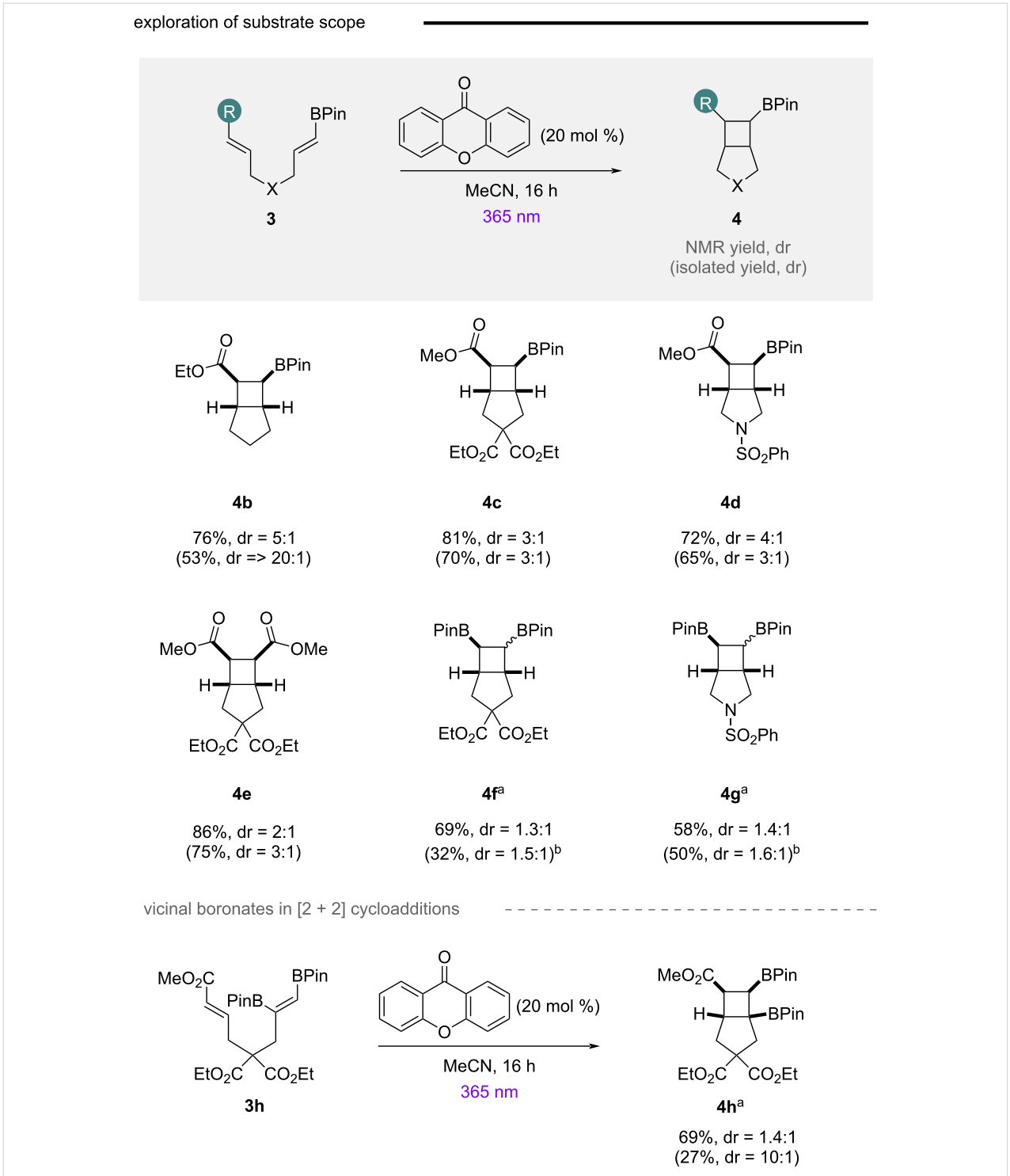

Scheme 1: Establishing the substrate scope. Conditions: **3** (1 equiv), xanthone (20 mol %), MeCN (0.03 M), under 365 nm irradiation, rt, 16 h; [a]xanthone (50 mol %) was used and reactions were run for 48 h; [b]to aid characterization of isolated material, the product was isolated after oxidation to the corresponding cyclobutyldiol.

substrate lifetime, intramolecular [2 + 2] reactivity with both acrylates and alkenylboronic esters was effective. The small 3D, boron-containing fragments could be derivatized to demonstrate the synthetic utility of the process. Although reactivity is currently limited to intramolecular quenching, it is envisaged the developed insights will serve as a blueprint for future endeavors to achieve sensitization using high energy photocatalysts, especially when considering recent advances enabling

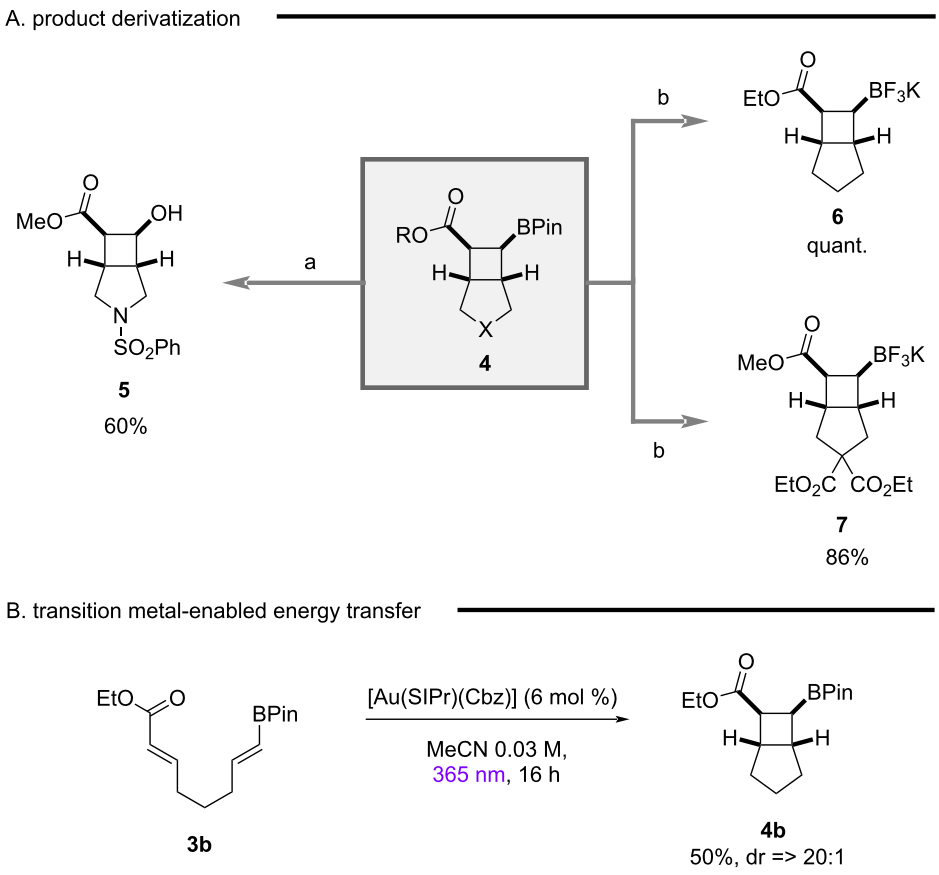

Scheme 2: A) Product derivatization and B) transition-metal EnT catalysis. Reaction conditions A): **4d** (1 equiv), H_2O_2 (30 wt % in H_2O), aq NaH_2PO_4, THF, 0 °C; B) **4** (1 equiv), KF (4 equiv), L-tartaric acid (2.1 equiv), MeOH, MeCN, H_2O, rt.

subsequent intramolecular H-atom abstraction [51] and efficient rearrangements [73,74].

Supporting Information

Supporting Information File 1

Experimental section, characterization, and copies of spectra.
[https://www.beilstein-journals.org/bjoc/content/supplementary/1860-5397-21-69-S1.pdf]

Acknowledgements

We thank Eduardo Garcia Alonso for preliminary results and Dr. Roza Bouchal for help with cyclic voltammetry experiments. We thank Prof. Steven Nolan for providing [Au(SIPr)(Cbz)] and for insightful discussions. We thank the Mass Spec department of the Institute for Chemistry and Biochemistry of Freie Universität.

Funding

We gratefully acknowledge financial support from the Max-Planck Society, The European Research Council (ERC) under the Horizon Europe research and innovation program (project number 101163783 LUMIBOR) and the Fonds der Chemischen Industrie, FCI.

ORCID® iDs

Peter H. Seeberger - https://orcid.org/0000-0003-3394-8466
John J. Molloy - https://orcid.org/0000-0001-5337-0353

Data Availability Statement

All data that supports the findings of this study is available in the published article and/or the supporting information of this article.

References

1. Hammond, G. S.; Turro, N. J. *Science* **1963,** *142,* 1541–1553. doi:10.1126/science.142.3599.1541
2. Roth, H. D. *Angew. Chem., Int. Ed. Engl.* **1989,** *28,* 1193–1207. doi:10.1002/anie.198911931

3. Schultz, D. M.; Yoon, T. P. *Science* **2014,** *343,* 1239176. doi:10.1126/science.1239176
4. Wang, H.; Tian, Y.-M.; König, B. *Nat. Rev. Chem.* **2022,** *6,* 745–755. doi:10.1038/s41570-022-00421-6
5. Goti, G.; Manal, K.; Sivaguru, J.; Dell'Amico, L. *Nat. Chem.* **2024,** *16,* 684–692. doi:10.1038/s41557-024-01472-6
6. Paterno, E.; Chieffi, G. *Gazz. Chim. Ital.* **1909,** *39,* 341–361.
7. D'Auria, M. *Photochem. Photobiol. Sci.* **2019,** *18,* 2297–2362. doi:10.1039/c9pp00148d
8. Franceschi, P.; Cuadros, S.; Goti, G.; Dell'Amico, L. *Angew. Chem., Int. Ed.* **2023,** *62,* e202217210. doi:10.1002/anie.202217210
9. Norrish, R. G. W.; Bamford, C. H. *Nature* **1937,** *140,* 195–196. doi:10.1038/140195b0
10. Yang, N. C.; Yang, D.-D. H. *J. Am. Chem. Soc.* **1958,** *80,* 2913–2914. doi:10.1021/ja01544a092
11. Chen, C. *Org. Biomol. Chem.* **2016,** *14,* 8641–8647. doi:10.1039/c6ob01214k
12. Liebermann, C. *Ber. Dtsch. Chem. Ges.* **1877,** *10,* 2177–2179. doi:10.1002/cber.187701002242
13. Ciamician, G.; Silber, P. *Ber. Dtsch. Chem. Ges.* **1908,** *41,* 1928–1935. doi:10.1002/cber.19080410272
14. Poplata, S.; Tröster, A.; Zou, Y.-Q.; Bach, T. *Chem. Rev.* **2016,** *116,* 9748–9815. doi:10.1021/acs.chemrev.5b00723
15. Dexter, D. L. *J. Chem. Phys.* **1953,** *21,* 836–850. doi:10.1063/1.1699044
16. Strieth-Kalthoff, F.; James, M. J.; Teders, M.; Pitzer, L.; Glorius, F. *Chem. Soc. Rev.* **2018,** *47,* 7190–7202. doi:10.1039/c8cs00054a
17. Dutta, S.; Erchinger, J. E.; Strieth-Kalthoff, F.; Kleinmans, R.; Glorius, F. *Chem. Soc. Rev.* **2024,** *53,* 1068–1089. doi:10.1039/d3cs00190c
18. Hammond, G. S.; Saltiel, J.; Lamola, A. A.; Turro, N. J.; Bradshaw, J. S.; Cowan, D. O.; Counsell, R. C.; Vogt, V.; Dalton, C. *J. Am. Chem. Soc.* **1964,** *86,* 3197–3217. doi:10.1021/ja01070a002
19. Neveselý, T.; Wienhold, M.; Molloy, J. J.; Gilmour, R. *Chem. Rev.* **2022,** *122,* 2650–2694. doi:10.1021/acs.chemrev.1c00324
20. Lu, Z.; Yoon, T. P. *Angew. Chem., Int. Ed.* **2012,** *51,* 10329–10332. doi:10.1002/anie.201204835
21. Tröster, A.; Alonso, R.; Bauer, A.; Bach, T. *J. Am. Chem. Soc.* **2016,** *138,* 7808–7811. doi:10.1021/jacs.6b03221
22. Daub, M. E.; Jung, H.; Lee, B. J.; Won, J.; Baik, M.-H.; Yoon, T. P. *J. Am. Chem. Soc.* **2019,** *141,* 9543–9547. doi:10.1021/jacs.9b04643
23. Großkopf, J.; Kratz, T.; Rigotti, T.; Bach, T. *Chem. Rev.* **2022,** *122,* 1626–1653. doi:10.1021/acs.chemrev.1c00272
24. Genzink, M. J.; Kidd, J. B.; Swords, W. B.; Yoon, T. P. *Chem. Rev.* **2022,** *122,* 1654–1716. doi:10.1021/acs.chemrev.1c00467
25. Ma, J.; Chen, S.; Bellotti, P.; Guo, R.; Schäfer, F.; Heusler, A.; Zhang, X.; Daniliuc, C.; Brown, M. K.; Houk, K. N.; Glorius, F. *Science* **2021,** *371,* 1338–1345. doi:10.1126/science.abg0720
26. Adak, S.; Hazra, P. S.; Fox, C. B.; Brown, M. K. *Angew. Chem., Int. Ed.* **2025,** *64,* e202416215. doi:10.1002/anie.202416215
27. Zhu, M.; Zhang, X.; Zheng, C.; You, S.-L. *Acc. Chem. Res.* **2022,** *55,* 2510–2525. doi:10.1021/acs.accounts.2c00412
28. Montalti, M.; Credi, A.; Prodi, L.; Gandolfi, M. T. *Handbook of Photochemistry,* 3rd ed.; CRC Press: Boca Raton, FL, USA, 2006. doi:10.1201/9781420015195
29. Strieth-Kalthoff, F.; Glorius, F. *Chem* **2020,** *6,* 1888–1903. doi:10.1016/j.chempr.2020.07.010
30. Nikitas, N. F.; Gkizis, P. L.; Kokotos, C. G. *Org. Biomol. Chem.* **2021,** *19,* 5237–5253. doi:10.1039/d1ob00221j
31. Martynova, E. A.; Voloshkin, V. A.; Guillet, S. G.; Bru, F.; Beliš, M.; Van Hecke, K.; Cazin, C. S. J.; Nolan, S. P. *Chem. Sci.* **2022,** *13,* 6852–6857. doi:10.1039/d2sc00864e
32. Schmid, L.; Glaser, F.; Schaer, R.; Wenger, O. S. *J. Am. Chem. Soc.* **2022,** *144,* 963–976. doi:10.1021/jacs.1c11667
33. Rehpenn, A.; Hindelang, S.; Truong, K.-N.; Pöthig, A.; Storch, G. *Angew. Chem., Int. Ed.* **2024,** *63,* e202318590. doi:10.1002/anie.202318590
34. Schlosser, L.; Rana, D.; Pflüger, P.; Katzenburg, F.; Glorius, F. *J. Am. Chem. Soc.* **2024,** *146,* 13266–13275. doi:10.1021/jacs.4c01352
35. Fernández, E. *Advances in Organoboron Chemistry towards Organic Synthesis,* 1st ed.; Thieme: Stuttgart, Germany, 2020. doi:10.1055/b-006-164898
36. Fyfe, J. W. B.; Watson, A. J. B. *Chem* **2017,** *3,* 31–55. doi:10.1016/j.chempr.2017.05.008
37. Marotta, A.; Fang, H.; Adams, C. E.; Sun Marcus, K.; Daniliuc, C. G.; Molloy, J. J. *Angew. Chem., Int. Ed.* **2023,** *62,* e202307540. doi:10.1002/anie.202307540
38. McGhie, L.; Marotta, A.; Loftus, P. O.; Seeberger, P. H.; Funes-Ardoiz, I.; Molloy, J. J. *J. Am. Chem. Soc.* **2024,** *146,* 15850–15859. doi:10.1021/jacs.4c02261
39. Chatterjee, S.; Tripathi, N. M.; Bandyopadhyay, A. *Chem. Commun.* **2021,** *57,* 13629–13640. doi:10.1039/d1cc05481c
40. Grams, R. J.; Santos, W. L.; Scorei, I. R.; Abad-García, A.; Rosenblum, C. A.; Bita, A.; Cerecetto, H.; Viñas, C.; Soriano-Ursúa, M. A. *Chem. Rev.* **2024,** *124,* 2441–2511. doi:10.1021/acs.chemrev.3c00663
41. Kazmi, M. Z. H.; Schneider, O. M.; Hall, D. G. *J. Med. Chem.* **2023,** *66,* 13768–13787. doi:10.1021/acs.jmedchem.3c01194
42. Kweon, B.; Blank, L.; Soika, J.; Messara, A.; Daniliuc, C. G.; Gilmour, R. *Angew. Chem., Int. Ed.* **2024,** *63,* e202404233. doi:10.1002/anie.202404233
43. Molloy, J. J.; Metternich, J. B.; Daniliuc, C. G.; Watson, A. J. B.; Gilmour, R. *Angew. Chem., Int. Ed.* **2018,** *57,* 3168–3172. doi:10.1002/anie.201800286
44. Faßbender, S. I.; Molloy, J. J.; Mück-Lichtenfeld, C.; Gilmour, R. *Angew. Chem., Int. Ed.* **2019,** *58,* 18619–18626. doi:10.1002/anie.201910169
45. Zähringer, T. J. B.; Wienhold, M.; Gilmour, R.; Kerzig, C. *J. Am. Chem. Soc.* **2023,** *145,* 21576–21586. doi:10.1021/jacs.3c07678
46. Molloy, J. J.; Schäfer, M.; Wienhold, M.; Morack, T.; Daniliuc, C. G.; Gilmour, R. *Science* **2020,** *369,* 302–306. doi:10.1126/science.abb7235
47. Wienhold, M.; Kweon, B.; McLaughlin, C.; Schmitz, M.; Zähringer, T. J. B.; Daniliuc, C. G.; Kerzig, C.; Gilmour, R. *Angew. Chem., Int. Ed.* **2023,** *62,* e202304150. doi:10.1002/anie.202304150
48. Liu, Y.; Ni, D.; Stevenson, B. G.; Tripathy, V.; Braley, S. E.; Raghavachari, K.; Swierk, J. R.; Brown, M. K. *Angew. Chem., Int. Ed.* **2022,** *61,* e202200725. doi:10.1002/anie.202200725
49. Liu, Y.; Ni, D.; Brown, M. K. *J. Am. Chem. Soc.* **2022,** *144,* 18790–18796. doi:10.1021/jacs.2c08777
50. Posz, J. M.; Sharma, N.; Royalty, P. A.; Liu, Y.; Salome, C.; Fessard, T. C.; Brown, M. K. *J. Am. Chem. Soc.* **2024,** *146,* 10142–10149. doi:10.1021/jacs.4c01557
51. Hanania, N.; Eghbarieh, N.; Masarwa, A. *Angew. Chem., Int. Ed.* **2024,** *63,* e202405898. doi:10.1002/anie.202405898

52. Fang, H.; García-Eguizábal, A.; Hsueh, Y. J.; Daniliuc, C. G.; Funes-Ardoiz, I.; Molloy, J. J. *Angew. Chem., Int. Ed.* **2025,** *64,* e202418651. doi:10.1002/anie.202418651
53. Coote, S. C.; Bach, T. *J. Am. Chem. Soc.* **2013,** *135,* 14948–14951. doi:10.1021/ja408167r
54. Murray, P. R. D.; Bussink, W. M. M.; Davies, G. H. M.; van der Mei, F. W.; Antropow, A. H.; Edwards, J. T.; D'Agostino, L. A.; Ellis, J. M.; Hamann, L. G.; Romanov-Michailidis, F.; Knowles, R. R. *J. Am. Chem. Soc.* **2021,** *143,* 4055–4063. doi:10.1021/jacs.1c01173
55. Scholz, S. O.; Kidd, J. B.; Capaldo, L.; Flikweert, N. E.; Littlefield, R. M.; Yoon, T. P. *Org. Lett.* **2021,** *23,* 3496–3501. doi:10.1021/acs.orglett.1c00938
56. Marotta, A.; Adams, C. E.; Molloy, J. J. *Angew. Chem., Int. Ed.* **2022,** *61,* e202207067. doi:10.1002/anie.202207067
57. Tanaka, T.; Yamaji, M.; Shizuka, H. *J. Chem. Soc., Faraday Trans.* **1998,** *94,* 1179–1187. doi:10.1039/a707820j
The effect of solvent polarity on EnT is well established.
58. Lee, C. F.; Diaz, D. B.; Holownia, A.; Kaldas, S. J.; Liew, S. K.; Garrett, G. E.; Dudding, T.; Yudin, A. K. *Nat. Chem.* **2018,** *10,* 1062–1070. doi:10.1038/s41557-018-0097-5
59. Schuster, D. I.; Widman, D. *Tetrahedron Lett.* **1971,** *12,* 3571–3574. doi:10.1016/s0040-4039(01)97233-8
60. Münster, N.; Parker, N. A.; van Dijk, L.; Paton, R. S.; Smith, M. D. *Angew. Chem., Int. Ed.* **2017,** *56,* 9468–9472. doi:10.1002/anie.201705333
61. Murai, H.; l'haya, Y. J. *Chem. Phys.* **1989,** *135,* 131–137. doi:10.1016/0301-0104(89)87012-0
62. Satzger, H.; Schmidt, B.; Root, C.; Zinth, W.; Fierz, B.; Krieger, F.; Kiefhaber, T.; Gilch, P. *J. Phys. Chem. A* **2004,** *108,* 10072–10079. doi:10.1021/jp047583+
63. Beckwith, A. L. J. *Tetrahedron* **1981,** *37,* 3073–3100. doi:10.1016/s0040-4020(01)98839-8
64. Marco-Contelles, J.; Sanchez, B. *J. Org. Chem.* **1993,** *58,* 4293–4297. doi:10.1021/jo00068a025
65. Hoffmann, N.; Buschmann, H.; Raabe, G.; Scharf, H.-D. *Tetrahedron* **1994,** *50,* 11167–11186. doi:10.1016/s0040-4020(01)89419-9
66. Demchuk, O. P.; Hryshchuk, O. V.; Vashchenko, B. V.; Kozytskiy, A. V.; Tymtsunik, A. V.; Komarov, I. V.; Grygorenko, O. O. *J. Org. Chem.* **2020,** *85,* 5927–5940. doi:10.1021/acs.joc.0c00265
67. Liashuk, O. S.; Grygorenko, O. O.; Volovenko, Y. M.; Waser, J. *Chem. – Eur. J.* **2023,** *29,* e202301650. doi:10.1002/chem.202301650
68. Lennox, A. J. J.; Lloyd-Jones, G. C. *Angew. Chem., Int. Ed.* **2012,** *51,* 9385–9388. doi:10.1002/anie.201203930
69. Guillet, S. G.; Logvinov, A. A.; Voloshkin, V. A.; Martynova, E. A.; Nolan, S. P. *Org. Lett.* **2023,** *25,* 1403–1408. doi:10.1021/acs.orglett.3c00136
70. Zhao, Y.; Voloshkin, V. A.; Martynova, E. A.; Maity, B.; Cavallo, L.; Nolan, S. P. *Chem. Commun.* **2024,** *60,* 3174–3177. doi:10.1039/d4cc00379a
71. Voloshkin, V. A.; Villa, M.; Martynova, E. A.; Beliš, M.; Van Hecke, K.; Ceroni, P.; Nolan, S. P. *Chem. Sci.* **2024,** *15,* 4571–4580. doi:10.1039/d3sc06675d
72. Zhao, Y.; Guillet, S. G.; Voloshkin, V. A.; Nolan, S. P. *Org. Lett.* **2024,** *26,* 10322–10327. doi:10.1021/acs.orglett.4c03919
73. Zheng, Y.; Dong, Q.-X.; Wen, S.-Y.; Ran, H.; Huang, H.-M. *J. Am. Chem. Soc.* **2024,** *146,* 18210–18217. doi:10.1021/jacs.4c04370
74. Wen, S.-Y.; Chen, J.-J.; Zheng, Y.; Han, J.-X.; Huang, H.-M. *Angew. Chem., Int. Ed.* **2025,** *64,* e202415495. doi:10.1002/anie.202415495

License and Terms

BEILSTEIN JOURNAL OF ORGANIC CHEMISTRY

Study of tribenzo[*b*,*d*,*f*]azepine as donor in D–A photocatalysts

Katy Medrano-Uribe*, Jorge Humbrías-Martín and Luca Dell'Amico*

Full Research Paper

Open Access

Address:
Department of Chemical Sciences, University of Padova, Via Francesco Marzolo 1, 35131, Padova, Italy

Email:
Katy Medrano-Uribe* - katyelizabeth.medranouribe@unipd.it;
Luca Dell'Amico* - luca.dellamico@unipd.it

* Corresponding author

Keywords:
donor–acceptor system; photocatalyst design; photoredox catalysis; organic photocatalyst

Beilstein J. Org. Chem. **2025,** *21,* 935–944.
https://doi.org/10.3762/bjoc.21.76

Received: 17 February 2025
Accepted: 17 April 2025
Published: 14 May 2025

This article is part of the thematic issue "Photocatalysis and photochemistry in organic synthesis".

Guest Editor: T. Noël

Abstract

Since the discovery of donor–acceptor (D–A) type molecules in the field of materials science, they have found great applicability in the field of photocatalysis. Most of these compounds are based on complex D–A–D structures or multi-D–A systems, such as 4CzIPN. Whereas these systems have been widely studied and applied as photocatalysts, simpler D–A structures remain less explored. Nevertheless, the simplicity of D–A structures makes them the ideal structures to further understand the structure–property relationship of D–A molecules for optimizing their photocatalytic performance by simpler modification of the different D–A subunits. In particular, D–A structures featuring sulfur-based acceptors and nitrogen donors have gained increasing attention for their use as photoredox catalysts. This study introduces a new family of D–A molecules by exploring various sulfur-based acceptors and nitrogen donors, including a novel tribenzo[*b*,*d*,*f*]azepine (TBA) unit and 5*H*-dibenz[*b*,*f*]azepine (IMD). Our findings demonstrate that these simple D–A structures exhibit promising photocatalytic properties, comparable to those of more complex D–A–D systems.

Introduction

In recent years, photocatalysis has emerged as a powerful tool for the construction and functionalization of organic molecules and materials. Thus, the scientific community has focused on the design and study of new organic molecules that can be used as photocatalysts, replacing generally more expensive metal-based complexes [1-3]. Furthermore, there is a particular interest in the obtainment of organic molecules with well-balanced redox potentials in the excited state that can act as bimodal photocatalysts, facilitating their use in oxidative and reductive quenching cycles. In this sense, it is crucial to understand the molecule's structure–properties dependence to modulate its optical and photoredox properties [4]. For instance, molecules with donor–acceptor (D–A) structures, classically used as OLED emitters, have gained relevance by finding alternative

applications in the field of photocatalysis [5]. In this type of structure, the electron density distribution in the charge transfer (CT) excited state is facilitated by the presence of an electron-rich moiety and an electron-poor part in the same molecule, increasing the lifetime in the excited state. One of the representative classes of molecules demonstrating dual use in materials chemistry and photocatalysis is the carbazolyl dicyanobenzene (CDCB) family. Since the initial report on the synthesis and photoluminescence study of 4CzIPN (**1**, Figure 1a) [6], the scientific community has recognized its potential under photocatalytic manifolds. This interest is attributed to: i) its absorption profile in the visible region, ii) a long lifetime of the excited states, and iii) balanced redox potentials in both the ground and excited states [7]. In 2018, Zeitler and her collaborators conducted an innovative and in-depth study on modulating the photochemical properties of a family of donor–acceptor cyanoarenes [8]. They employed various nitrogen donor molecules attached to diversely substituted acceptor cores. This systematic approach allowed the authors to develop new organic photocatalysts (PCs) with strong reductive or oxidative properties based on the different redox potentials.

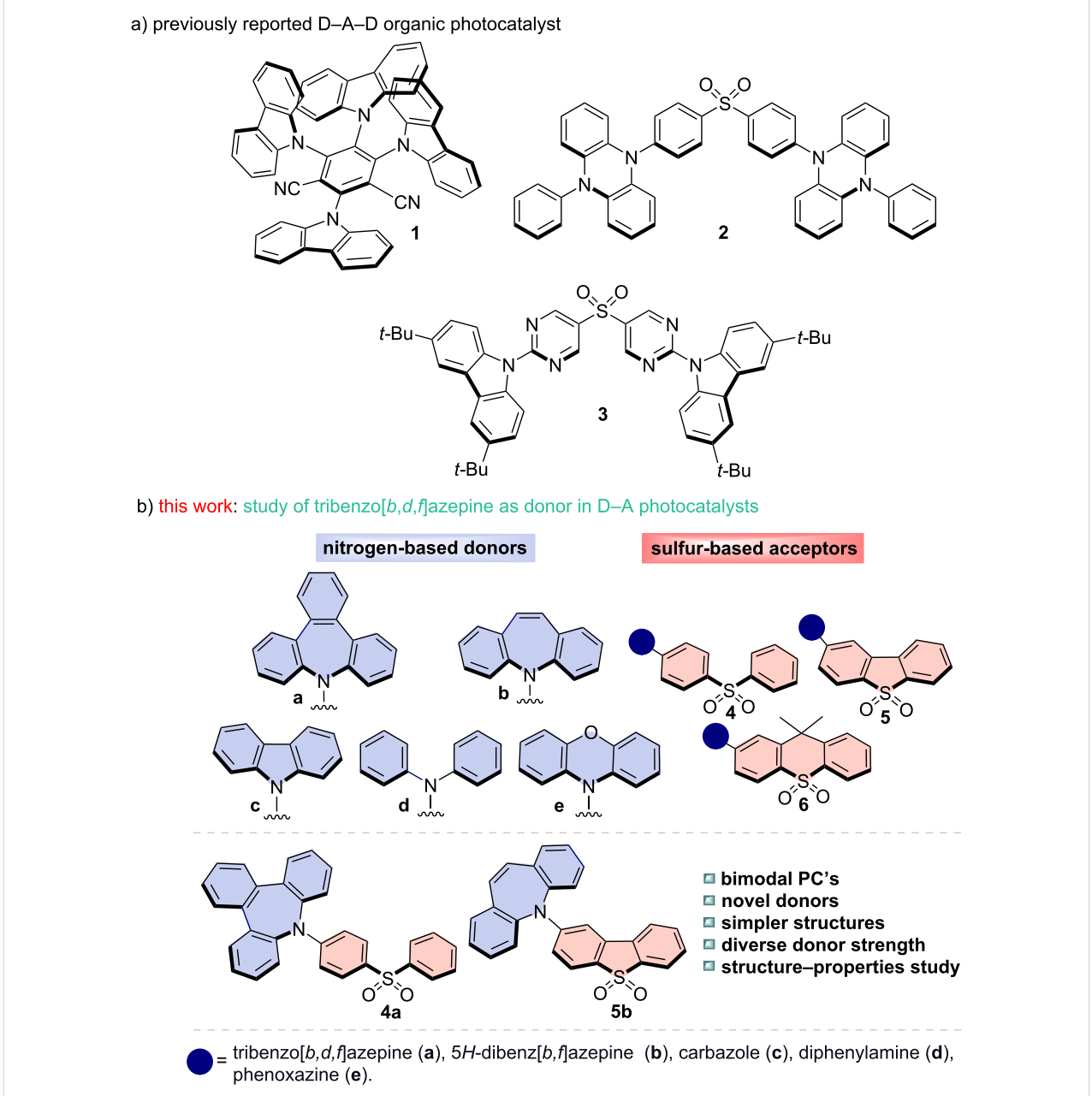

Figure 1: D–A–D organic PCs previously reported and our new D–A bimodal organic PCs.

Although diverse scaffolds have been reported in the literature, the identification and use of novel PCs with tunable and diverse optical and redox properties can pave the way to uncharted reactivity. In this context, sulfur-based cores, widely used as acceptors in photoelectric materials [9-14], and dyes [15,16] serve as promising structures for constructing and designing novel PCs. These structures show a high electron affinity, stability, and the possibility of tuning their physicochemical properties by substituting the two aromatic rings. In 2018, Sang Kwon and co-workers reported a computational study to design new PCs to be employed in atom transfer radical polymerization (O-ATRP) [17]. Notably, the sulfur-based structure **2** showed excellent performance for this transformation. One year later, the same research group reported its use in a reversible addition-fragmentation chain-transfer (RAFT) polymerization [18]. Moreover, in 2022, Zysman-Colman and collaborators showed that molecule **3**, initially synthesized as a TADF (thermally activated delayed fluorescence) emitter [14], can be used as a PC under electron-transfer (ET) and energy-transfer (EnT) processes (Figure 1a) [19]. All the main reports in the field focused on D–A–D (donor–acceptor–donor) structures. Quite surprisingly, the potential use as PCs of structurally simpler D–A molecules has been largely overlooked.

Aliphatic and aromatic nitrogen donors are widely used in synthesizing fluorescent emitters due to their electron-donating strength. The development of stronger donors to enhance luminescence remains a key area of research [20-22]. Recently, azepine-based analogs, such as tribenzo[*b,d,f*]azepine (TBA, **a**), have been explored due to their photoluminescence properties [23-27]. This antiaromatic core offers unique features, including twisted structures, reduced π–π stacking, and enhanced reverse intersystem crossing rates, becoming a better donor compared to fully planar compounds as carbazole (**c**). Similarly, 5*H*-dibenz[*b,f*]azepine (IMD, **b**) has been incorporated into D–A–D structures, showing interesting photophysical properties compared to common substrates like **c**, diphenylamine (**d**), and phenoxazine (**e**) [28-30]. However, their potential as D-unit in organic PCs remains unexplored. For this reason, studying this avenue could unlock new opportunities for the synthesis and design of more powerful, efficient and versatile organic photocatalysts.

We herein present the design, synthesis and study of a new sulfur-based D–A family using diverse nitrogen donors (Figure 1b). We performed complete photophysical characterization of the diverse D–A molecules to analyze the structure–properties relationships. We further studied their photocatalytic potential as bimodal PCs and demonstrated their potential use in different reductive and oxidative quenching processes.

Results and Discussion

Photophysical properties analysis

We started our study with three different sulfur-based acceptors, namely: diphenyl sulfone (**4**), dibenzo[*b,d*]thiophene 5,5-dioxide (**5**), and 9,9-dimethyl-9*H*-thioxanthene 10,10-dioxide (**6**). The selection of these scaffolds was aimed at investigating the effect of conjugation and rigidity/flexibility on the presence of the same donor (TBA, **a**). In the case of the D–A compounds **4a** and **6a**, we observed a blue-shifted absorption profile due to the break of the conjugation in sulfur-based acceptors. Compounds **4a** and **6a** presented a similar absorption profile, while molecule **5a** showed a red-shifted spectrum tailing up to the visible region (Figure 2a). The lack of a significant charge transfer (CT) character in scaffolds **4a** and **6a** can be attributed to the absence of a complete conjugated system.

On the other hand, the fluorescence profile showed more differences in the analysis of the three members of the D–A family. Again, **5a** revealed a bathochromic effect compared with the less conjugated scaffolds. Interestingly, molecule **4a**, which has the most flexible acceptor core, exhibited a dual emission (DE) profile (Figure 2a). This behavior may be connected to the phenomenon known as PISP (photoinduced structural planarization), which has been reported for the TBA N-substituted with an electron-withdrawing group [31]. Additionally, it is possible that the mobility of core **4** contributes to this behavior, as evidenced by the observation that the DE is not present in the more rigid structures **5a** and **6a**. In this compound, we did not observe changes in the absorption profile during the solvatochromism analysis (see Supporting Information File 1, Figure S4). The structural characteristics of compound **5a** conferred the biggest value in terms of Stokes shift parameter, indicating an increased excited state's charge transfer (CT) character (Table 1). Similarly, this behavior was observed experimentally in the solvatochromism study of fluorescence using solvents with diverse polarities (see Supporting Information File 1, Figure S9). Indeed, the density functional theory (DFT) calculation performed at WB97XD/Def2TZVP level of theory showed the lowest value for the HOMO–LUMO energy gap in compound **5a** (3.9 eV) as a consequence of the extended π conjugation compared with **4a** and **6a** (4.4 and 4.4 eV, respectively). Interestingly, compound **6a**, which possesses the weakest sulfur-based acceptor, showed an inversion in the LUMO distribution, localizing it in the TBA core – this behavior of the named antiaromatic compound as an acceptor was previously reported (Figure 2) [31].

The dibenzo[*b,d*]thiophene 5,5-dioxide (**5**) was chosen for further investigation because of its red-shifted absorption. From a photochemical perspective, this characteristic can facilitate the use of less energetic light sources. Additionally, we aim to eval-

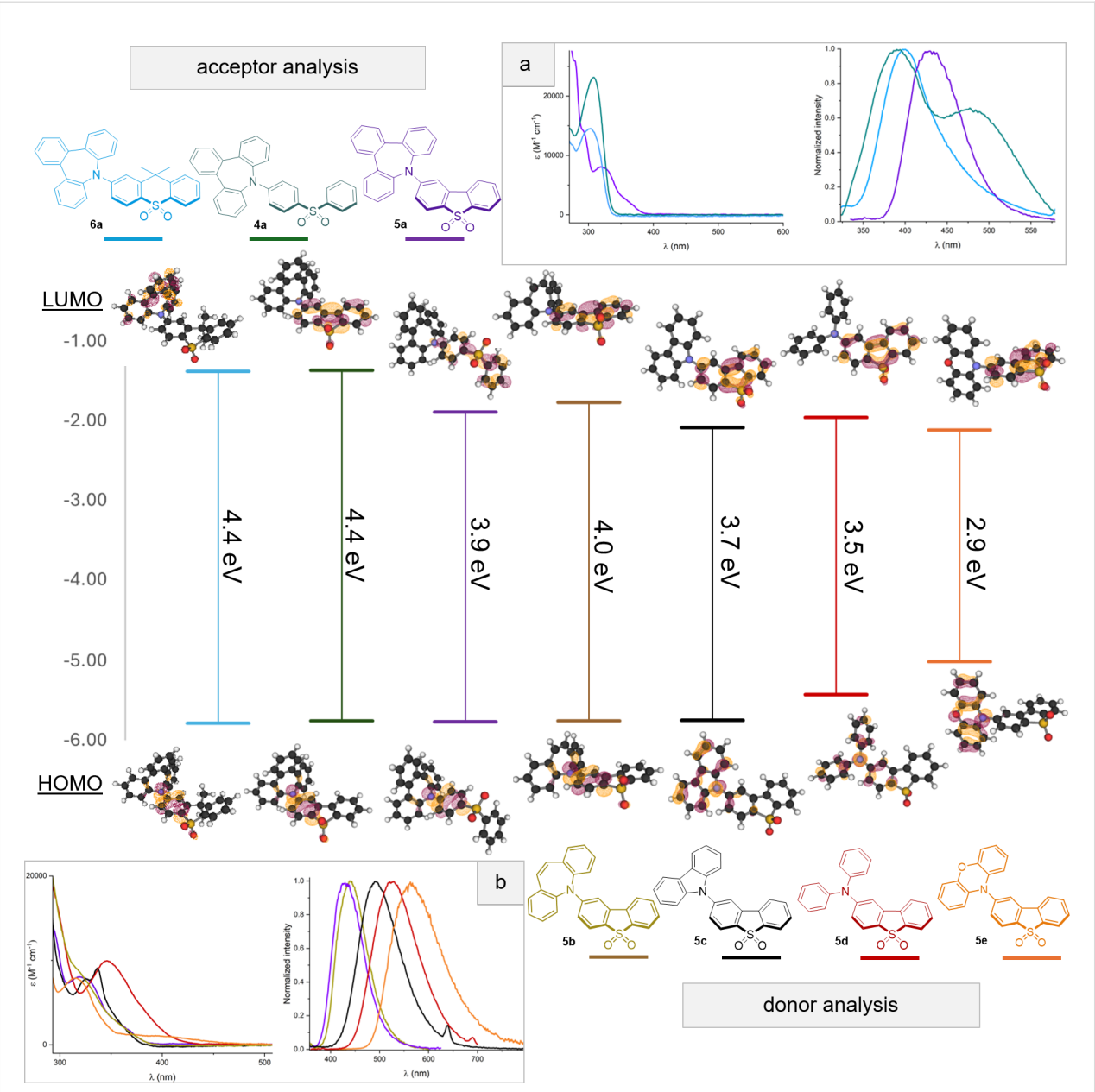

Figure 2: Selected frontier MOs and relative calculated energies of D–A photocatalysts (**4a**,**5a–e**, and **6a**). Absorption and emission profiles of D–A compounds (**4a**,**5a–e**, and **6a**) measured in MeCN.

uate the unique effect of the TBA donor unit (**a**) compared to other donors. We next synthesized diverse D–A structures employing common nitrogen-based compounds widely used in materials chemistry like carbazole (**c**), diphenylamine (**d**), and phenoxazine (**e**). Furthermore, we wanted to study the diverse or similar properties between the antiaromatic molecules **a** and **b**, in which the main difference is the presence of a third aromatic ring. According to the literature, the presence of the third benzene ring in the TBA (**a**) differentiates the conformations of structures **a** and **b** in the excited state. This results in a consistently planar conformation for donor **b**, while donor **a** can exhibit either a planar or bent conformation, depending on the nature of the substituent, as previously mentioned. This duality between planar and bent shapes is significant, as it contributes to the aromatic character that is acquired in the excited state by structures that are antiaromatic in the ground state, following Baird's rule. Intrigued by this diverse behavior, we wanted to investigate if the possible structural differences between both compounds (**5a** and **5b**) were important for photocatalytic activity.

Analyzing the diverse absorption profiles, we can observe an increase in the red-shifted behavior related to the donor strength in compounds **5e**, **5d**, and **5c**. In contrast, the azepine-derived compounds are the most blue-shifted (Table 1, entry 5). The same trend is observed in the emission (Figure 2b). The Stokes shift values for the classical nitrogen donors (**c**, **d,** and **e**) demonstrate a more pronounced CT character with respect to **5a** and **5b** (Table 1, entry 8), also corroborated by the theoretical descriptor Δr (Table 1, entry 11) that describes the charge transfer character [32,33]. Moreover, this CT behavior is supported by the DFT studies, which suggested a better spatial separation between the HOMO and LUMO. As expected, the HOMO–LUMO energy gap followed a trend that is dependent on the electron-donating capacity of the nitrogen heterocycles and amine present in compounds **5e** (2.9 eV), **5d** (3.5 eV)**,** and **5c** (3.7 eV). At the same time, **5a** and **5b** showed bigger values (3.9 eV and 4.0 eV, respectively) (Figure 2).

The strength of common donors plays a crucial role in influencing quantum yield (QY) measurements. As shown in Table 1, we observe a notable decrease in QY across the PCs **5e**, **5d**, and **5c**, with values of 16%, 14%, and 14%, respectively. The lowest values were obtained for molecules **5a** and **5b** (7% and 6%, each).

Remarkably, compound **5e** demonstrated minimal luminescence in nearly all solvents at room temperature. This behavior has been previously reported and is believed to be due to strong CT stabilization of the first excited state of the molecule [34]. This observation is further supported by the orthogonal D–A conformation calculated using DFT, which indicates a decoupled interaction between the HOMO and the LUMO (Figure 2). Moreover, compound **5e** is the only member of the family in which the HOMO orbital is not delocalized in one of the aromatic rings of the acceptor core.

Redox properties analysis

We started our analysis by looking at the impact of the diverse sulfur-based cores on the redox properties. Here, we can observe similar E_{ox} values ranging from 1.41 V to 1.46 V vs SCE. This behavior is consistent with preserving the same donor core (**a**) within the structure. In contrast, a significant difference was observed for the E_{red} values. By adjusting the acceptor strength of the sulfur core, we observed a trend where the D–A structure with the weakest acceptor (**6a**) yielded the most negative value (E_{red} = −2.4 vs SCE) (see Supporting Information File 1, Table S1). In contrast, molecule **5a**, which has the strongest acceptor displayed the most positive one (E_{red} = −1.9 V vs SCE).

We next investigated the diverse donors. For D–A molecules **5c**, **5d**, and **5e**, the redox potential calculated for the ground state is slightly more positive than the one measured for the single donor (**c**, **d**, and **e**, respectively). For example, for

Table 1: Summary of the excited- and ground-state photoredox properties.[a]

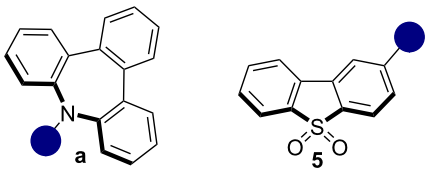

Entry	●, PC	4a	5a	6a	5b	5c	5d	5e
1	E_{ox} (V)[a]	1.46	1.41	1.43	1.32	1.42	1.12	0.75
2	E^*_{ox} (V)	–2.24	–1.89	–2.27	–1.88	–1.68	–1.78	–1.85
3	E_{red} (V)[a]	–2.35	–1.95	–2.4	–1.96	–1.75	–1.86	–1.74
4	E^*_{red} (V)	1.35	1.35	1.3	1.24	1.35	1.04	0.86
5	λ_{abs} (nm)	308	320	292	312	336	346	393
6	λ_{em}(nm)	400,478	430	398	441	493	525	564
7	$E_{0,0}$ (eV)	3.7	3.3	3.7	3.2	3.1	2.9	2.6
8	Stokes shift (nm)	81	110	106	129	157	179	171
9	τ (ns)	0.9[b]	2.2[b]	2.0[b]	0.7	11.6	9.1	4.4[b]
10	QY (%)	12	7	10	6	14	14	16
11	Δr[c]	3.31 Å	2.62 Å	2.82 Å	2.40 Å	3.57 Å	3.52 Å	4.97 Å

[a]All potentials were measured in MeCN. Values are reported in V versus SCE (see Supporting Information File 1). [b]τ_{AvInt}. [c]The Δr parameter describes the charge transfer character.

phenoxazine (**e**) we measured an E_{ox} = 0.67 V, while for compound **5e** the E_{ox} = 0.75 V vs SCE. In contrast, the azepine cores (**a** and **b**) showed a stronger impact in the E_{ox} of the D–A structures. For instance, IMD (**b**) with an oxidation potential of 0.73 V when present in the molecule **5b** resulted in a considerably different E_{ox} of 1.32 V (Figure 3).

A molecule that in the excited state exhibits both strong oxidative power (E^*_{ox} up to −1.5 V) and strong reductive power (E^*_{red} up to 1.5 V) can be classified as a bimodal photocatalyst. This type of molecule is capable of driving both oxidative and reductive reactions, thereby offering significant versatility to achieve photocatalytic transformations. To our delight, molecule **5a** possesses a promising E^*_{ox} =−1.89 V vs SCE (Table 1, entries 1 and 2) and a useful E_{ox} = 1.41 V. For E_{red}, **5a** maintains a good balance between the redox potentials in both the ground and excited states, showing values of E_{red} = −1.95 V and E^*_{red} = 1.35 V vs SCE (Table 1, entries 3 and 4). Comparing it with its analog **5b**, we observe similar redox potentials except for E_{ox} and E^*_{red} values.

The redox window is more limited for the other members of the D–A family. For example, for molecule **5e** the E_{ox} is 0.75 V, which is the lowest value among all family members (Table 1, entry 1). This observation can be explained by the nonexistent electronic coupling between the donor and the acceptor due to the highly twisted structure [35] as shown in the HOMO. As a consequence, the E_{ox} of molecule **5e** is similar to the E_{ox} of the phenoxazine core, with respect to the rest of the family (**5a**–**d**) that possesses higher E_{ox} since their HOMO is localized in both the donor and acceptor.

Photocatalytic studies and synthetic applications

After establishing structure–property relationships, we aimed to use the synthesized donor–acceptor (D–A) compounds to investigate their photocatalytic activity. We found that most members of the D–A family exhibited promising redox potentials in their excited states, indicating their potential to function as effective bimodal photocatalysts. Additionally, our photophysical characterization provided essential insights into their

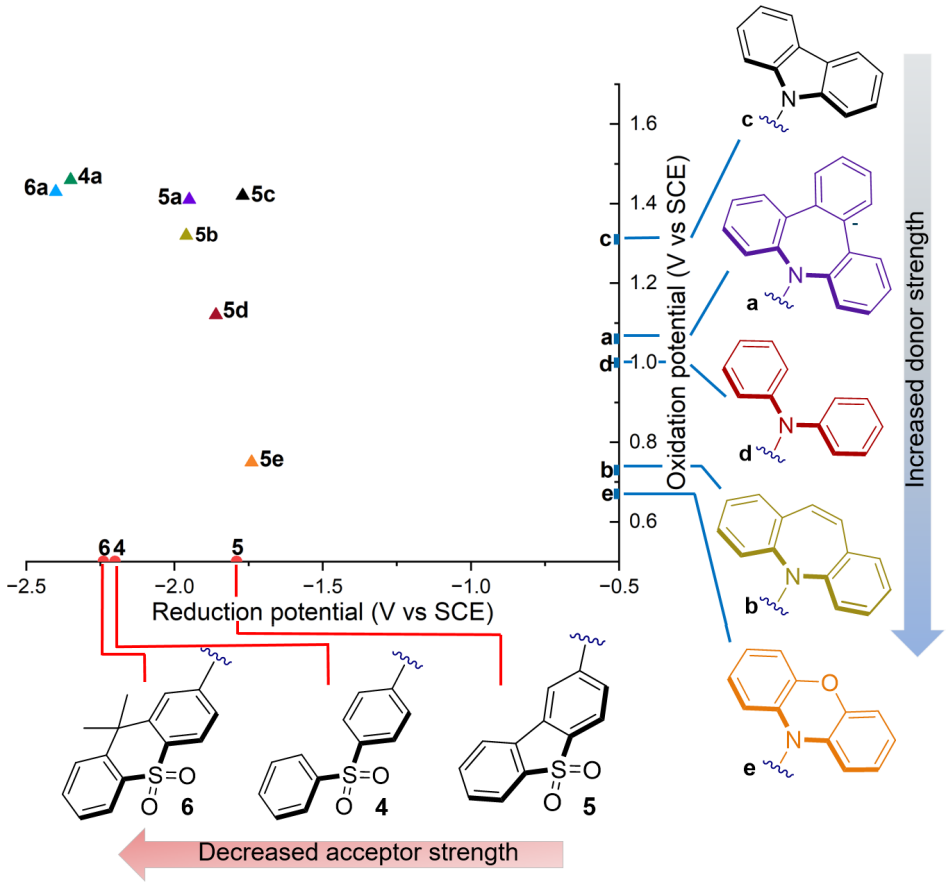

Figure 3: Comparison of the ground state redox potential of the acceptor moieties (**4**–**6**), the donor moieties (**a**–**e**), and D–A compounds (**4a**, **5a**–**e**, and **6a**).

behavior in the excited state and stability. We initiated the study of the photocatalytic activity of all family members in an oxidative quenching cycle for the dehalogenation of 4-bromobenzonitrile (**7**). Typically, this type of chemical transformation requires highly reducing PCs or the use of UV light [36]. First, we evaluated the photocatalytic performance of molecules **4a**, **5a**, and **6a** (see Supporting Information File 1, Table S3). As we expected, due to the blue-shifted absorption presented in molecules **4a** and **6a**, it was impossible to excite them under visible light (400 nm). Gratifyingly, PC **5a** delivered product **8** with a promising 63% NMR yield.

Next, we compare the photocatalytic behavior of compound **5a** with the other family members utilizing the same dehalogenation manifold. Here, even slightly changes in the redox properties have an influence on the yield of the reaction. The D–A with the azepine analog (**5b**), gave the dehalogenated product **8** in 58% NMR yield (Table 2, entry 2). Quite surprisingly, **5e** showed only traces of **8**, even with an E^*_{ox} of −1.85 V (Table 2, entry 5).

Under the oxidative quenching study, we also evaluated the photocatalytic potential of the new family of D–A compounds in the atom transfer radical addition (ATRA) reaction involving styrene and tosyl chloride (TsCl), as previously reported by Zysman-Colman and co-workers [19]. Compound **5d** showed the best performance with a 27% calculated NMR yield (20%, isolated yield) (Table 3, entry 3), while the azepine derivatives **5a** and **5b** led the transformation at 13 and 8%, respectively (Table 3, entries 1 and 2). However, these results are comparable to those obtained by the same author using the well-established PCs **1** and **3** (Table 3, entries 6 and 7)

Table 2: Dehalogenation of 4-bromobenzonitrile (**7**).

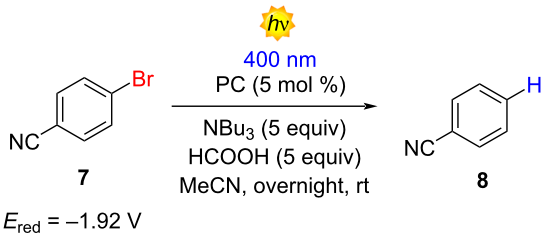

Entry	PC	^{1}H NMR yield[a] (%)
1	**5a**	63
2	**5b**	58
3	**5c**	56
4	**5d**	44
5	**5e**	traces

[a]CH_2Br_2 as internal standard.

Next, we wanted to analyze the use of the PCs in reductive quenching mechanisms. For this purpose, we selected the Giese-type addition between the *N*-Cbz-Pro (**12**, E_{ox} = 0.95 V vs SCE) and the dimethyl maleate (**13**), which is a standard benchmark reaction for the evaluation of novel PCs [37]. In this case, we obtained the best result using compound **5a** with a 76% NMR yield (65%, isolated yield) (Table 4, entry 1). Com-

Table 3: ATRA reaction between tosyl chloride (**9**) and styrene (**10**).

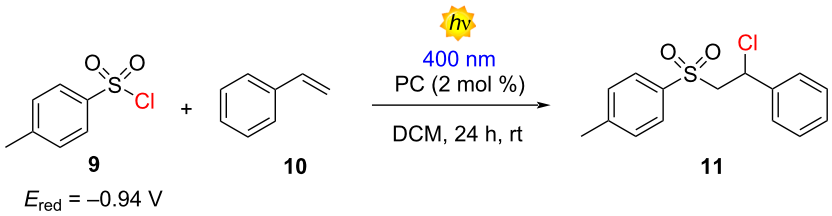

Entry	PC	Yield[a] (%)
1	**5a**	13
2	**5b**	8
3	**5c**	27 (20)
4	**5d**	12
5	**5e**	21
6[b]	**1**	10
7[b]	**3**	16

[a]Yields determined by ^{1}H NMR analysis of the crude mixture using CH_2Br_2 as internal standard. Isolated yield in parentheses. [b]Yields reported in reference [19].

Table 4: Giese addition using N-Cbz-Pro (**12**) and dimethyl maleate (**13**).

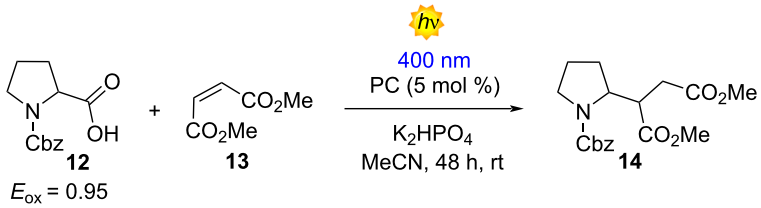

Entry	PC	Yield[a] (%)
1	**5a**	78 (65)
2	**5b**	59
3	**5c**	65
4	**5d**	43
5	**5e**	5
6[b]	**1**	99
7[b]	**3**	64

[a]Yields determined by ^{1}H NMR analysis of the crude mixture using CH_2Br_2 as internal standard. Isolated yield in parentheses. [b]Yields reported in reference [19].

pounds **5b** and **5c**, whose redox potential in the ground and excited state are similar to **5a**, lead to the formation of the **14** in 59% and 65% NMR yield, each (Table 4, entries 2 and 3). Interestingly, compounds **5d** and **5e** showed the worst photocatalytic performances that can be attributed to their inferior E^*_{red} (Table 4, entries 4 and 5). Gratifyingly, our PC **5a** showed a better performance in comparison with the D–A–D compound **3** (Table 3, entry 7).

Furthermore, we obtained pleasing outcomes when we tried the photocatalyzed reductive pinacol coupling of benzaldehyde (**15**), as reported by Rueping [38]. In this methodology, the reduction of compound **15** is facilitated by reduced photocatalyst (PC) and the interaction of **15** with the radical cation of DIPEA. The best result, again, was attributed to molecule **5a** with 60% isolated yield (Table 5, entry 1). In contrast, molecule **5b** showed the worst performance with 41% NMR yield (Table 5, entry 2). For compounds **5c**–**e**, the NMR yield calculated for product **16** was similar (55–51%), probably due to the comparable reductive properties in both ground and excited states (Table 5, entries 3, 4 and 5). Unfortunately, for this reaction, all the members of the D–A family delivered the product in a lower yield compared with molecules **1** and **3** (Table 5, entries 6 and 7).

Table 5: Pinacol coupling of benzaldehyde (**15**).

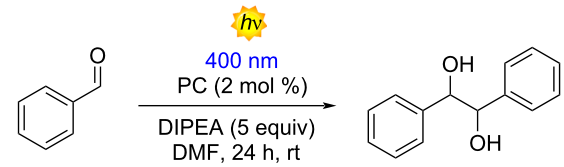

Entry	PC	Yield[a] (%)
1	**5a**	69 (60)
2	**5b**	41
3	**5c**	55
4	**5d**	51
5	**5e**	51
6[b]	**1**	76
7[b]	**3**	80

[a]Yields determined by ^{1}H NMR analysis of the crude mixture using CH_2Br_2 as internal standard and refer to the combined yield of meso:dl isomers. Isolated yield in parenthesis. [b]Yields reported in reference [19].

Conclusion

In conclusion, we explored the potential of tribenzo[*b*,*d*,*f*]azepine (TBA) as a donor in donor–acceptor (D–A) organic photocatalysts (PCs). We synthesized a new series of sulfur-based D–A compounds and compared their photophysical and photoredox properties with TBA, its analog 5*H*-dibenz[*b*,*f*]azepine (IMD), and common nitrogen donors. The excited state redox potentials of these compounds suggest their suitability for challenging photocatalytic reactions through oxidative and reducing quenching cycles. TBA showed a well-balanced redox window, making it a promising candidate for new PC designs. While TBA and IMD displayed similar charac-

teristics, the D–A IMD compound showed a shorter lifetime, which proved unfavorable in photocatalytic tests. The differing excited state conformations (bend vs planar) reported for these azepine analogs did not negatively impact photocatalytic activity, showing similar results in some of the benchmark reactions carried out during this analysis. Our findings suggest that antiaromatic compounds like TBA could replace traditional nitrogen donors in PCs, offering good redox potentials and competitive photophysical properties in addition to the previously reported characteristics like highly twisted structures that can be useful in designing new PCs with TADF behavior. We hope this study inspires the construction of new PCs that could combine azepine derivatives, exemplifying the valuable incorporation of widely used structures in materials chemistry to photocatalysis.

Supporting Information

Supporting Information File 1

Reactivity studies, general experimental procedures, product isolation and characterization, spectroscopic data for new compounds, and copies of NMR spectra.
[https://www.beilstein-journals.org/bjoc/content/supplementary/1860-5397-21-76-S1.pdf]

Acknowledgements

L. D. and K. M. U. thank Dr. Ilaria Fortunati for her technical support during the lifetime measurements.

Funding

The financial support of the authors is provided by the Ministero dell'Università e della Ricerca (MUR, C93C22007660006, K.M.U), Fondazione Cariparo (Starting Package C93C22008360007, K.M.U.) and European Research Council (ERC-Starting Grant 2021 SYNPHOCAT 101040025, J.H.M., L.D.).

Author Contributions

Katy Medrano-Uribe: conceptualization; funding acquisition; investigation; methodology; project administration; visualization; writing – original draft. Jorge Humbrías-Martín: formal analysis; investigation; writing – review & editing. Luca Dell'Amico: funding acquisition; project administration; resources; supervision; writing – review & editing.

ORCID® iDs

Katy Medrano-Uribe - https://orcid.org/0000-0001-9801-9524
Jorge Humbrías-Martín - https://orcid.org/0000-0002-0245-727X
Luca Dell'Amico - https://orcid.org/0000-0003-0423-9628

Data Availability Statement

All data that supports the findings of this study is available in the published article and/or the supporting information of this article.

Preprint

A non-peer-reviewed version of this article has been previously published as a preprint: https://doi.org/10.3762/bxiv.2025.11.v1

References

1. Romero, N. A.; Nicewicz, D. A. *Chem. Rev.* **2016,** *116,* 10075–10166. doi:10.1021/acs.chemrev.6b00057
2. Bortolato, T.; Cuadros, S.; Simionato, G.; Dell'Amico, L. *Chem. Commun.* **2022,** *58,* 1263–1283. doi:10.1039/d1cc05850a
3. Hari, D. P.; König, B. *Chem. Commun.* **2014,** *50,* 6688–6699. doi:10.1039/c4cc00751d
4. Vega-Peñaloza, A.; Mateos, J.; Companyó, X.; Escudero-Casao, M.; Dell'Amico, L. *Angew. Chem., Int. Ed.* **2021,** *60,* 1082–1097. doi:10.1002/anie.202006416
5. Bryden, M. A.; Zysman-Colman, E. *Chem. Soc. Rev.* **2021,** *50,* 7587–7680. doi:10.1039/d1cs00198a
6. Uoyama, H.; Goushi, K.; Shizu, K.; Nomura, H.; Adachi, C. *Nature* **2012,** *492,* 234–238. doi:10.1038/nature11687
7. Shang, T.-Y.; Lu, L.-H.; Cao, Z.; Liu, Y.; He, W.-M.; Yu, B. *Chem. Commun.* **2019,** *55,* 5408–5419. doi:10.1039/c9cc01047e
8. Speckmeier, E.; Fischer, T. G.; Zeitler, K. *J. Am. Chem. Soc.* **2018,** *140,* 15353–15365. doi:10.1021/jacs.8b08933
9. Yang, S.-Y.; Tian, Q.-S.; Yu, Y.-J.; Zou, S.-N.; Li, H.-C.; Khan, A.; Wu, Q.-H.; Jiang, Z.-Q.; Liao, L.-S. *J. Org. Chem.* **2020,** *85,* 10628–10637. doi:10.1021/acs.joc.0c01200
10. Zhang, Q.; Li, B.; Huang, S.; Nomura, H.; Tanaka, H.; Adachi, C. *Nat. Photonics* **2014,** *8,* 326–332. doi:10.1038/nphoton.2014.12
11. Gudeika, D.; Lee, J. H.; Lee, P.-H.; Chen, C.-H.; Chiu, T.-L.; Baryshnikov, G. V.; Minaev, B. F.; Ågren, H.; Volyniuk, D.; Bezvikonnyi, O.; Grazulevicius, J. V. *Org. Electron.* **2020,** *83,* 105733. doi:10.1016/j.orgel.2020.105733
12. Bezvikonnyi, O.; Gudeika, D.; Volyniuk, D.; Mimaite, V.; Sebastine, B. R.; Grazulevicius, J. V. *J. Lumin.* **2019,** *206,* 250–259. doi:10.1016/j.jlumin.2018.10.018
13. Zhang, D.; Wei, H.; Wang, Y.; Dai, G.; Zhao, X. *Dyes Pigm.* **2020,** *174,* 108028. doi:10.1016/j.dyepig.2019.108028
14. dos Santos, P. L.; Chen, D.; Rajamalli, P.; Matulaitis, T.; Cordes, D. B.; Slawin, A. M. Z.; Jacquemin, D.; Zysman-Colman, E.; Samuel, I. D. W. *ACS Appl. Mater. Interfaces* **2019,** *11,* 45171–45179. doi:10.1021/acsami.9b16952
15. Jia, X.; Han, W.; Xue, T.; Zhao, D.; Li, X.; Nie, J.; Wang, T. *Polym. Chem.* **2019,** *10,* 2152–2161. doi:10.1039/c8py01778f
16. Zhou, H.; Huang, Q.; Liu, X.; Xu, D.; Zhang, W.; Fu, S.; Feng, X.; Zhang, Z. *Dyes Pigm.* **2021,** *184,* 108868. doi:10.1016/j.dyepig.2020.108868
17. Singh, V. K.; Yu, C.; Badgujar, S.; Kim, Y.; Kwon, Y.; Kim, D.; Lee, J.; Akhter, T.; Thangavel, G.; Park, L. S.; Lee, J.; Nandajan, P. C.; Wannemacher, R.; Milián-Medina, B.; Lüer, L.; Kim, K. S.; Gierschner, J.; Kwon, M. S. *Nat. Catal.* **2018,** *1,* 794–804. doi:10.1038/s41929-018-0156-8
18. Song, Y.; Kim, Y.; Noh, Y.; Singh, V. K.; Behera, S. K.; Abudulimu, A.; Chung, K.; Wannemacher, R.; Gierschner, J.; Lüer, L.; Kwon, M. S. *Macromolecules* **2019,** *52,* 5538–5545. doi:10.1021/acs.macromol.9b00940

19. Bryden, M. A.; Millward, F.; Matulaitis, T.; Chen, D.; Villa, M.; Fermi, A.; Cetin, S.; Ceroni, P.; Zysman-Colman, E. *J. Org. Chem.* **2023,** *88,* 6364–6373. doi:10.1021/acs.joc.2c01137
20. Wang, C.; Zhao, Y.; Su, R.; Li, D.; Guo, Y.; Su, W.; Yu, T. *Dyes Pigm.* **2023,** *208,* 110880. doi:10.1016/j.dyepig.2022.110880
21. Tian, X.; Yao, M.; Liang, X.; Zhou, C.; Xiao, S.; Gao, Y.; Liu, H.; Zhang, S.-T.; Yang, B. *Dyes Pigm.* **2022,** *205,* 110463. doi:10.1016/j.dyepig.2022.110463
22. Wu, Q.; Li, J.; Liu, D.; Mei, Y.; Liu, B.; Wang, J.; Xu, M.; Li, Y. *Dyes Pigm.* **2023,** *217,* 111421. doi:10.1016/j.dyepig.2023.111421
23. Lei, B.; Huang, Z.; Li, S.; Liu, J.; Bin, Z.; You, J. *Angew. Chem., Int. Ed.* **2023,** *62,* e202218405. doi:10.1002/anie.202218405
24. Wu, Y.; Liu, X.; Liu, J.; Yang, G.; Han, S.; Yang, D.; Cao, X.; Ma, D.; Bin, Z.; You, J. *Mater. Horiz.* **2023,** *10,* 3785–3790. doi:10.1039/d3mh00617d
25. Xiao, X.; Lei, B.; Wu, D.; Bin, Z. *Chem. Commun.* **2023,** *59,* 6556–6559. doi:10.1039/d3cc01235b
26. Mamada, M.; Aoyama, A.; Uchida, R.; Ochi, J.; Oda, S.; Kondo, Y.; Kondo, M.; Hatakeyama, T. *Adv. Mater. (Weinheim, Ger.)* **2024,** *36,* 202402905. doi:10.1002/adma.202402905
27. Chen, Y.-K.; Lei, J.; Wu, T.-L. *Chem. Sci.* **2024,** *15,* 10146–10154. doi:10.1039/d4sc02351j
28. Wang, Z.; Wang, Z.; Lu, P.; Wang, Y. *Chem. – Asian J.* **2020,** *15,* 3519–3526. doi:10.1002/asia.202000980
29. Yu, L.; Wu, Z.; Xie, G.; Luo, J.; Zou, Y.; Ma, D.; Yang, C. *J. Mater. Chem. C* **2020,** *8,* 12445–12449. doi:10.1039/d0tc02412k
30. Bezvikonnyi, O.; Gudeika, D.; Volyniuk, D.; Rutkis, M.; Grazulevicius, J. V. *Dyes Pigm.* **2020,** *175,* 108104. doi:10.1016/j.dyepig.2019.108104
31. Chen, Y.; Tseng, S.-M.; Chang, K.-H.; Chou, P.-T. *J. Am. Chem. Soc.* **2022,** *144,* 1748–1757. doi:10.1021/jacs.1c11231
32. Peach, M. J. G.; Benfield, P.; Helgaker, T.; Tozer, D. J. *J. Chem. Phys.* **2008,** *128,* 044118. doi:10.1063/1.2831900
33. Guido, C. A.; Cortona, P.; Mennucci, B.; Adamo, C. *J. Chem. Theory Comput.* **2013,** *9,* 3118–3126. doi:10.1021/ct400337e
34. Data, P.; Pander, P.; Okazaki, M.; Takeda, Y.; Minakata, S.; Monkman, A. P. *Angew. Chem.* **2016,** *128,* 5833–5838. doi:10.1002/ange.201600113
35. Higginbotham, H. F.; Yi, C.-L.; Monkman, A. P.; Wong, K.-T. *J. Phys. Chem. C* **2018,** *122,* 7627–7634. doi:10.1021/acs.jpcc.8b01579
36. Discekici, E. H.; Treat, N. J.; Poelma, S. O.; Mattson, K. M.; Hudson, Z. M.; Luo, Y.; Hawker, C. J.; de Alaniz, J. R. *Chem. Commun.* **2015,** *51,* 11705–11708. doi:10.1039/c5cc04677g
37. Mateos, J.; Rigodanza, F.; Vega-Peñaloza, A.; Sartorel, A.; Natali, M.; Bortolato, T.; Pelosi, G.; Companyó, X.; Bonchio, M.; Dell'Amico, L. *Angew. Chem., Int. Ed.* **2020,** *59,* 1302–1312. doi:10.1002/anie.201912455
38. Nakajima, M.; Fava, E.; Loescher, S.; Jiang, Z.; Rueping, M. *Angew. Chem.* **2015,** *127,* 8952–8956. doi:10.1002/ange.201501556

License and Terms

BEILSTEIN JOURNAL OF ORGANIC CHEMISTRY

General method for the synthesis of enaminones via photocatalysis

Paula Pérez-Ramos, Raquel G. Soengas* and Humberto Rodríguez-Solla*

Letter

Open Access

Address:
Department of Organic and Inorganic Chemistry, and Instituto Universitario de Química Organometálica Enrique Moles, University of Oviedo, Julián Clavería 8, 33006, Oviedo, Spain

Email:
Raquel G. Soengas* - rsoengas@uniovi.es;
Humberto Rodríguez-Solla* - hrsolla@uniovi.es

* Corresponding author

Keywords:
chromones; dehalogenation; enaminones; nickel; photocatalysis

Beilstein J. Org. Chem. **2025,** *21,* 1535–1543.
https://doi.org/10.3762/bjoc.21.116

Received: 09 May 2025
Accepted: 25 July 2025
Published: 29 July 2025

This article is part of the thematic issue "Photocatalysis and photochemistry in organic synthesis" and is dedicated to the memory of our friend and colleague Prof. Iván Lavandera García.

Guest Editor: T. Noël

Abstract

Enaminones are key intermediates in the synthesis of several derivatives with important applications in medicinal chemistry. Furthermore, many marketed drugs feature the enaminone structural moiety. In this context, we have developed a photoredox and nickel catalytic system to rapidly forge the enaminone scaffold from 3-bromochromones via a Michael reaction of an amine with an electron-deficient alkene moiety and subsequent photocatalyzed debromination. With this dual catalytic system, a range of structurally diverse enaminone derivatives have been achieved in good yields with total *trans* selectivity. Mechanistic studies indicate that the key to the success of this process is the formation of an unexplored ternary Ni-complex with 3-bromochromone and a pyridinium salt, which is crucial for the effective activation of the α,β-unsaturated system towards the nucleophilic addition.

Introduction

Enaminones are relevant intermediates in organic chemistry and the pharmaceutical industry [1-6]. These enamines have a carbonyl group conjugated to a carbon–carbon double bond, owing its great versatility in organic synthesis to its ability to act as both electrophiles and nucleophiles [7]. This makes enaminones very reactive, providing an excellent scaffold for organic synthesis. Thus, enaminones are valuable building blocks in the preparation of several carbocyclic [8-11], heterocyclic [12-18] as well as acyclic compounds [19-23]. Furthermore, the enaminone structural moiety represents the key framework of many drug classes, including antibiotic (**1**) [24], anti-inflammatory (**2**) [25], antinociceptive (**3**) [26], anticonvulsant (**4**) [27], antitubercular (**5**) [28], and antitumor (**6**) [29] agents (Figure 1).

In view of the important biological roles of enaminones and their relevance as synthetic intermediates, it is not surprising that there has been a continuous focus on developing general, straightforward, and efficient strategies for their synthesis.

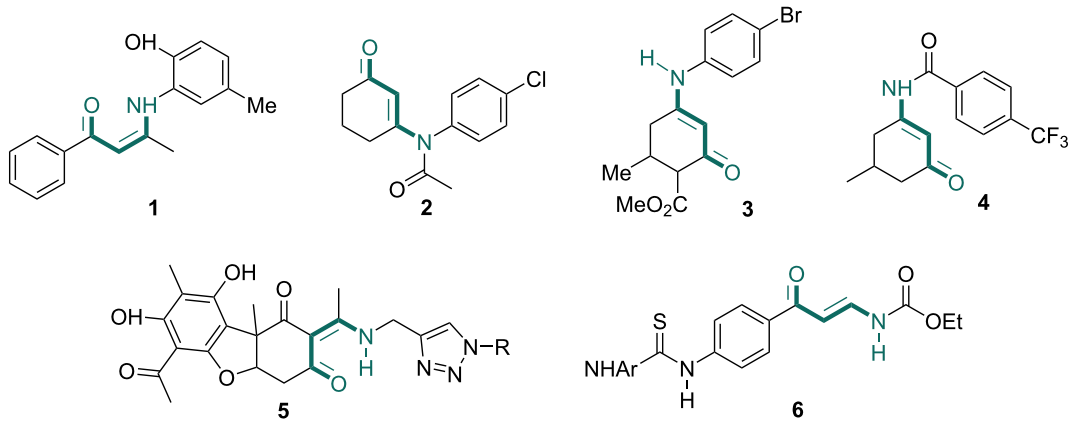

Figure 1: Examples of compounds with medicinal effects containing an enaminone structural moiety.

Enaminones are usually accessed by condensation of 1,3-dicarbonyl compounds with amines [30]. While this approach is simple and straightforward, it often leads to a mixture of constitutional isomers in which the two different α-positions of the ketone have been functionalized. Therefore, the development of novel methods for the synthesis of enaminones has attracted much attention over the past decades.

Kuwano's group described the synthesis of enaminones from ethyl ketones via a nickel-catalyzed selective β-amination (Scheme 1A) [31]. The preparation of enaminones can also be achieved by the reaction of aldehydes and calcium carbide in the presence of amines and CuI as catalyst, as reported by Zhang and co-workers (Scheme 1B) [32]. On the other hand, Li et al. disclosed a silver-catalyzed amination of propargyl alcohols to afford enaminones (Scheme 1C) [33].

Although these new methods provide a wide variety of enaminones, there are limitations such as expensive and unavailable reagents, long reaction times and drastic reaction conditions. Furthermore, the increasing emphasis on economic and environmental factors has highlighted the limitations of traditional

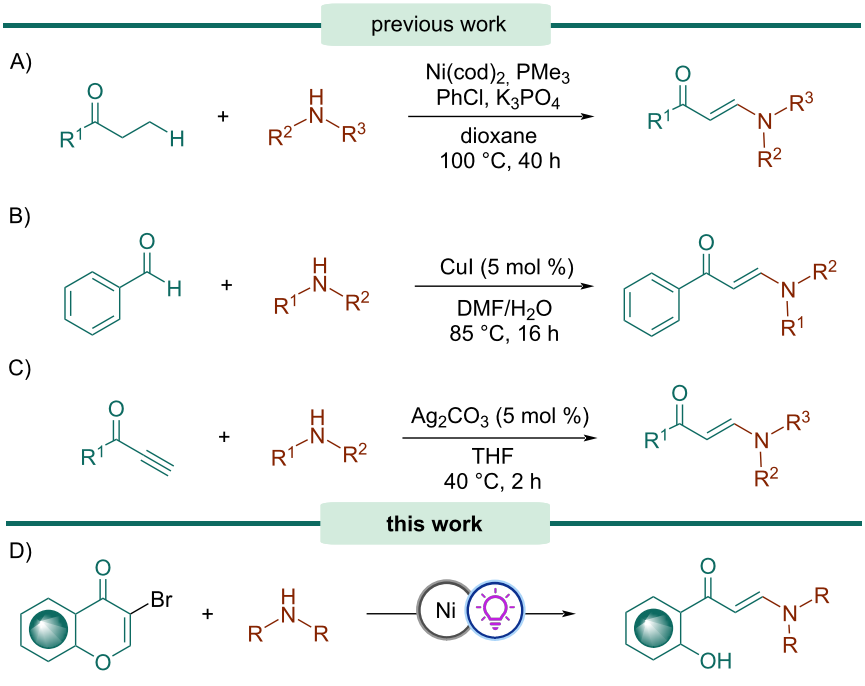

Scheme 1: Synthesis of enaminones.

methods for enaminone synthesis to align with the modern understanding of organic chemistry.

With the increasing concern on the environmental impact of organic synthesis, photocatalysis emerged as a powerful synthetic tool in organic chemistry, offering new ways to deliver diverse organic products via mild, easy to handle, and environmentally benign operations [34-36]. Thus, the use of visible light as an energy source provides more efficient chemical transformations and minimize the use of harmful reagents, the generation of waste and the consumption of energy, fulfilling several principles of Green Chemistry and promoting greener opportunities for organic synthesis [37,38]. In this context, the reactivity of enaminones under visible-light-mediated reaction conditions has attracted significant attention [39]. However, it is rather surprising that a photocatalytic approach for the synthesis of enaminones has yet to be explored.

Herein, we report the first light-mediated reaction for the synthesis of enaminones from 3-bromochromones (Scheme 1D). Initially, a Ni(II)-catalyzed hydroamination protocol affords the intermediate 2-amino-3-bromochromanones, which upon photocatalytic dehalogenation and subsequent opening of the heterocyclic ring provide the corresponding enaminones. This transformation is simple, straightforward, and proceeds under mild conditions.

Results and Discussion

The initial challenge in achieving the desired reactivity was the activation of the unsaturated system towards the nucleophilic addition of the amine. The most common strategy to increase the reactivity of unsaturated esters towards an aza-Michael addition is the use of transition metal complexes as catalysts/promoters [40-42]. Considering this background, we reasoned that Ni(II) could be a suitable catalyst for the amination of unsaturated systems.

Initial investigations were carried out by using 3-bromochromone (**7a**) and morpholine (**8a**) as model substrates in the presence of Ni(II) salt (5 mol %) and ligand (5 mol %), a pyridinium salt (1 equiv) and a photocatalyst (1 mol %) under 427 nm blue LEDs. After carefully screening of the reaction parameters (Table 1 and Tables S1–S7, Supporting Information File 1), we found that a combination of 1-[1-(*tert*-butoxycarbonyl)piperidin-4-yl]-2,4,6-triphenylpyridin-1-ium (**PS1**), $NiBr_2$·diglyme, 4,4'-dimethoxy-2,2'-bipyridine (dmbpy), and 10-(3,5-dimethoxyphenyl)-9-mesityl-1,3,6,8-tetramethoxyacridin-10-ium tetrafluoroborate (**PC1**) in *N*,*N*-dimethylformamide (DMF) at 20 °C afforded the best results, giving the desired product **9a** in 70% isolated yield (Table 1, entry 1). Changing $NiBr_2$·diglyme to other nickel salts, such as $Ni(OTf)_2$ and $NiCl_2$·diglyme led to lower yields (Table 1, entries 2 and 3). Similarly, changing the ligand for dtbbpy or phenantroline also resulted in a decrease in the efficiency of the process (Table 1, entries 4 and 5). The pyridinium salt has also a significant effect on reactivity; thus, when 1-benzyl-2,4,6-triphenylpyridin-1-ium (**PS2**) was used, enaminone **9a** was isolated in only 34% yield (Table 1, entry 6). Replacing DMF by DME, DMSO or acetone diminished the product yields (Table 1, entries 7–9). The reactivity of acridinium **PC1** was superior to that of other photocatalysts, including 4-CzIPN (**PC2**) and $[Ir(dF(CF_3)ppy)_2(dtbbpy)]PF_6$ (**PC3**) (Table 1, entries 10 and 11).

Attempts to increase the temperature of the process resulted in a complex reaction mixture in which only traces of the desired enaminone **9a** were detected (Table 1, entry 12). Longer reaction times also led to significant degradation, isolating the desired enaminone in only 18% yield (Table 1, entry 13). The reaction with 3-chlorochromone gives lower yield while 3-iodochromone failed to provide the desired enaminone **9a** (Table S7, Supporting Information File 1).

Control experiments including the reaction in the absence of visible-light or photocatalyst, showed no product formation (Table 1, entries 16 and 17). Interestingly, the yield of **9a** dropped to 30% in the absence of Ni salt and 33% in the absence of the pyridinium salt (Table 1, entries 14 and 15).

With the optimal reaction conditions, we first studied the substrate scope of 3-bromochromones **7** (Scheme 2).

It was determined that the process was compatible with various halochromones bearing electron-withdrawing (F, Cl, Br) or electron-donating (Me, OMe) groups at different positions of the aromatic ring, affording the corresponding enaminone products **9a**–**h** in moderate to good yields (45–70%). Of particular relevance is the effective formation of enaminones **9d** and **9e** containing bromo and chloro moieties, respectively, since they could enable further chemical transformations. Unfortunately, when 2-methyl-3-bromochromone was employed as the substrate, the process failed to afford the desired enaminone product, which was possibly caused by a combination of increased steric hindrance and decreased electrophilicity of the β-carbon due to the electron-donating nature of the methyl group.

Subsequently, we turned our attention to investigate a range of amine derivatives **8** under the standard conditions. When morpholine was replaced by piperidine, the expected enaminone **9g** was provided, albeit in lower yield. Similarly, 4-methylpiperidine and *N*-*tert*-butoxycarbonylpiperazine

Table 1: Optimization of reaction conditions.

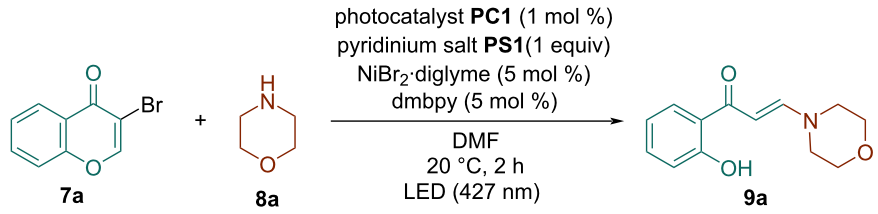

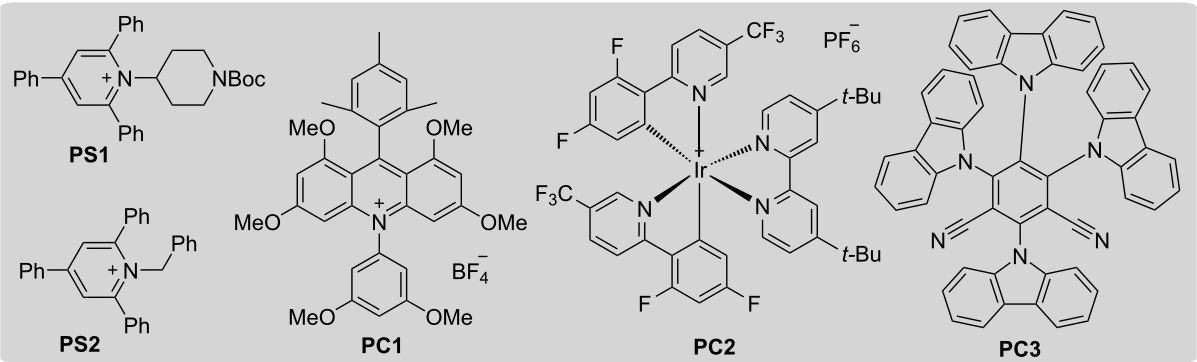

Entry	Deviation from the standard conditions[a]	Yield (%)[b]
1	none	70
2	$Ni(OTf)_2$ instead $NiBr_2$·diglyme	62
3	$NiCl_2$·diglyme instead $NiBr_2$·diglyme	49
4	dtbbpy instead dmbpy	66
5	phenantroline instead dmbpy	49
6	**PS2** instead **PS1**	34
7	acetone instead DMF	51
8	DMSO instead DMF	55
9	DME instead DMF	57
10	**PC2** instead **PC1**	46
11	**PC3** instead **PC1**	57
12	40 °C instead 20 °C	traces
13	16 h instead 2 h	18
14	no **PS**	33
15	no Ni salt and ligand	30
16	no **PC**	n.r.[c]
17	no light	n.r.

[a]3-Bromochromone **7a** (0.2 mmol), morpholine **8a** (0.3 mmol), **PC1** (1.0 mol %), $NiBr_2$·diglyme (5.0 mol %), dmbpy (5.0 mol %) and **PS1** (1.0 equiv) in DMF under N_2, irradiation with a 427 nm LED lamp at 20 °C for 2 hours. [b]Isolated yield of **9a** after flash column chromatography. [c]No reaction.

afforded the corresponding enaminones **9i** and **9j**, respectively, in moderate yields. Gratifyingly, 1-(pyridin-2-yl)piperazine was also tolerated, providing the expected product **9h** in 46% yield. Considering that pyridine is one of the core components of drug derivative formulations, present in more than 7,000 active pharmaceutical compounds [43], the possibility of introducing a pyridine ring into the enaminone structure could be useful for the development of new drug candidates.

When pyrrolidine was used as amine reagent, the target enaminone **9k** was obtained, albeit in low yield. Regrettably, this transformation failed to provide the corresponding enaminone products by replacing alicyclic amines by diisopropylamine, probably due to steric hindrance. Steric factors could also explain the lack of reactivity of seven-membered azepane. In view of these results, it seems evident that six-membered cyclic amines have the optimal ring size for the photocatalyzed enam-

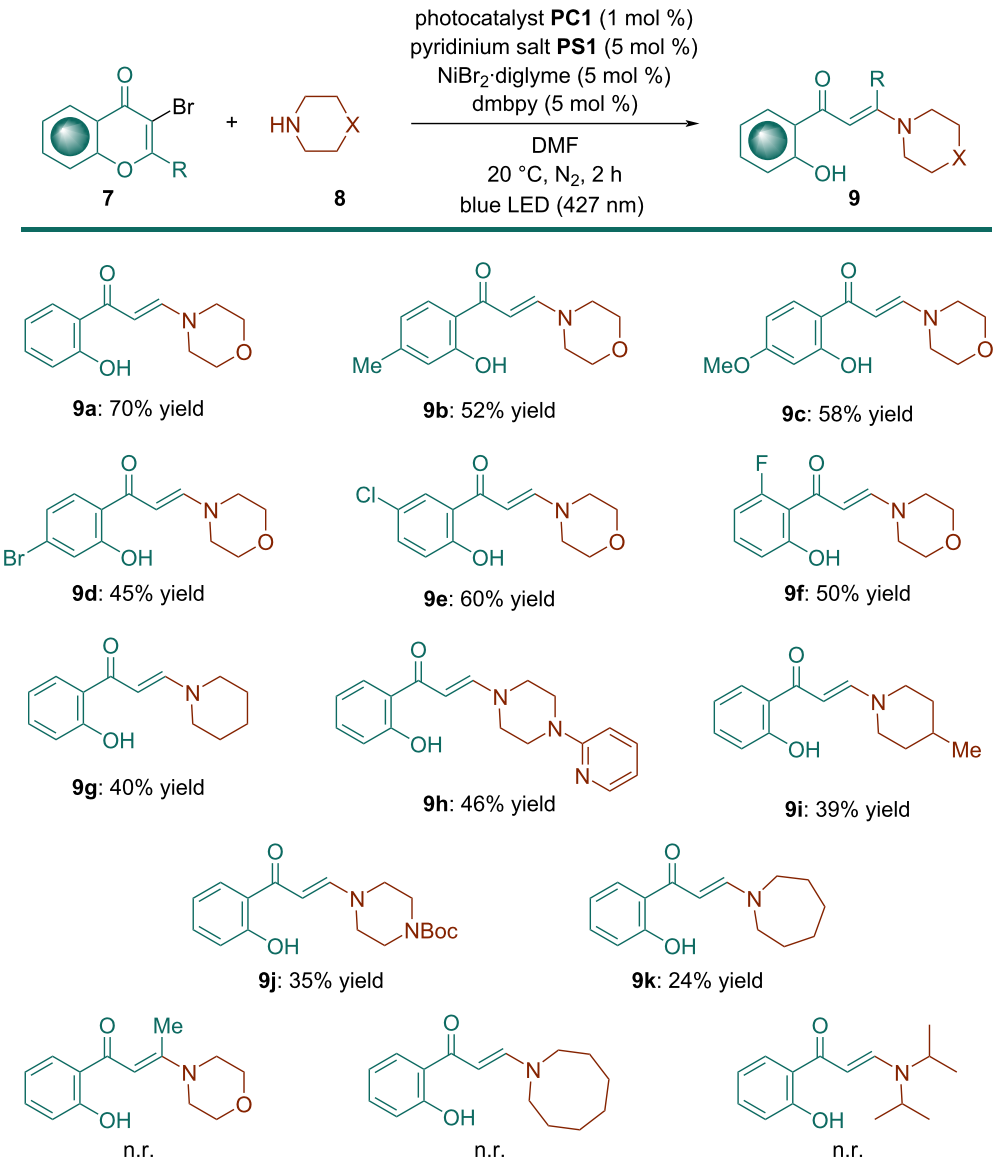

Scheme 2: Substrate scope.

inone formation process. For enaminones **9b–k** the remaining mass balance comprised mainly unreacted starting materials.

The scalability of the process was demonstrated in semipreparative scale for the reaction of 3-bromochromone (**7a**, 5.0 mmol) to afford enaminone **9a** in a 68% isolated yield (Scheme 3).

In terms of the reaction mechanism, TEMPO completely inhibited the reaction, implying the possibility of a radical intermediate in the reaction (Scheme 4A). Moreover, the TEMPO adduct **10** was identified using GC–MS (Figure S1, Supporting Information File 1). When the reaction was performed under air-equilibrated conditions, the intended product **9a** was obtained in a 31% yield, indicating that air influenced the interaction between the Ni-catalyst and the α,β-unsaturated carbonyl function (Scheme 4B). Furthermore, when the reaction of chromone **10** was carried out under standard conditions, the starting material was recovered unaltered, evidencing that the photocatalyzed dehalogenation step is crucial to enable the ring opening (Scheme 4C).

In order to determine the role of Ni(II) in this process, UV–vis studies were carried out. Thus, upon addition of **PS1** and **7a** to a solution of $NiBr_2$-dmbpy, a charge transfer (CT) band at 688 nm was visible in the UV–vis spectrum (Figure S2, Supporting Information File 1). This observation is consistent with

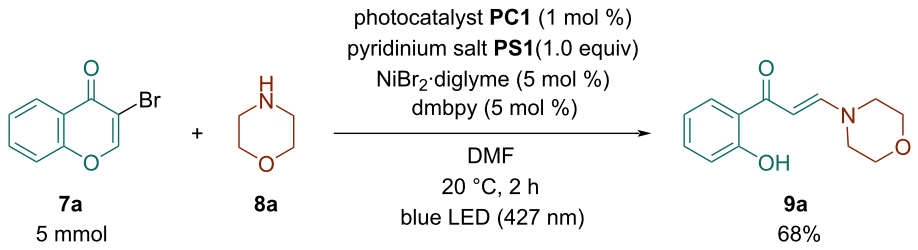

Scheme 3: Scale-up synthesis of enaminone **9a**.

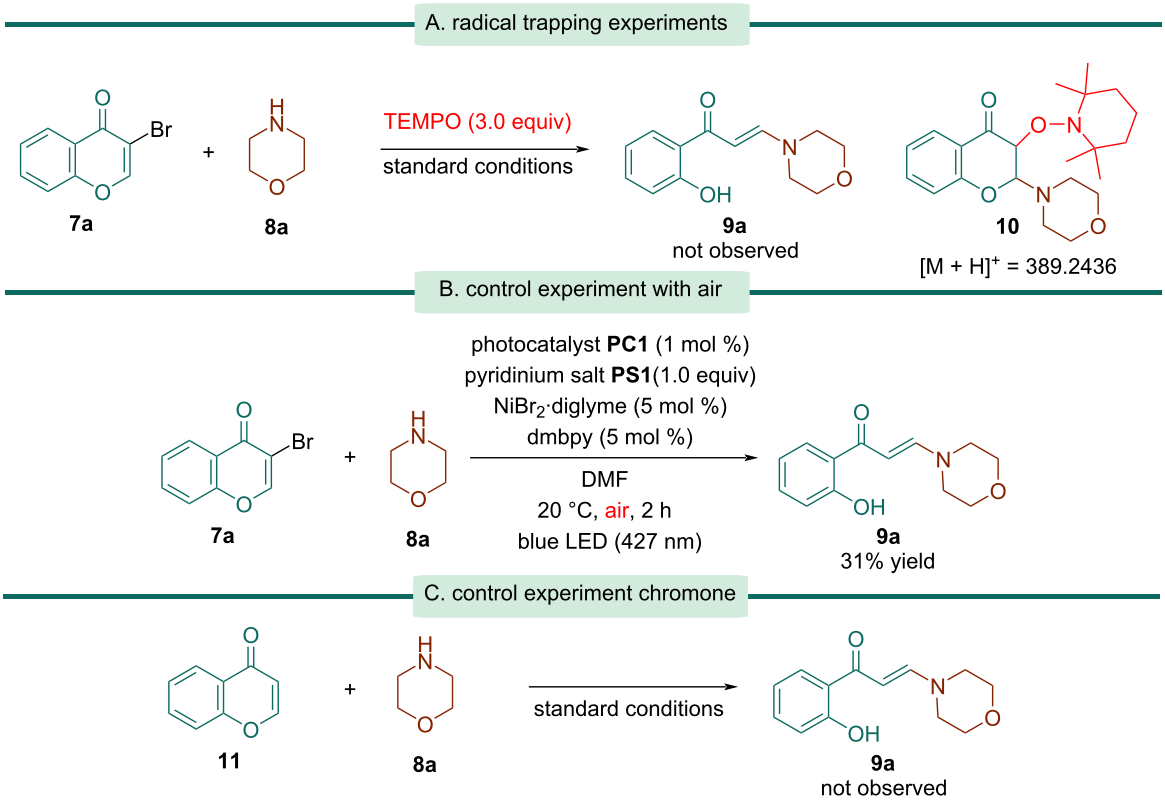

Scheme 4: Mechanistic studies.

the formation of a six-coordinate, pseudo-octahedral Ni(II) complex [44] involving the carbonyl groups of **PS1** and **7a**, which is further activated on aggregation of the pyridinium salt and the chromone aromatic ring through π–π stacking.

Then, **PC1** was submitted to Stern–Volmer quenching experiments. Whereas no interaction occurred between the excited form of **PC1** and 3-bromochromone (**7a**), a direct interaction occurred between **PC1*** and morpholine (**8a**, Figure S3, Supporting Information File 1). Based on these results, the most plausible scenario might be that the reaction starts with the excitation of **PC1** at 427 nm to generate the highly oxidative state **PC1*** that interacts with morpholine (**8a**) to generate the corresponding aminium radical cation.

To gain a better understanding of the process, the formation of the enaminone product **9a** was monitored overtime by ^{1}H NMR, which confirmed that the the reaction was complete within 2 h. Furthermore, the rate of the reaction is independent of the concentration of the 3-bromochromone substrate **7a** and amine **8a** (Figure S4, Supporting Information File 1).

Based on the above experiments and prior work on the photocatalytic reductive halogenation using acridinium photocata-

lysts [45,46], a possible mechanism for this reaction is proposed in Scheme 5.

A ternary complex is initially formed upon complexation of 3-bromochromone (**7a**) with $NiBr_2$-dmbpy. By virtue of being coordinated to a Ni-center, the β-carbon is activated toward nucleophilic attack of the amine, furnishing 2-amino-3-bromochromenone **I**. Simultaneously, acridinium photocatalyst **PC1** absorbed energy and transitioned from the ground state to excited state under visible-light irradiation. This excited state **PC1*** is quenched by the amine, generating the amine radical cation and **PC1** radical via a single-electron transfer (SET) process. Then, the C−Br bond of **I** is cleaved by **PC1**•, generating a C-centered radical **II**, which can be further reduced to give an enolate **III**, that ultimately evolves to the more stable anion **IV** and undergoes protonation to afford the final enaminone product **9a**.

Conclusion

In summary, a simple and effective nickel-assisted photocatalytic protocol for the direct formation of enaminones from 3-bromochromones is reported. The process involves a Ni(II)-catalyzed hydroamination, followed by photocatalytic reductive debromination. Mechanistic studies suggest that the key step of this transformation is the complexation of the starting 3-bromochromones to Ni(II) and a pyridinium salt, giving rise to a ternary Ni-complex which activates the α,β-unsaturated carbonyl compound towards nucleophilic addition. The presented method is operationally simple and can be conducted using low catalyst loadings of a Ni-catalyst and an inexpensive organic photocatalyst.

Supporting Information

Supporting Information File 1

Additional optimization details, mechanistic studies, experimental details, characterization data and NMR spectra for enaminones **9**.
[https://www.beilstein-journals.org/bjoc/content/supplementary/1860-5397-21-116-S1.pdf]

Acknowledgements

We would like to thank Prof. Jose Manuel Costa-Fernández for his help with the spectroscopic studies.

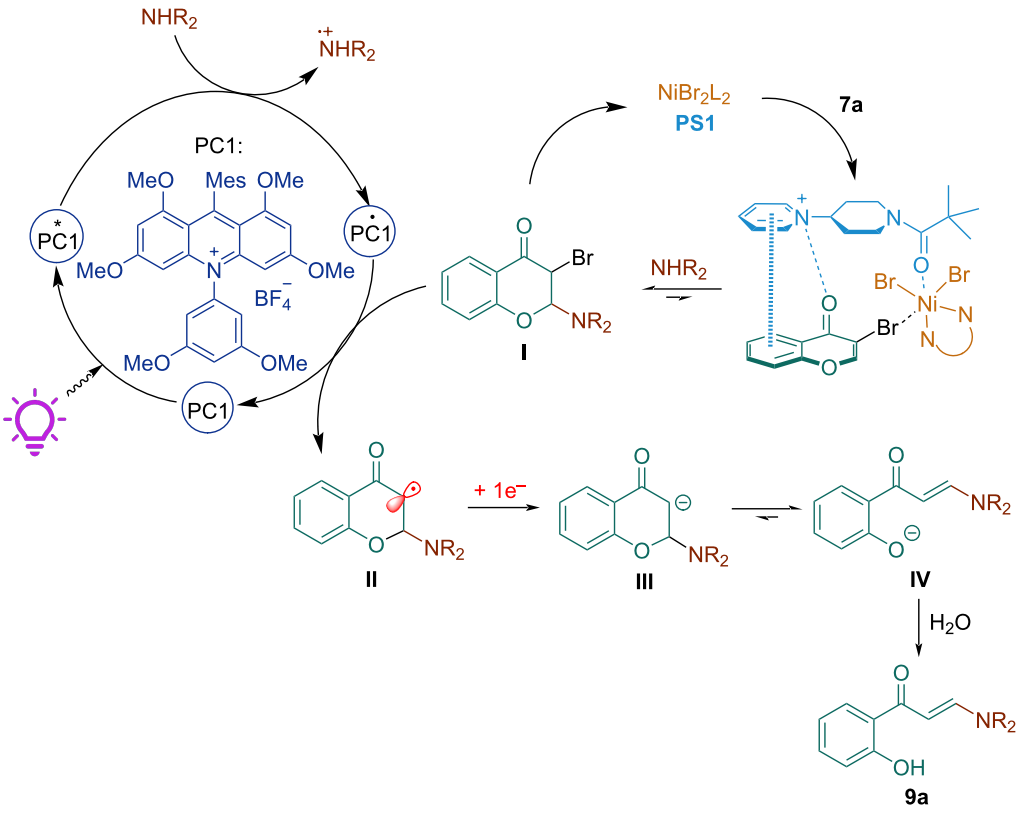

Scheme 5: Proposed mechanism.

Funding

This work has received financial support from MCI (PID2022-137893OB-I00), Principado de Asturias (SEK-25-GRU-GIC-24-054) and INGENIUM Alliance of European Universities (ERASMUS-EDU-2022-EUR-UNIV-2, Project number 101090042). P.P.R. thanks "Programa Investigo" for a predoctoral contract (AYUD/2022/9313, EU Next Generation).

Author Contributions

Paula Pérez-Ramos: investigation; writing – review & editing. Raquel G. Soengas: conceptualization; funding acquisition; supervision; writing – original draft. Humberto Rodríguez-Solla: conceptualization; funding acquisition; supervision; writing – review & editing.

ORCID® iDs

Raquel G. Soengas - https://orcid.org/0000-0001-8178-0034
Humberto Rodríguez-Solla - https://orcid.org/0000-0002-5394-5177

Data Availability Statement

All data that supports the findings of this study is available in the published article and/or the supporting information of this article.

Preprint

A non-peer-reviewed version of this article has been previously published as a preprint: https://doi.org/10.3762/bxiv.2025.32.v1

References

1. Cao, S.; Jing, Y.; Liu, Y.; Wan, J. *Chin. J. Org. Chem.* **2014,** *34,* 876–885. doi:10.6023/cjoc201312016
2. Chattopadhyay, A. K.; Hanessian, S. *Chem. Commun.* **2015,** *51,* 16450–16467. doi:10.1039/c5cc05892a
3. Huang, J.; Yu, F. *Synthesis* **2021,** *53,* 587–610. doi:10.1055/s-0040-1707328
4. Wang, Y.; Zhang, C.; Li, S.; Liu, L.; Feng, X. *ChemistrySelect* **2022,** *7,* e202103345. doi:10.1002/slct.202103345
5. Chen, X. Y.; Zhang, X.; Wan, J.-P. *Org. Biomol. Chem.* **2022,** *20,* 2356–2369. doi:10.1039/d2ob00126h
6. Wang, Z.; Zhao, B.; Liu, Y.; Wan, J.-P. *Adv. Synth. Catal.* **2022,** *364,* 1508–1521. doi:10.1002/adsc.202200144
7. Amaye, I. J.; Haywood, R. D.; Mandzo, E. M.; Wirick, J. J.; Jackson-Ayotunde, P. L. *Tetrahedron* **2021,** *83,* 131984. doi:10.1016/j.tet.2021.131984
8. Zhou, S.; Wang, J.; Wang, L.; Song, C.; Chen, K.; Zhu, J. *Angew. Chem., Int. Ed.* **2016,** *55,* 9384–9388. doi:10.1002/anie.201603943
9. Yang, L.; Wei, L.; Wan, J.-P. *Chem. Commun.* **2018,** *54,* 7475–7478. doi:10.1039/c8cc03514h
10. Liu, M.; Yan, K.; Wen, J.; Liu, W.; Wang, M.; Wang, L.; Wang, X. *Adv. Synth. Catal.* **2022,** *364,* 512–517. doi:10.1002/adsc.202101181
11. Fang, Z.; Ma, Y.; Dong, J. *Tetrahedron Lett.* **2022,** *102,* 153944. doi:10.1016/j.tetlet.2022.153944
12. Liang, X.; Guo, P.; Yang, W.; Li, M.; Jiang, C.; Sun, W.; Loh, T.-P.; Jiang, Y. *Chem. Commun.* **2020,** *56,* 2043–2046. doi:10.1039/c9cc08582c
13. Zheng, X.; Liu, Y.; Wan, J.-P. *Chin. J. Org. Chem.* **2021,** *41,* 2700–2706. doi:10.6023/cjoc202104053
14. Wang, F.; Fu, R.; Chen, J.; Rong, J.; Wang, E.; Zhang, J.; Zhang, Z.; Jiang, Y. *Chem. Commun.* **2022,** *58,* 3477–3480. doi:10.1039/d2cc00383j
15. Dattatri; Singam, M. K. R.; Nanubolu, J. B.; Reddy, M. S. *Org. Biomol. Chem.* **2022,** *20,* 6363–6367. doi:10.1039/d2ob00839d
16. Ying, J.; Liu, T.; Liu, Y.; Wan, J.-P. *Org. Lett.* **2022,** *24,* 2404–2408. doi:10.1021/acs.orglett.2c00671
17. Guo, Y.; Liu, Y.; Wan, J.-P. *Chin. Chem. Lett.* **2022,** *33,* 855–858. doi:10.1016/j.cclet.2021.08.003
18. Liang, Y.; Wang, R. *Tetrahedron Lett.* **2023,** *114,* 154287. doi:10.1016/j.tetlet.2022.154287
19. Duan, X.; Li, H.; Li, W.; Wang, J.; Liu, N. *ChemistrySelect* **2021,** *6,* 6478–6482. doi:10.1002/slct.202101726
20. Liu, T.; Wei, L.; Zhao, B.; Liu, Y.; Wan, J.-P. *J. Org. Chem.* **2021,** *86,* 9861–9868. doi:10.1021/acs.joc.1c00862
21. Lu, F.; Zhang, K.; Yao, Y.; Yin, Y.; Chen, J.; Zhang, X.; Wang, Y.; Lu, L.; Gao, Z.; Lei, A. *Green Chem.* **2021,** *23,* 763–766. doi:10.1039/d0gc03590d
22. Yu, Q.; Liu, Y.; Wan, J.-P. *Chin. Chem. Lett.* **2021,** *32,* 3514–3517. doi:10.1016/j.cclet.2021.04.037
23. Zheng, Y.; Liu, Z.-W.; Li, T.; Li, X.; Li, S.-H. *Org. Lett.* **2022,** *24,* 7533–7537. doi:10.1021/acs.orglett.2c02824
24. Cindrić, M.; Rubčić, M.; Hrenar, T.; Pisk, J.; Cvijanović, D.; Lovrić, J.; Vrdoljak, V. *J. Mol. Struct.* **2018,** *1154,* 636–642. doi:10.1016/j.molstruc.2017.10.078
25. Kumar, R.; Saha, N.; Purohit, P.; Garg, S. K.; Seth, K.; Meena, V. S.; Dubey, S.; Dave, K.; Goyal, R.; Sharma, S. S.; Banerjee, U. C.; Chakraborti, A. K. *Eur. J. Med. Chem.* **2019,** *182,* 111601. doi:10.1016/j.ejmech.2019.111601
26. Masocha, W.; Kombian, S. B.; Edafiogho, I. O. *Sci. Rep.* **2016,** *6,* 21582. doi:10.1038/srep21582
27. Amaye, I. J.; Heinbockel, T.; Woods, J.; Wang, Z.; Martin-Caraballo, M.; Jackson-Ayotunde, P. *Int. J. Environ. Res. Public Health* **2018,** *15,* 1784. doi:10.3390/ijerph15081784
28. Bangalore, P. K.; Vagolu, S. K.; Bollikanda, R. K.; Veeragoni, D. K.; Choudante, P. C.; Misra, S.; Sriram, D.; Sridhar, B.; Kantevari, S. *J. Nat. Prod.* **2020,** *83,* 26–35. doi:10.1021/acs.jnatprod.9b00475
29. Ghorab, M. M.; Ragab, F. A.; Heiba, H. I.; El-Gazzar, M. G.; El-Gazzar, M. G. M. *Bioorg. Med. Chem. Lett.* **2018,** *28,* 1464–1470. doi:10.1016/j.bmcl.2018.03.089
30. Liu, J.-Y.; Cao, G.-E.; Xu, W.; Cao, J.; Wang, W.-L. *Appl. Organomet. Chem.* **2010,** *24,* 685–691. doi:10.1002/aoc.1667
31. Ueno, S.; Shimizu, R.; Kuwano, R. *Angew. Chem., Int. Ed.* **2009,** *48,* 4543–4545. doi:10.1002/anie.200900892
32. Yu, D.; Sum, Y. N.; Ean, A. C. C.; Chin, M. P.; Zhang, Y. *Angew. Chem., Int. Ed.* **2013,** *52,* 5125–5128. doi:10.1002/anie.201301019
33. Li, M.; Fang, D.; Geng, F.; Dai, X. *Tetrahedron Lett.* **2017,** *58,* 4747–4749. doi:10.1016/j.tetlet.2017.09.054
34. Marzo, L.; Pagire, S. K.; Reiser, O.; König, B. *Angew. Chem., Int. Ed.* **2018,** *57,* 10034–10072. doi:10.1002/anie.201709766
35. Shaw, M. H.; Twilton, J.; MacMillan, D. W. C. *J. Org. Chem.* **2016,** *81,* 6898–6926. doi:10.1021/acs.joc.6b01449
36. Narayanam, J. M. R.; Stephenson, C. R. J. *Chem. Soc. Rev.* **2011,** *40,* 102–113. doi:10.1039/b913880n
37. Crisenza, G. E. M.; Melchiorre, P. *Nat. Commun.* **2020,** *11,* 803. doi:10.1038/s41467-019-13887-8

38. Yoon, T. P.; Ischay, M. A.; Du, J. *Nat. Chem.* **2010,** *2,* 527–532. doi:10.1038/nchem.687
39. Han, Y.; Zhou, L.; Wang, C.; Feng, S.; Ma, R.; Wan, J.-P. *Chin. Chem. Lett.* **2024,** *35,* 108977. doi:10.1016/j.cclet.2023.108977
40. Kim, S.; Kang, S.; Kim, G.; Lee, Y. *J. Org. Chem.* **2016,** *81,* 4048–4057. doi:10.1021/acs.joc.6b00341
41. Lapointe, S.; Zargarian, D. *Dalton Trans.* **2016,** *45,* 15800–15810. doi:10.1039/c6dt02105k
42. Yamuna, P.; Philip, R. M.; Anilkumar, G. *Tetrahedron* **2022,** *122,* 132936. doi:10.1016/j.tet.2022.132936
43. De, S.; Kumar S K, A.; Shah, S. K.; Kazi, S.; Sarkar, N.; Banerjee, S.; Dey, S. *RSC Adv.* **2022,** *12,* 15385–15406. doi:10.1039/d2ra01571d
44. Goldcamp, M. J.; Edison, S. E.; Squires, L. N.; Rosa, D. T.; Vowels, N. K.; Coker, N. L.; Krause Bauer, J. A.; Baldwin, M. J. *Inorg. Chem.* **2003,** *42,* 717–728. doi:10.1021/ic025860q
45. Maji, T.; Karmakar, A.; Reiser, O. *J. Org. Chem.* **2011,** *76,* 736–739. doi:10.1021/jo102239x
46. Nguyen, J. D.; D'Amato, E. M.; Narayanam, J. M. R.; Stephenson, C. R. J. *Nat. Chem.* **2012,** *4,* 854–859. doi:10.1038/nchem.1452

License and Terms